Computational Aerodynamics

ANDREW NING

Brigham Young University

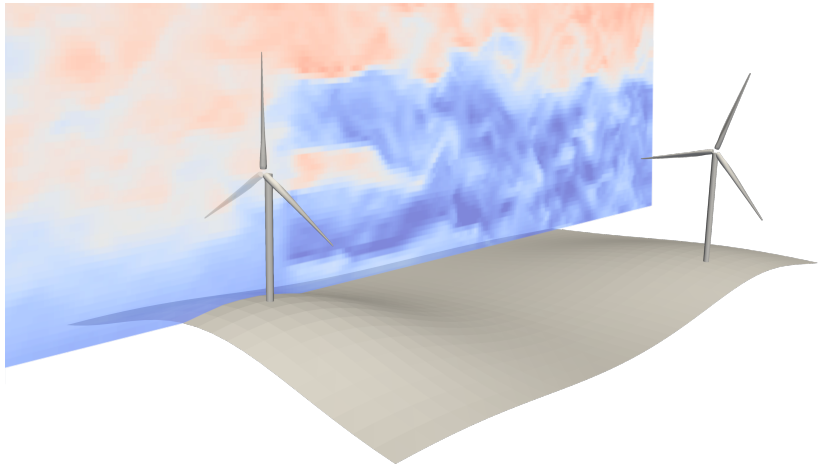

Compiled on Monday 11th April, 2022 at 09:39

Copyright
© 2022 Andrew Ning. All rights reserved.

Publication
First electronic edition: January 2020.

Contents

Preface

This book is designed for graduate students to provide additional depth beyond an introductory course in aerodynamics. A major focus is on computational theory and implementation of modern aerodynamic methods.

Acknowledgements

The cover figure was provided by Denis-Gabriel Caprace. The layout of this book was greatly improved based in part on a template provided by Max Opgenoord. Judd Mehr transcribed some of the equations and figures from the author's lecture notes.

1 Fundamentals

This chapter reviews various concepts that are covered in an introductory fluids or aerodynamics course, but with greater depth.

1.1 Density

A simple definition of density is mass per volume:

$$\rho = \frac{m}{\forall} \,. \tag{1.1}$$

However, the definition is not precise enough for a fluid as the size of the volume if not defined. If the control volume is large then the the density may vary significantly at different locations within the volume.

The need for a small volume leads to the next most common definition of density:

$$\rho = \lim_{\Delta\forall \to 0} \frac{\Delta m}{\Delta\forall} \,. \tag{1.2}$$

However, this definition is also problematic. Fluids are made up of individual molecules. Imagine freezing all of these particles, within some control volume, in order to make a density measurement. Suppose the volume is small enough so that there is only a couple of air particles in it and we sum up their mass and divide by the volume. Now suppose we make the volume a bit bigger so there is now a half dozen particle in it and we repeat the measurement. Because there are so few particles, as the volume changes size, the density measurement varies erratically as shown on the left side of Fig. 1.1.

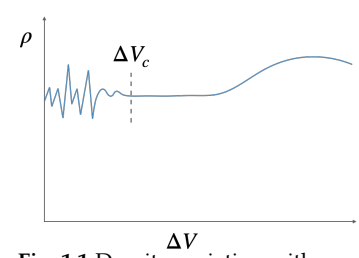

Fig. 1.1 Density variation with control volume size (logarithmic scale). The behavior is erratic at small scales because there are few molecules in the control volume. At some point the number of particles is so large that the fluid acts like a continuum with a volume we denote as $\Delta\forall_c$.

As we increase the size of the control volume eventually the number of particles contained within the volume is so large that the fluid acts like a continuum (we refer to this continuum volume as $\Delta\forall_c$). After this point, the density measurement begins to level out. For air at standard temperature and pressure the size of this control volume is a cube with sides approximately 1 micron in length. This control volume would have about 30 million air molecules in it. That is a large enough number that, statistically speaking, the density in the control volume is constant. However, if we continued to increase the volume then at some point our

density measurements would change because of spatial variation as noted at the beginning of this section. So, a better definition of density is:

$$\rho = \lim_{\Delta \forall \to \Delta \forall_c} \frac{\Delta m}{\Delta \forall} . \tag{1.3}$$

If we operate at scales above $\Delta \forall_c$ we are said to employ the *continuum* assumption. This means that we can treat the fluid not as individual molecules, but as a continuous medium. Everything we consider in this book will assume that the fluid is a continuum. While this assumption is reasonable for most aerodynamic applications, it is not always a good assumption. For example, at very high altitudes, air molecules are spread out far enough that we can no longer reliably use the Navier-Stokes equations. Instead, we could use the Boltzman transport equations that uses a statistical description to model particle transport.

One major categorization of fluids, related to density, is a distinction between *incompressible* versus *compressible*. No fluid can be truly incompressible, but it is a useful mathematical idealization. For now we will think of incompressible as a fluid with constant density, but we will see shortly that is an overly restrictive definition of incompressibility.

1.2 Pressure

Pressure is defined as

$$p = \lim_{\Delta A \to 0} = \frac{\Delta F}{\Delta A} . \tag{1.4}$$

Again, we should keep in mind that the limit doesn't really go to zero, but rather to a small enough control volume to where the continuum assumption is still valid. But for simplicity we won't continue to make that distinction.

Let us first consider why a fluid creates pressure. One way to visualize the effect of pressure is to consider the individual air molecules bouncing off a solid surface. The momentum transfer of the molecules is proportional to their mass times their velocity. Since the force is momentum per unit time, the pressure is then proportional to the momentum flux:

$$p \propto \rho V^2 . \tag{1.5}$$

For an ideal gas, temperature is proportional to the mean kinetic energy of the particles:

$$T \propto V^2 \tag{1.6}$$

Combining these equations yields:

$$p \propto \rho T \tag{1.7}$$

For an *ideal gas* the proportionality constant is the *specific gas constant* R:

$$p = \rho R T \tag{1.8}$$

For dry air the constant is:

$$R = 287.058 \frac{\mathrm{J}}{\mathrm{kg} \cdot \mathrm{K}} \tag{1.9}$$

We motivated pressure by imaging particles bouncing off a surface, but we know there is a pressure in a fluid away from surfaces as well. If there is no surface nearby to exchange momentum with, how is there a pressure? At first we might think the pressure arises because of collisions between the molecules, but this is not the case and in fact one of the assumptions for an ideal gas is that there are no interactions between particles. As long as there is a large number of particles, the situation is exactly the same as the case with a wall nearby as shown in Fig. 1.2. For any molecule leaving, statistically speaking, another will be entering. The momentum flux through the control volume is the same (if the entering/leaving particle was straight on, then the change in momentum would be $2mV$ since the momentum has the same magnitude but different signs in entering/leaving).

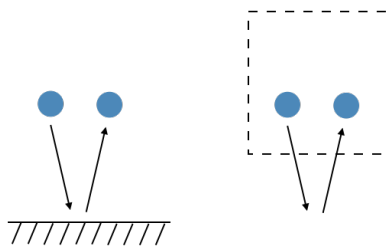

Fig. 1.2 Momentum transfer against a wall or momentum flux though a control volume is the same.

1.3 Shear Stress

Just like density and pressure, we can understand shear stresses better by considering a molecular description of air. Imagine a bunch of faster moving air particles next to a bunch of slower moving air particles as shown in Fig. 1.3. The molecules exchange momentum causing the faster particles to slow down and the slower particles to speed up. On average the velocity profile would look something like that shown on the right of Fig. 1.3. The forces acting on the particles arise from shear stresses.

Now let us consider fluid particles moving next to a solid object. The same principle applies. The molecules in the solid object have zero

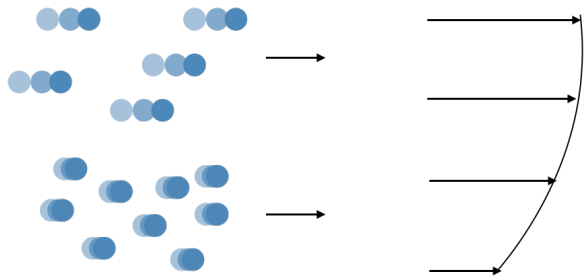

Fig. 1.3 Shear profile created from faster moving particles above lower moving particles.

velocity. Because of the momentum exchange between particles the fluid particles next to the wall must then also have zero velocity on average (in the reference frame of the solid object). This is called the *no slip condition* and is depicted in Fig. 1.4.

The layer of slow moving air near a solid surface is called a *boundary layer*. The velocity gradient creates a shear stress given by:

$$\tau = \mu \frac{\partial V}{\partial y}, \tag{1.10}$$

where μ is called the *dynamic viscosity* of the fluid.

Another common fluid categorization is *viscous* versus *inviscid*. An inviscid fluid is one where the viscosity is zero. A truly inviscid fluid doesn't exist, but is often a good mathematical approximation.

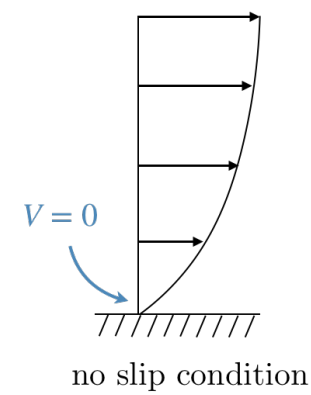

Fig. 1.4 The no slip condition requires that the velocity at a solid wall is zero.

1.4 Forces and Moments

All aerodynamics forces and moments arise from just pressure and shear stresses (Fig. 1.5). Pressure can only act normal to a body, shear stresses act tangential to the surface but can have a component in the normal direction as well (more on this later). Once we know pressure and shear stress everywhere on the surface of a body we can integrate to get total forces.

Pressure is very important to aerodynamic flows. A few examples will help illustrate. Consider the airfoils and cylinder depicted in Fig. 1.6. For a Reynolds number of 1 million all of these shapes have the same amount of drag, which is a rather surprising result. The airfoils have low pressure drag because of their streamlined shape, but have significant skin friction drag (resulting from shear) because of their large surface area. The cylinder on the other hand has little skin friction drag, but because it is blunt it has a large wake with significant pressure drag. Even though the cylinder is much smaller the blunt shape creates drag as high as the much larger airfoils. This is why aerodynamicists often mention the need for streamlined shapes. This also explains why many

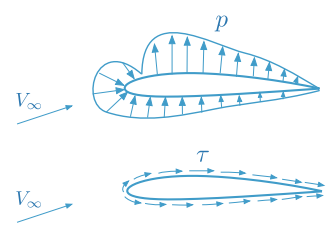

Fig. 1.5 top: pressure, bottom: shear stresses.

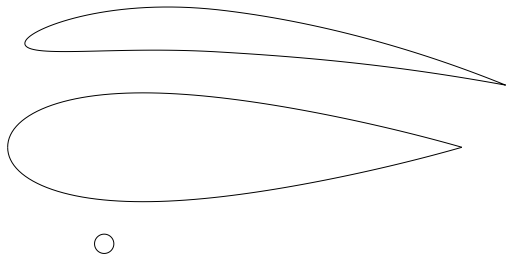

Fig. 1.6 A NACA 6409 airfoil at 5 degrees angle of attack, a NACA 0024 airfoil at 0 degrees angle of attack, and a cylinder at the scales of this figure, all have the same drag force for a Reynolds number of 1 million.

World War I era planes had such poor performance. Lots of wire bracing, usually with biplanes, was required for structural reinforcement, but the blunt shapes of circular wires created a large amount of drag. Between the two world wars semi-monoconque designs (skin stiffened, like an egg shell) and high-strength aluminum allowed for sufficient structural strength without wire bracing.

Example 1.1 Atmospheric pressure

Pressure plays such an important role because the pressure in our atmosphere is quite high. At sea level the pressure is about 2,000 lbs/ft^2. A flat plate the size of a piece of paper could carry 65 pounds by creating just a 5% pressure differential from top to bottom.

When plotting pressure we generally use the nondimensional *pressure coefficient*:

$$C_p = \frac{p - p_\infty}{\frac{1}{2}\rho V_\infty^2} \tag{1.11}$$

which is the gauge pressure divided by the dynamic pressure. For the idealized inviscid flow around a cylinder we could plot the pressure as a function of the azimuthal angle of the cylinder as shown in Fig. 1.7. Because the cylinder is symmetric only one curve is shown to represent both the top and bottom half.

Notice that the pressure starts high at the stagnation point, drops as the flow speeds up around the cylinder, and then recovers the same high pressure on the back side. Because the pressure distribution is perfectly symmetric, there is no drag in this inviscid scenario. The curve is reminiscent of rolling a ball down a frictionless hill. In the absence of friction you should be able to return to the same height.

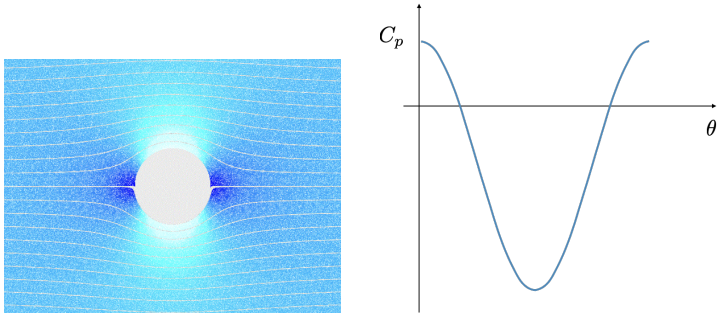

Fig. 1.7 Pressure coefficient around an idealized inviscid cylinder.

The presence of viscosity, however, alters the flow field. The flow separates from the cylinder creating a large wake. The pressure distribution does not recover to the same high pressure on the back side, resulting in drag (Fig. 1.8). Notice that on the forward half of the

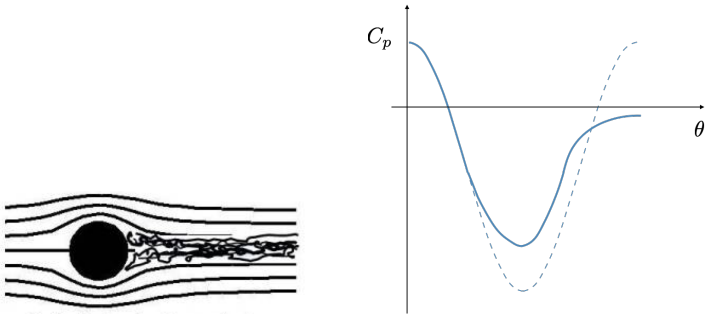

Fig. 1.8 Pressure coefficient around an viscous cylinder.

cylinder the pressure changes from high to low. We call this a *favorable pressure gradient* as to pressure accelerates the flow. On the back half of the cylinder, the flow moves from a low pressure region to a high pressure one. This is called an *adverse pressure gradient*. The fluid must work against the adverse pressure gradient, and in the presence of viscosity some energy is loss so it will not return all the around the cylinder. Instead the fluid decreases in momentum and eventually has zero velocity in the direction along the cylinder leading to flow separation. The void is filled in with a low pressure wake.

Most of the time we are interested in streamlined bodies. The pressure coefficient distribution for an airfoil is depicted in Fig. 1.9 An airfoil, however, is not symmetric, so we see two curves: one for the upper surface and one for the lower surface. Also note that the y-axis plots the negative of the pressure coefficient. This is a common convention because the upper surface (or suction side) is associated with low pressures, whereas the lower surface (or pressure side) is associated with higher pressures. Thus, by plotting the negative of the

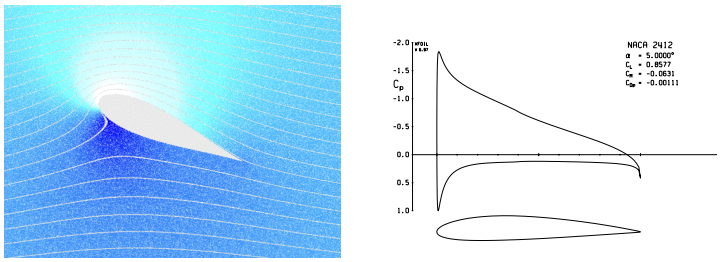

Fig. 1.9 Pressure coefficient around an airfoil.

pressure coefficient, the upper curve corresponds to the upper surface and lower curve corresponds to the lower surface. The two curves start at the stagnation point (which for an inviscid, incompressible flow, corresponds to $C_p = 1$ as we will see in the next chapter). For the upper surface we see rapid acceleration into the low pressure region just aft of the nose, and then a long gradual pressure recovery, in an adverse gradient, towards the trailing edge. It is important that the pressure recovery in the adverse region is gradual, otherwise the flow will separate. As we will also see in the next chapter, the force in the vertical direction is given by the area between these two curves (Eq. 2.126). Thus, we see that most of the lift (which is not quite the same as the force in the vertical direction, as discussed below) is generated by the upper surface. This is generally true, and is primarily why many instruments for aircraft are located on the lower surface where disrupting the flow field is less consequential.

The integration of the pressure and shear stresses over a body results in forces and moments that could be resolved into any coordinate system. For aerodynamic bodies some common conventions are discussed below. By definition we define drag as the force in the direction of the freestream (depicted in Fig. 1.10), and lift is always defined perpendicular to the freestream. The force normal to the body is called the normal force (not to be confused with lift). These forces are related by a simple coordinate transformation:

$$L = N \cos\alpha - A \sin\alpha \tag{1.12}$$

$$D = N \sin\alpha + A \cos\alpha \tag{1.13}$$

Note also from the figure that the angle of attack is defined as the angle between the freestream and the chord line, or some other reference line of the vehicle.

As we will discuss in more detail later, nondimensional parameters are critically important in aerodynamics. The lift and drag are normalized as follows:

$$C_L = \frac{L}{\frac{1}{2}\rho V_\infty^2 S} \tag{1.14}$$

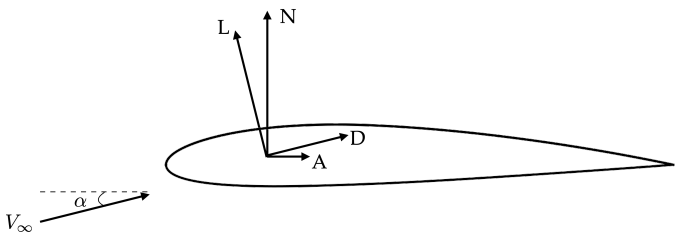

Fig. 1.10 Lift acts perpendicular to the freestream.

$$C_D = \frac{D}{\frac{1}{2}\rho V_\infty^2 S}, \tag{1.15}$$

where the symbol S is a reference area. Anything can be used for the reference area (it is just a reference), as long as one is consistent, but there are general conventions depending on the application. The force coefficients are meaningless without also defining what reference area was used. For example, if you look up tables of drag coefficients for various objects they will always define what type of reference area should be used. Streamlined objects tend to use projected areas parallel to the freestream (because the drag scales more with the skin friction area), whereas blunt objects often use projected cross-sectional areas normal to the freestream (because the drag is more pressure dominant scaling with the projected frontal area).

The pitching moment is normalized as shown below, where c is an additional reference length (e.g., chord for an airfoil)

$$C_M = \frac{M}{\frac{1}{2}\rho V_\infty^2 S c}. \tag{1.16}$$

A moment causing the body to nose-up is typically considered positive.

In addition, to the 3D coefficients, we also have 2-D expressions for the aerodynamic coefficients. The symbols are lowercase to indicate 2D. These expressions for lift, drag, and moment respectively are:

$$c_\ell = \frac{\ell}{\frac{1}{2}\rho V_\infty^2 c} \tag{1.17}$$

$$c_d = \frac{d}{\frac{1}{2}\rho V_\infty^2 c} \tag{1.18}$$

$$c_m = \frac{m}{\frac{1}{2}\rho V_\infty^2 c^2}. \tag{1.19}$$

The lift coefficient is a function of angle of attack as shown in Fig. 1.11 (and potentially other nondimensional parameters like Reynolds number and Mach number). For a positively cambered airfoil (not symmetric) the airfoil begins producing lift at a negative angle of attack called

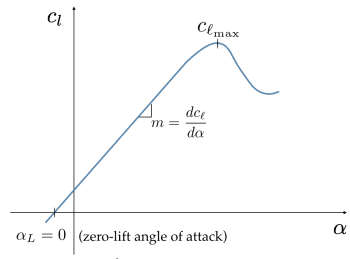

Fig. 1.11 Lift curve.

the *zero-lift angle of attack*. The lift then increases linearly with a slope m, called the lift curve slope. At some point, viscous effects dominant, the flow separates and the lift drops (a phenomenon called *stall*). The highest lift coefficient is called $c_{l_{max}}$ (pronounced: c-ell-max). For the linear portion of the curve we can write:

$$c_l = m(\alpha - \alpha_0) \tag{1.20}$$

Similarly, we can plot the drag coefficient either as a function of angle of attack or as a function of lift coefficient as shown in Fig. 1.12 Drag generally varies quadratically with lift (and thus with angle of attack) over much of the drag polar.

Pitching moment coefficient (not shown) is usually negative and relatively flat with respect to angle of attack for an airfoil.

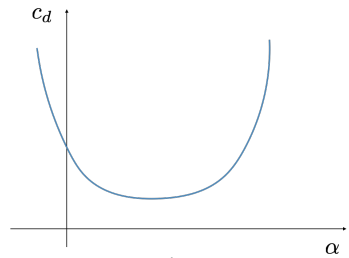

Fig. 1.12 Drag polar.

1.5 Frequently Used Math Concepts

The gradient operator acts on a scalar and produces a vector:

$$\nabla p = \frac{\partial p}{\partial x}\hat{x} + \frac{\partial p}{\partial y}\hat{y} + \frac{\partial p}{\partial z}\hat{z} \tag{1.21}$$

The gradient is a vector that points in the direction where the scalar field is increasing the fastest.

Divergence is a scalar quantity that acts on vectors:

$$\nabla \cdot \vec{V} = \frac{\partial V_x}{\partial x} + \frac{\partial V_y}{\partial y} + \frac{\partial V_z}{\partial z} \tag{1.22}$$

It can be thought of as a measure of how much something is expanding or contracting. If the vector $\vec{V}$ is velocity its divergence measures volume change per unit mass (or the rate of change of density). Thus, for incompressible flows the divergence is zero (we will derive this more rigorously shortly).

$$\nabla \cdot \vec{V} = 0 \;\rightarrow\; \text{incompressible} \tag{1.23}$$

The curl is a vector quantity and it acts on vectors:

$$\nabla \times \vec{V} = \left(\frac{\partial V_z}{\partial y} - \frac{\partial V_y}{\partial V_z}\right)\hat{x} + \left(\frac{\partial V_x}{\partial z} - \frac{\partial V_z}{\partial V_x}\right)\hat{y} + \left(\frac{\partial V_y}{\partial x} - \frac{\partial V_x}{\partial V_y}\right)\hat{z} \tag{1.24}$$

The curl measures the tendency of a vector field to create rotation. If the vector $\vec{V}$ is velocity then its curl is called vorticity ($\vec{\omega}$):

$$\vec{\omega} = \nabla \times \vec{V} \tag{1.25}$$

Vorticity is an important aerodynamic quantity we will discuss later. It is related to rotation as vorticity is twice the angular velocity.

Stoke's theorem relates the contour integral of a vector around a path to the curl (or rotation) of that vector inside the area.

$$\oint_C \vec{V} \cdot d\vec{\ell} = \int_A \left(\nabla \times \vec{V}\right) \cdot d\vec{A} \tag{1.26}$$

The divergence theorem relates the flux of some vector leaving a control volume to the divergence of that vector inside the enclosed volume.

$$\int_A \vec{V} \cdot d\vec{A} = \int_{\forall} \left(\nabla \cdot \vec{V}\right) d\forall \tag{1.27}$$

Index notation, also known as Einstein notation, or sometimes tensor notation, is a convenient representation often used in differential forms of fluid equations. In this notation a single index represents all three vector components. The same index may be used in separate terms indicating a free index that is repeated for all three vector components. Thus,

$$\frac{\partial(\rho u_i)}{\partial t} + \frac{\partial p}{\partial x_i} = 0 \tag{1.28}$$

is a shorthand for three equations:

$$\frac{\partial(\rho u_1)}{\partial t} + \frac{\partial p}{\partial x_1} = 0 \tag{1.29}$$

$$\frac{\partial(\rho u_2)}{\partial t} + \frac{\partial p}{\partial x_2} = 0 \tag{1.30}$$

$$\frac{\partial(\rho u_3)}{\partial t} + \frac{\partial p}{\partial x_3} = 0 \tag{1.31}$$

where the subscripts $1, 2, 3$ correspond to separate Cartesian directions, typically the x, y, z directions.

A repeated index, in the same term, represents a summation. Thus, $\partial u_i / \partial x_i$ is shorthand for:

$$\sum_{i=1}^{3} \frac{\partial u_i}{\partial x_i} \tag{1.32}$$

or

$$\frac{\partial u_i}{\partial x_i} = \frac{\partial u_1}{\partial x_1} + \frac{\partial u_2}{\partial x_2} + \frac{\partial u_3}{\partial x_3} = \nabla \cdot \vec{V} \tag{1.33}$$

We can combine the two types of indices (free index and summation index) as shown in the expression below:

$$\frac{\partial(\rho u_i)}{\partial t} + \frac{\partial(\rho u_i u_j)}{\partial x_j} = 0 \tag{1.34}$$

In this case index j is repeated in the same term, which indicates a summation. Whereas the index i appears once in each term and is thus the free index representing separate equations. There can only be one free index, but there can be multiple summations, generally indicated with additional indices. Written explicitly the above equations expands out to:

$$\frac{\partial(\rho u_1)}{\partial t} + \frac{\partial(\rho u_1 u_1)}{\partial x_1} + \frac{\partial(\rho u_1 u_2)}{\partial x_2} + \frac{\partial(\rho u_1 u_3)}{\partial x_3} = 0 \tag{1.35}$$

$$\frac{\partial(\rho u_2)}{\partial t} + \frac{\partial(\rho u_2 u_1)}{\partial x_1} + \frac{\partial(\rho u_2 u_2)}{\partial x_2} + \frac{\partial(\rho u_2 u_3)}{\partial x_3} = 0 \tag{1.36}$$

$$\frac{\partial(\rho u_3)}{\partial t} + \frac{\partial(\rho u_3 u_1)}{\partial x_1} + \frac{\partial(\rho u_3 u_2)}{\partial x_2} + \frac{\partial(\rho u_3 u_3)}{\partial x_3} = 0 \tag{1.37}$$

$$\tag{1.38}$$

While this shorthand takes some getting used to, once we are familiar with it we can express many equations more concisely and clearly. This shorthand becomes particularly useful once tensors are involved.

1.6 Dynamic Similarity

Nondimensional numbers are critically important in fluids. They provide insight across problems of different scales. For example, a lift of 60 N doesn't mean much without context (is that a lot of lift or a little?). On the other hand, we can tell if a lift coefficient is large or small regardless of whether it is from a dragonfly or an airliner as the lift coefficient falls along a narrow range.

Nondimensional numbers also also the basis of wind tunnel testing, and similarity modeling in general. They also provide critical insight by reducing the dimensionality of the problem, and highlight fundamental relationships. Let's illustrate with some examples.

Example 1.2 Nondimensional parameters for wind turbine power production

Consider a wind turbine. The data we explore could come from experimental measurements or computations, it doesn't matter, but in this case it is simulation data with added noise. As depicted in Fig. 1.13, we are interested in understanding the relationship between the power the turbine produces and two inputs: the incoming velocity and the rotation speed of the rotor.

For the purposes of this example, we let the inputs fall within the following ranges with uniform probability:

$$\begin{aligned} V_\infty &\in [5, 15]\ \mathrm{m/s} \\ \Omega &\in [1, 30]\ \mathrm{RPM} \end{aligned} \tag{1.39}$$

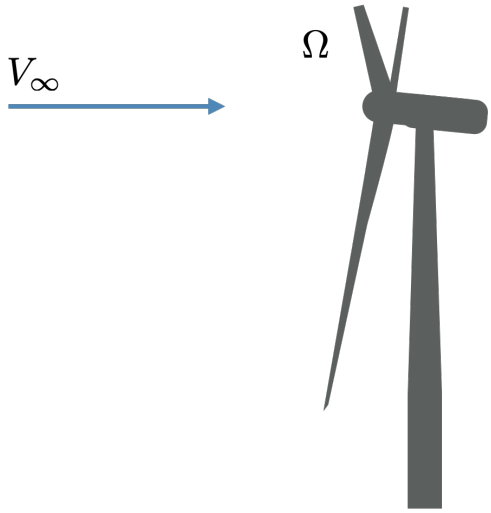

Fig. 1.13 A wind turbine with an incoming wind speed and a rotor rotation speed.

We observe the output of many "experiments" in Fig. 1.14.

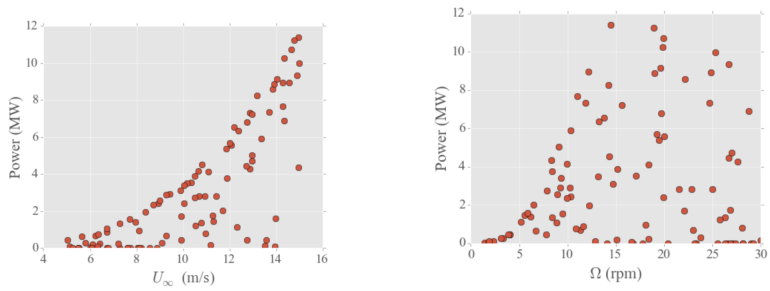

power vs windspeed power vs rotation speed

Fig. 1.14 The power produced by the wind turbine as we randomly vary wind speed and rotation speed.

There appears to be very little structure in this data. In other words, if you were given a wind speed, you wouldn't be able to predict the power output (although it appears as if we could predict a maximum power, which is true). The same conclusion applies for the rotation speed. Imagine that your supervisor has given you the assignment to create a predictive model for the turbine power as a function of two variables. So far, the data doesn't appear promising to allow this. What would you do?

Perhaps, evaluating random samples was the problem. Let's instead try holding the rotation speed constant, and just vary V_∞. In Fig. 1.15 we perform that experiment for four different rotation speeds.

This appears much more promising. Clear structure is visible. Perhaps we would create a polynomial fit for each rotation speed separately, and then a separate curve fit for the polynomial coefficients as a function of the rotation speeds. This is still rather problematic, it's fairly complex, and the curves seem to go to zero power at different points making interpolation challenging.

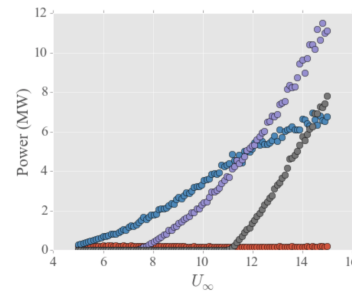

Fig. 1.15 Power as a function of windspeed for four different rotation speeds.

Formally, what we are trying to understand is a functional relationship to predict power as a function of all inputs (including some we are holding constant):

$$P = f(V_\infty, \Omega, \rho, R) \tag{1.40}$$

and perhaps other variables like viscosity. From previous courses you have learned that appropriately chosen nondimensional parameters can simplify the relationships between variables. Perhaps greater insight is available through nondimensionalization.

While the Buckingham-Pi theorem can help us formally quantify how many nondimensional parameters we need, most of the time it is straightforward to determine an appropriate set. First, let's nondimensionalize the velocities. There are numerous possibilities but for wind turbines the standard convention for normalizing the speeds is to use the tip-speed ratio, which is a ratio of the tip-speed relative to the freesteam:

$$\lambda = \frac{\Omega R}{V_\infty} \tag{1.41}$$

The power could also be nondimensionalized many ways, but the standard way is to use the freesteam dynamic pressure times the rotor disk area (producing a force) then multiplying by the freestream velocity once more to obtain power. This is called the power coefficient:

$$C_P = \frac{P}{\frac{1}{2}\rho V_\infty^3 \pi R^2} \tag{1.42}$$

All of the parameters have been used in the nondimensionalization so these are all the Pi groups. Our new equation now looks like:

$$C_P = f(\lambda) \tag{1.43}$$

Let's try plotting the data as suggested by this nondimensionalization. The data from Fig. 1.14 is shown in Fig. 1.16. and for Fig. 1.15 the results are shown in Fig. 1.17.

Now the relationship is very clear. Given a velocity V_∞ and rotation speed Ω we can now provide a quite good prediction for the wind turbine's power. Note that we are able to do this without knowing anything about the physics involved in the function f.

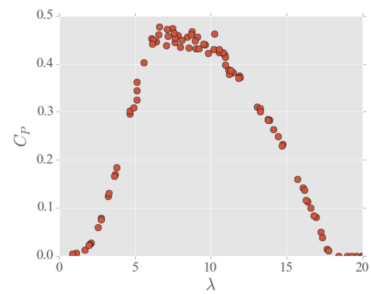

Fig. 1.16 Power coefficient as a function of tip speed.

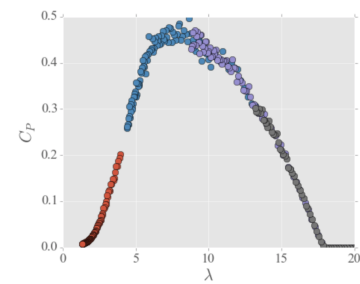

Fig. 1.17 Same figure but color coded by the rotation speed.

Imagine an object/vehicle that we wish to predict aerodynamic drag for. We could write the relationship as:

$$D = f(V_\infty, \rho, \mu, a, \alpha, \text{shape}) \tag{1.44}$$

where a is the speed of sound, and α the angle of attack. Through nondimensionalization the function is reduced to:

$$C_D = f(\alpha, Re, M, \text{shape}^*) \tag{1.45}$$

where $shape^*$ means a nondimensional shape, and M is the Mach number. If we added gravity to the list of inputs then we would another nondimensional parameter, the Froude number. Adding time would yield another nondimensional parameter: the Strouhaul number. But for most aerodynamic flows buoyancy is negligible and only Reynolds number and Mach number are significant.

This equation means that if we have two identical shapes at different scales (e.g., a full scale aircraft, and a small model) if we match the Reynolds number and the Mach number then we can predict the drag of the full scale model by performing tests on the small scale.

Now let us explore this concept a bit more rigorously from the governing equations. As a simple case, we will look at just the x component of the 2D incompressible Navier-Stokes equation

$$u\frac{\partial u}{\partial x} + v\frac{\partial u}{\partial y} = -\frac{1}{\rho}\frac{\partial p}{\partial x} + \frac{\mu}{\rho}\left(\frac{\partial^2 u}{\partial x^2} + \frac{\partial^2 u}{\partial y^2}\right). \tag{1.46}$$

We would like to nondimensionalize this equation. The first term has two velocity terms in the numerator and one length in the denominator. We can multiply the whole equation as follows using V_∞ as a relevant velocity and c as a relevant length scale (e.g., the chord length of an airfoil):

$$\frac{c}{V_\infty^2}\left[u\frac{\partial u}{\partial x} + v\frac{\partial u}{\partial y} = -\frac{1}{\rho}\frac{\partial p}{\partial x} + \frac{\mu}{\rho}\left(\frac{\partial^2 u}{\partial x^2} + \frac{\partial^2 u}{\partial y^2}\right)\right] \tag{1.47}$$

For convenience we define the following nondimensional variables:

$$u^* = \frac{u}{V_\infty}, \quad v^* = \frac{v}{V_\infty}, \quad x^* = \frac{x}{c}, \quad y^* = \frac{y}{c} \tag{1.48}$$

We first focus on the first two terms, which nondimensionalize in a straightforward way:

$$u^*\frac{\partial u^*}{\partial x^*} + v^*\frac{\partial u^*}{\partial y^*} = -\frac{1}{\rho V_\infty^2}\frac{\partial p}{\partial x^*} + \frac{\mu c}{\rho V_\infty^2}\left(\frac{\partial^2 u}{\partial x^2} + \frac{\partial^2 u}{\partial y^2}\right) \tag{1.49}$$

For pressure we could nondimensionalize as follows:

$$p^* = \frac{p}{\rho V_\infty^2} \tag{1.50}$$

Although convention is to use the following (called the *pressure coefficient*):

$$p^* = C_p = \frac{p - p_\infty}{\frac{1}{2}\rho V_\infty^2}, \tag{1.51}$$

because it is only pressure differences that matters in computing loads. For the concept at hand it doesn't matter. Either way, the term p_∞ is

constant and so drops out of the derivative. We'll just use the simpler nondimensionalization for this example.

$$u^*\frac{\partial u^*}{\partial x^*} + v^*\frac{\partial u^*}{\partial y^*} = -\frac{\partial p^*}{\partial x^*} + \frac{\mu c}{\rho V_\infty^2}\left(\frac{\partial^2 u}{\partial x^2} + \frac{\partial^2 u}{\partial y^2}\right) \tag{1.52}$$

For the last term there is one velocity term in the numerator (and we already have a velocity in the denominator we can use to nondimensionalize). There are two length scales in the denominator and so we need to multiply and divide the last equation by c.

$$u^*\frac{\partial u^*}{\partial x^*} + v^*\frac{\partial u^*}{\partial y^*} = -\frac{\partial p^*}{\partial x^*} + \frac{\mu c^2}{\rho V_\infty^2 c}\left(\frac{\partial^2 u}{\partial x^2} + \frac{\partial^2 u}{\partial y^2}\right) \tag{1.53}$$

$$u^*\frac{\partial u^*}{\partial x^*} + v^*\frac{\partial u^*}{\partial y^*} = -\frac{\partial p^*}{\partial x^*} + \frac{\mu}{\rho V_\infty c}\left(\frac{\partial^2 u^*}{\partial x^{*2}} + \frac{\partial^2 u^*}{\partial y^{*2}}\right) \tag{1.54}$$

The equation is now nondimensional. We note that the factor appearing at the beginning of the last term is one over the Reynolds number:

$$u^*\frac{\partial u^*}{\partial x^*} + v^*\frac{\partial u^*}{\partial y^*} = -\frac{\partial p^*}{\partial x^*} + \frac{1}{Re}\left(\frac{\partial^2 u^*}{\partial x^{*2}} + \frac{\partial^2 u^*}{\partial y^{*2}}\right) \tag{1.55}$$

The insight from this equation, is that if we match Reynolds numbers for two similar geometries and boundary conditions then all of the nondimensional fluid properties (velocity, pressure, density, etc.) will be identical in the entire flow field.

If we used the compressible Navier-Stokes equation then another parameter would emerge: the Mach number. If the unsteady term was added then the Strouhaul number would emerge, and if the gravity term was added then the Froude number would emerge.

Example 1.3 Matching Reynolds number

In practice, matching some of these parameters isn't so easy. Consider trying to match the Reynolds number between a full scale aircraft and a 1:20 scale model for use in a wind tunnel. The ratio of kinematic viscosity at 35,000 ft (typical altitude for a transport aircraft) as compared to sea level is about three ($\nu_{alt} = 3\nu_{wt}$). If we equate the Reynolds number at altitude (alt) and the wind tunnel model (wt):

$$\frac{V_{alt} l_{alt}}{\nu_{alt}} = \frac{V_{wt} l_{wt}}{\nu_{wt}} \tag{1.56}$$

Solving for the velocity ratio shows that the velocity in the wind tunnel must be about seven times that of the aircraft's velocity! This is rather problematic. Some possible ways to address this include using a pressurized tunnel, or

a cryogenic tunnel, but both of these solutions are expensive and generally require smaller tunnels which makes the problem harder.

In practice, many wind tunnel experiments don't match Reynolds number. That isn't always as bad as it sounds. For example, consider the drag coefficient around a sphere (Fig. 1.18). Notice how the Reynolds number varies across a wide range in the figure from 1 to 100 million. Most other nondimensional parameters vary along a small range, near 1. Reynolds number is an exception, effectively it varies with log scaling rather than linear scaling. The upshot is that one generally only needs to match Reynolds number within the same order of magnitude. In fact, we can often get away with not even getting close to matching Reynolds number as long as we are in the same flow regime (laminar or turbulent). The exception is near transition from laminar to turbulent flow (the steep drop in the figure). For our aircraft example, the wind tunnel may be at too low of a Reynolds number to naturally have turbulent flow, whereas the full-scale aircraft will be turbulent much earlier. A common approach for wind tunnel testing in these scenarios is to intentionally trip turbulence at the desired location by adding zigzag tape, or a roughness patch. Matching Reynolds number is generally only critical in the boundary layer where viscous effects are large, and so tripping the boundary layer can work reasonably well without actually matching the Reynolds number.

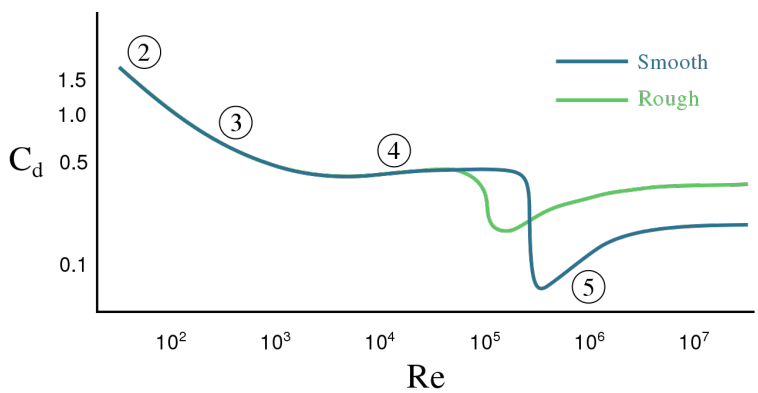

Fig. 1.18 Drag coefficient of a sphere as a function of Reynolds number. Public domain image.

1.7 Governing Equations

Sometimes we call the governing equations in fluid mechanics conservation laws. However, that is a bit of a misnomer. Momentum, for

example, isn't conserved. Newton's second law doesn't say $dp/dt = 0$, but rather equates forces with changes in momentum. Balance laws is perhaps a more apt terminology.

The balance laws in fluid mechanics are analogous to the principles of balancing your bank account, which we can write in a generic way as:

$$\text{accumulation} = \text{inflow - outflow + production} \tag{1.57}$$

For finances, the accumulation is the total in your bank account, inflow is deposits, outflow is withdraws, and production is interest. The same idea works in fluids although we generally reorder, combine inflow/outflow, and speak of rates:

$$\text{rate of accumulation} + \text{rate of net outflow} = \text{rate of production} \tag{1.58}$$

Let's apply this principle to the mass in a control volume. First, mass accumulates in a control volume as the change in time of the total mass integrated over the volume:

$$\frac{\partial}{\partial t}\int_{\forall} \rho d\forall \tag{1.59}$$

The net outflow is an integral over the mass entering or leaving the surface area per unit time:

$$\int_A \rho \vec{V} \cdot d\vec{A} = 0 \tag{1.60}$$

Finally, mass cannot be produced within the control volume. Putting these pieces together yields:

$$\frac{\partial}{\partial t}\int_{\forall} \rho d\forall + \int_A \rho \vec{V} \cdot d\vec{A} = 0 \tag{1.61}$$

This is the integral form of the mass equation.

We can obtain the differential form through a few additional steps. For the first term we move the derivative inside the integral. Differentiation and integration commute (as long as the function and its derivative are continuous) and so we can swap the order. For the second term we apply the divergence theorem (Eq. 1.27):

$$\int_{\forall} \frac{\partial \rho}{\partial t} d\forall + \int_{\forall} \nabla \cdot \left(\rho \vec{V}\right) d\forall = 0 \tag{1.62}$$

Next, we combine the equations into one integral:

$$\int_{\forall} \left(\frac{\partial \rho}{\partial t} + \nabla \cdot \left(\rho \vec{V}\right)\right) d\forall = 0 \tag{1.63}$$

Because this equation must apply for every control volume in the fluid, the integrand must be zero everywhere:

$$\frac{\partial \rho}{\partial t} + \nabla \cdot \left(\rho \vec{V}\right) = 0 \tag{1.64}$$

This is the differential form of the mass equation.

Let's now explore what the implications are for an incompressible flow. First, we need to understand what the total derivative of density looks like. The density in a fluid can vary with position and time:

$$\rho(x, y, z, t) \tag{1.65}$$

Let's take the derivative of this function with respect to time, realizing that the position x, y, z of the fluid particle can also vary with time.

$$\frac{d\rho}{dt} = \frac{\partial \rho}{\partial t} + \frac{\partial \rho}{\partial x}\frac{dx}{dt} + \frac{\partial \rho}{\partial y}\frac{dy}{dt} + \frac{\partial \rho}{\partial y}\frac{dz}{dt} \tag{1.66}$$

Noting that $dx/dt = u$, the x-component of velocity, and similarly for the other components:

$$\frac{d\rho}{dt} = \frac{\partial \rho}{\partial t} + \frac{\partial \rho}{\partial x}u + \frac{\partial \rho}{\partial y}v + \frac{\partial \rho}{\partial y}w \tag{1.67}$$

Finally, we can write this in a generic vector notation (independent of coordinate system choice):

$$\frac{d\rho}{dt} = \frac{\partial \rho}{\partial t} + \nabla \rho \cdot \vec{V} \tag{1.68}$$

In fluid mechanics we often give this total derivative the special name: material derivative or substantial derivative and denote it with a big D (although mathematically a little d has the same meaning, its just a total derivative):

$$\frac{D()}{Dt} = \frac{\partial()}{\partial t} + \nabla() \cdot \vec{V} \tag{1.69}$$

The first term in the substantial derivative tell us how a fluid property changes in time at a fixed point, whereas the second term tells us how a fluid property changes due to fluid motion. This is perhaps most easily visualized with temperature. Imagine a cold region of air and a hot region of air and that the entire volume of air was static (i.e., temperature is not changing in time). In this case the first term would be zero, but a fluid particle moving from the cold to the hot region would experience a change a temperature from the convective (second) term. Now imagine that the entire mass of air (both cold and

hot regions) was heated up. Now the first term would be increasing even without moving. As we track the fluid particle the total change in temperature is due to the convective motion and the temporal change in temperature. The total derivative captures this full change.

With that background we can now understand that an incompressible flow has:

$$\frac{D\rho}{Dt} = \frac{\partial \rho}{\partial t} + \nabla \rho \cdot \vec{V} = 0 \tag{1.70}$$

This means for an incompressible flow it is not necessary that both terms in the substantial derivative are zero, but rather only that their sum is zero. Thus, while all constant density flows are incompressible, not all incompressible flows are constant density. Common examples of the latter are mixtures of two fluids (e.g., salt water with fresh water, or helium mixed with air). The density at a given fixed point changes in time, and if you moved between the two types of water the density also changes. However, the density following a given fluid particle does not change (if incompressible). Another way to state this is that the density is constant in a Lagrangian frame, not an Eulerian one.

Let's now go back to our mass balance equation and apply the definition of incompressibility. Repeating the mass balance equation (Eq. 1.64):

$$\frac{\partial \rho}{\partial t} + \nabla \cdot \left(\rho \vec{V}\right) = 0\,. \tag{1.71}$$

First, we apply the differential operator across the variables in the second term:

$$\frac{\partial \rho}{\partial t} + \nabla \rho \cdot \vec{V} + \rho \nabla \cdot \vec{V} = 0\,. \tag{1.72}$$

We see that the first two terms are the substantial derivative so this equation becomes:

$$\frac{D\rho}{Dt} + \rho \nabla \cdot \vec{V} = 0\,. \tag{1.73}$$

For an incompressible flow the substantial derivative of density is zero, thus the mass balance equation simplifies for an incompressible flow to:

$$\nabla \cdot \vec{V} = 0\,. \tag{1.74}$$

Again, if the density is constant we would arrive at this same conclusion, but we can also arrive at this conclusion for non-constant density flows that are still incompressible. We will use this formula multiple times throughout the book to apply incompressibility assumptions. This definition should make sense from what a divergence represents. This formula tells us that for an incompressible fluid, the volume of a particular quantity of fluid mass cannot expand or contract.

Let's now apply our balance law to momentum. The first, two terms (accumulation and net outflow) are nearly the same as that for mass, but are multiplied by another velocity to produce momentum. In this case we won't worry about moving control volumes. For momentum, there are production terms, which come from forces (via Newton's second law). For aerodynamics these forces arise from pressure and shear stresses.

$$\frac{\partial}{\partial t}\int_{\forall}\rho\vec{V}d\forall + \int_{A}\rho\vec{V}\left(\vec{V}\cdot d\vec{A}\right) = -\int_{A}pd\vec{A} + \int_{A}\overleftrightarrow{\tau}\cdot d\vec{A} \tag{1.75}$$

where $\overleftrightarrow{\tau}$ is the stress tensor.

We can put this equation in differential form using the divergence theorem in the same manner as in the mass balance. This is easiest to do using Einstein notation. The integral equation becomes:

$$\frac{\partial}{\partial t}\int_{\forall}\rho u_i d\forall + \int_{A}\rho u_i u_j dA_j = -\int_{A}pdA_i + \int_{A}\tau_{ij}dA_j \tag{1.76}$$

In index form the divergence theorem (Eq. 1.27) is:

$$\int_{A}u_j dA_j = \int_{\forall}\frac{\partial u_j}{\partial x_j}d\forall \tag{1.77}$$

Applying the divergence theorem to Eq. 1.76 and moving the derivative under the integral results in:

$$\int_{\forall}\frac{\partial(\rho u_i)}{\partial t}d\forall + \int_{\forall}\frac{\partial(\rho u_i u_j)}{\partial x_j}d\forall = -\int_{\forall}\frac{\partial p}{\partial x_i}d\forall + \int_{\forall}\frac{\partial \tau_{ij}}{\partial x_j}d\forall \tag{1.78}$$

Combining the integrals into one integral and noting that the equation must apply for any control volume and so the integrand must be zero, gives the differential form of the momentum equation:

$$\frac{\partial(\rho u_i)}{\partial t} + \frac{\partial(\rho u_i u_j)}{\partial x_j} = -\frac{\partial p}{\partial x_i} + \frac{\partial \tau_{ij}}{\partial x_j} \tag{1.79}$$

Note that since i appears once in each term it represents a vector equation (three equations in x, y and z). The index j appears twice in some terms indicating a summation over $j = 1 \ldots 3$.

We can simplify this equation by expanding the derivatives (focusing on the just the left hand side):

$$\frac{\partial(\rho u_i)}{\partial t} + \frac{\partial(\rho u_i u_j)}{\partial x_j} = \tag{1.80}$$

$$\rho\frac{\partial u_i}{\partial t} + u_i\frac{\partial \rho}{\partial t} + u_i\frac{\partial(\rho u_j)}{\partial x_j} + \rho u_j\frac{\partial(u_i)}{\partial x_j} \tag{1.81}$$

Next, we use the continuity equation (Eq. 1.64) in differential form:

$$\frac{\partial \rho}{\partial t} + \frac{\partial(\rho u_j)}{\partial x_j} = 0 \tag{1.82}$$

The second and third terms in Eq. 1.81 is exactly u_i times the continuity equation and so those two terms sum to zero. The remaining two terms are the definition of the substantial derivative:

$$\rho \frac{\partial u_i}{\partial t} + \rho u_j \frac{\partial(u_i)}{\partial x_j} = \rho \frac{Du_i}{Dt} \tag{1.83}$$

Substituting this new left hand side back into the momentum equations results in the following formula:

$$\boxed{\rho \frac{Du_i}{Dt} = -\frac{\partial p}{\partial x_i} + \frac{\partial \tau_{ij}}{\partial x_j}} \tag{1.84}$$

Or if we really want to be compact we can define the total stress as the combination of pressure and shear stress:

$$\sigma_{ij} = -p\delta_{ij} + \tau_{ij} \tag{1.85}$$

where δ_{ij} is the Kronecker delta:

$$\delta_{ij} = \begin{cases} 1 & \text{if } i = j \\ 0 & \text{if } i \neq j \end{cases} \tag{1.86}$$

Then the momentum equation becomes:

$$\boxed{\rho \frac{Du_i}{Dt} = \frac{\partial \sigma_{ij}}{\partial x_j}} \tag{1.87}$$

1.8 Stress Tensor

The only term that may be unfamiliar in this equation is the stress tensor τ. To formulate the stress tensor we need a relationship between stresses and strains, which is called a *constitutive equation*. Stresses are related to the velocity gradients:

$$\frac{\partial u_i}{\partial x_j} \tag{1.88}$$

We can write the velocity gradient in the equivalent form:

$$\frac{\partial u_i}{\partial x_j} = \frac{1}{2}\left(\frac{\partial u_i}{\partial x_j} + \frac{\partial u_j}{\partial x_i}\right) + \frac{1}{2}\left(\frac{\partial u_i}{\partial x_j} - \frac{\partial u_j}{\partial x_i}\right) \tag{1.89}$$

Notice that the second and fourth terms cancel, and the first and second add back to the original relationship. This seems a rather unnecessary complication, but the usefulness is that the first two terms together form a symmetric tensor, and the last two form an antisymmetric tensor.* A tensor a_{ij} is antisymmetric if $a_{ij} = -a_{ji}$. For convenience we will express these two groupings as:

*Any rank 2 tensor can be decomposed into the sum of a symmetric and an antisymmetric tensor.

$$\frac{\partial u_i}{\partial x_j} = \epsilon_{ij} + \omega_{ij} \tag{1.90}$$

The first term, the symmetric portion, we call the *strain tensor*.†

†Actually it is a rate of strain tensor as these are velocities, not deflections.

$$\epsilon_{ij} = \frac{1}{2}\left(\frac{\partial u_i}{\partial x_j} + \frac{\partial u_j}{\partial x_i}\right) \tag{1.91}$$

The strain tensor describes deformations. The antisymmetric, second term, is the *vorticity tensor* and it describes pure rotation. Like pure translations, pure rotation does not create stresses. Thus, the stress tensor is related only to the strain tensor (the symmetric portion of the velocity gradients).

For a *Newtonian fluid* we assume that the stress-strain relationship is linear. Most fluids are quite accurately classified as linear, including air. However, there are non-Newtonian fluids where the stress-strain relationship is nonlinear and thus the viscosity varies with stress. Common examples are blood, ketchup, honey, and paint.

In a general case the relationship would look like:

$$\tau_{ij} = K_{ijkl}\epsilon_{kl} \tag{1.92}$$

where K is a fourth-order tensor with $3^4 = 81$ constants relating the nine stress components ($\tau_{xx}, \tau_{xy}, \ldots$) to the nine strain components. However, because fluids are isotropic (fluid properties are the same in all directions) tensor theory shows that the most general isotropic fourth order tensor is as follows:

$$K_{ijkl} = \lambda\delta_{ij}\delta_{kl} + \mu\delta_{ik}\delta_{jl} + \nu\delta_{il}\delta_{jk} \tag{1.93}$$

where λ, μ and ν are all constants (down to 3 constants from the original 81).

Because we know that the stress tensor is also symmetric we can exchange the ij components:

$$K_{ijkl} = K_{jikl} = \lambda\delta_{ji}\delta_{kl} + \mu\delta_{jk}\delta_{il} + \nu\delta_{jl}\delta_{ik} \tag{1.94}$$

Comparing with the previous equation we see that the first term is identical, since the Kronecker delta is symmetric $\delta_{ij} = \delta_{ji}$. Comparing

the latter two terms we see that $\mu = \nu$, and so a general isotropic, symmetric, fourth-order tensor is expressed as:

$$K_{ijkl} = \lambda\delta_{ij}\delta_{kl} + \mu\left(\delta_{ik}\delta_{jl} + \delta_{il}\delta_{jk}\right) \tag{1.95}$$

Note that there are only two unique constants, μ and λ, which for a fluid we call the first and second coefficients of viscosity.[‡]

[‡]This is exactly the same situation with isotropic structural materials where the constitutive equation relating stress and strain requires only two constants: the modulus of elasticity E and Poisson's ratio ν.

We now plug this general tensor relationship (Eq. 1.95) into the constitutive equation (Eq. 1.92):

$$\tau_{ij} = \left[\lambda\delta_{ij}\delta_{kl} + \mu\left(\delta_{ik}\delta_{jl} + \delta_{il}\delta_{jk}\right)\right]\epsilon_{kl} \tag{1.96}$$

One of the rules of the Kronecker delta is that it can be contracted as follows (note the sum over i):

$$a_i\delta_{ij} = a_j, \tag{1.97}$$

which can be seen to be true because δ_{ij} is zero unless $i = j$. Thus, the stress tensor simplifies as:

$$\begin{aligned}\tau_{ij} &= \left[\lambda\delta_{ij}\delta_{kl} + \mu\left(\delta_{ik}\delta_{jl} + \delta_{il}\delta_{jk}\right)\right]\epsilon_{kl} \\ &= \lambda\delta_{ij}\delta_{kl}\epsilon_{kl} + \mu\left(\delta_{ik}\delta_{jl}\epsilon_{kl} + \delta_{il}\delta_{jk}\epsilon_{kl}\right) \\ &= \lambda\delta_{ij}\epsilon_{kk} + \mu\left(\epsilon_{ij} + \epsilon_{ji}\right) \\ &= \lambda\delta_{ij}\epsilon_{kk} + 2\mu\epsilon_{ij}\end{aligned} \tag{1.98}$$

where the last line was simplified because the strain tensor is symmetric. Finally, expanding the strain tensor explicitly (Eq. 1.91) gives the expression:

$$\tau_{ij} = \mu\left(\frac{\partial u_i}{\partial x_j} + \frac{\partial u_j}{\partial x_i}\right) + \lambda\left(\frac{\partial u_k}{\partial x_k}\right)\delta_{ij}\,. \tag{1.99}$$

The second coefficient of viscosity λ is a bit problematic because it adds another unknown that we don't have an equation for. Fortunately in many cases the last term in Eq. 1.99 is zero: inviscid flow (viscosity coefficients are zero), incompressible flow (the divergence $\partial u_k/\partial x_k = \nabla\cdot\vec{V} = 0$), or in boundary layers where viscous shear stresses are much larger than viscous normal stresses. However, for viscous compressible flows that term is not zero and we need a model to address it.

To motivate this model, let us consider the hydrostatic and deviatoric components of the stress tensor.[§] The hydrostatic value is just the average of the three diagonal components, and in matrix form is placed along the diagonals. This portion is invariant to rotation, and thus acts like pressure. The deviatoric component is just the original tensor minus the hydrostatic tensor.[¶] In this case the hydrostatic component is:

[§]Any rank 2 tensor can be separated into the sum of a hydrostatic and a deviatoric tensor.

[¶]As another structural analogue, this is exactly the same process whereby von Mises stress is derived (via distortional energy theory). It is the deviatoric compoinent of the stress that is assumed to be related to failure.

$$
\begin{aligned}
h_{ij} &= \frac{1}{3}\text{trace}(\tau)\delta_{ij} \\
&= \frac{1}{3}\tau_{kk}\delta_{ij} \\
&= \frac{1}{3}\left(2\mu\frac{\partial u_k}{\partial x_k} + 3\lambda\frac{\partial u_l}{\partial x_l}\right)\delta_{ij} \\
&= \left(\frac{2}{3}\mu + \lambda\right)\frac{\partial u_k}{\partial x_k}\delta_{ij} \\
&= \kappa\frac{\partial u_k}{\partial x_k}\delta_{ij}
\end{aligned}
\tag{1.100}
$$

In the second line we used $\delta_{kk} = 3$ from the definition of the Kronecker delta, and in the third line we combined the two terms since the summation indices were both arbitrary dummy indices. Finally, the quantity $2/3\mu + \lambda$ is known as the *bulk viscosity*, κ, and was thus simplified for convenience in the last line.

The deviatoric component is then:

$$
\begin{aligned}
d_{ij} &= \tau_{ij} - h_{ij} \\
&= \mu\left(\frac{\partial u_i}{\partial x_j} + \frac{\partial u_j}{\partial x_i}\right) - \frac{2}{3}\mu\left(\frac{\partial u_k}{\partial x_k}\right)\delta_{ij}\,.
\end{aligned}
\tag{1.101}
$$

Stoke's hypothesis is that the bulk viscosity κ is zero. The rationale is that we expect the hydrostatic component of the shear stress to be zero. In other words the effective pressure, often called the mechanical pressure, is exactly the same as the thermodynamic pressure, which assumes that thermodynamic equilibrium occurs rapidly. The shear stress then only produces deviatoric components (only shear and no pure volume dilation/compression).

This hypothesis is widely used, and generally produces good results. Some theoretical arguments and limited experiments (it is difficult to measure the bulk viscosity) suggest that κ is negligible for some gases. However, in other scenarios have shown it to be quite large. More recent arguments suggest that it is not the bulk viscosity that is negligible but rather that the product $\kappa\nabla\cdot\vec{V}$ (seen in Eq. 1.100) is typically negligible compared to the thermodynamic pressure.[1] Both assumptions result in the hydrostatic component vanishing (although the latter argument is more physically defensible).

1. Buresti, *A note on Stokes' hypothesis*, 2015.

Using this hypothesis, the stress tensor retains only the deviatoric component:

$$
\tau_{ij} = \mu\left(\frac{\partial u_i}{\partial x_j} + \frac{\partial u_j}{\partial x_i}\right) - \frac{2}{3}\mu\left(\frac{\partial u_k}{\partial x_k}\right)\delta_{ij}
\tag{1.102}
$$

For an incompressible flow, the stress tensor portion simplifies considerably. First, the second term in the stress tensor vanishes because $\partial u_k/\partial x_k = \nabla \cdot \vec{V} = 0$ for an incompressible flow. Next, we need to take the derivative of the stress tensor since that is how it appears in the Navier-Stokes equations. For an incompressible flow μ is constant (not true for compressible flows where μ is function of temperature) and so we can pull it out of the derivative.

$$\frac{\partial \tau_{ij}}{\partial x_j} = \mu \left(\frac{\partial^2 u_i}{\partial x_j^2} + \frac{\partial^2 u_j}{\partial x_i \partial x_j} \right) \tag{1.103}$$

But since the divergence of the velocity field is zero for an incompressible flow ($\partial u_j/\partial x_j = 0$), the second term vanishes. Plugging this simplification into Eq. 1.84 yields the *incompressible momentum equation*:

$$\rho \frac{D\vec{V}}{Dt} = -\nabla p + \mu \nabla^2 \vec{V} \tag{1.104}$$

For an incompressible flow there are only four unknowns: the three components of velocity and pressure (the density is either constant or known for the incompressible case). There are also four equations: mass and three momentum equations. For compressible flows we have two additional unknowns (e.g., temperature and density) and two additional equations: the energy equation and a thermodynamic equation of state (e.g., ideal gas equation).

1.9 Vorticity Equation

In this section we derive the vorticity equation, an alternative form of the Navier–Stokes equation useful in some contexts. Before doing so we review a few vector calculus identities:

$$\nabla \times (\phi \vec{A}) = \phi(\nabla \times \vec{A}) + \nabla\phi \times \vec{A} \tag{1.105}$$

$$\nabla \times (\nabla \phi) = 0 \tag{1.106}$$

$$\nabla \cdot (\nabla \times \vec{A}) = 0 \tag{1.107}$$

$$\frac{1}{2}\nabla(\vec{A} \cdot \vec{A}) = (\vec{A} \cdot \nabla)\vec{A} + \vec{A} \times (\nabla \times \vec{A}) \tag{1.108}$$

$$\nabla \times (\vec{A} \times \vec{B}) = \vec{A}(\nabla \cdot \vec{B}) - \vec{B}(\nabla \cdot \vec{A}) + (\vec{B} \cdot \nabla)\vec{A} - (\vec{A} \cdot \nabla)\vec{B} \tag{1.109}$$

We can derive the vorticity equation by taking the curl of the Navier-Stokes equation.

$$\nabla \times \left(\frac{\partial \vec{V}}{\partial t} + (\vec{V} \cdot \nabla)\vec{V} \right) = -\frac{1}{\rho}\nabla p + \frac{1}{\rho}\nabla \cdot \tau \tag{1.110}$$

Expanding terms by recalling that vorticity is the curl of velocity (Eq. 1.25), and using some of the above identities (Eqs. 1.105, 1.106, and 1.108) gives:

$$\frac{\partial \vec{\omega}}{\partial t} + \nabla \times \left(\frac{1}{2} \nabla(\vec{V} \cdot \vec{V}) - \vec{V} \times (\nabla \times \vec{V}) \right) = \frac{1}{\rho^2} \nabla \rho \times \nabla p + \nabla \times \left(\frac{1}{\rho} \nabla \cdot \tau \right) \tag{1.111}$$

Let's now focus on the second term:

$$\nabla \times \left(\frac{1}{2} \nabla(\vec{V} \cdot \vec{V}) - \vec{V} \times (\nabla \times \vec{V}) \right) = \nabla \times \left(\nabla \left(\frac{V^2}{2} \right) - \vec{V} \times \omega \right) \tag{1.112}$$

where V is the magnitude of $\vec{V}$. Since V^2 is just a scalar, this first term drops out by Eq. 1.106.

$$\nabla \times \left(\frac{1}{2} \nabla(\vec{V} \cdot \vec{V}) - \vec{V} \times (\nabla \times \vec{V}) \right) = \nabla \times \left(\omega \times \vec{V} \right) \tag{1.113}$$

We now expand the right hand side using Eq. 1.109

$$\nabla \times \left(\frac{1}{2} \nabla(\vec{V} \cdot \vec{V}) - \vec{V} \times (\nabla \times \vec{V}) \right) = \tag{1.114}$$

$$= \vec{\omega}(\nabla \cdot \vec{V}) - \vec{V}(\cancel{\nabla \cdot \vec{\omega}}) + (\vec{V} \cdot \nabla)\vec{\omega} - (\vec{\omega} \cdot \nabla)\vec{V} \tag{1.115}$$

where the second term dropped out by Eq. 1.106 We now put these terms back into the original equation to yield the vorticity equation.

$$\begin{aligned} \underbrace{\frac{\partial \vec{\omega}}{\partial t} + (\vec{V} \cdot \nabla)\vec{\omega}}_{D\vec{\omega}/Dt} = \underbrace{(\vec{\omega} \cdot \nabla)\vec{V}}_{\substack{\text{vortex stretching} \\ \text{and tilting}}} - \underbrace{\vec{\omega}(\nabla \cdot \vec{V})}_{\substack{\text{vortex stretching} \\ \text{due to} \\ \text{compressibility}}} \\ + \underbrace{\frac{1}{\rho^2} \nabla \rho \times \nabla p}_{\text{baroclinic term}} + \underbrace{\nabla \times \left(\frac{1}{\rho} \nabla \cdot \tau \right)}_{\substack{\text{vorticity diffusion} \\ \text{due to viscosity}}} \end{aligned} \tag{1.116}$$

The baroclinic term is zero if density is constant, if the fluid is incompressible and homogenous, or if density is only a function of pressure, which is called a *barotropic* fluid and includes many liquids. For these cases, the vorticity equation simplifies to:

$$\frac{D\vec{\omega}}{Dt} = (\vec{\omega} \cdot \nabla)\vec{V} + \nu \nabla^2 \vec{\omega} \tag{1.117}$$

The first term on the right hand side is nonzero when the vorticity is stretched or tilted. The last term, is the vorticity diffusion due to

viscosity. It is perhaps more easily understood by comparing to the heat diffusivity equation:

$$\frac{dT}{dt} = k\nabla^2 T \tag{1.118}$$

where T is temperature and k is the heat diffusivity. These equation describes how temperature spreads based on the heat diffusivity. This term in the vorticity equation has the same form, describing how vorticity spreads based on the viscosity.

1.10 Rotating Reference Frame

Fluid moving in a rotating reference frame introduces additional apparent forces. Imagine an inertial frame defined by the Cartesian coordinates $\hat{\imath}, \hat{\jmath}, \hat{k}$, and a second rotating frame, rotating at some speed Ω relative to the inertial frame, defined by the Cartesian coordinates $\hat{x}, \hat{y}, \hat{z}$ (Fig. 1.19). We use the subscript I to refer to quantities measured relative to the inertial frame, and subscript R for quantities measured relative to the rotating frame. Then, from the perspective of the inertial frame, $\hat{\imath}$ is fixed. Mathematically this is expressed as:

$$\left(\frac{d\hat{\imath}}{dt}\right)_I = 0 \tag{1.119}$$

Similarly, from the perspective of the rotating frame, $\hat{x}$ is fixed.

$$\left(\frac{d\hat{x}}{dt}\right)_R = 0 \tag{1.120}$$

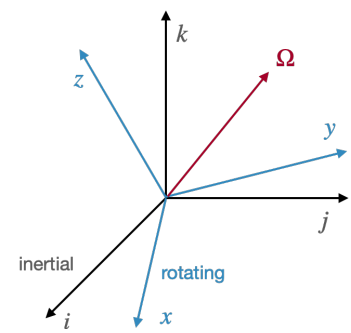

Fig. 1.19 An inertial frame and a rotating reference frame.

However, from the perspective of the inertial frame $\hat{x}$ is not fixed, it is rotating, and so its time derivative is not zero. We can show that this derivative is given by:*

$$\left(\frac{d\hat{x}}{dt}\right)_I = \vec{\Omega} \times \hat{x} \tag{1.121}$$

*This is shown in any dynamics textbook. It is straightforward to derive from drawing out the geometry.

With that result, let us consider a position vector $\vec{r} = x\hat{x} + y\hat{y} + z\hat{z}$, which indicates the position of some fluid particle. We have chosen to represent the vector in the basis of the rotating coordinate frame, but it is the same vector for both frames (we are assuming the origins are coincident for this case). If we take derivatives in our rotating frame then we have:

$$\left(\frac{d\vec{r}}{dt}\right)_R = \dot{x}\hat{x} + \dot{y}\hat{y} + \dot{z}\hat{z} \tag{1.122}$$

where the dot superscript indicates a time derivative (note that the unit vectors are fixed in this frame so the result is straightforward).

These derivatives $(\dot{x}, \dot{y}, \dot{z})$ are unambiguous quantities because they are scalars and so are the same in any reference frame.

Let's now repeat the same derivative, but take derivatives in the inertial reference frame. Because the unit vectors $\hat{x}, \hat{y}, \hat{z}$ are not fixed in this reference frame, we have additional terms from the chain rule.

$$\begin{aligned}\left(\frac{d\vec{r}}{dt}\right)_I &= \dot{x}\hat{x} + x\left(\frac{d\hat{x}}{dt}\right)_I + \dot{y}\hat{y} + y\left(\frac{d\hat{y}}{dt}\right)_I + \dot{z}\hat{z} + z\left(\frac{d\hat{z}}{dt}\right)_I \\ &= \dot{x}\hat{x} + x(\vec{\Omega}\times\hat{x}) + \dot{y}\hat{y} + y(\vec{\Omega}\times\hat{y}) + \dot{z}\hat{z} + z(\vec{\Omega}\times\hat{z}) \\ &= \left(\frac{d\vec{r}}{dt}\right)_R + \vec{\Omega}\times\vec{r}\end{aligned} \tag{1.123}$$

Since the time derivative of position is velocity $\vec{v}$, we can write this more succinctly as:

$$\vec{v}_I = \vec{v}_R + \vec{\Omega}\times\vec{r} \tag{1.124}$$

Thus, we the velocity we measure in the relative frame needs to modified with an addition term to represent an inertial velocity.

We now repeat the process once more to determine accelerations. Note that Eq. 1.123 provides a general rule for any vector:

$$\left(\frac{d\square}{dt}\right)_I = \left(\frac{d\square}{dt}\right)_R + \vec{\Omega}\times\square \tag{1.125}$$

where $\square$ is any vector. We now take derivatives of Eq. 1.123:

$$\left(\frac{d^2\vec{r}}{dt^2}\right)_I = \frac{d}{dt}_I\left(\frac{d\vec{r}}{dt}\right)_R + \frac{d\vec{\Omega}}{dt}_I\times\vec{r} + \vec{\Omega}\times\left(\frac{d\vec{r}}{dt}\right)_I \tag{1.126}$$

We expand the first term using Eq. 1.125

$$\vec{a}_I = \left(\frac{d^2\vec{r}}{dt^2}\right)_R + \vec{\Omega}\times\left(\frac{d\vec{r}}{dt}\right)_R + \frac{d\vec{\Omega}}{dt}_I\times\vec{r} + \vec{\Omega}\times\left(\frac{d\vec{r}}{dt}\right)_I \tag{1.127}$$

We recognize the first term as $\vec{a}_R$, the acceleration as measured in the relative frame. For the third term $\vec{\Omega}$ is already defined in the inertial frame so the derivative is straightforward.

$$\vec{a}_I = \vec{a}_R + \vec{\Omega}\times\left(\frac{d\vec{r}}{dt}\right)_R + \dot{\vec{\Omega}}\times\vec{r} + \vec{\Omega}\times\left(\frac{d\vec{r}}{dt}\right)_I \tag{1.128}$$

We now expand the last term using Eq. 1.123:

$$\vec{a}_I = \vec{a}_R + \vec{\Omega}\times\left(\frac{d\vec{r}}{dt}\right)_R + \dot{\vec{\Omega}}\times\vec{r} + \vec{\Omega}\times\left(\frac{d\vec{r}}{dt}\right)_R + \vec{\Omega}\times(\vec{\Omega}\times\vec{r}) \tag{1.129}$$

The second and fourth term are identical and so can be summed. If the rotation occurs at a constant rate, then the third term is zero. This leaves us with:

$$\vec{a}_I = \vec{a}_R + 2\vec{\Omega} \times \vec{v}_R + \vec{\Omega} \times (\vec{\Omega} \times \vec{r}) \tag{1.130}$$

We now see that, because of rotation, the acceleration as seen in the inertial frame differs from that of that in the rotating frame with two new terms (the dropped term should be reinserted if the rotation rate is not constant). The second term is called the Coriolis acceleration, and the third term is the centripetal acceleration.

We can insert these accelerations as apparent forces (per unit mass) in the momentum equation (Eq. 1.84), with a negative sign since force appears on the opposite of acceleration in the momentum equation. The result is:

$$\boxed{\frac{D\vec{V}}{Dt} = -\frac{1}{\rho}\nabla p + \frac{1}{\rho}\nabla\cdot\overleftrightarrow{\tau} - \underbrace{2\vec{\Omega} \times \vec{V}}_{\text{Coriolis}} - \underbrace{\vec{\Omega} \times (\vec{\Omega} \times \vec{r})}_{\text{centripetal}}} \tag{1.131}$$

Even though all fluid motion on the Earth is in a rotating frame, these last two terms are generally negligible. One notable exception is some large-scale atmospheric flows. There are also scenarios, within a boundary layer, where the flow speeds are slow enough that even though these extra forces are small their impact is important. One such case is discussed in Section 6.3.1.

1.11 Far Field Forces

In Section 1.7 we developed both integral and differential forms of the governing equations. In this section we are going to apply the integral form to yield some key insights. As discussed, if we want to determine the forces and moments on a body, we need to find the pressure and shear stress all along the body and integrate. In this section, we will see that there is an alternative approach. Through a control volume analysis we can determine the forces on a body by integrating in the far-field. This is a useful result that is the basis of some wind tunnel measurement techniques, and is directly used in several theorems related to the lift and drag of bodies as we will see. Generally, we can shortcut some of the steps shown in this analysis, but we will be fully rigorous this first time.

Consider, a body with a control volume as shown in Fig. 1.20. The outer surface is far away from the body. The figure is not two control

volumes (one around the body and one in the far field), but rather one control volume, which we have created by making a small cut to allow a continuous shape that wraps around the body from the far field control volume. In other words, as defined, the control volume contains only fluid (not the body).

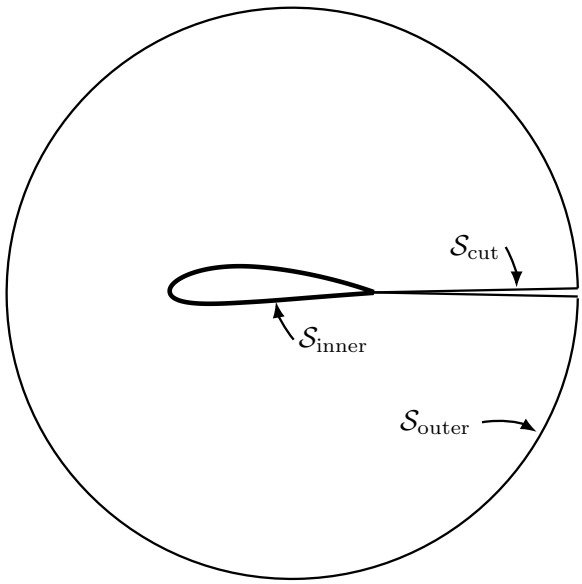

Fig. 1.20 A control volume with a branch cut so that the volume contains only fluid on the interior.

We now apply the integral form of the momentum equation to this control volume. The standard equation is shown below, but in this case we will assume the flow is steady so the time dependent term drops off.

$$\cancel{\frac{\partial}{\partial t}\int_{\forall} \rho\vec{V}d\forall} + \int_A \rho\vec{V}\left(\vec{V}\cdot d\vec{A}\right) = -\int_A p d\vec{A} + \int_A \overleftrightarrow{\tau}\cdot d\vec{A} \tag{1.132}$$

All of the remaining integrals are only surface integrals so we combine them into one integral and we redefine $d\vec{A}$ as $\hat{n}dA$ for convenience. By convention the surface normal always points "out" of the control volume:

$$\int_A \left(\rho\vec{V}\left(\vec{V}\cdot\hat{n}\right) + p\hat{n} - \overleftrightarrow{\tau}\,\hat{n}\right) dA = 0 \tag{1.133}$$

Next, we divide the surface integration into three parts: integration along the inner surface, integration along the outer surface, and integration along the cut surface. The integration along the cut surface will go to zero. The reason is that the velocity and pressure must vary continuously and so we be identical on either side of the cut. However, the unit normal $\hat{n}$ will change sign from one side of the cut to the other

and so the sum of those integrals will cancel:

$$\int_{S_{\text{inner}}} (\ )dA + \int_{S_{\text{outer}}} (\ )dA + \cancel{\int_{S_{\text{cut}}} (\ )dA} = 0 \tag{1.134}$$

Let's look at the remaining terms. For the inner surface $\hat{V} \cdot \hat{n}$ must be zero since fluid cannot pass through the body (and the control volume is right against the body). This is called the *no flow through* condition, which is true for a solid body whether the flow is viscous or inviscid (no slip occurs only for viscous flows).

$$\int_{S_{\text{inner}}} \left(\cancel{\rho \vec{V} \left(\vec{V} \cdot \hat{n} \right)} + p\hat{n} - \overleftrightarrow{\tau}\ \hat{n} \right) dA \tag{1.135}$$

What remains is the the definition for the body force (i.e., the integral of pressure and shear stress over the body is the force that acts on the body):

$$\int_{S_{\text{inner}}} \left(p\hat{n} - \overleftrightarrow{\tau}\ \hat{n} \right) dA = \vec{F}_b \tag{1.136}$$

This integral represents the force on the fluid, but usually we care about the force of the fluid on the body. Thus, we would need a negative sign. However, because of the way we have defined our control volume, "out" for the control volume points into the body. This is opposite of our convention for positive pressures. Thus, we need another negative sign and so the two signs cancel out.

For the outer surface we are far enough away from the body that any shear stresses would be negligible.

$$\int_{S_{\text{outer}}} \left(\rho \vec{V} \left(\vec{V} \cdot \hat{n} \right) + p\hat{n} - \cancel{\overleftrightarrow{\tau}\ \hat{n}} \right) dA \tag{1.137}$$

If we put this all together we are left with:

$$\boxed{\vec{F}_b = -\int_{S_{\text{outer}}} \left(\rho \vec{V} \left(\vec{V} \cdot \hat{n} \right) + p\hat{n} \right) dA} \tag{1.138}$$

This is a significant result! It means that we can determine the forces on the body just by measuring velocities and pressures in a domain surrounding the body. Furthermore, if the outer boundary is unconfined (e.g., not in a wind tunnel) then the pressure term also goes to zero and we only need the velocity term.

Now that we've done it rigorously we note that you will get the exact same result if just use one outer control volume with no cut. In this case, the body force is an internal force acting in the control volume that we need to include with the other forces (pressure and shear stress).

We will also need to include a negative sign because the equation uses the force of the body on the fluid and F_b is the force of the fluid on the body. This approach is easier, and one will shortcut to from now on. However, it is worth rigorously justifying that we can include a body in a control volume when all the governing equations are for the fluid only.

Potential Flow

2

Potential flow is an extremely useful theory for low-speed aerodynamics, and forms the basis of panel methods widely used in many conceptual design studies.

2.1 Irrotational Flow

To begin, we will need a few more definitions. The equation below defines *circulation*:

$$\Gamma = \oint \vec{V} \cdot d\vec{l} = \int_S \left(\nabla \times \vec{V}\right) \cdot d\vec{A} \tag{2.1}$$

The integral on the left is a contour integral, and the one on the right is a transformed version using Stoke's theorem (Eq. 1.26). Referring to Fig. 2.1, the circulation in contour A is zero, whereas the circulation in contour B is proportional to the lift generated by the airfoil. Circulation is a concept that, roughly speaking, measures the rotation of the flow. This is also suggested by the second form of the integral that shows that circulation is related to the curl of the velocity field (which is proportional to rotation).

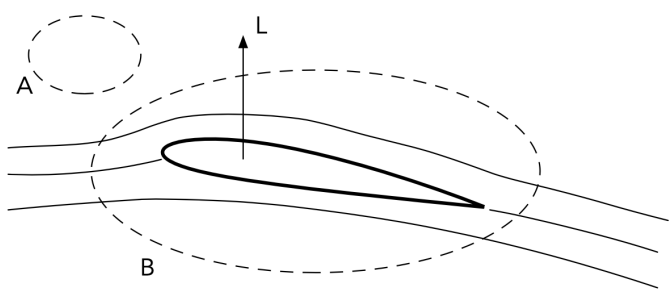

Fig. 2.1 Circulation is defined from a contour integral.

Recall the definition for vorticity:

$$\vec{\omega} = \nabla \times \vec{V} \tag{2.2}$$

We call a flow field *irrotational* if:

$$\nabla \times \vec{V} = 0 \tag{2.3}$$

It is convenient to identify flow situations that can be approximated as irrotational. One reason is that if the above equation is true we can always represent the velocity field as a scalar potential function ϕ:

$$\vec{V} = \nabla\phi \tag{2.4}$$

That is because the curl of any gradient is always zero (a vector identity):

$$\nabla \times \nabla\phi = 0 \tag{2.5}$$

One significance of this form is that ϕ is a scalar and so it simplifies our representation from a three-dimensional velocity field to a one-dimensional scalar function.

A flow field is irrotational if the upstream flow is irrotational and the flow field is inviscid (shear stresses introduce rotation/vorticity). An irrotational flow field can only have conservative forces, like gravity, and not nonconservative ones like those arising from viscosity. In other words, an irrotational flow field is inviscid. However, the opposite is not necessarily true. One can have an inviscid flow field that is rotational.

Perhaps the most useful reason for identifying an irrotational flow occurs if the flow is both irrotational *and* incompressible. Recall that for an incompressible flow continuity requires that:

$$\nabla \cdot \vec{V} = 0 \tag{2.6}$$

If we now substitutue in the vector potential for irrotational flow (Eq. 2.4) we have:

$$\nabla \cdot \nabla\phi = 0 \tag{2.7}$$

or

$$\boxed{\nabla^2\phi = 0} \tag{2.8}$$

This is Laplace's equation. In Cartesian coordinates this equations is expressed as:

$$\frac{\partial^2\phi}{\partial x^2} + \frac{\partial^2\phi}{\partial y^2} + \frac{\partial^2\phi}{\partial z^2} = 0 \tag{2.9}$$

It is a very useful equation that shows up in multiple applications. We could solve Laplace's equation on a grid in a similar (but much simpler) manner to what is done with computational fluid dynamics (discussed in Chapter 7). However, that isn't necessary. The reason why it is so useful is that it is a *linear* PDE. That means that if we have two vector fields that satisfy Laplace's equation, then their sum also satisfies Laplace's equation (the principle of *superposition*). There

are many known solutions to Laplace's equation that are relevant to flow fields. This means that we can build up complex flow fields from simple vector fields that are known solutions to the governing equations. In this manner we can, for example, analyze the flow over a complicated aircraft shape, using a superposition of known vector field solutions by adjusting their strengths appropriately to satisfy the boundary conditions. This is the basis of panel methods that are widely used in applied aerodynamics.

Note that the above derivation only needed to assume that the flow was incompressible and irrotational. It applies in 2D and 3D and for both steady and unsteady flows.

2.2 Potential Flow

The governing equation for potential flow is Laplace's equation.

$$\nabla^2 \phi = 0 \tag{2.10}$$

Recall that the two main assumptions to this equation were incompressible and irrotational flow. For aerodynamics an incompressible flow occurs for low Mach numbers, approximately less than $M = 0.3$. Viscosity always introduces rotation (except in some contrived cases), whereas an inviscid flow does not. Thus, we need an inviscid flow in order for it to be irrotational. That is a necessary but not sufficient condition. However, if the flow starts irrotational, *and* the fluid is inviscid, then it will remain irrotational. For many aerodynamic cases we have a constant freestream (which is irrotational) and so outside of the boundary layer the flow field will be irrotational. So while the assumptions of incompressible and irrotational flow seem rather restrictive, there are still a useful approximation for many aerodynamic applications: namely low-speed flows outside of the boundary layer. As we will learn later, we can actual extend the methods into flow fields that are moderately compressibile, meaning the methods are useful even up to low transonic Mach numbers.

2.2.1 Stream Function

There is an alternative way to come to the same governing equations using stream functions. By construction, a streamline automatically satisfies continuity for an incompressible flow. The incompressible continuity equation (Eq. 1.74) in 2D is:

$$\frac{\partial u}{\partial x} + \frac{\partial v}{\partial y} = 0 \tag{2.11}$$

If we define:

$$u = \frac{\partial \psi}{\partial y} \tag{2.12}$$

$$v = -\frac{\partial \psi}{\partial x} \tag{2.13}$$

for some stream function ψ then we automatically satisfy the above equation since the mixed partials must be equal. A stream function has its name because lines of constant ψ (contour lines) are streamlines.

If we then add the restriction of irrotationality (Eq. 2.3)

$$\frac{\partial v}{\partial x} - \frac{\partial u}{\partial y} = 0 \Rightarrow \frac{\partial^2 \psi}{\partial x^2} + \frac{\partial^2 \psi}{\partial y^2} = 0\,, \tag{2.14}$$

then we obtain Laplace's equation.

In other words, the potential formulation automatically satisfies irrotationality ($\vec{V} = \nabla\phi$) and we impose continuity to get Laplace's equation. The stream function does the opposite. It automatically satisfies continuity and we impose irrotationality to get Laplace's equation. The downside of the stream function approach is that, as outlined, it only works in 2D. Describing three-dimensional flows requires two stream functions. The potential form automatically works in 3D, and is simpler with just one function so is widely used.

The main usefulness of introducing the stream function is to note that both the potential and stream functions satisfy the Cauchy Riemann equations (used frequently in complex analysis):

$$\frac{\partial \phi}{\partial x} = \frac{\partial \psi}{\partial y} \tag{2.15}$$

$$\frac{\partial \phi}{\partial y} = -\frac{\partial \psi}{\partial x} \tag{2.16}$$

This means that potential lines and streamlines are orthogonal (see Fig. 2.2):

$$\nabla\phi \cdot \nabla\psi = \frac{\partial \phi}{\partial x}\frac{\partial \psi}{\partial x} + \frac{\partial \phi}{\partial y}\frac{\partial \psi}{\partial y} \tag{2.17}$$

$$= \frac{\partial \phi}{\partial x}\left(-\frac{\partial \phi}{\partial y}\right) + \frac{\partial \phi}{\partial y}\frac{\partial \phi}{\partial x} \tag{2.18}$$

$$= 0 \tag{2.19}$$

This concept helps us to attribute physical significance to potential lines.

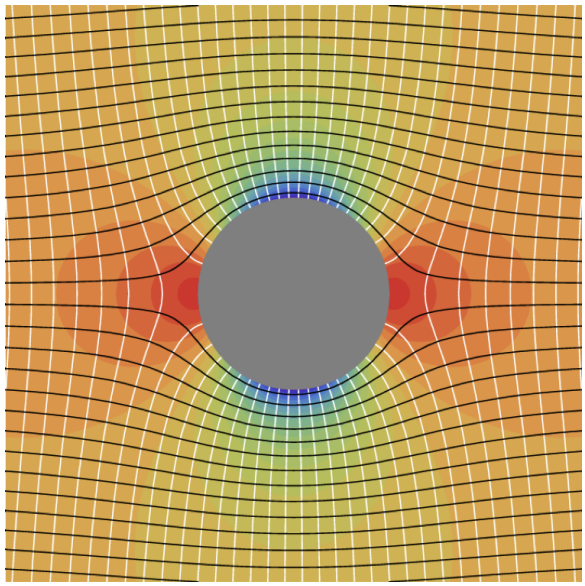

Fig. 2.2 Streamlines in black and potential lines in white are always orthogonal in 2D. By Incredio, CC BY-SA 3.0, Wikimedia Commons.

2.2.2 Elementary Solutions to Laplace's Equation

There are various known elementary solutions to Laplace's equation. As discussed in the previous section, these elementary solutions are particularly useful because the governing equation is linear. Thus, we will use distributions of elementary solutions, and solve for their strengths to satisfy requisite boundary conditions. There are four main elementary solutions that are used. The first is uniform flow (Fig. 2.3), which has the following potential function, stream function, and velocity components.

$$\phi = V\cos(\alpha x) + V\sin(\alpha y) \tag{2.20}$$

$$\psi = -V\sin(\alpha x) + V\cos(\alpha y) \tag{2.21}$$

$$V_x = V\cos(\alpha) \tag{2.22}$$

$$V_y = V\sin(\alpha) \tag{2.23}$$

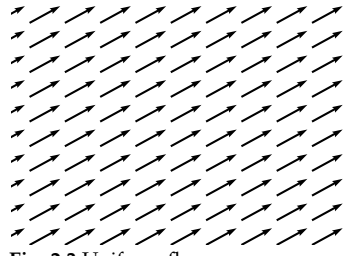

Fig. 2.3 Uniform flow.

The next solution is called a *source*, or if its strength is negative, it is called a *sink*. In a source/sink all the flow is radial (Fig. 2.4). In terms

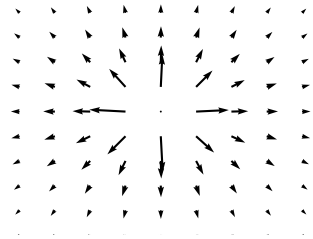

Fig. 2.4 Source/sink.

of potential/stream functions and velocity components it is defined as:

$$\phi = \frac{\Lambda}{2\pi}\ln(r) \tag{2.24}$$

$$\psi = \frac{\Lambda}{2\pi}\theta \tag{2.25}$$

$$V_r = \frac{\Lambda}{2\pi r} \tag{2.26}$$

$$V_\theta = 0 \tag{2.27}$$

The next solution is called a *vortex*, and it produces only tangential flow (Fig. 2.5). Its mathematical description is:

$$\phi = -\frac{\Gamma}{2\pi}\theta \tag{2.28}$$

$$\psi = \frac{\Gamma}{2\pi}\ln(r) \tag{2.29}$$

$$V_r = 0 \tag{2.30}$$

$$V_\theta = -\frac{\Gamma}{2\pi r} \tag{2.31}$$

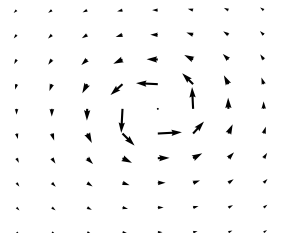

Fig. 2.5 A point vortex (with negative circulation).

Those are all the first-order singularities. A commonly-used second order singularity is a doublet, which could be thought of as a source and a sink brought infinitely close together (Fig. 2.6). Its mathematical description is:

$$\phi = \frac{\kappa\cos(\theta)}{2\pi r} \tag{2.32}$$

$$\psi = -\frac{\kappa\sin(\theta)}{2\pi r} \tag{2.33}$$

$$V_r = -\frac{\kappa\cos(\theta)}{2\pi r^2} \tag{2.34}$$

$$V_\theta = -\frac{\kappa\sin(\theta)}{2\pi r^2} \tag{2.35}$$

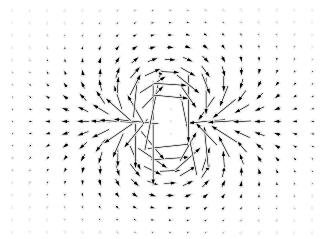

Fig. 2.6 A doublet.

Note that Λ, Γ, and κ refer to the strength of the source/sink, vortex, and doublet respectively.

As a simple example of superposition, combining uniform flow and a source yields a shape called the Rankine oval (Fig. 2.7).* By combining these two singularities there exists a stagnation streamline. If we replaced the stagnation streamline with a solid body, the outer flow represents the flow around a body with the shape of a Rankine oval (for incompressible/inviscid flow.† The inner flow is not meaningful. Through an an appropriate choice of singularities and their strengths, we can potentially represent the flow around any arbitrary body as will be discussed later in this chapter.

*If we add a sink downstream then a closed oval is created.

†Another common example is uniform flow plus a doublet, which creates flow around a cylinder. This is a good exercise to implement on your own in a numerical simulation. Adjust the strength of the doublet and observe the behavior.

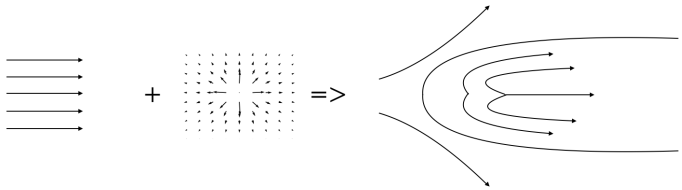

Fig. 2.7 A Rankine oval form by the superposition of uniform flow and source.

A simple way these solutions are used to represent solid surfaces, is to simulate flow near the ground, or to simulate *ground effect*. For example, a lifting body will a pair of counter-rotating vortices as shown on the top of Fig. 2.8.‡. In order to represent the fluid behavior of a wing near the ground, we produce *mirror vortices*, which are vortices on the other side of the ground, the same distance away, with circulation in the opposite direction (e.g., like a mirror). This is a useful trick as the combination of induced velocities creates a no-flow-through condition at the ground. In other words, in the same way we can use these singularities to represent flow around a body, we can use them to simulate flow near the ground. This simple model can help us understand what happens to a lifting body near the ground. Notice that the mirror vortices induce an upwash on the body. This is a real effect, that aircraft flying near the ground can reduce the amount of lift they need to produce and thus reduce their drag. Birds sometimes take advantage of this effect. This idea is sometimes used where a complex body can be simulated near ground by mirroring all of the singularities across the ground plane. However, the computational cost can be fairly high as it doubles the number of singularities and this is an n-body problem (the number of interactions between the singularities scales as n^2).

‡The behavior of wake vortices is reviewed in more detail in Chapter 4

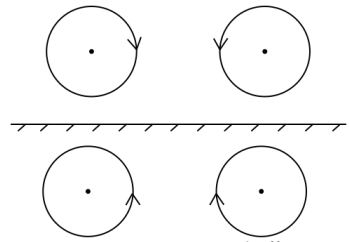

Fig. 2.8 A wing in ground effect simulated by a set of mirror vortices.

2.3 D'Alembert's Paradox and the Kutta-Joukowski Theorem

It turns out the in potential flow, the drag around any shape is always zero. This is a somewhat puzzling outcome that is called *D'Alembert's Paradox*.* Even for cases when the predicted flow field is not symmetric (like an oval or airfoil at an angle of attack), the integration of the pressures to compute drag always sums to zero. The problem is that for geometries with rapid changes, like around the back end of an airfoil at an angle of attack, unrealistic flow fields are predicted (Fig. 2.9). This is because without viscosity, infinite pressure gradients can be supported, and thus rapid changes in direction will occur. However, this mathematical solution is unstable. Even a tiny amount of viscosity will make such rapid changes impossible leading to flow separation.† The potential flow solutions actually admit an infinite number of solutions.

*Historically this led to some difficulty between mathematicians and engineers.

†A topic discussed in more detail in Chapter 3.

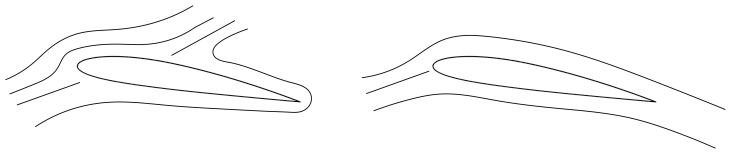

Fig. 2.9 Illustration of flow around airfoil predicted by potential flow (left), and the actual flow field (right).

In order for potential flow to produce useful solutions we will need to add an addition condition, to force a physically meaningful solution, a criteria that will be expanded upon later (Section 2.5.6).

The Kutta-Joukowsi theorem relates circulation to the force generated, which by definition is lift (perpendicular). As a corollary this equation predicts that the drag is zero for 2D incompressible, inviscid flow (D'Alembert's paradox).

$$\vec{L} = \rho_\infty \vec{V} \times \vec{\Gamma} \tag{2.36}$$

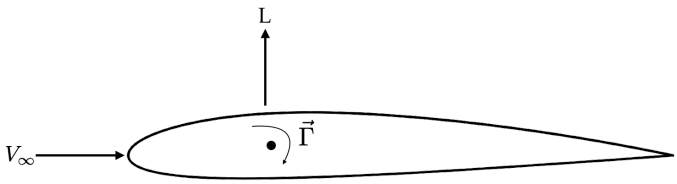

Fig. 2.10 The Kutta Joukowski theorem defines the direction of the lift force based on the incoming velocity and the circulation.

2.4 Pressure Coefficient for Incompressible Flow

The Bernoulli equation can be derived either from the momentum equation or the conservation of mechanical energy equation.

$$p + \frac{1}{2}\rho V^2 = \text{constant} \tag{2.37}$$

It is a redundant equation as we already have four equations and four unknowns, but is often convenient. The large number of assumptions/limitations required to use the equation should be kept in mind: applies only along a streamline, flow must be steady, inviscid, and incompressible, and there cannot be any work or heat transfer along the streamline.

The main reason to bring it up at this point, is that for an irrotational flow Bernoulli's equation applies not just along a streamline, but can apply between any two points in the flow (assuming no work or heat transfer). Equating between any two arbitrary points greatly extends the utility of the equation.

The pressure coefficient was introduced earlier, but is defined as:

$$C_p = \frac{p - p_\infty}{\frac{1}{2}\rho V_\infty^2} \tag{2.38}$$

For an incompressible, irrotational flow we can simplify by using Bernoulli's equation:

$$p_\infty + \frac{1}{2}\rho V_\infty^2 = p + \frac{1}{2}\rho V^2 \tag{2.39}$$

$$p - p_\infty = \frac{1}{2}\rho V_\infty^2 - \frac{1}{2}\rho V^2 \tag{2.40}$$

Substituting into the pressure coefficient definition results in:

$$C_p = 1 - \left(\frac{V}{V_\infty}\right)^2 \tag{2.41}$$

Thus, at a stagnation point (for an incompresible, irrotational flow) $C_p = 1$.

2.5 Thin Airfoil Theory

In an introductory aerodynamics text you may have learned that you can combine various point singularities to form interesting flows. For example, freestream + source + sink can be used to create a Rankine oval, whereas freestream + doublet can be used to create a cylinder and freestream + doublet + vortex can create a lifting cylinder. While interesting, we would like to be able to predict flow fields around arbitrary geometries. Thus, we are interested in the inverse problem: given a geometry what should be the strengths and positions of the singularities in order to create a flow field around the geometry? Thin airfoil theory is the first method we will explore with this goal in mind. Thin airfoil theory requires some simplifying assumptions but in return allows for some analytic solutions. With modern computing capabilities, thin airfoil theory has been replaced by more general approaches like panel methods, which we'll discuss afterwords. But, the insights that analytic solutions provide are still useful.

2.5.1 Airfoil

For convenience we will align our airfoil along the x axis, and separate the upper and lower surfaces on either side of this chord line (Fig. 2.11). The thickness distribution is then given by:

$$t(x) = y_u(x) - y_l(x) \tag{2.42}$$

and the camber distribution is:

$$\bar{y}(x) = \frac{1}{2}\left(y_u(x) + y_l(x)\right) \tag{2.43}$$

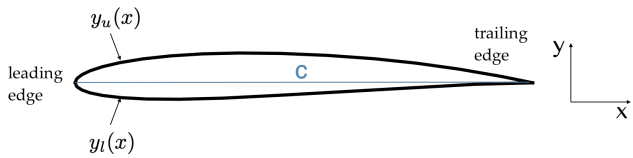

Fig. 2.11 Definitions of upper and lower surfaces, leading and trailing edges, and the chord length c.

When we refer to thickness or camber we generally mean the maximum thickness or camber (normalized by chord):

$$\text{thickness: } \frac{t}{c} = \tau = \frac{\max\left[t(x)\right]}{c} \tag{2.44}$$

$$\text{camber: } \frac{\max\left[\bar{y}(x)\right]}{c} \tag{2.45}$$

2.5.2 Line Distributions

Recall that one of the key ideas of potential flow is that we can use superposition because the governing equation is linear. We will divide the total potential function into three parts: a component for the freestream, a component for airfoil thickness, and a component for airfoil camber.

$$\phi = \phi_\infty + \phi_t + \phi_c \tag{2.46}$$

Representing the freestream component is straightforward as a known elementary solution to potential flow:

$$\phi_\infty = V_\infty \cos(\alpha x) + V_\infty \sin(\alpha y) \tag{2.47}$$

Next, we wish to model a thick airfoil (with no camber). Motivated by some of the basic solutions (e.g., Rankine oval), sources seem like a natural fit to model the thickness distribution of an airfoil. However, we would like to model any airfoil shape and so rather than use a few discrete sources we will use an infinite number of infinitely weak sources. This is the same concept as used in statics, where, as an alternative to discrete forces you use distributed loads that represent the force per unit length. In this case we will use a source line distribution along the airfoil chord line where $q(s)$ represents the source strength per unit length (Fig. 2.12).

Fig. 2.12 Source line distribution along the chord line.

Before considering the distribution of sources, let's first consider a point source (Fig. 2.13). From introductory aerodynamics recall that a

point source creates only radial velocity and has the following potential function:

$$\phi = \frac{\Lambda}{2\pi}\ln(r) \tag{2.48}$$

$$V_r = \frac{\Lambda}{2\pi r} \tag{2.49}$$

where Λ is the strength of the source and r is the radial distance from the center of the source. Since our airfoil is defined in a cartesian coordinate system we will decompose the radial velocity into x and y components:

$$u = \frac{\Lambda\cos\theta}{2\pi r} \tag{2.50}$$

$$v = \frac{\Lambda\sin\theta}{2\pi r} \tag{2.51}$$

Now for the line distribution the strength for some infinitesimal length ds is $d\Lambda = q ds$. We can express the potential function as an integral along this distribution.

$$\phi = \frac{1}{2\pi}\int_0^c q(s)\ln r ds \tag{2.52}$$

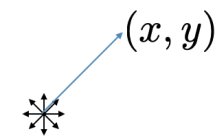

Fig. 2.13 A point source.

For the velocities, we would like to convert to cartesian coordinates. The vector r is the vector from the infinitesimal source to the evaluation point. While the evaluation point is fixed, the local source location s changes as we integrate across the line (see Fig. 2.14). The velocity at some point x, y from the contributions of the total line distribution is (using $\cos\theta = (x-s)/r$ and $\sin\theta = y/r$):

$$u(x,y) = \frac{1}{2\pi}\int_0^c q(s)\frac{x-s}{(x-s)^2+y^2}ds \tag{2.53}$$

$$v(x,y) = \frac{1}{2\pi}\int_0^c q(s)\frac{y}{(x-s)^2+y^2}ds \tag{2.54}$$

As the evaluation crosses the velocity sheet ($y \to 0$) the velocity u is continuous but v is discontinuous. This should make sense conceptually as we consider the nature of sources.

Next, we need to model the camber line of the airfoil. From introductory aerodynamics we find that vortices can be used to create lift, so a vortex line seems a natural choice. The procedure is much the same.

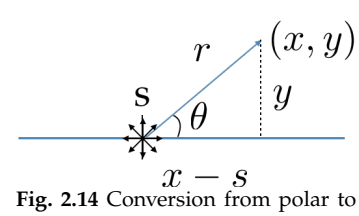

Fig. 2.14 Conversion from polar to cartesian coordinates in describing relative position of evaluation point and the source.

First, recall the potential and velocities for a point vortex (Fig. 2.15).

$$\phi = -\frac{\Gamma}{2\pi}\theta \tag{2.55}$$

$$V_\theta = -\frac{\Gamma}{2\pi r} \tag{2.56}$$

where Γ is the point vortex length. We again break the tangential velocity into x and y components:

$$u = \frac{\Gamma \sin\theta}{2\pi r} \tag{2.57}$$

$$v = -\frac{\Gamma \cos\theta}{2\pi r} \tag{2.58}$$

We now consider a line of vortices with strength per unit length γ (Fig. 2.16). That means the vortex strength per some length ds is $d\Gamma = \gamma ds$. We can express the potential function as an integral along this distribution.

$$\phi = -\frac{1}{2\pi}\int_0^c \gamma(s)\theta ds \tag{2.59}$$

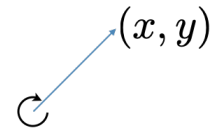

Fig. 2.15 A point vortex.

The velocities induced from the vortex distribution look similar to those from the source distribution:

$$u(x,y) = \frac{1}{2\pi}\int_0^c \gamma(s)\frac{y}{(x-s)^2+y^2}ds \tag{2.60}$$

$$v(x,y) = -\frac{1}{2\pi}\int_0^c \gamma(s)\frac{x-s}{(x-s)^2+y^2}ds \tag{2.61}$$

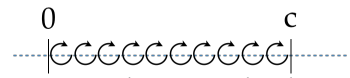

Fig. 2.16 A line vortex distribution along the chord line.

As we cross the velocity sheet ($y \to 0$) the velocity v is continuous but u is discontinuous. This should also make sense as you consider the nature of vortices.

2.5.3 Boundary Conditions

We now have a model, but need a way to solve for the unknown distributions $q(s)$ and $\gamma(s)$ that will produce the desired flow field around an arbitrary airfoil shape. To do this we need to impose the boundary conditions.

The first boundary condition is that the induced velocity must go to zero in the farfield. This boundary condition is automatically satisfied by the choice of singularities (sources and vortices). The other boundary condition we need to satisfy is flow tangency. We require that the total velocity vector is tangent to the airfoil surface, or in other words that the normal component of velocity is zero (no flow-through condition). Mathematically we can say that the slope of the airfoil is related to the local velocity as (Fig. 2.17):

$$\frac{v}{u} = \frac{dy}{dx} \tag{2.62}$$

Fig. 2.17 Illustration of flow tangency condition.

Using the airfoil coordinate system we established earlier we can write the two surfaces as:

$$y_u(x) = \bar{y}(x) + \frac{1}{2}t(x) \tag{2.63}$$

$$y_l(x) = \bar{y}(x) - \frac{1}{2}t(x) \tag{2.64}$$

Substituting these expressions into our flow tangency condition yields:

$$\frac{v}{u} = \frac{dy}{dx} = \frac{d\bar{y}}{dx} \pm \frac{1}{2}\frac{dt}{dx} \tag{2.65}$$

Using our decomposition, we can write the velocity components as:

$$u = V_\infty \cos\alpha + u_t + u_c \tag{2.66}$$

$$v = V_\infty \sin\alpha + v_t + v_c \tag{2.67}$$

The resulting boundary condition is then:

$$\frac{V_\infty \sin\alpha + v_t + v_c}{V_\infty \cos\alpha + u_t + u_c} = \frac{d\bar{y}}{dx} \pm \frac{1}{2}\frac{dt}{dx} \tag{2.68}$$

In order to provide this condition in a form that we can solve analytically three simplifications are made. All of these assumptions are based on small disturbances, or in other words that the the airfoil is *thin*, and with a small angle of attack, thus the name *thin airfoil theory*. The first assumption is that α is small enough to where we can approximately $\sin\alpha \approx \alpha$ and $\cos\alpha \approx 1$. This assumption is actually not necessarily to solve the equations analytically, but is conventionally done, simplifies the equations, and is consistent with the other assumptions and so it used here:

$$\frac{V_\infty \alpha + v_t + v_c}{V_\infty + u_t + u_c} = \frac{d\bar{y}}{dx} \pm \frac{1}{2}\frac{dt}{dx} \tag{2.69}$$

The second assumption is that the x-components of the induced velocity are much smaller than the freestream velocity and so can be neglected *in the boundary condition*.

$$\frac{V_\infty \alpha + v_t + v_c}{V_\infty} = \frac{d\bar{y}}{dx} \pm \frac{1}{2}\frac{dt}{dx} \tag{2.70}$$

The final simplification is to use the exact airfoil slope, but impose the boundary condition at $y = \pm 0$ rather than at the actual surface (y_u, y_l). The resulting boundary condition is then:

$$(v_t + v_c)_{y=\pm 0} = V_\infty \left(\frac{d\bar{y}}{dx} \pm \frac{1}{2}\frac{dt}{dx} - \alpha \right) \tag{2.71}$$

Finally, since the sources were designed to address the thickness distribution and the vortices the camber, we assume the former only involves the thickness part of the boundary condition and the latter the camber portion:

$$v_t(y=0) = \pm V_\infty \frac{1}{2}\frac{dt}{dx} \tag{2.72}$$

$$v_c(y=0) = V_\infty \left(\frac{d\bar{y}}{dx} - \alpha\right) \tag{2.73}$$

2.5.4 Induced Velocities

Let's now work out the induced velocities from the sources and vortices. Previously, we derived the induced velocity for a line of sources:

$$u(x,y) = \frac{1}{2\pi}\int_0^c q(s)\frac{x-s}{(x-s)^2+y^2}ds \tag{2.74}$$

$$v(x,y) = \frac{1}{2\pi}\int_0^c q(s)\frac{y}{(x-s)^2+y^2}ds \tag{2.75}$$

but now we need to evaluate the integrals as $y \to 0$. The first, we can evaluate directly, the second is less straightforward so we'll leave in the form of a limit for now.

$$u_t(x, y \to 0^+) = \frac{1}{2\pi}\int_0^c \frac{q(s)}{(x-s)}ds \tag{2.76}$$

$$v_t(x, y \to 0^+) = \frac{1}{2\pi}\lim_{y\to 0^+}\int_0^c q(s)\frac{y}{(x-s)^2+y^2}ds \tag{2.77}$$

The second integral is zero everywhere except when $x = s$. Thus, $q(s)$ becomes $q(x)$ and can come out of the integral. Additionally, because the function is zero everywhere else we can extend the limits of integration to $-\infty$ to ∞ without changing the solution

$$v_t(x, y \to 0^+) = \frac{q(x)}{2\pi}\int_{-\infty}^{\infty} \frac{y}{(x-s)^2+y^2}ds \tag{2.78}$$

We divide the top and bottom of the integrand by y^2:

$$v_t(x, y \to 0^+) = \frac{q(x)}{2\pi}\int_{-\infty}^{\infty} \frac{1/y}{\left(\frac{x-s}{y}\right)^2+1}ds \tag{2.79}$$

We now introduce the change of variables $z = (x-s)/y$ and $ds = -ydz$:

$$v_t(x, y \to 0^+) = \frac{q(x)}{2\pi}\int_{\infty}^{-\infty} \frac{-1}{(z)^2+1}dz \tag{2.80}$$

or switching the limits of integration:

$$v_t(x, y \to 0^+) = \frac{q(x)}{2\pi} \int_{-\infty}^{\infty} \frac{1}{(z)^2 + 1} dz \tag{2.81}$$

The integrand has a known solution:

$$v_t(x, y \to 0^+) = \frac{q(x)}{2\pi} \left[\tan^{-1} z\right]_{-\infty}^{\infty} \tag{2.82}$$

Finally, evaluating the integral gives:

$$v_t(x, y \to 0^+) = \frac{q(x)}{2} \tag{2.83}$$

The solution is the same if we approach from $y \to 0^-$ except with a negative sign. Thus we arrive at:

$$\boxed{v_t(x, y \to \pm 0) = \pm \frac{q(x)}{2}} \tag{2.84}$$

The vortex line has the same types of integral but reversed in order for u and v:

$$u_c(x, y = 0) = \pm \frac{\gamma(x)}{2} \tag{2.85}$$

$$v_c(x, y = 0) = -\frac{1}{2\pi} \int_0^c \frac{\gamma(s)}{x - s} ds \tag{2.86}$$

We can now plug these into the boundary conditions (Eqs. 2.72 and 2.73):

$$\pm \frac{q(x)}{2} = \pm V_\infty \frac{1}{2} \frac{dt}{dx} \tag{2.87}$$

$$-\frac{1}{2\pi} \int_0^c \frac{\gamma(s)}{x - s} ds = V_\infty \left(\frac{d\bar{y}}{dx} - \alpha \right) \tag{2.88}$$

The first equation shows that we can determine the source distribution simply from the known airfoil thickness distribution:

$$\boxed{q(x) = V_\infty \frac{dt}{dx}} \tag{2.89}$$

The vortex distribution is not as simple, and requires solving an integral equation with a known angle of attack and camber distribution:

$$\boxed{\frac{1}{2\pi} \int_0^c \frac{\gamma(s)}{x - s} ds = V_\infty \left(\alpha - \frac{d\bar{y}}{dx} \right)} \tag{2.90}$$

2.5.5 Symmetric Airfoil

The integral equation is easiest to solve if the airfoil is symmetric. For a symmetric airfoil the camber is zero and so the integral equation simplifies to:

$$\int_0^c \frac{\gamma(s)}{x-s} ds = 2\pi V_\infty \alpha \tag{2.91}$$

To solve this equation we will use a coordinate transformation. This is a common coordinate transformation which transforms the airfoil into cosine spacing:

$$x = \frac{c}{2}(1-\cos\theta)\,, \quad \theta = 0\ldots\pi \tag{2.92}$$

$$s = \frac{c}{2}(1-\cos\phi) \tag{2.93}$$

$$ds = \frac{c}{2}\sin\phi d\phi \tag{2.94}$$

With this transformation the integral becomes:

$$\int_0^\pi \frac{\gamma(\phi)\sin\phi}{\cos\phi-\cos\theta} d\phi = 2\pi V_\infty \alpha \tag{2.95}$$

A useful integral that we will use again later when we discuss finite wing theory is:

$$\int_0^\pi \frac{\cos(n\phi)}{\cos\phi-\cos\theta} d\phi = \pi\frac{\sin(n\theta)}{\sin\theta} \tag{2.96}$$

For convenience, we enumerate two solutions below. For $n = 0$:

$$\int_0^\pi \frac{1}{\cos\phi-\cos\theta} d\phi = 0 \tag{2.97}$$

and for $n = 1$:

$$\int_0^\pi \frac{\cos\phi}{\cos\phi-\cos\theta} d\phi = \pi \tag{2.98}$$

Referring back to Eqs. 2.95 and 2.98 we see that

$$\gamma(\phi) = \frac{2V_\infty\alpha}{\tan\phi} \tag{2.99}$$

is a solution. However, referring to Eq. 2.97 we see that adding on a second term like that shown below is also a solution:

$$\gamma(\phi) = \frac{2V_\infty\alpha}{\tan\phi} + \frac{k}{\sin\phi} \tag{2.100}$$

where k is an arbitrary constant. This last equation is the most general solution. However, it presents a problem. Since the equation is satisfied for any value of k that means that γ has an infinite number of solutions that satisfy the boundary conditions. That's not helpful as that means the lift has an infinite number of possibilities. We need some additional information to close this equation.

The missing piece we use is the *Kutta condition*. As we've seen, potential flow allows for an infinite number of solutions for the flow field around an airfoil. However, at a sharp trailing edge the real flow must leave smoothly at the trailing edge. If not, an infinitely large pressure gradient would be required to force the flow around the sharp corner. In a real flow, the large adverse pressure gradient would lead to flow separation.

2.5.6 Kutta Condition

Potential flow analysis suggest that at a sharp trailing edge the velocity will either be infinite, or it must leave smoothly at the bisection of the training edge angle. The real fluid cannot permit such a large velocity as that would require navigating a huge adverse pressure gradient and the flow would separate. Thus, the latter is what occurs in reality.

Referring back to Eq. 2.85 we see that the predicted velocity is discontinuous at the trailing edge (Fig. 2.18) unless $\gamma(c) = 0$. This requirement ($\gamma(c) = 0$) is the Kutta condition. Adding in the thickness contribution it means that the flow speed on upper and lower surfaces are equal at the trailing edge.

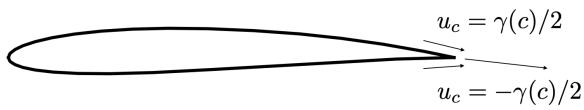

Fig. 2.18 A depiction of the Kutta condition and the discontinuous jump in u_c unless $\gamma(c) = 0$.

While the above derivation was motivated for a sharp airfoil, the same condition can be applied to a blunt airfoil. In that case we assume that the wake is thin and straight and does not support a pressure difference. In other words the velocities at the trailing edge will still be equal. The Kutta condition in this form cannot be used for unsteady flows or applications like airfoils with jet flaps.

Referring back to our equation for the vortex distribution:

$$\gamma(\phi) = \frac{2V_\infty \alpha}{\tan\phi} + \frac{k}{\sin\phi} \tag{2.101}$$

with the Kutta condition expressed in our cosing spacing: $\gamma(\pi) = 0$, we can see that at $\phi = \pi$ the circulation is infinite unless:

$$k = 2V_\infty \alpha \tag{2.102}$$

Inserting this into the above equation yields:

$$\gamma(\phi) = \frac{2V_\infty \alpha}{\sin\phi}(1 + \cos\phi) \tag{2.103}$$

We can see that $\gamma(\pi) = 0$ by applying L'Hopital's rule. While this removes the infinite velocities at the trailing edge, there are still infinite velocities at the leading edge. This is just a consequence of the fact that at the leading edge the small disturbance assumption, on which thin airfoil theory is based, is clearly violated. Later we will discuss a method called Riegel's correction to help address this issue.

While we did the derivation in a transformed coordinate system, we now wish to transform back to our original coordinate system. We can rearrange Eq. 2.92 as:

$$\cos\phi = 1 - \frac{2x}{c} \tag{2.104}$$

Then with that definition, and the aid of Fig. 2.19, we can write an expression for $\sin\phi$ in terms of x (just using the Pythagorean theorem):

$$\sin\phi = 2\left[\frac{x}{c}\left(1 - \frac{x}{c}\right)\right]^{1/2}. \tag{2.105}$$

The resulting circulation distribution for a symmetric airfoil is then:

$$\gamma(x) = 2V_\infty \alpha \frac{\sqrt{1 - x/c}}{\sqrt{x/c}} \tag{2.106}$$

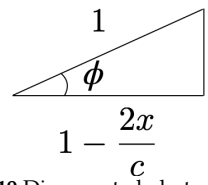

Fig. 2.19 Diagram to help transform from cosine coordinate system back to original coordinate system.

2.5.7 Cambered Airfoil

The cambered case is a bit more difficult, but we start with the same equation (Eq. 2.90), including camber this time, and apply the same coordinate transformation (Eq. 2.92):

$$\int_0^\pi \frac{\gamma(\phi)\sin\phi}{\cos\phi - \cos\theta} d\phi = 2\pi V_\infty(\alpha - b(\theta)) \tag{2.107}$$

where

$$b(\theta) = \frac{d\bar{y}}{dx}(x(\theta)) \tag{2.108}$$

We also need the Kutta condition:

$$\gamma(\pi) = 0 \tag{2.109}$$

To find a solution we use the same form we found from the symmetric solution (Eq. 2.103) and additional terms using a Fourier sine series. In order to ensure that the Kutta condition can be meet we chose a form of the equation that automatically satisfies this condition:

$$\gamma(\phi) = 2V_\infty \left[A_0 \frac{(1+\cos\phi)}{\sin\phi} + \sum_n A_n \sin(n\phi) \right] \tag{2.110}$$

where A_i are Fourier coefficients. By plugging into our governing equation Eq. 2.107, and using the integral in Eq. 2.96, we can compute the coefficients from the known camber distribution as follows:

$$A_0 = \alpha - \frac{1}{\pi} \int_0^\pi b(\theta) d\theta \tag{2.111}$$

$$A_n = \frac{2}{\pi} \int_0^\pi b(\theta) \cos(n\theta) d\theta \tag{2.112}$$

The evaluation process is then:

1. Get the camber line shape of the airfoil $\bar{y}$.
2. Differentiate to get $d\bar{y}/dx$.
3. Perform a variable substitution in terms of θ (Eq. 2.92).
4. Evaluate the above integrals to get the Fourier coefficients.

The Fourier series converges even if the camber line does not have a continuous slope (e.g., flaps and slats). Once we have the coefficients then we have a known solution for $\gamma(\phi)$ (Eq. 2.110).

2.5.8 Pressure

With computed source and vortex distributions we can now evaluate pressure along the airfoil, and the resulting forces and moments. Recall the definition of pressure coefficient for an incompressible, irrotational flow:

$$C_p = 1 - \left(\frac{V}{V_\infty} \right)^2 \tag{2.113}$$

In this case, the velocity is:

$$V^2 = u^2 + v^2 \tag{2.114}$$

$$= (V_\infty \cos\alpha + u_t + u_c)^2 + (V_\infty \sin\alpha + v_t + v_c)^2 \tag{2.115}$$

Note that we retain all of the terms, as it is no longer necessary to ignore some as we had to do in the boundary condition. Retaining all terms improves the accuracy of the pressure distribution.

As hinted at earlier, one problem with thin airfoil theory is that it leads to unrealistically large velocities near the leading edge because the small disturbance assumption is not justified there. One way to address this is to use Riegel's correction. The method is simple, the velocity is just multiplied by the cosine of the local airfoil slope:

$$V_{mod} = V \cos\beta \tag{2.116}$$

Note that at the leading edge where $\beta = 90°$ this correction allows for a stagnation point. In terms of our airfoil camber and thickness we can rewrite this equation as:

$$V_{mod} = V \frac{1}{\sqrt{1 + \left(\frac{d\bar{y}}{dx} \pm \frac{1}{2}\frac{dt}{dx}\right)^2}} \tag{2.117}$$

This modified velocity is used in the pressure coefficient calculation:

$$C_p = 1 - \left(\frac{V_{mod}}{V_\infty}\right)^2 \tag{2.118}$$

2.5.9 Forces and Moments

With known pressures we can integrate along the surface to compute forces and moments. We will use the coordinate system shown in Fig. 2.20. On the upper surface the pressure over an incremental

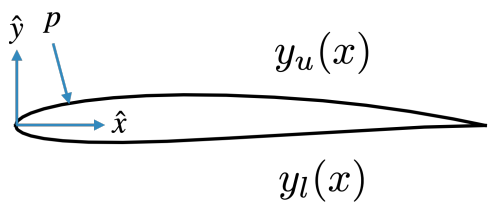

Fig. 2.20 Normal and tangential directions for integration.

surface ds leads to the following forces in the x-direction:

$$F'_x = -p_u ds \cos\beta \tag{2.119}$$

and y-direction:

$$F'_y = p_u ds \sin\beta \tag{2.120}$$

where β is the local slope (Fig. 2.21). Using the substitution:

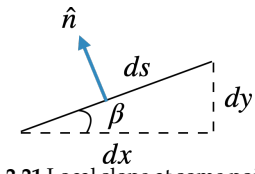

Fig. 2.21 Local slope at some point on the body.

$$\cos\beta = \frac{dx}{ds} \tag{2.121}$$

and

$$\sin\beta = \frac{dy}{ds} = \frac{\frac{dy}{dx}dx}{ds} \tag{2.122}$$

and including the lower surface leads to the following forces and moments (per unit depth):

$$F'_x = \int_0^c \left(p_u \frac{dy_u}{dx} - p_l \frac{dy_l}{dx}\right) dx \tag{2.123}$$

$$F'_y = \int_0^c (p_l - p_u)\, dx \tag{2.124}$$

$$M'_{le} = \int_0^c \left[p_u\left(x + y_u \frac{dy_u}{dx}\right) - p_l\left(x + y_l \frac{dy_l}{dx}\right)\right] dx \tag{2.125}$$

If we nondimensionalize we have:

$$c_n = \int_0^1 \left(C_{p_l} - C_{p_u}\right) d\left(\frac{x}{c}\right) \tag{2.126}$$

$$c_a = \int_0^1 \left(C_{p_u} \frac{dy_u}{dx} - C_{p_l} \frac{dy_l}{dx}\right) d\left(\frac{x}{c}\right) \tag{2.127}$$

$$c_{mle} = \int_0^1 \left[C_{p_u}\left(\frac{x}{c} + \frac{y_u}{c}\frac{dy_u}{dx}\right) - C_{p_l}\left(\frac{x}{c} + \frac{y_l}{c}\frac{dy_l}{dx}\right)\right] d\left(\frac{x}{c}\right) \tag{2.128}$$

where c_n and c_a are the normal force coefficient and axial force coefficient corresponding to the y and x direction respectively, for our body-aligned coordinate system.

We can evaluate the lift and drag from the above integrals (Eq. 1.13):

$$c_l = c_n \cos\alpha - c_a \sin\alpha \tag{2.129}$$

$$c_d = c_n \sin\alpha + c_a \cos\alpha \tag{2.130}$$

or more simply we can use the Kutta-Joukowski theorem. The total circulation is given by the integrating the vorticity:

$$\Gamma = \int_0^c \gamma(s) ds \tag{2.131}$$

To perform the integral we use our coordinate transformation (Eq. 2.94):

$$\Gamma = \int_0^c \gamma(s) ds \tag{2.132}$$

$$= \frac{c}{2}\int_0^\pi \gamma(\phi)\sin\phi d\phi \tag{2.133}$$

We then substitute the general solution for the vortex distribution (Eq. 2.110) into the integral:

$$\Gamma = \frac{c}{2}\int_0^\pi 2V_\infty \left[A_0 \frac{(1+\cos\phi)}{\sin\phi} + \sum_n A_n \sin(n\phi)\right] \sin\phi d\phi \tag{2.134}$$

$$= V_\infty c \left[A_0 \int_0^\pi (1+\cos\phi)d\phi + \sum_n A_n \int_0^\pi \sin\phi \sin(n\phi)d\phi\right] \tag{2.135}$$

$$= V_\infty c \left[A_0 \left(\phi + \sin\phi\right)_0^\pi + \sum_n A_n \int_0^\pi \sin\phi \sin(n\phi)d\phi\right] \tag{2.136}$$

$$= V_\infty c \left[A_0\pi + \sum_n A_n \int_0^\pi \sin\phi \sin(n\phi)d\phi\right] \tag{2.137}$$

From the orthogonality of the Fourier terms:

$$\int_0^\pi \sin(n\theta)\sin(m\theta) = 0 \text{ for } n \neq m \tag{2.138}$$

we see that the last integral vanishes for every term in the Fourier series except $n = 1$.

$$\Gamma = V_\infty c \left[A_0\pi + A_1 \int_0^\pi \sin^2\phi d\phi\right] \tag{2.139}$$

$$= V_\infty c \left[A_0\pi + A_1 \frac{\pi}{2}\right] \tag{2.140}$$

$$= V_\infty c\pi \left[A_0 + \frac{A_1}{2}\right] \tag{2.141}$$

To get the lift we then use the Kutta Joukowski theorem:

$$L' = \rho V_\infty \Gamma \tag{2.142}$$

$$L' = \rho V_\infty^2 c\pi \left[A_0 + \frac{A_1}{2}\right] \tag{2.143}$$

Integrating the drag leads to:

$$D' = 0 \tag{2.144}$$

as expected.

Let's analyze the equations in a bit more detail to see what insights the analytic expression can offer. As usual, we will want to nondimensionalize the lift:

$$c_l = \frac{L'}{\frac{1}{2}\rho V_\infty^2 c} = 2\pi\left(A_0 + \frac{A_1}{2}\right) \tag{2.145}$$

$$= 2\pi\left[\alpha - \frac{1}{\pi}\int_0^\pi b(\theta)(1-\cos\theta)d\theta\right] \tag{2.146}$$

If we compare this with the standard form for the lift curve (prior to stall):

$$c_l = m(\alpha - \alpha_0) \tag{2.147}$$

We notice the remarkable and useful result that no matter what shape the airfoil is *the theoretical lift curve slope is always* 2π:

$$m = 2\pi \tag{2.148}$$

In practice, the lift curve slope of real airfoils is generally a bit less than 2π because of viscous effects, but is still quite close. The second part gives the zero lift angle of attack:

$$\alpha_0 = \frac{1}{\pi}\int_0^{\pi} b(\theta)(1 - \cos\theta)d\theta \tag{2.149}$$

which would be zero for an uncambered airfoil ($b(\theta) = 0$) as expected.

The pitching moment can be derived about an arbitrary point x as shown in **??**. The integral is:

$$M(x) = -\rho V_\infty \int_0^c \gamma(s)(s - x)ds \tag{2.150}$$

where the negative sign is used since a pitch up is considered a positive moment. Using our coordinate transformations (Eqs. 2.92 to 2.94) results in:

$$M(x) = -\frac{\rho V_\infty c^2}{4}\int_0^{\pi} \gamma(\phi)\sin\phi(\cos\theta - \cos\phi)d\phi \tag{2.151}$$

$$= \frac{\rho V_\infty c}{2}\left[\cos\theta\int_0^{\pi}\gamma(\phi)\sin\phi d\phi - \int_0^{\pi}\gamma(\phi)\sin\phi\cos\phi d\phi\right] \tag{2.152}$$

The first integral is the same as the one we evaluated for lift earlier (Eq. 2.133), excepting the constant $c/2$ term and evaluates to Eq. 2.141 (times $2/c$).

$$M(x) = -\frac{\rho V_\infty c^2}{4}\left[\cos\theta\, 2V_\infty\pi\left(A_0 + \frac{A_1}{2}\right) - \int_0^{\pi}\gamma(\phi)\sin\phi\cos\phi d\phi\right] \tag{2.153}$$

Let's consider only the second integral now:

$$\int_0^\pi \gamma(\phi)\sin\phi\cos\phi d\phi \tag{2.154}$$

$$= 2V_\infty\left[A_0\int_0^\pi \cos\phi(1+\cos\phi) + \sum_n A_n\int_0^\pi \sin\phi\cos\phi\sin(n\phi)\right] \tag{2.155}$$

$$= 2V_\infty\left[A_0\frac{\pi}{2} + A_1\int_0^\pi \cos\phi\sin\phi\sin(\phi) + A_2\int_0^\pi \cos\phi\sin\phi\sin(2\phi)\right. \tag{2.156}$$

$$\left. A_3\int_0^\pi \cos\phi\sin\phi\sin(3\phi) + \ldots\right] \tag{2.157}$$

The A_1 term integrates to zero, as does A_3 and all higher order terms. The A_2 term integrates to $\pi/4$.

$$\int_0^\pi \gamma(\phi)\sin\phi\cos\phi d\phi = 2V_\infty\left[A_0\frac{\pi}{2} + A_2\frac{\pi}{4}\right] \tag{2.158}$$

We now plug this result back into Eq. 2.153 yielding:

$$M(x) = -\frac{\rho V_\infty c^2}{4}\left[\cos\theta\, 2V_\infty\pi\left(A_0 + \frac{A_1}{2}\right) - 2V_\infty\left(A_0\frac{\pi}{2} + A_2\frac{\pi}{4}\right)\right] \tag{2.159}$$

$$= -\frac{\rho V_\infty^2 c^2\pi}{2}\left[\cos\theta\left(A_0 + \frac{A_1}{2}\right) - \left(A_0\frac{1}{2} + A_2\frac{1}{4}\right)\right] \tag{2.160}$$

$$= -\frac{\rho V_\infty^2 c^2\pi}{2}\left[A_0\left(\cos\theta - \frac{1}{2}\right) + A_1\frac{\cos\theta}{2} - \frac{A_2}{4}\right] \tag{2.161}$$

$$\tag{2.162}$$

Let's now express this in terms of x using our inverse transformation (Eq. 2.104):

$$M(x) = -\frac{\rho V_\infty^2 c^2\pi}{2}\left[A_0\left(\frac{1}{2} - \frac{2x}{c}\right) + A_1\left(\frac{1}{2} - \frac{x}{c}\right) - \frac{A_2}{4}\right] \tag{2.163}$$

Now for convenience, we distribute a $c/2$ from the outside term through the parenthesis:

$$M(x) = -\rho V_\infty^2 c\pi\left[A_0\left(\frac{c}{4} - x\right) + A_1\left(\frac{c}{4} - \frac{x}{2}\right) - A_2\frac{c}{8}\right] \tag{2.164}$$

The definition of the aerodynamic center is the point about which the pitching moment is independent of angle of attack $dM/d\alpha = 0$. The

only Fourier coefficient that depends on angle of attack is A_0:

$$A_0 = \alpha - \frac{1}{\pi}\int_0^{\pi} b(\phi)d\phi \tag{2.165}$$

So from the moment equation we can see that the point at which $dM/d\alpha = 0$ is when $x = c/4$. This is another highly useful result from thin airfoil theory, namely that *the airfoil quarter chord is the theoretical location of the aerodynamic center*.

$$\boxed{x_{ac} = \frac{c}{4}} \tag{2.166}$$

We can also compute the pitching moment coefficient about the aerodynamic center, but that depends on the specific airfoil shape.

$$M_{ac} = M(x = c/4) = -\rho V_\infty^2 c\pi \left[A_1\frac{c}{8} - A_2\frac{c}{8}\right] \tag{2.167}$$

$$= -\frac{\rho V_\infty^2 c^2 \pi}{8}(A_1 - A_2) \tag{2.168}$$

$$c_{m\,\mathrm{ac}} = \frac{M_{ac}}{\frac{1}{2}\rho V_\infty^2 c^2} \tag{2.169}$$

$$= -\frac{\pi}{4}(A_1 - A_2) \tag{2.170}$$

Example 2.1 Parabolic camber

Let's consider an example of an airfoil with parabolic camber as shown in Fig. 2.22 and given in equation form as:

$$\bar{y} = 4\epsilon\frac{x}{c}(c - x) \tag{2.171}$$

where ϵ is the the maximum camber.

We now follow the steps outlined at the end of Section 2.5.7. With the camber line defined we now differentiate:

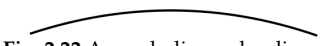

Fig. 2.22 A parabolic camber line.

$$\frac{d\bar{y}}{dx} = 4\epsilon\left(1 - \frac{2x}{c}\right) \tag{2.172}$$

Then apply the variable substitution $x = \frac{c}{2}(1 - \cos\phi)$:

$$b(\phi) = 4\epsilon\cos\phi \tag{2.173}$$

We now perform the integrals for the Fourier coefficients:

$$A_0 = \alpha - \frac{4\epsilon}{\pi}\int_0^{\pi}\cos\phi d\phi \tag{2.174}$$

$$= \alpha \tag{2.175}$$

$$A_1 = \frac{8\epsilon}{\pi}\int_0^{\pi} \cos^2(\phi)d\phi \tag{2.176}$$

$$= 4\epsilon \tag{2.177}$$

$$A_2 = \frac{8\epsilon}{\pi}\int_0^{\pi} \cos(\phi)\cos(2\phi)d\phi \tag{2.178}$$

$$= 0 \tag{2.179}$$

Similarly, $A_n = 0$ for all $n \geq 2$.

Using the equation for lift we have:

$$L' = \pi\rho V_\infty^2 c(\alpha + 2\epsilon) \tag{2.180}$$

2.5.10 Lumped Vortex Method

The following discussion is a bit of an aside, but uses the results of thin airfoil theory and will be useful in a later chapter. Let's consider a model as shown in Fig. 2.23. Rather than using a distribution of vortices, we want to lump all the vorticity into one point vortex. This model will be used later in a vortex lattice method where we need a simple way to model the camber and will use results of thin airfoil theory to do so. With only one point vortex we can only satisfy the flow tangency boundary condition at one point (the control point denoted by x). The question then is where should we place the point vortex (distance a), and where should we place the control point (distance b)?

In Eq. 2.73 we derived that the flow tangency boundary condition for the vertical velocity is:

$$v_c = V_\infty\left(\frac{d\bar{y}}{dx} - \alpha\right) \tag{2.181}$$

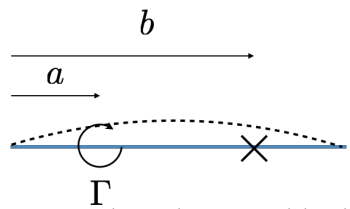

Fig. 2.23 A lumped vortex model and a control point marked with x.

For a point vortex we know that the induced velocity is given by $V_\theta = \Gamma/(2\pi r)$ or in this case the velocity of the vortex induced at the control point where we will impose the boundary condition is:

$$-\frac{\Gamma}{2\pi(b-a)} = V_\infty\left(\frac{d\bar{y}}{dx} - \alpha\right) \tag{2.182}$$

As we know nothing about the airfoil at this stage, we will assume a parabolic camber as that seems reasonably flexible will still retaining simplicity. The previous example provides the camber line slope, which is given by the following equation when evaluated at the control point:

$$\left.\frac{d\bar{y}}{dx}\right|_{x=b} = 4\epsilon\left(1 - \frac{2b}{c}\right) \tag{2.183}$$

Similarly, the previous example solved for the lift of a parabolic camber airfoil, which we can relate to circulation through the Kutta-Joukowski theorem:

$$L' = \pi\rho V_\infty^2 c(\alpha + 2\epsilon) = \rho V_\infty \Gamma \tag{2.184}$$

Solving for Γ and using some algebra on the above equation results in the following:

$$\left(\frac{c}{b-a}\right)\alpha + \left(\frac{2c}{b-1}\right)\epsilon = (2)\,\alpha - \left(8\left(1 - 2\frac{b}{c}\right)\right)\epsilon \tag{2.185}$$

For this equation to be satisfied the coefficients in front of α must be equal, as must the coefficients in front of ϵ. This gives two equations for two unknowns:

$$a = \frac{1}{4}c \tag{2.186}$$

$$b = \frac{3}{4}c \tag{2.187}$$

Thus, using the results of thin airfoil theory suggests that we should put the vortex at the quarter chord and the control point at three-quarters chord.

2.6 Hess-Smith Panel Method

Thin airfoil theory is quite clever, but comes with a few significant limitations. The most problematic limitation is the assumption of small disturbances. This means that near stagnation points, which exist for all airfoils, the pressure distributions are not well predicted. Significant inaccuracies may also exist for airfoils with high camber or large thickness.

We will reuse the ideas of thin airfoil theory where complex solutions are built up from distributions of sources, vortices, etc. The advantage to this approach is that the governing equation (Laplace) is automatically satisfied, as is the farfield boundary condition. We only need to worry about satisfying flow tangency and the Kutta condition. The main deviation we make from thin airfoil theory is to place the source/vortex distributions on the surface of the body rather than at the chord line, and use the exact flow tangency conditions imposed at the surface. The approach is to discretize the geometry into segments that we call *panels*. The integral equations developed in this chapter can be applied on each panel leading to a system of linear equations. The methodology is called a *panel method*, and can be applied in 3D. There are many different types of panel methods of varying sophistication. Modern

panel methods often use sources and doublets rather than vortices. In this section we will study one of the simplest but still useful panel methods for two-dimensional flow. It was developed by Hess and Smith of Douglas Aircraft in 1966 and was the first practical panel method.

We still use the same key idea that we will model the flow as a contribution of three potential functions: freestream, line source distributions (Eq. 2.52), and vortex line distributions (Eq. 2.59).

$$\phi = \phi_\infty + \phi_t + \phi_c \tag{2.188}$$

$$= V_\infty \cos(\alpha x) + V_\infty \sin(\alpha y) + \int_0^c \frac{q(s)}{2\pi} \ln r ds - \int_0^c \frac{\gamma(s)}{2\pi} \theta ds \tag{2.189}$$

The above integrals are difficult to evaluate on arbitrary shapes so a common simplification is to approximate the airfoil with straight line segments. These segments form the "panels", and they will be numbered as shown in Fig. 2.24. With that simplification the equation becomes a summation of integrals that occur over flat panels:

$$\phi = V_\infty \cos(\alpha x) + V_\infty \sin(\alpha y) + \sum_{i=1}^{N} \int_{\text{panel } i} \left[\frac{q(s)}{2\pi} \ln r - \frac{\gamma(s)}{2\pi} \theta \right] ds \tag{2.190}$$

Fig. 2.24 An airfoil discretized into straight line panels.

The Hess/Smith model makes the following simplifications. First, that the source strength ($q(s)$) is constant on a given panel, but can vary from panel to panel. These strengths will be varied to satisfy flow tangency at control points, one for each panel (N strengths and N boundary conditions). Next, they chose to have the vortex strength ($\gamma(s)$) be constant over the entire airfoil (and thus constant on each panel). This leads to one additional unknown to satisfy the one additional equation: the Kutta condition.

A panel with constant source/vortex strength produces infinite velocities at the ends of each panel and so control points cannot be at the end points. The midpoint is the most logical choice but that could be the midpoint of the panel or the midpoint of the actual surface. For this model it works better (and is simpler) to have the control points at the midpoints of the panel. This is because numerical errors can occur if the control point is too close to a singularity. Similarly, the Kutta condition

is applied at the control points on the middle of the trailing edge panels highlighted in Fig. 2.25. Note that with this method the Kutta condition is then not quite at the trailing edge. The real flow, with viscosity, does not have a stagnation point right at the trailing edge anyway, so it turns out this approximation fortuitously often yields better predictions than a more numerically accurate boundary condition would.

Fig. 2.25 Location of control points (x) and direction of normal for an arbitrary panel, and the controls points (x) on the trailing edge-panels for the Kutta condition.

Let us consider a generic panel as described in Fig. 2.26. From known end point locations (x_i, y_i), we need to determine the control point locations, the angle, and the normal and tangent vectors. Because we chose to model control points at the center of the panels rather than at the center of the surface they are easily computed:

$$\bar{x}_i = \frac{x_i + x_{i+1}}{2} \tag{2.191}$$

$$\bar{y}_i = \frac{y_i + y_{i+1}}{2} \tag{2.192}$$

As we will see, the methodology doesn't actually need θ but rather $\sin\theta$ and $\cos\theta$. These can be computed as:

$$\sin\theta_i = \frac{y_{i+1} - y_i}{l_i} \tag{2.193}$$

$$\cos\theta_i = \frac{x_{i+1} - x_i}{l_i} \tag{2.194}$$

Based on our numbering scheme (Fig. 2.24) the body is to the right when progressing from i to $i+1$ and the surface normal always points out (away from the body). Thus, the normal and tangential vectors are given by:

$$\hat{t}_i = \cos\theta_i \hat{x} + \sin\theta_i \hat{y} \tag{2.195}$$

$$\hat{n}_i = -\sin\theta_i \hat{x} + \cos\theta_i \hat{y} \tag{2.196}$$

The velocity at panel i will be the velocity calculated at control point i:

$$u_i \equiv u(\bar{x}_i, \bar{y}_i) \tag{2.197}$$

$$v_i \equiv v(\bar{x}_i, \bar{y}_i) \tag{2.198}$$

With that setup we can now write our boundary conditions in equation form. First, the no-flow-through, or flow tangency, condition is:

$$\vec{V} \cdot \hat{n} = 0 \tag{2.199}$$

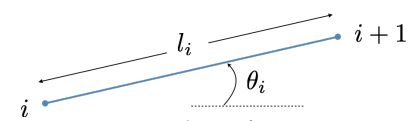

Fig. 2.26 Nomenclature for a generic panel i.

Using the vectors we defined earlier we can express this as:

$$-u_i \sin\theta_i + v_i \cos\theta_i = 0 \tag{2.200}$$

which is applied at each panel. Next, as we saw, one way to state the Kutta condition is that the tangential velocity at the trailing edge is the same on the upper and lower surfaces:

$$V_{t1} = -V_{tn} \tag{2.201}$$

or using our panel notation:

$$u_1 \cos\theta_1 + v_1 \sin\theta_1 = -u_N \cos\theta_N - v_N \sin\theta_N \tag{2.202}$$

To build up the solution we need to be able to compute the influence of a panel on another panel. To start, we compute u^*_{sij} and v^*_{sij}, which is the x and y components of velocity at panel i induced by a source distribution at panel j (see Fig. 2.27).

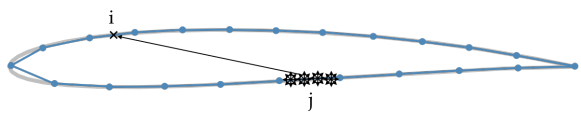

Fig. 2.27 Computing induced velocity at panel i from a line source distribution along panel j.

To determine the velocities, we need to consider a generic panel j as shown in Fig. 2.28. For convenience we use a rotated coordinate system aligned with the panel (x^*, y^*). In the rotated coordinate system, we already know the how to compute the velocities. This is exactly what we derived previously: the velocities induced by a line source distribution over a finite segment (Eqs. 2.53 and 2.54), except in this case the source strength is constant over the panel.

$$u^*_{sij} = \frac{q_j}{2\pi} \int_0^{l_j} \frac{x^* - s}{(x^* - s)^2 + (y^*)^2} ds \tag{2.203}$$

$$v^*_{sij} = \frac{q_j}{2\pi} \int_0^{l_j} \frac{y^*}{(x^* - s)^2 + (y^*)^2} ds \tag{2.204}$$

With q out of the integral, both of these integrals can be solved analytically (recall that x^* and y^* are constants in the integral as they are just an evaluation point).

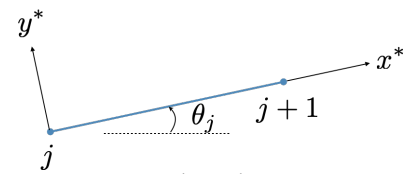

Fig. 2.28 A rotated coordinate system aligned with an arbitrary panel j.

$$
\begin{aligned}
u^*_{sij} &= \frac{q_j}{2\pi}\int_0^{l_j} \frac{x^* - s}{(x^* - s)^2 + (y^*)^2} ds \\
&= \frac{q_j}{2\pi}\left(\frac{1}{-2}\right)\int_0^{l_j} \frac{-2(x^* - s)}{(x^* - s)^2 + (y^*)^2} ds \\
&= \frac{q_j}{2\pi}\left(\frac{1}{-2}\right)\left[\ln\left((x^* - s)^2 + (y^*)^2\right)\right]_0^{l_j} \\
&= \frac{q_j}{2\pi}\left(\frac{1}{-2}\right)\left[\ln\left((x^* - l_j)^2 + (y^*)^2\right) - \ln\left((x^*)^2 + (y^*)^2\right)\right] \\
&= \frac{-q_j}{2\pi}\left(\frac{1}{2}\right)\ln\left[\frac{(x^* - l_j)^2 + (y^*)^2}{(x^*)^2 + (y^*)^2}\right] \\
&= \frac{-q_j}{2\pi}\ln\left[\frac{\sqrt{(x^* - l_j)^2 + (y^*)^2}}{\sqrt{(x^*)^2 + (y^*)^2}}\right]
\end{aligned}
\tag{2.205}
$$

The v integral can also be found analytically:

$$
\begin{aligned}
v^*_{sij} &= \frac{q_j}{2\pi}\int_0^{l_j} \frac{y^*}{(x^* - s)^2 + (y^*)^2} ds \\
&= \frac{q_j}{2\pi}\int_0^{l_j} \frac{1/y^*}{\left(\frac{x^* - s}{y^*}\right)^2 + 1} ds
\end{aligned}
\tag{2.206}
$$

If we let $z = (x^* - s)/y^*$ then $dz = -ds/y^*$ and the integral becomes:

$$
\begin{aligned}
v^*_{sij} &= \frac{q_j}{2\pi}\int_{x^*/y^*}^{(x^* - l_j)/y^*} \frac{-1}{z^2 + 1} dz \\
&= \frac{q_j}{2\pi}\int_{(x^* - l_j)/y^*}^{x^*/y^*} \frac{1}{z^2 + 1} dz \\
&= \frac{q_j}{2\pi}\left[\tan^{-1} z\right]_{(x^* - l_j)/y^*}^{x^*/y^*} \\
&= \frac{q_j}{2\pi}\left[\tan^{-1}\left(\frac{x^*}{y^*}\right) - \tan^{-1}\left(\frac{x^* - l_j}{y^*}\right)\right]
\end{aligned}
\tag{2.207}
$$

These equations are a bit cumbersome but fortunately we can simplify them quite a bit by looking at the geometry of the problem. Consider the figure shown in Fig. 2.29. Examining the geometry we see that our equations can be simplified as:

$$
\begin{aligned}
u^*_{sij} &= \frac{-q_j}{2\pi}\ln\left(\frac{r_{ij+1}}{r_{ij}}\right) \\
v^*_{sij} &= \frac{q_j}{2\pi}(\alpha - \theta) \rightarrow v^*_{sij} = q_j\frac{\beta_{ij}}{2\pi}
\end{aligned}
\tag{2.208}
$$

An additional benefit of this simplification is that our equations no longer depend upon the rotated coordinate system x^*, y^*.

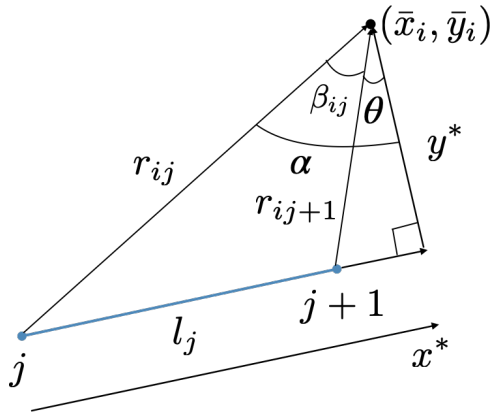

Fig. 2.29 A depiction of the geometry for an evaluation point on panel i from singularities integrating across panel j.

We need to be careful when computing β. There are various trigonometry approaches we could use, but we may run into problems for large angles. Consider two vectors starting from a common point as shown in Fig. 2.30. The definitions of the cross and dot product yield:

$$\vec{a} \times \vec{b} = |a||b| \sin\theta \tag{2.209}$$

$$\vec{a} \cdot \vec{b} = |a||b| \cos\theta \tag{2.210}$$

If we divide these two equations and solve for θ we get:

$$\theta = \tan^{-1} \frac{\vec{a} \times \vec{b}}{\vec{a} \cdot \vec{b}} \tag{2.211}$$

Using our geometry leads to the following equation for β:

$$\beta_{ij} = \begin{cases} \text{atan2}\left(\frac{(x_j-\bar{x}_i)(y_{j+1}-\bar{y}_i)-(y_j-\bar{y}_i)(x_{j+1}-\bar{x}_i)}{(x_j-\bar{x}_i)(x_{j+1}-\bar{x}_i)+(y_j-\bar{y}_i)(y_{j+1}-\bar{y}_i)}\right) & \text{if } i \neq j \\ \pi & \text{if } i = j \end{cases} \tag{2.212}$$

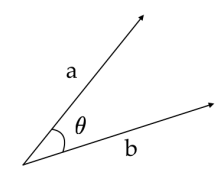

Fig. 2.30 Two vectors originating from a common origin.

The equation for β_{ii} is not obvious. The angle approaches π or $-\pi$ depending on which direction you approach from. In our case, we always come from the outside based on the way we defined our geometry and the fact that we only care about external flow so that is why $\beta_{ii} = \pi$. We need to make sure we force this. If we rely on the first equation to compute the self-induction then some panels will evaluate to something close to π and others close to $-\pi$ based on small numerical errors.

While this equation is a bit long, it is reliable. If we use the `atan2` function then the domain is $(-\pi, \pi]$ and we don't have to worry about

what quadrant we are in. This formula works equally well in three dimensions.

For vortices the procedure is essentially the same. As we've seen with thin airfoil theory the integrals are just swapped between x and y with a sign change. The result is:

$$\begin{aligned} u^*_{vij} &= \gamma \frac{\beta_{ij}}{2\pi} \\ v^*_{vij} &= \frac{\gamma}{2\pi} \ln\left(\frac{r_{ij+1}}{r_{ij}}\right) \end{aligned} \tag{2.213}$$

Recall that we computed all the velocities in the rotated (starred) coordinate system (Fig. 2.28). We need to rotate the velocities back to the original x, y coordinate system:

$$\begin{aligned} u &= u^* \cos\theta_j - v^* \sin\theta_j \\ v &= u^* \sin\theta_j + v^* \cos\theta_j \end{aligned} \tag{2.214}$$

Now, we can put everything together. Recall that the flow tangency boundary condition is (Eq. 2.200):

$$-u_i \sin\theta_i + v_i \cos\theta_i = 0 \tag{2.215}$$

Each velocity is the sum of the freestream velocity and the sources and vortices from each panel:

$$\begin{aligned} u_i &= V_\infty \cos\alpha + \sum_{j=1}^{N} u_{sij} + \sum_{j=1}^{N} u_{vij} \\ v_i &= V_\infty \sin\alpha + \sum_{j=1}^{N} v_{sij} + \sum_{j=1}^{N} v_{vij} \end{aligned} \tag{2.216}$$

We now have to make a bunch of substitutions. First, the coordinate transformation (Eq. 2.214):

$$\begin{aligned} u_i &= V_\infty \cos\alpha + \sum_{j=1}^{N} (u^*_{sij} \cos\theta_j - v^*_{sij} \sin\theta_j + u^*_{vij} \cos\theta_j - v^*_{vij} \sin\theta_j) \\ v_i &= V_\infty \sin\alpha + \sum_{j=1}^{N} (u^*_{sij} \sin\theta_j + v^*_{sij} \cos\theta_j + u^*_{vij} \sin\theta_j + v^*_{vij} \cos\theta_j) \end{aligned} \tag{2.217}$$

Next, we substititue in the panel velocities (Eqs. 2.208 and 2.213):

$$
\begin{aligned}
u_i &= V_\infty \cos\alpha + \sum_{j=1}^{N}\left[\frac{-q_j}{2\pi}\ln\left(\frac{r_{ij+1}}{r_{ij}}\right)\cos\theta_j\right.\\
&\left.-q_j\frac{\beta_{ij}}{2\pi}\sin\theta_j + \gamma\frac{\beta_{ij}}{2\pi}\cos\theta_j - \frac{\gamma}{2\pi}\ln\left(\frac{r_{ij+1}}{r_{ij}}\right)\sin\theta_j\right]\\
&= V_\infty \cos\alpha + \sum_{j=1}^{N}\left[\frac{-q_j}{2\pi}\left(\ln\left(\frac{r_{ij+1}}{r_{ij}}\right)\cos\theta_j + \beta_{ij}\sin\theta_j\right)\right.\\
&\left.+\frac{\gamma}{2\pi}\left(\beta_{ij}\cos\theta_j - \ln\left(\frac{r_{ij+1}}{r_{ij}}\right)\sin\theta_j\right)\right]\\
v_i &= V_\infty \sin\alpha + \sum_{j=1}^{N}\left[\frac{-q_j}{2\pi}\ln\left(\frac{r_{ij+1}}{r_{ij}}\right)\sin\theta_j\right.\\
&\left.+q_j\frac{\beta_{ij}}{2\pi}\cos\theta_j + \gamma\frac{\beta_{ij}}{2\pi}\sin\theta_j + \frac{\gamma}{2\pi}\ln\left(\frac{r_{ij+1}}{r_{ij}}\right)\cos\theta_j\right]\\
&= V_\infty \sin\alpha + \sum_{j=1}^{N}\left[\frac{q_j}{2\pi}\left(-\ln\left(\frac{r_{ij+1}}{r_{ij}}\right)\sin\theta_j + \beta_{ij}\cos\theta_j\right)\right.\\
&\left.+\frac{\gamma}{2\pi}\left(\beta_{ij}\sin\theta_j + \ln\left(\frac{r_{ij+1}}{r_{ij}}\right)\cos\theta_j\right)\right]
\end{aligned}
\tag{2.218}
$$

Now we substitute into the boundary condition (Eq. 2.200):

$$
\begin{aligned}
&-V_\infty\cos\alpha\sin\theta_i + \sum_{j=1}^{N}\left[\frac{q_j}{2\pi}\left(\ln\left(\frac{r_{ij+1}}{r_{ij}}\right)\cos\theta_j\sin\theta_i + \beta_{ij}\sin\theta_j\sin\theta_i\right)\right.\\
&\left.-\frac{\gamma}{2\pi}\left(\beta_{ij}\cos\theta_j\sin\theta_i - \ln\left(\frac{r_{ij+1}}{r_{ij}}\right)\sin\theta_j\sin\theta_i\right)\right]\\
&+V_\infty\sin\alpha\cos\theta_i + \sum_{j=1}^{N}\left[\frac{q_j}{2\pi}\left(-\ln\left(\frac{r_{ij+1}}{r_{ij}}\right)\sin\theta_j\cos\theta_i + \beta_{ij}\cos\theta_j\cos\theta_i\right)\right.\\
&\left.+\frac{\gamma}{2\pi}\left(\beta_{ij}\sin\theta_j\cos\theta_i + \ln\left(\frac{r_{ij+1}}{r_{ij}}\right)\cos\theta_j\cos\theta_i\right)\right] = 0
\end{aligned}
\tag{2.219}
$$

Grouping like terms:

$$
\begin{aligned}
&\sum_{j=1}^{N}\left[\frac{q_j}{2\pi}\left(\ln\left(\frac{r_{ij+1}}{r_{ij}}\right)(\cos\theta_j\sin\theta_i - \sin\theta_j\cos\theta_i) + \beta_{ij}(\sin\theta_j\sin\theta_i + \cos\theta_j\cos\theta_i)\right)\right.\\
&\left.+\frac{\gamma}{2\pi}\left(\beta_{ij}(\sin\theta_j\cos\theta_i - \cos\theta_j\sin\theta_i) + \ln\left(\frac{r_{ij+1}}{r_{ij}}\right)(\sin\theta_j\sin\theta_i + \cos\theta_j\cos\theta_i)\right)\right]\\
&= V_\infty\cos\alpha\sin\theta_i - V_\infty\sin\alpha\cos\theta_i
\end{aligned}
\tag{2.220}
$$

Now we can simplify using trig identities:

$$\begin{aligned}
&\sum_{j=1}^{N}\left[\frac{q_j}{2\pi}\left(\ln\left(\frac{r_{ij+1}}{r_{ij}}\right)\sin(\theta_i-\theta_j)+\beta_{ij}\cos(\theta_i-\theta_j)\right)\right.\\
&\left.+\frac{\gamma}{2\pi}\left(-\beta_{ij}\sin(\theta_i-\theta_j)+\ln\left(\frac{r_{ij+1}}{r_{ij}}\right)\cos(\theta_i-\theta_j)\right)\right]\\
&=V_\infty\sin(\theta_i-\alpha)
\end{aligned} \tag{2.221}$$

Finally, we can write this a linear set of equations for q_j and γ of the form:

$$\sum_{j=1}^{N} A_{ij}q_j + A_{i,N+1}\gamma = b_i \tag{2.222}$$

where

$$\begin{aligned}
A_{ij} &= \left[\ln\left(\frac{r_{ij+1}}{r_{ij}}\right)\sin(\theta_i-\theta_j)+\beta_{ij}\cos(\theta_i-\theta_j)\right]\\
A_{iN+1} &= \sum_{j=1}^{N}\left[\ln\left(\frac{r_{ij+1}}{r_{ij}}\right)\cos(\theta_i-\theta_j)-\beta_{ij}\sin(\theta_i-\theta_j)\right]\\
b_i &= 2\pi V_\infty\sin(\theta_i-\alpha)
\end{aligned} \tag{2.223}$$

We need to be careful when computing the angles θ. Note that they only appear as sums and differences within sin and cosine function. We can use the sum and difference formulas:

$$\sin(\theta_i-\theta_j) = \sin\theta_i\sin\theta_j - \cos\theta_i\cos\theta_j \tag{2.224}$$

$$\cos(\theta_i-\theta_j) = \cos\theta_i\cos\theta_j + \sin\theta_i\sin\theta_j \tag{2.225}$$

With these expansions we never need to explicitly compute θ, but rather just use the formulas show in Eqs. 2.193 and 2.194 for $\sin\theta_i$ and $\cos\theta_i$. Alternatively, we can compute each θ_i directly, but we must use the `atan2` function. This is because $\sin^{-1}(0.5)$, for example, has multiple solutions, and the default implementation does not account for which quadrant we are. The function `atan2` on the other hand, looks at the signs of the components to determine the quadrant, and thus return a unique angle.

Now we have to enforce the Kutta condition (Eq. 2.202) and follow

more or less the same procedure. First, we substitute in (Eq. 2.216):

$$
\begin{aligned}
& u_1 \cos\theta_1 + v_1 \sin\theta_1 = -u_N \cos\theta_N - v_N \sin\theta_N \\
& \quad \Rightarrow \\
& \left(V_\infty \cos\alpha + \sum_{j=1}^{N} u_{s1j} + \sum_{j=1}^{N} u_{v1j} \right) \cos\theta_1 \\
& + \left(V_\infty \sin\alpha + \sum_{j=1}^{N} v_{s1j} + \sum_{j=1}^{N} v_{v1j} \right) \sin\theta_1 \\
& = -\left(V_\infty \cos\alpha + \sum_{j=1}^{N} u_{sNj} + \sum_{j=1}^{N} u_{vNj} \right) \cos\theta_N \\
& - \left(V_\infty \sin\alpha + \sum_{j=1}^{N} v_{sNj} + \sum_{j=1}^{N} v_{vNj} \right) \sin\theta_N
\end{aligned}
\tag{2.226}
$$

Next, we introduce the coordinate system transformation (Eq. 2.214):

$$
\begin{aligned}
& \left(V_\infty \cos\alpha + \sum_{j=1}^{N} \left(u^*_{s1j} \cos\theta_j - v^*_{s1j} \sin\theta_j + u^*_{v1j} \cos\theta_j - v^*_{v1j} \sin\theta_j \right) \right) \cos\theta_1 \\
& + \left(V_\infty \sin\alpha + \sum_{j=1}^{N} \left(u^*_{s1j} \sin\theta_j + v^*_{s1j} \cos\theta_j + u^*_{v1j} \sin\theta_j + v^*_{v1j} \cos\theta_j \right) \right) \sin\theta_1 \\
& = -\left(V_\infty \cos\alpha + \sum_{j=1}^{N} \left(u^*_{sNj} \cos\theta_j - v^*_{sNj} \sin\theta_j + u^*_{vNj} \cos\theta_j - v^*_{vNj} \sin\theta_j \right) \right) \cos\theta_N \\
& - \left(V_\infty \sin\alpha + \sum_{j=1}^{N} \left(u^*_{sNj} \sin\theta_j + v^*_{sNj} \cos\theta_j + u^*_{vNj} \sin\theta_j + v^*_{vNj} \cos\theta_j \right) \right) \sin\theta_N
\end{aligned}
\tag{2.227}
$$

Now the panel velocities (Eqs. 2.208 and 2.213):

$$
\begin{aligned}
&\left(V_\infty \cos\alpha + \sum_{j=1}^{N}\left(\frac{-q_j}{2\pi}\ln\left(\frac{r_{1j+1}}{r_{1j}}\right)\cos\theta_j - q_j\frac{\beta_{1j}}{2\pi}\sin\theta_j\right.\right.\\
&\quad\left.\left.+\gamma\frac{\beta_{1j}}{2\pi}\cos\theta_j - \frac{\gamma}{2\pi}\ln\left(\frac{r_{1j+1}}{r_{1j}}\right)\sin\theta_j\right)\right)\cos\theta_1\\
&+\left(V_\infty \sin\alpha + \sum_{j=1}^{N}\left(\frac{-q_j}{2\pi}\ln\left(\frac{r_{1j+1}}{r_{1j}}\right)\sin\theta_j + q_j\frac{\beta_{1j}}{2\pi}\cos\theta_j\right.\right.\\
&\quad\left.\left.+\gamma\frac{\beta_{1j}}{2\pi}\sin\theta_j + \frac{\gamma}{2\pi}\ln\left(\frac{r_{1j+1}}{r_{1j}}\right)\cos\theta_j\right)\right)\sin\theta_1\\
&= -\left(V_\infty \cos\alpha + \sum_{j=1}^{N}\left(\frac{-q_j}{2\pi}\ln\left(\frac{r_{Nj+1}}{r_{Nj}}\right)\cos\theta_j - q_j\frac{\beta_{Nj}}{2\pi}\sin\theta_j\right.\right.\\
&\quad\left.\left.+\gamma\frac{\beta_{Nj}}{2\pi}\cos\theta_j - \frac{\gamma}{2\pi}\ln\left(\frac{r_{Nj+1}}{r_{Nj}}\right)\sin\theta_j\right)\right)\cos\theta_N\\
&-\left(V_\infty \sin\alpha + \sum_{j=1}^{N}\left(\frac{-q_j}{2\pi}\ln\left(\frac{r_{Nj+1}}{r_{Nj}}\right)\sin\theta_j + q_j\frac{\beta_{Nj}}{2\pi}\cos\theta_j\right.\right.\\
&\quad\left.\left.+\gamma\frac{\beta_{Nj}}{2\pi}\sin\theta_j + \frac{\gamma}{2\pi}\ln\left(\frac{r_{Nj+1}}{r_{Nj}}\right)\cos\theta_j\right)\right)\sin\theta_N
\end{aligned}
\tag{2.228}
$$

Next we group terms:

$$
\begin{aligned}
&V_\infty(\sin\alpha\sin\theta_1+\cos\alpha\cos\theta_1)\\
&+\sum_{j=1}^{N}\left[\frac{-q_j}{2\pi}\ln\left(\frac{r_{1j+1}}{r_{1j}}\right)\left(\cos\theta_j\cos\theta_1+\sin\theta_j\sin\theta_1\right)\right.\\
&\qquad\left.+q_j\frac{\beta_{1j}}{2\pi}\left(\cos\theta_j\sin\theta_1-\sin\theta_j\cos\theta_1\right)\right]\\
&+\sum_{j=1}^{N}\left[\gamma\frac{\beta_{1j}}{2\pi}(\sin\theta_j\sin\theta_1+\cos\theta_j\cos\theta_1)\right.\\
&\qquad\left.+\frac{\gamma}{2\pi}\ln\left(\frac{r_{1j+1}}{r_{1j}}\right)(\cos\theta_j\sin\theta_1-\sin\theta_j\cos\theta_1)\right]\\
&=-V_\infty(\cos\alpha\cos\theta_N+\sin\alpha\sin\theta_N)\\
&+\sum_{j=1}^{N}\left[\frac{q_j}{2\pi}\ln\left(\frac{r_{Nj+1}}{r_{Nj}}\right)(\cos\theta_j\cos\theta_N+\sin\theta_j\sin\theta_N)\right.\\
&\qquad\left.-q_j\frac{\beta_{Nj}}{2\pi}(\cos\theta_j\sin\theta_N-\sin\theta_j\cos\theta_N)\right]\\
&+\sum_{j=1}^{N}\left[-\gamma\frac{\beta_{Nj}}{2\pi}(\sin\theta_j\sin\theta_N+\cos\theta_j\cos\theta_N)\right.\\
&\qquad\left.-\frac{\gamma}{2\pi}\ln\left(\frac{r_{Nj+1}}{r_{Nj}}\right)(\cos\theta_j\sin\theta_N-\sin\theta_j\cos\theta_N)\right]
\end{aligned}
\quad , \tag{2.229}
$$

use trig identities:

$$
\begin{aligned}
&V_\infty\cos(\theta_1-\alpha)\\
&+\sum_{j=1}^{N}\left[\frac{-q_j}{2\pi}\ln\left(\frac{r_{1j+1}}{r_{1j}}\right)\cos(\theta_1-\theta_j)+q_j\frac{\beta_{1j}}{2\pi}\sin(\theta_1-\theta_j)\right]\\
&+\sum_{j=1}^{N}\left[\gamma\frac{\beta_{1j}}{2\pi}\cos(\theta_1-\theta_j)+\frac{\gamma}{2\pi}\ln\left(\frac{r_{1j+1}}{r_{1j}}\right)\sin(\theta_1-\theta_j)\right]\\
&=-V_\infty\cos(\theta_N-\alpha)\\
&+\sum_{j=1}^{N}\left[\frac{q_j}{2\pi}\ln\left(\frac{r_{Nj+1}}{r_{Nj}}\right)\cos(\theta_N-\theta_j)-q_j\frac{\beta_{Nj}}{2\pi}\sin(\theta_N-\theta_j)\right]\\
&+\sum_{j=1}^{N}\left[-\gamma\frac{\beta_{Nj}}{2\pi}\cos(\theta_N-\theta_j)-\frac{\gamma}{2\pi}\ln\left(\frac{r_{Nj+1}}{r_{Nj}}\right)\sin(\theta_N-\theta_j)\right]
\end{aligned}
\quad , \tag{2.230}
$$

and simplify

$$\begin{aligned}
&\sum_{j=1}^{N}\Bigg[q_j\beta_{1j}\sin(\theta_1-\theta_j)-q_j\ln\left(\frac{r_{1j+1}}{r_{1j}}\right)\cos(\theta_1-\theta_j)\\
&+q_j\beta_{Nj}\sin(\theta_N-\theta_j)-q_j\ln\left(\frac{r_{Nj+1}}{r_{Nj}}\right)\cos(\theta_N-\theta_j)\\
&+\gamma\beta_{1j}\cos(\theta_1-\theta_j)+\gamma\ln\left(\frac{r_{1j+1}}{r_{1j}}\right)\sin(\theta_1-\theta_j)\\
&+\gamma\beta_{Nj}\cos(\theta_N-\theta_j)+\gamma\ln\left(\frac{r_{Nj+1}}{r_{Nj}}\right)\sin(\theta_N-\theta_j)\Bigg]\\
&=-2\pi V_\infty(\cos(\theta_1-\alpha)+\cos(\theta_N-\alpha))
\end{aligned} \tag{2.231}$$

We can write this in the linear form:

$$\sum_{j=1}^{N}A_{N+1,j}q_j+A_{N+1,N+1}\gamma=b_{N+1} \tag{2.232}$$

where

$$\begin{aligned}
A_{N+1,j}&=\sum_{k=1\text{ and }N}\left[\beta_{kj}\sin(\theta_k-\theta_j)-\ln\left(\frac{r_{kj+1}}{r_{kj}}\right)\cos(\theta_k-\theta_j)\right]\\
A_{N+1,N+1}&=\sum_{k=1\text{ and }N}\left(\sum_{j=1}^{N}\left[\beta_{kj}\cos(\theta_k-\theta_j)+\ln\left(\frac{r_{kj+1}}{r_{kj}}\right)\sin(\theta_k-\theta_j)\right]\right)\\
b_{N+1}&=-2\pi V_\infty\left[\cos(\theta_1-\alpha)+\cos(\theta_N-\alpha)\right]
\end{aligned} \tag{2.233}$$

Now we can assemble the no-flow-through conditions and the Kutta condition in one large matrix:

$$\begin{bmatrix} A_{11} & \cdots & A_{1N} & A_{1,N+1}\\ \vdots & & \vdots & \vdots\\ A_{N1} & \cdots & A_{NN} & A_{N,N+1}\\ A_{N+1,1} & \cdots & A_{N+1,N} & A_{N+1,N+1}\end{bmatrix}\begin{bmatrix} q_1\\ \vdots\\ q_N\\ \gamma\end{bmatrix}=\begin{bmatrix} b_1\\ \vdots\\ b_N\\ b_{N+1}\end{bmatrix} \tag{2.234}$$

This is a linear system that we can solve for q and γ. With known source and vortex strengths we then compute the pressure coefficient.

We know the normal velocity is zero at each panel so we just need to compute the tangential velocity (using Eq. 2.195), substituting in the velocity components (Eq. 2.216), making a coordinate transformation (Eq. 2.214), grouping terms, and using trig identities:

$$
\begin{aligned}
V_{ti} &= u_i \cos\theta_i + v_i \sin\theta_i \\
&= \left(V_\infty \cos\alpha + \sum_{j=1}^{N}(u_{sij} + u_{vij})\right)\cos\theta_i + \left(V_\infty \sin\alpha + \sum_{j=1}^{N}(v_{sij} + v_{vij})\right)\sin\theta_i \\
&= \left(V_\infty \cos\alpha + \sum_{j=1}^{N}(u^*_{sij}\cos\theta_j - v^*_{sij}\sin\theta_j + u^*_{vij}\cos\theta_j - v^*_{vij}\sin\theta_j)\right)\cos\theta_i \\
&\quad + \left(V_\infty \sin\alpha + \sum_{j=1}^{N}(u^*_{sij}\sin\theta_j + v^*_{sij}\cos\theta_j + u^*_{vij}\sin\theta_j + v^*_{vij}\cos\theta_j\right)\sin\theta_i \\
&= V_\infty \cos(\theta_i - \alpha) \\
&\quad + \sum_{j=1}^{N}\left[u^*_{sij}\cos(\theta_i - \theta_j) + v^*_{sij}\sin(\theta_i - \theta_j) + u^*_{vij}\cos(\theta_i - \theta_j) + v^*_{vij}\sin(\theta_i - \theta_j)\right]
\end{aligned}
\tag{2.235}
$$

We now substitute in the panel velocities (Eqs. 2.208 and 2.213):

$$
\begin{aligned}
&= V_\infty \cos(\theta_i - \alpha) \\
&\quad + \sum_{j=1}^{N}\left[\frac{-q_j}{2\pi}\ln\left(\frac{r_{ij+1}}{r_{ij}}\right)\cos(\theta_i - \theta_j)\right. \\
&\quad + q_j\frac{\beta_{ij}}{2\pi}\sin(\theta_i - \theta_j) \\
&\quad + \gamma\frac{\beta_{ij}}{2\pi}\cos(\theta_i - \theta_j) \\
&\quad \left. + \frac{\gamma}{2\pi}\ln\left(\frac{r_{ij+1}}{r_{ij}}\right)\sin(\theta_i - \theta_j)\right]
\end{aligned}
\tag{2.236}
$$

The final result is then:

$$
\begin{aligned}
V_{t\,i} &= V_\infty \cos(\theta_i - \alpha) \\
&\quad + \frac{1}{2\pi} \sum_{j=1}^{N} \left[q_j \left(\beta_{ij} \sin(\theta_i - \theta_j) - \ln\left(\frac{r_{ij+1}}{r_{ij}}\right) \cos(\theta_i - \theta_j) \right) \right] \\
&\quad + \frac{\gamma}{2\pi} \sum_{j=1}^{N} \left[\beta_{ij} \cos(\theta_i - \theta_j) + \ln\left(\frac{r_{ij+1}}{r_{ij}}\right) \sin(\theta_i - \theta_j) \right]
\end{aligned}
\tag{2.237}
$$

The pressure coefficient is then given by (since the normal velocity is zero):

$$
C_p(\bar{x}_i, \bar{x}_j) = 1 - \left(\frac{V_{ti}}{V_\infty}\right)^2 \tag{2.238}
$$

and is assumed to be constant over a given panel.

Viscous Flow

3

In the last chapter we saw that panel methods are an effective technique for irrotational flows, a reasonable assumption for attached, low speed flows, outside the boundary layer. To extend the utility of the methods we turn our attention to numerical methods for resolving boundary layers and computing drag.

3.1 Boundary Layer Fundamentals

The presence of viscosity alters flow behavior. Recall the discussion on shear stress and the no slip condition discussed in Section 1.3. The shear stress is proportional to the velocity gradients (Eq. 1.10). Because the velocity is zero at a solid wall, near the wall the velocity gradients will be large, and thus the shear stresses will be significant. For a streamlined body, only this near-wall region is significantly affected by viscosity — a region we call the *boundary layer*. It is called the boundary layer because it only occurs near the boundary of the solid object, and is generally small relative to the size of the body.

Within the boundary layer viscous effects are important, and outside of the boundary layer we can treat the flow as inviscid. This behavior allows us to re-use the inviscid flow behavior studied in the previous chapter, with some modifications confined to a small region. To be clear, the behavior is continuous and there is no actual clear line that divides viscous behavior from inviscid. Still, it will be useful to define a boundary layer "height", and we will discuss a few definitions for boundary layer size in this chapter.

For blunt bodies, or streamlined bodies at high angles of attack (which act like a blunt body), flow separation occurs and a wake develops. Once flow separation occurs there is no longer a boundary layer and viscous behavior extends across a large region comparable to the body size. We can no longer "correct" inviscid flow solutions as the viscous effects are widespread.

Figure 3.1 depicts many of the features seen in a boundary layer and viscous flows in general. For now we will just run through a quick overview, and subsequently will discuss these features in more

detail. Starting from a stagnation point the boundary layer begins as laminar. Over some region the boundary layer instabilities become significant and the boundary layer transitions to a turbulent boundary layer. Eventually, the boundary layer will separate from the body and leave behind a wake. Ideally, for a streamlined body, this separation occurs right at the trailing edge of the body. From this figure we see two mechanism for drag. The first, is drag from the shear stresses acting over the body. We call this *skin-friction drag*. The second, is the momentum deficit caused by the wake and depicted on the right of Fig. 3.1. This deficit leads to a lower pressure on the trailing-edge side, and we call this *pressure drag*. It is primarily affected by the shape of the body. Note that while separation was shown as occurring after turbulent flow in Fig. 3.1, separation can sometimes occur in the laminar region.

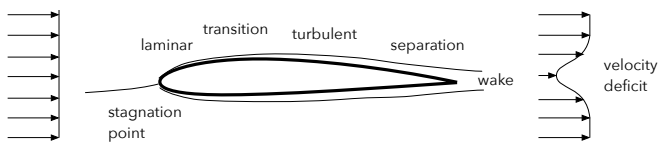

Fig. 3.1 Depiction of salient features for viscous flow around a body.

The word *laminar* suggests multiple laminae, or layers. Conceptually, it is meant to describe flow behavior that acts like multiple distinct layers passing over each other (i.e., slow layers near the wall and faster layers away from the wall). In laminar flow there is mixing across the layers, but it not readily visible as the mixing primarily occurs at molecular scales. In contrast a *turbulent* flow has unsteady mixing across multiple scales (small to large). Because the mixing occurs on larger scales the flow is affected across a larger region and thus the boundary layer height is larger as compared to laminar flow (see Fig. 3.2). Also because a turbulent boundary creates more mixing, the velocity gradient is larger at the wall, and thus the shear stress at the wall is also larger (see again Fig. 3.2).

The shear stress at the wall is given by:

$$\tau_w = \mu \left.\frac{\partial u}{\partial y}\right|_{y=0} \tag{3.1}$$

Because we are often interested in normalized values, we normalize this shear stress in the *skin friction coefficient*:

$$c_f = \frac{\tau_w}{\frac{1}{2}\rho V_e^2} \tag{3.2}$$

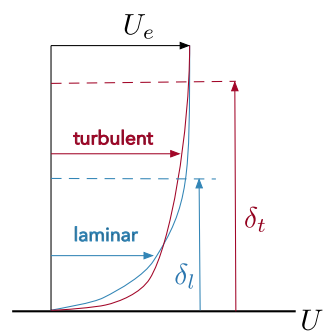

Fig. 3.2 An overlaid laminar and turbulent boundary layer.

where V_e is called the *edge velocity*, or the velocity just outside of the boundary layer.

Transition refers to the change from a laminar boundary layer to a turbulent one. We often think of transition occurring at a specific point, but it really occurs over a region. The mechanism of transition is the growth of instabilities in the boundary layer. For low Reynolds number instabilities are damped (the viscous forces are high relative to inertial) and the flow remains laminar. For high Reynolds numbers the instabilities are amplified causing the large-scale mixing of turbulent flow. For a flat plate transition occurs at a Reynolds number of approximately: $Re = 2 \times 10^5$–3×10^6. As the flow progresses over a solid surface, the length of the boundary layer becomes longer, and thus the local Reynolds number grows, eventually leading to transition.

The primary factors that affect transition are discussed below. The freestream conditions are a significant factor (i.e., density, viscosity, speed, turbulence level, noise). If the incoming flow is already highly turbulent, then transition will occur more quickly. Pressure gradients are a major factor. Even a very small adverse gradient can cause transition. The surface roughness of the body is another major factor. A rougher surface will amplify instabilities and lead to earlier transition. As discussed in the paragraphs following Ex. 1.3, sometimes roughness elements are intentionally added over a wing to trigger turbulent flow. Heat transfer is a less common, but potentially important factor. Cooling can be used to stabilize a boundary layer. Suction and blowing is an active strategy that is sometimes used to delay boundary layer transition.

Separation refers to the flow detaching from the surface and creating a wake. The process is depicted in Fig. 3.3. Recall the discussion surrounding Fig. 1.8 regarding an adverse pressure gradient. In an adverse pressure gradient, the fluid near the wall slows down until eventually the velocity gradient is zero (vertical), the flow separates, and after that point the flow near the wall may be reversed in the eddies of the resultant wake. Because the velocity gradient is zero at the point of separation, the shear stress is also zero (Eq. 3.1). Checking for zero shear stress is one way to detect separation numerically. This fact also explains why one should avoid creating stagnation points in an adverse pressure gradient. Slowing the velocity to zero means the flow is guaranteed to separate. A common engineering solution is to use a fairing to avoid the stagnation.

Separation generally leads to a massive increase in drag, and a significant drop in lift. Once separation occurs, the flow may reattach, especially if it occurs early on the body. When this occurs, the separation

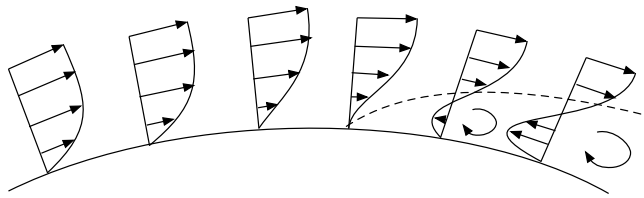

Fig. 3.3 Fluid near the wall slows down until eventually it separates.

and reattachment points envelope a recirculating region known as a *separation bubble* (and because this has to occur early on the body to provide a chance to reattach, it usually separates in the laminar region, becomes turbulent then reattaches, and is called a laminar separation bubble).

As shown in Fig. 3.2, a turbulent boundary layer has higher velocities closer to the surface, and is thus more resistant to separation. This creates a common design tradeoff where turbulent flow may be desirable in delaying pressure drag increases, but at a cost of higher skin friction drag. A classic example is a golf ball. From Fig. 1.8 we note the large drop in drag for a cylinder, which occurs after the transition to turbulence. This is because the turbulent boundary layer delays separation longer, resulting in a smaller wake, and less pressure drag. For higher Reynolds numbers, the skin friction drag grows and so the curve starts to rise again.

For a streamlined body the pressure drag is (hopefully) significantly smaller than the skin friction drag, and so more substantial laminar flow may be desirable. However, a 100% laminar flow airfoil is actually not very useful. For it to not separate it would have to be made very thin and be restricted to a narrow range of small lift coefficients. So although laminar flow is desirable to a point, we still want the airfoil to transition to turbulent flow at some point so it is more robust against separation across various conditions. Even if separation does not occur, the presence of viscosity can significantly alter the pressure distribution (or equivalently can be thought of as altering the effective shape of the body). We will revisit this idea again later in this chapter.

While the discussion of this section focused on drag, as that is the primary effect of viscosity, it also affects the lift. Notably the lift curve slope is often slightly reduced by the presence of viscosity. And, once separated, a precipitous drop in lift occurs, which is known as *stall* (see Fig. 3.4).

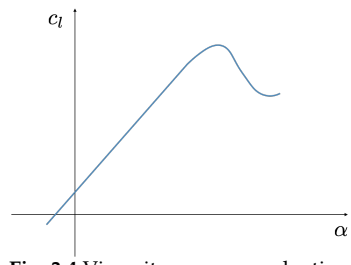

Fig. 3.4 Viscosity causes a reduction in lift curve slope and flow separation causes stall.

3.2 Boundary Layer Equations

In this section we would like to deriver a simplified version of the Navier Stokes equations that is applicable within the boundary layer. We start with the steady, compressible, 2D Navier Stokes equations (neglecting the normal shear stresses τ_{xx} and τ_{yy}, which are typically insignificant).

$$\begin{aligned}
\frac{\partial(\rho u)}{\partial x} + \frac{\partial(\rho v)}{\partial y} &= 0 \\
\rho\left(u\frac{\partial u}{\partial x} + v\frac{\partial u}{\partial y}\right) &= -\frac{\partial p}{\partial x} + \frac{\partial}{\partial y}\left[\mu\left(\frac{\partial u}{\partial y} + \frac{\partial v}{\partial x}\right)\right] \\
\rho\left(u\frac{\partial v}{\partial x} + v\frac{\partial v}{\partial y}\right) &= -\frac{\partial p}{\partial y} + \frac{\partial}{\partial x}\left[\mu\left(\frac{\partial u}{\partial y} + \frac{\partial v}{\partial x}\right)\right]
\end{aligned} \tag{3.3}$$

In the boundary layer, we use the coordinate direction x to follow the surface that the boundary layer is developing on, and y as a direction normal to the local surface (Fig. 3.5). Our first assumption is that we can still use the Cartesian form of our governing equations shown above, but with our boundary layer definition of x and y, which are not actually Cartesian. This assumes that the boundary layer height is very small relative to the local radius of curvature, a reasonable assumption for most streamlined shapes (similar like the locally flat assumption of the ground we might use when predicting local behavior, even though the Earth surface is curved). A centrifugal pressure gradient term can be added if the curvature is significant, but for our purposes we will assume that it is not.

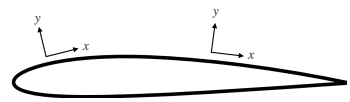

Fig. 3.5 Local coordinates in boundary layer that follow the profile of the blade.

Within the boundary layer we anticipate that some of the terms are much smaller than others, and thus can be neglected to give us a simplified set of equations appropriate for analysis only within the boundary layer. We derive this simplified set of equations by examining the order of magnitude of each term. We assume that the boundary layer height (δ) is much smaller than the distance the boundary layer covers (L). Those lengths also provide appropriate length scales for y and x respectively. We know that the horizontal velocity is V_e just outside the boundary layer, by definition, and zero at the surface, so a typical order of magnitude for the horizontal velocity is V_e. Then, from an order-of-magnitude analysis using the continuity equation above (ignoring the minor changes in density), we know that the two terms must balance each other so we expect that:

$$\frac{V_e}{L} \propto \frac{v}{\delta} \tag{3.4}$$

Or, in other words:

$$v \propto \frac{\delta}{L} V_e \tag{3.5}$$

This provides us with a scale for the vertical velocities in the boundary layer, which we see will be much smaller than the horizontal velocities.

Examining the first and second terms of the x momentum equation, with an order of magnitude analysis, we expect that:

$$\rho u \frac{\partial u}{\partial x} \propto \frac{\rho V_e^2}{L} \tag{3.6}$$

and

$$\rho v \frac{\partial u}{\partial y} \propto \rho \frac{\delta}{L} V_e \frac{V_e}{\delta} \propto \frac{\rho V_e^2}{L^2} \tag{3.7}$$

Thus, we see that both of these inertial terms are of similar magnitudes.

Pressure just outside the boundary layer is proportional to the dynamic pressure of the edge velocity, so we assume that

$$\frac{\partial p}{\partial x} \propto \frac{\rho V_e^2}{L}, \tag{3.8}$$

which is also of the same magnitude.

The viscous terms are:

$$\frac{\partial}{\partial y}\left[\mu \frac{\partial u}{\partial y}\right] \propto \mu \frac{V_e}{\delta^2} \tag{3.9}$$

and

$$\frac{\partial}{\partial y}\left[\mu \frac{\partial v}{\partial x}\right] \propto \mu \frac{V_e}{L^2} \tag{3.10}$$

Comparing these two terms we see that the first is much larger than the second, and so the second term can be neglected within the boundary layer.

We know that we cannot neglect both viscous terms as compared to our inertial terms, otherwise this wouldn't be much of a boundary layer, so that means that those two terms must be of similar magnitudes:

$$\frac{\rho V_e^2}{L} \propto \mu \frac{V_e}{\delta^2} \tag{3.11}$$

or

$$\mu \propto \frac{\rho V_e \delta^2}{L} \tag{3.12}$$

We can express this in terms of a Reynolds number for the flow just outside the boundary layer:

$$\frac{\delta}{L} = \frac{1}{\sqrt{Re_L}} \tag{3.13}$$

where $Re_L = \rho V_e L/\mu$ In other words, are assumption that δ is small compared to L is analogous to assuming that the Reynolds number is large.

We now apply the same analysis to the y momentum equation. The order of magnitude analysis results in:

$$\rho u \frac{\partial v}{\partial x} \propto \frac{\rho V_e^2 \delta}{L^2} \tag{3.14}$$

$$\rho v \frac{\partial v}{\partial y} \propto \frac{\rho V_e^2 \delta}{L^2} \tag{3.15}$$

$$\frac{\partial p}{\partial y} \propto \frac{\rho V_e^2}{\delta} \tag{3.16}$$

$$\frac{\partial}{\partial x}\left[\mu \frac{\partial u}{\partial y}\right] \propto \frac{\rho V_e^2 \delta}{L^2} \tag{3.17}$$

$$\frac{\partial}{\partial x}\left[\mu \frac{\partial v}{\partial x}\right] \propto \frac{\rho V_e^2 \delta^3}{L^4} \tag{3.18}$$

If we factor out $\rho V_e^2/L$ from each term, for easier comparison, we see that the first, second, and fourth terms are of magnitude δ/L whereas the pressure term is of magnitude $1/(\delta/L)$, and the last is $(\delta/L)^3$. In other words, the pressure term is much larger than all the other terms and so we can neglect all others except pressure.

Dropping all of the small terms (one viscous term in x momentum, and all but the pressure term in the y momentum) results in the *boundary layer equations*:

$$\begin{aligned} \frac{\partial(\rho u)}{\partial x} + \frac{\partial(\rho v)}{\partial y} &= 0 \\ \rho\left(u\frac{\partial u}{\partial x} + v\frac{\partial u}{\partial y}\right) &= -\frac{\partial p}{\partial x} + \frac{\partial}{\partial y}\left(\mu\frac{\partial u}{\partial y}\right) \\ \frac{\partial p}{\partial y} &= 0 \end{aligned} \tag{3.19}$$

The last equation says that pressure is independent of y. In other words, at a given x location, the pressure at the surface of the object will be the same as the pressure at the edge of the boundary layer. This is quite fortunate as it means the pressure field we find from an inviscid solution is the same pressure felt directly by the body without modification by the boundary layer (as long as we account for the effective shape changes caused by the boundary layer—a topic discussed later). While the boundary layer equations are an approximation of the full Navier Stokes equations, experimental data supports this conclusion.

If pressure is not dependent on y then it is only a function of x and the partial derivative becomes a total derivative:

$$\frac{\partial p}{\partial x} \rightarrow \frac{dp}{dx} \tag{3.20}$$

Furthermore, since the pressure just outside the boundary layer, is the same all the way through the boundary layer (not a function of y), then we can compute dp/dx just outside the boundary layer. If just outside the boundary layer, then we can assume the flow is inviscid and use Euler's equation. We use the subscript e to refer to "edge" properties, or in other words the inviscid solution just outside the boundary layer. Euler's equation gives:

$$\frac{dp}{dx} = -\rho V_e \frac{dV_e}{dx} \tag{3.21}$$

We substitute the above into the boundary layer equations.

$$\begin{aligned} \frac{\partial(\rho u)}{\partial x} + \frac{\partial(\rho v)}{\partial y} &= 0 \\ \rho\left(u\frac{\partial u}{\partial x} + v\frac{\partial u}{\partial y}\right) &= \rho V_e \frac{dV_e}{dx} + \frac{\partial}{\partial y}\left(\mu\frac{\partial u}{\partial y}\right) \end{aligned} \tag{3.22}$$

If will also make the assumption of incompressibility then we can pull density out of the first equation, and viscosity can come out of the derivative (normally it is a function of temperature, but if the flow is incompressible then temperature is constant).

$$\begin{aligned} \frac{\partial u}{\partial x} + \frac{\partial v}{\partial y} &= 0 \\ u\frac{\partial u}{\partial x} + v\frac{\partial u}{\partial y} &= V_e \frac{dV_e}{dx} + \nu\frac{\partial^2 u}{\partial y^2} \end{aligned} \tag{3.23}$$

Keep in mind, that V_e is not an unknown, but rather an input from the outer inviscid solution.

This set of equations is still nonlinear, but it is easier to solve than the original Navier Stokes equations. The Navier Stokes are an *elliptic* PDE because it contains second derivatives in both x and y. Physically, an elliptic PDE requires defining boundary conditions in all directions. The boundary layer equations are a *parabolic* PDE because second derivatives only appear in one variable, y. Parabolic PDEs do not require boundary conditions in all directions, but instead can use a "time" marching approach (like the wave equation). That means we just need to specify conditions on one end (i.e., upstream), and then we can march the solution downstream.

Even though the equations are simpler, few analytic solutions exist. We will explore one of these, but for the most part these analytic solutions are of less interest as their pertain to simplified geometries and flow conditions. Typically we are interested in arbitrary geometries and so will use numerical solutions to solve for boundary layers. These methods are useful as long as the boundary layers remain attached, and do not have excessive curvature.

3.2.1 Displacement and Momentum Thickness

While we have talked about the "height" of the boundary layer, it is not clear how we should quantify this, and in fact multiple approaches exist. The two most important ones are the displacement thickness and the momentum thickness. The displacement thickness is the distance we would need to displace the wall so that an exterior inviscid flow (i.e., at V_e) would have the same mass flow rate as that actual flow. For example, the left side of Fig. 3.6 shows a boundary layer, and the mass flow deficit is the area colored in red. On the right side of figure we have an inviscid flow with the body displaced just enough so that the red area is equal to corresponding area on the left. From the above definition, δ^* is the height of the red rectangle on the right.

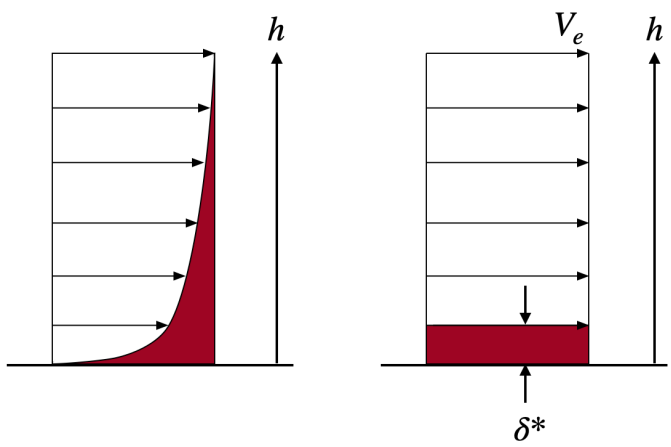

Fig. 3.6 A depiction of displacement thickness, where the actual flow is on the left, and the idealized displacement thickness is shown on the right.

The mass flow rate on the left is:

$$\dot{m} = \int_0^h \rho u dy \tag{3.24}$$

and on the right the mass flow rate is (we keep the first term as an integral for convenience in the rest of the derivation):

$$\int_0^h \rho_e V_e dy - \rho_e V_e \delta^* \tag{3.25}$$

We now equate these two mass flow rates:

$$\int_0^h \rho u dy = \int_0^h \rho_e V_e dy - \rho_e V_e \delta^* \tag{3.26}$$

Rearraning:

$$\rho_e V_e \delta^* = \int_0^h (\rho_e V_e - \rho u) dy \tag{3.27}$$

Then solving for δ^* gives:

$$\delta^* = \int_0^h \left(1 - \frac{\rho u}{\rho_e V_e}\right) dy \tag{3.28}$$

As $y \to h$ the term $\rho u \to \rho_e V_e$ and so the integrand approaches zero. Thus, we can extend the integration limits without changing the result. By convention, since the end limit h is not precise, the integration is extended to infinity.

$$\boxed{\delta^* = \int_0^\infty \left(1 - \frac{\rho u}{\rho_e V_e}\right) dy} \tag{3.29}$$

If incompressible, then the densities cancel out.

One physical meaning of the displacement thickness is that it tells us how much larger we should to make the body in the inviscid flow simulation to simulate the presence of the boundary layer (Fig. 3.7). The actual viscous flow experiences a decrease in mass flow because of the boundary layer, which could be treated as an inviscid flow around a larger body (larger by the displacement thickness).

Thus, one approach to account for the boundary layer is to first solve the inviscid flow (e.g., panel method) with the original body to get V_e, then solve the boundary layer equations to get δ^*, next modify the body shape using the displacement thickness, and repeat the process as needed. The main difficulty with this approach is that it requires modifying the geometry and repaneling the geometry, which can be challenging and computationally expensive.

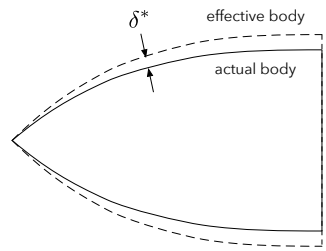

Fig. 3.7 The displacement thickness provides an "effective" shape for the body in a viscous flow.

An easier, and more common approach, is to keep the geometry as is but modify the boundary condition using the *transpiration velocity*. For the original inviscid flow solution the surface boundary condition is the no flow through condition $V_n = 0$. However, with a boundary layer we are actually solving the inviscid solution outside of the boundary layer, and at the edge of the boundary layer the normal velocity is not necessarily zero. Thus, if can find an expression for V_n we can use our original geometry but modify the boundary condition.

To find an appropriate value for V_n, we first apply the continuity equation in the boundary layer:

$$\frac{\partial(\rho u)}{\partial x} + \frac{\partial(\rho v)}{\partial y} = 0 \tag{3.30}$$

and in the external flow:

$$\frac{\partial(\rho_e V_e)}{\partial x} + \frac{\partial(\rho_e V_n)}{\partial y} = 0 \tag{3.31}$$

where V_n is the normal velocity We subtract the second equation from the first, and integrate across the boundary layer.

$$\int_0^h \frac{\partial}{\partial x}(\rho_e V_e - \rho u)dy = \int_0^h \frac{\partial}{\partial y}(\rho v - \rho_e V_n)dy \tag{3.32}$$

The order of differentiating and integrating can be swapped for the first term, and in the second term the integral and differentiation cancel out.

$$\frac{\partial}{\partial x}\left[\rho_e V_e \left(\int_0^h \left(1 - \frac{\rho u}{\rho V_e}\right) dy\right)\right] = [\rho v - \rho_e V_e]_0^h \tag{3.33}$$

$$= (\rho_e V_n - \rho_e V_n) - (0 - \rho_e V_n) \tag{3.34}$$

$$= \rho_e V_n \tag{3.35}$$

The term in parenthesis on the left is the displacement thickness. Thus, we have our new boundary condition:

$$V_n = \frac{1}{\rho_e}\frac{d}{dx}(\rho_e V_e \delta^*) \tag{3.36}$$

For incompressible flow this simplifes to:

$$\boxed{V_n = \frac{d}{dx}(V_e \delta^*)} \tag{3.37}$$

The alternate procedure then is to analyze the geometry using an inviscid analysis to obtain V_e, then solve the boundary layer equations to obtain δ^*, next reanalyze the inviscid analysis using the modified boundary condition (with fixed geometry/paneling), and repeat as needed. Rather than a fixed point iteration, a more effective approach is to solve the equations in a coupled manner using Newton's method.

An alternative measure of boundary layer height is the momentum thickness, which we call θ. This is the distance we would need to displace the wall so that an exterior inviscid flow (i.e., at V_e) would have the same momentum flow rate as that actual flow.

On the left of Fig. 3.8 the true momentum flow rate is:

$$\int_0^h \rho u^2 dy \tag{3.38}$$

On the right side the momentum flow of this hypothetical scenario is:

$$\dot{m} V_e - \rho_e V_e^2 \theta \tag{3.39}$$

where the mass flow rate is reduced because of the displacement as shown in Eq. 3.24. Inserting that equation gives the following for the

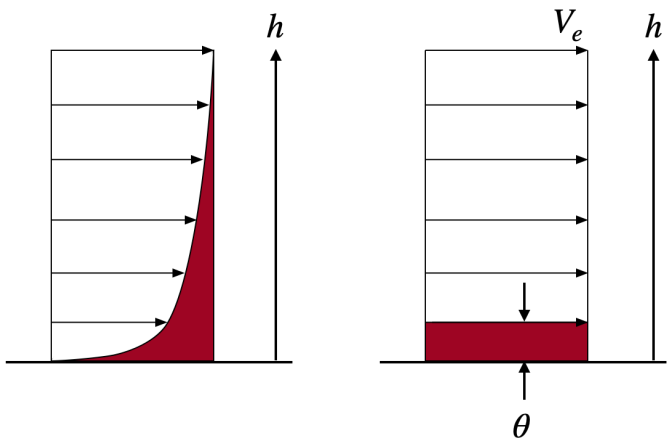

Fig. 3.8 A depiction of momentum thickness, where the actual flow is on the left, and the idealized momentum thickness is shown on the right.

right hand side:

$$\int_0^h \rho u V_e dy - \rho_e V_e^2 \theta \tag{3.40}$$

Equating the two momentum flow rates gives:

$$\int_0^h \rho u^2 dy = \int_0^h \rho u V_e dy - \rho_e V_e^2 \theta \tag{3.41}$$

Rearranging

$$\rho_e V_e^2 \theta = \int_0^h (\rho u V_e - \rho u^2) dy \tag{3.42}$$

then solving for θ and again extending the upper limit to infinity gives:

$$\theta = \int_0^\infty \frac{\rho u}{\rho_e V_e} \left(1 - \frac{u}{V_e}\right) dy \tag{3.43}$$

The primary usefulness of the momentum thickness is that it is a measure of momentum deficit, and thus is directly related to drag. For

example, the skin friction drag on a flat plate is proportional to the momentum thickness at the end of the plate:

$$D' = \rho V_e^2 \theta_L \tag{3.44}$$

where θ_L indicates the momentum thickness at $x = L$.

3.2.2 Laminar Flat Plate: Blasius Solution

There are a few analytic solutions to the boundary layer equations, and one that is particularly useful is the Blasius solution. It is a solution to laminar, incompressible, boundary layers over a flat plate with no pressure gradient. In this text we are less interested in analytic solutions to simple geometries and more interested in numerical solutions around arbitrary shapes so we will skip the derivation.

The results are:

$$\delta^* = \frac{1.72x}{\sqrt{Re_x}} \tag{3.45}$$

$$\theta = \frac{0.664x}{\sqrt{Re_x}} \tag{3.46}$$

where

$$Re_x = \frac{\rho V x}{\mu} \tag{3.47}$$

is the local Reynolds number.

The local skin friction coefficient is:

$$c_f = \frac{\tau}{q_\infty} = \frac{0.664}{\sqrt{Re_x}} \tag{3.48}$$

and the total skin friction coefficient, integrated across the plate, is:

$$C_f = \frac{1}{q_\infty L} \int_0^L \tau dx = \frac{1}{L} \int_0^L c_f dx = \frac{1.328}{\sqrt{Re_L}} \tag{3.49}$$

Notice the $1/\sqrt{x}$ behavior of the skin friction coefficient, suggesting that most of the skin friction drag occurs near the leading edge (at least within the laminar portion of the boundary layer).

The boundary layer equations can be solved for compressible laminar boundary layers also, but the result is a set of coupled ODEs that requires a numerical solution.

3.2.3 Turbulent Flat Plate: Schlichting

There is no analytic solution to turbulent boundary layers, so instead we rely on empirical fits. There are many such fits, one popular one

was developed by Schlichting for turbulent incompressible boundary layers on flat plates without a pressure gradient.

$$\delta^* = \frac{0.046x}{Re_x^{0.2}} \tag{3.50}$$

$$\theta = \frac{0.036x}{Re_x^{0.2}} \tag{3.51}$$

$$c_f = \frac{0.0592}{Re_x^{0.2}} \tag{3.52}$$

$$C_f = \frac{0.074}{Re_L^{0.2}} \tag{3.53}$$

Notice that, as expected, the boundary layer height and skin friction increases faster with x for a turbulent boundary layer as opposed to laminar.

3.2.4 Momentum Integral Equation

Exact solutions of the boundary layer equations are difficult to impossible in general cases. One of the main quantities we are interested in, with regards to a boundary layer analysis, is drag. An integral approach allows us to approximate the skin friction drag in a boundary layer. Just like differential and integral forms of the governing equation are both useful, we will derive an integral form of the mass and momentum equations within the boundary layer.

We consider a general case, and only at the end simplify for incompressible flow. Consider a control volume as shown in Fig. 3.9 for a small slice of the boundary layer. The control volume has a small width $\Delta x \to 0$, and it extends until the boundary layer reaches the edge velocity (or using standard boundary layer notation as $y/\delta \to \infty$). We will apply a mass and momentum balance to this control volume.

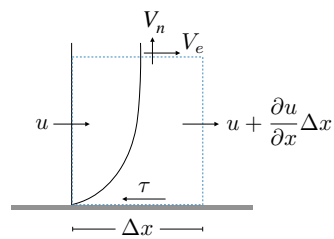

Fig. 3.9 A control volume within a boundary layer.

Steady mass balance:

The standard equation for a steady mass balance is:

$$\int \rho \vec{V} \cdot d\vec{A} = 0 \tag{3.54}$$

There is a boundary layer profile coming in on the left, and a different one leaving on the right, and there is also potentially some vertical velocity V_n of unknown magnitude and sign leaving through the top of the control volume as noted on the figure.

$$-\int_0^h \rho u dy + \int_0^h \left(\rho u + \frac{\partial(\rho u)}{\partial x}\Delta x\right) dy + \rho_e V_n \Delta x = 0 \tag{3.55}$$

The first integral cancels with part of the second integral, and then Δx cancels out of the remaining terms leaving:

$$\int_0^h \frac{\partial(\rho u)}{\partial x} dy + \rho_e V_n = 0 \tag{3.56}$$

Thus, we can solve for the unknown vertical velocity at the edge of the boundary layer.

$$V_n = -\frac{1}{\rho_e} \int_0^h \frac{\partial(\rho u)}{\partial x} dy \tag{3.57}$$

Steady momentum balance in the x-direction:

The general form for a steady momentum balance in the x-direction is:

$$\int \rho V_x (\vec{V} \cdot d\vec{A}) = -\int p d\vec{A}_x + F_x \tag{3.58}$$

Applying to our situation yields:

$$\begin{aligned} -\int_0^h \rho u^2 dy + \int_0^h \left(\rho u^2 + \frac{\partial(\rho u^2)}{\partial x}\Delta x\right) dy + V_e \rho_e V_n \Delta x = \\ \int_0^h p dy - \int_0^h \left(p + \frac{\partial p}{\partial x}\Delta x\right) dy - \tau \Delta x \end{aligned} \tag{3.59}$$

Most of the terms are straightforward. The mass flow rate out of the top is the same, but is multiplied by its x-component of velocity V_e. The pressure on the top surface is unknown, but because it is a vertical face it does not contribute any force in the x-direction. The shear stress creates a force on the fluid in the negative x-direction.

We can cancel terms just like in the mass balance:

$$\int_0^h \frac{\partial(\rho u^2)}{\partial x} dy + V_e \rho_e V_n = -\int_0^h \frac{\partial p}{\partial x} dy - \tau \tag{3.60}$$

Solving for τ and substituting in V_n from the mass balance (Eq. 3.57) gives the following expression for the shear stress:

$$\tau = -\int_0^h \frac{\partial p}{\partial x} dy - \int_0^h \frac{\partial(\rho u^2)}{\partial x} dy + V_e \int_0^h \frac{\partial(\rho u)}{\partial x} dy \tag{3.61}$$

Euler (outside boundary layer)

We can remove the pressure by using the 1D Euler momentum equation in differential form. Because we are considering the flow outside of the boundary layer, the flow is inviscid and so the Euler equation applies:

$$dp = -\rho V dV \tag{3.62}$$

Thus,

$$\frac{dp_e}{dx} = -\rho_e V_e \frac{dV_e}{dx} \tag{3.63}$$

The pressure derivative in Eq. 3.61 is actual a total derivative (and not a partial derivative) because according to the boundary layer approximation ($dp/dy = 0$) so p is only a function of x. Also the value of p is constant across the boundary layer (thus $p(x) = p_e(x)$. Thus, we can substitute this equation directly in.

Simplifying

Substituting this result back into Eq. 3.61 yields

$$\tau = \int_0^h \rho_e V_e \frac{dV_e}{dx} dy - \int_0^h \frac{\partial(\rho u^2)}{\partial x} dy + V_e \int_0^h \frac{\partial(\rho u)}{\partial x} dy \tag{3.64}$$

We can swap out the last term by using the chain rule:

$$\frac{\partial(\rho u V_e)}{\partial x} = \rho u \frac{\partial V_e}{\partial x} + V_e \frac{\partial(\rho u)}{\partial x} \tag{3.65}$$

Rearranging:

$$V_e \frac{\partial(\rho u)}{\partial x} = \frac{\partial(\rho u V_e)}{\partial x} - \rho u \frac{\partial V_e}{\partial x} \tag{3.66}$$

Substituting this result into Eq. 3.64 (and noting that V_e does not vary with y by definition and so the derivative is a total derivative) yields:

$$\tau = \int_0^h \rho_e V_e \frac{dV_e}{dx} dy - \int_0^h \frac{\partial(\rho u^2)}{\partial x} dy + \int_0^h \left(\frac{\partial(\rho u V_e)}{\partial x} - \rho u \frac{dV_e}{dx} \right) dy \tag{3.67}$$

We now collect like terms

$$\tau = \int_0^h (\rho_e V_e - \rho u) \frac{dV_e}{dx} dy + \int_0^h \frac{\partial(\rho u (V_e - u))}{\partial x} dy \tag{3.68}$$

In the first integral we note that dV_e/dx is independent of y and can thus be pulled out of the integral. We then multiply and divide that term by $\rho_e V_e$. For the second integral, we reverse the order of integration and differentiation, and multiply and divide that term by $\rho_e V_e^2$

$$\tau = \frac{dV_e}{dx} \rho_e V_e \int_0^h \left(1 - \frac{\rho u}{\rho_e V_e}\right) dy + \frac{\partial}{\partial x} \left(\rho_e V_e^2 \int_0^h \frac{\rho u}{\rho_e V_e} \left(1 - \frac{u}{V_e}\right) dy \right) \tag{3.69}$$

We see that the first integral is the definition of the displacement thickness δ^*, and the second integral is the definition of the momentum thickness θ.

$$\tau = \frac{dV_e}{dx} \rho_e V_e \delta^* + \frac{\partial}{\partial x} \left(\rho_e V_e^2 \theta \right) \tag{3.70}$$

Expanding the second derivative and noting the the partial derivative is a total derivative since all of the quantities do not change in y results in:

$$\tau = \frac{dV_e}{dx}\rho_e V_e \delta^* + \rho_e V_e^2 \frac{d\theta}{dx} + 2\rho_e V_e \frac{dV_e}{dx}\theta + \frac{d\rho_e}{dx} V_e^2 \theta \tag{3.71}$$

Dividing by $\rho_e V_e^2$ and collecting like terms gives:

$$\frac{\tau}{\rho_e V_e^2} = \frac{dV_e}{dx}\frac{1}{V_e}(\delta^* + 2\theta) + \frac{d\theta}{dx} + \frac{d\rho_e}{dx}\frac{1}{\rho_e}\theta \tag{3.72}$$

We now multiply the first term by $1/2$ on the top and bottom and use the definition of the local skin friction coefficient. For the second term we factor out θ and define a new variable called the shape factor: $H = \delta^*/\theta$. The variable H is related to the "health" of the boundary layer (with smaller H as healthier). A flat plate, for example, has a value of $H < 2.59$ for a favorable pressure gradient, and $H > 2.59$ for an adverse one. As H exceeds approximately 2.2 a laminar boundary layer will typically transition, whereas a turbulent boundary layer will typically separate.

$$\frac{1}{2}c_f = \frac{dV_e}{dx}\frac{\theta}{V_e}(H + 2) + \frac{d\theta}{dx} + \frac{d\rho_e}{dx}\frac{1}{\rho_e}\theta \tag{3.73}$$

Finally, we would like to relate the derivative of density to the derivative of velocity. If we assume that the flow outside the boundary layer is isentropic (an assumption that is consistent with the irrotationality assumption), that we can use the isentropic relationship

$$\frac{p}{\rho^\gamma} = \text{ constant} \tag{3.74}$$

Taking derivatives yields:

$$\frac{dp}{dx} = \frac{\gamma p}{\rho}\frac{d\rho}{dx} \tag{3.75}$$

Using the definition of the speed of sound gives

$$\frac{dp}{dx} = a^2 \frac{d\rho}{dx} \tag{3.76}$$

We again, make use of Euler's equation (since the flow can be assumed inviscid outside of the boundary layer), to relate pressure to velocity:

$$\frac{dp}{dx} = a^2 \frac{d\rho}{dx} = -\rho V \frac{dV}{dx} \tag{3.77}$$

Thus,

$$\frac{d\rho_e}{dx} = -\rho_e M_e^2 \frac{1}{V_e}\frac{dV_e}{dx} \tag{3.78}$$

We now substitute this expression into Eq. 3.73

$$\frac{1}{2}c_f = \frac{dV_e}{dx}\frac{\theta}{V_e}(H+2) + \frac{d\theta}{dx} + -M_e^2\frac{1}{V_e}\frac{dV_e}{dx}\theta \tag{3.79}$$

We can now combine like terms yielding the final result:

$$\frac{1}{2}c_f = \frac{d\theta}{dx} + \frac{dV_e}{dx}\frac{\theta}{V_e}\left(H+2-M_e^2\right) \tag{3.80}$$

This is the Von Kármán Momentum Integral Equation. We've been able to express the mass and momentum balance in a compact equation relating the important quantities in the boundary layer. If the flow is incompressible then that means $M_e \longrightarrow 0$ and we have the incompressible form:

$$\frac{1}{2}c_f = \frac{d\theta}{dx} + \frac{dV_e}{dx}\frac{\theta}{V_e}(H+2) \tag{3.81}$$

This equation contains too many unknowns to solve by itself (θ, H, c_f), but can be solved in connection with empirical relationships for laminar or turbulent boundary layers.

3.3 Thwaites' Method: Numerical Solution of Laminar Incompressible Boundary Layers

Consider a generic boundary layer as shown in Fig. 3.10. We typically draw it with the axes the other way, so that the boundary layer is vertical, but drawing it this way is more natural to look at the slope and curvature.

At the wall ($y = 0$) we know that $u = 0$ and $v = 0$. The only relevant velocity scale is V_e and a natural length scale is the momentum thickness θ. Thus, at the wall we expect that:

$$\left(\frac{\partial u}{\partial y}\right)_w \propto \frac{V_e}{\theta} \tag{3.82}$$

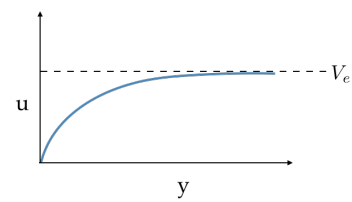

Fig. 3.10 A depiction of the boundary layer (rotated from our typical perspective).

Thwaites postulated that for a laminar boundary layer the proportionality is linear, so we can write this as an equality by multiplying by some unknown scalar l.

$$\left(\frac{\partial u}{\partial y}\right)_w = \frac{V_e}{\theta}l \tag{3.83}$$

Similarly, we expect the curvature to follow the form:

$$\left(\frac{\partial u^2}{\partial y^2}\right)_w \propto -\frac{V_e}{\theta^2} \tag{3.84}$$

Again, the assumption is that we can multiply by a unknown scalar (λ) to form an equality:

$$\left(\frac{\partial u^2}{\partial y^2}\right)_w = -\frac{V_e}{\theta^2}\lambda \tag{3.85}$$

In the above we have assumed negative curvature (which is indicative of a healthy boundary layer), but the sign of λ will allow the curvature to change.

We use our boundary layer momentum equation (Eq. 3.23):

$$u\frac{\partial u}{\partial x} + v\frac{\partial u}{\partial y} = V_e\frac{dV_e}{dx} + \nu\frac{\partial^2 u}{\partial y^2} \tag{3.86}$$

and substitute in values at the wall.

$$0 = V_e\frac{dV_e}{dx} - \nu\frac{V_e}{\theta^2}\lambda \tag{3.87}$$

From the above we find that:

$$\lambda = \frac{\theta^2}{\nu}\frac{dV_e}{dx} \tag{3.88}$$

Recall the momentum integral equation:

$$\frac{c_f}{2} = \frac{d\theta}{dx} + \frac{dV_e}{dx}\frac{\theta}{V_e}(H+2) \tag{3.89}$$

Let us relate c_f to the velocity gradient at the wall so we can make use of Eq. 3.83.

$$\frac{c_f}{2} = \frac{\tau_w}{\rho V_e^2} = \frac{1}{\rho V_e^2}\mu\frac{\partial u}{\partial y}\bigg|_w = \frac{\nu}{V_e^2}\frac{V_e}{\theta}l = \frac{\nu l}{\theta V_e} \tag{3.90}$$

Substitution this into the momentum integral equation, and solving Eq. 3.88 for $\frac{dV_e}{dx}$ and substituting that in as well gives:

$$\frac{\nu l}{\theta V_e} = \frac{d\theta}{dx} + \frac{\lambda\nu}{\theta^2}\frac{\theta}{V_e}(H+2) \tag{3.91}$$

We move the unknown terms l, λ to one side:

$$\frac{V_e}{\nu}\theta\frac{d\theta}{dx} = l - \lambda(H+2) \tag{3.92}$$

Thwaites found that plotting the left hand side (which is nondimensional) for numerous exact solutions of the boundary layer equations resulted in a remarkably good linear relationship.

$$\frac{V_e}{\nu}\theta\frac{d\theta}{dx} = 0.225 - 3\lambda \tag{3.93}$$

That form suggests that both H and l are functions of only λ. The above equations is an ODE that we can use to solve for θ.

$$\frac{d\theta}{dx} = 0.225\frac{\nu}{V_e\theta} - 3\lambda\frac{\nu}{V_e\theta} \tag{3.94}$$

Finally, substituting in Eq. 3.88 gives the ODE:

$$\boxed{\frac{d\theta}{dx} = \frac{0.225\nu}{V_e\theta} - \frac{3\theta}{V_e}\frac{dV_e}{dx}} \tag{3.95}$$

With some additional algebraic manipulations we can solve this ODE analytically, however the results requires an integral that typically still requires a numerical solution. Thus, it is generally easiest just to numerically solve the ODE using the above expression.

We now need expressions for l and H, which we showed should be functions only of λ. Notice from Eq. 3.88 that a positive value of λ corresponds to a favorable pressure gradient (and negative curvature in the boundary layer Eq. 3.85). The opposite is true for negative λ, thus we expect as λ becomes increasingly negative the boundary layer will transition (or possibly separate). Data fits for l and H come from Cebeci and Bradshaw [2]:

2. Cebeci and Bradshaw, *Physical and Computational Aspects of Convective Heat Transfer*, 1988.

$$\left.\begin{aligned} l &= 0.22 + 1.57\lambda - 1.8\lambda^2 \\ H &= 2.61 - 3.75\lambda - 5.24\lambda^2 \end{aligned}\right\} \text{ if } 0 \leq \lambda \leq 0.1 \tag{3.96}$$

$$\left.\begin{aligned} l &= 0.22 + 1.402\lambda + \frac{0.018\lambda}{0.107 + \lambda} \\ H &= 2.088 + \frac{0.0731}{0.14 + \lambda} \end{aligned}\right\} \text{ if } -0.1 < \lambda < 0 \tag{3.97}$$

If $\lambda \leq -0.1$ then laminar separation is predicted. The data fits do not extend beyond $\lambda > 0.1$, but we can just use the value at $\lambda = 0.1$ for larger values of λ.

Once, we solve the ODE for θ we compute λ from Eq. 3.88, l and H from the above expressions, and δ^* from the definition of H ($H = \delta^*/\theta$). The skin friction coefficient we compute from Eq. 3.90:

$$c_f = \frac{2\nu l}{\theta V_e} \tag{3.98}$$

The only remaining piece needed to solve the ODE is an inital condition. For a flat plate the initial boundary layer height is zero. In the analytic form we can use that directly, but for the numerical solution starting from $\theta_0 = 0$ causes numerical problems as can be seen from Eq. 3.95.

Instead we can start from small value like $x_0 = 10^{-6}$ and initialize θ_0 with the corresponding height from the Blasius solution:

$$\theta_0 = \frac{0.664 x_0}{\sqrt{Re_{x_0}}} \tag{3.99}$$

For an airfoil the boundary layer height is nonzero at the stagnation point (bottom half of Fig. 3.11). Moran derives an expression for the initial height at a stagnation point based on a Taylor series expansion of the edge velocity [3]. The result is:

3. Moran, *An Introduction to Theoretical and Computational Aerodynamics*, 1984.

$$\theta_0 = \left[\frac{0.075\nu}{(dV_e/dx)_0} \right]^{1/2} \tag{3.100}$$

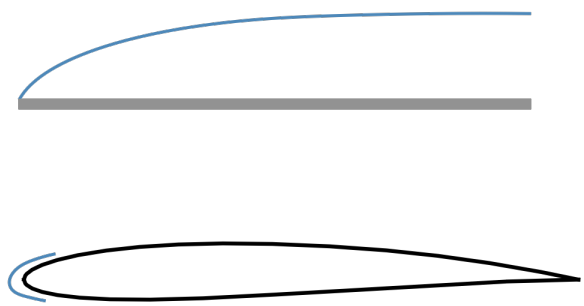

Fig. 3.11 Boundary layer height starts from zero for a flat plate, but has a nonzero height for an airfoil at the stagnation point.

The ODE should be terminated if there is laminar separation ($\lambda < -0.1$ as discussed above), or when transition is predicted (see Section 3.5.1).

Analytic Solution The above presentation focused on a numerical solution of the ODE, but it can also be solved analytically. The numerical solution is clearer, and more naturally leads to reusing similar methodology for the turbulent boundary layer solution (which must be solved numerically). However for hand calculations an analytic solution can be useful.

Starting with Eq. 3.95 moving one term to the other side and multiplying through by $2\theta V_e^6$ gives:

$$\frac{d\theta}{dx} + \frac{3\theta}{V_e}\frac{dV_e}{dx} = \frac{0.225\nu}{V_e\theta} \tag{3.101}$$

$$2\theta\frac{d\theta}{dx}V_e^6 + 6\theta^2 V_e^5 \frac{dV_e}{dx} = 0.45\nu V_e^5 \tag{3.102}$$

$$\frac{d}{dx}(\theta^2 V_e^6) = 0.45\nu V_e^5 \tag{3.103}$$

Now we integrate from 0 the starting point of boundary layer to x_p the x point along the boundary layer we wish to evaluate at:

$$\int_0^{x_p} \frac{d}{dx}(\theta^2 V_e^6)dx = \int_0^{x_p} 0.45\nu V_e^5 dx \tag{3.104}$$

$$\theta^2 V_e^6\Big|_0^{x_p} = \int_0^{x_p} 0.45\nu V_e^5 dx \tag{3.105}$$

$$\theta(x_p)^2 = \frac{\theta_0^2 V_{e0}^6}{V_e(x_p)^6} + \frac{0.45\nu}{V_e(x_p)^6}\int_0^{x_p} V_e(x)^5 dx \tag{3.106}$$

This expression provides an integral-based solution to solve for the momentum thickness at any point, as an alternative from the ODE approach.

3.4 Head's Method: Numerical Solution of Turbulent Incompressible Boundary Layers

A corresponding approach for turbulent boundary layers is Head's method. There is an improved method called Green's method, that is particularly useful if rapid flow changes exist. Its numerical solution is not any more difficult, but the equations are quite a bit longer, so we will present Head's method for simplicity.

We start with the same figure we used in deriving the momentum integral equation Fig. 3.9, and the intermediate result relating the normal velocity the velocity gradient across the control volume (Eq. 3.57). In this case the flow is assumed to be incompressible and so the density is cancelled out. We also assume that this "entrainment velocity" is pulled into the control volume rather than using the default out direction and so the sign is reversed:

$$V_n = \int_0^{\delta} \frac{\partial u}{\partial x} dy \tag{3.107}$$

The integral extends out to some arbitrary distance δ. Head assumed that the normalized entrainment velocity, was self-similar with the mean velocity profile, namely with H.

$$\frac{V_n}{V_e} = f(H) \tag{3.108}$$

Thus, for our boundary layer we have:

$$\frac{V_n}{V_e} = \frac{1}{V_e}\int_0^{\delta} \frac{\partial u}{\partial x} dy = f(H) \tag{3.109}$$

We now apply a series of algebraic manipulations:

$$\frac{\partial}{\partial x}\int_0^\delta u dy = V_e f(H) \tag{3.110}$$

$$\frac{\partial}{\partial x}\int_0^\delta (V_e - V_e + u) dy = V_e f(H) \tag{3.111}$$

$$\frac{\partial}{\partial x}\int_0^\delta V_e \left[1 - \left(1 - \frac{u}{V_e}\right)\right] dy = V_e f(H) \tag{3.112}$$

$$\frac{\partial}{\partial x}\left(V_e(\delta - \delta^*)\right) = V_e f(H) \tag{3.113}$$

We define the following new variable for convenience:

$$H_1 = \frac{\delta - \delta^*}{\theta} \tag{3.114}$$

The above equation then becomes:

$$\frac{d}{dx}(V_e \theta H_1) = V_e f(H) \tag{3.115}$$

From experimental measurements Head determined a relationship for $f(H)$ and between H_1 and H:

$$f(H) = 0.306(H_1 - 3)^{-0.6169} \tag{3.116}$$

$$H_1 = \begin{cases} 0.8234(H - 1.1)^{-1.287} + 3.3 & H \leq 1.6 \\ 1.5501(H - 0.6778)^{-3.064} + 3.3 & H > 1.6 \end{cases} \tag{3.117}$$

To solve the ODE we need to expand Eq. 3.115:

$$\frac{dV_e}{dx}\theta H_1 + \frac{d\theta}{dx}V_e H_1 + \frac{dH_1}{dx}V_e\theta = V_e\ 0.0306(H_1 - 3)^{-0.6169} \tag{3.118}$$

Solving for dH_1/dx gives:

$$\frac{dH_1}{dx} = \frac{0.0306}{\theta}(H_1 - 3)^{-0.6169} - \frac{dV_e}{dx}\frac{H_1}{V_e} - \frac{d\theta}{dx}\frac{H_1}{\theta} \tag{3.119}$$

This equation is undefined if $H_1 < 3$ and so we need to protect against that. An H_1 value that low corresponds to a large H (separation) and so we simply set $dH_1/dx = 0$ if that occurs.

We also have the momentum integral equation, which we rearrange for $d\theta/dx$:

$$\frac{d\theta}{dx} = \frac{c_f}{2} - \frac{dV_e}{dx}\frac{\theta}{V_e}(H + 2) \tag{3.120}$$

These two equations form a set of coupled linear ODEs where we solve for H_1 and θ simultaneously.

The remaining difficulties are that we have H_1 as a function of H, but need its inverse, and we have too many unknowns: θ, H_1 and c_f. The equation for H_1 (Eq. 3.117) can be easily inverted:

$$H = \begin{cases} 0.86(H_1 - 3.3)^{-0.777} + 1.1 & H_1 \geq 5.3 \\ 1.1538(H_1 - 3.3)^{-0.326} + 0.6778 & H_1 < 5.3 \end{cases} \tag{3.121}$$

These equations are undefined if $H_1 < 3.3$. As H_1 approaches 3.3 from above, the value of H approaches infinity (corresponding to separation). Thus, if $H_1 < 3.3$ we could simply return $H = 3.0$ (a typical large value for H corresponding to separation).

The skin friction coefficient can be estimated using the following semi-empirical formula:

$$c_f = 0.246 \times 10^{-0.678H} Re_\theta^{-0.268} \tag{3.122}$$

where

$$Re_\theta = \frac{V_e \theta}{\nu} \tag{3.123}$$

We now need two initial conditions. When the turbulent boundary layer is initiated from a laminar boundary layer on the same surface we assume continuity of the momentum thickness. In other words θ_0 is the final value of θ in the laminar section. After transition the value of H drops. As an initial value, we use the H value for a turbulent flat plate: $H = 1.28$ (see Eqs. 3.50 and 3.51). This value of H corresponds to a starting value of $H_1 = 10.6$ using Eq. 3.117.

Separation is predicted as H becomes large. The skin friction coefficient from the above formula goes to zero as H approaches infinity. Near separation the shape factor increases rapidly, so specifying a precise number makes little difference. A typical value is to assign $H = 3$ to correspond to separation, in which case the ODE should be terminated.

3.5 Transition Prediction Methods

Now that we know how to simulate a laminar boundary layer, and a turbulent boundary layer, we need to be able to predict when transition occurs. Before discussing a specific method, we discuss the mechanism of transition and some critical factors.

Transition is fundamentally caused by instability, on in other words the amplification of disturbances. At low Reynolds numbers, the

viscous forces are large compared to inertial forces so disturbances that arise are damped. Thus, the flow can remain laminar. For large Reynolds numbers the viscous forces are comparatively small. In this case there is not enough damping in the system to prevent rapid growth in disturbances and so turbulent flow develops. As the Reynolds number in the boundary layer increases, from an increasing length that the boundary layer traverses, eventually the disturbances will grow and turbulence will develop. While we will often predict a point of transition we should keep in mind that there is no actual point, but rather a region over which the flow transitions from laminar behavior to turbulence.

Some of the most relevant factors that affect turbulence are freestream conditions, surface roughness, and pressure gradients. If the incoming air is already turbulent or is disturbed to a greater degree, transition will occur sooner. A rough surface introduces larger and more frequent disturbances in the flow leading to earlier transition. This affect is sometimes used intentionally in wind tunnels as discussed in Ex. 1.3. While favorable pressure gradients can stabilize a boundary layer, as discussed earlier in this chapter, even a slightly adverse pressure gradient can induce transition.

Two other factors that affect transition, but don't as often naturally are suction/blowing and heating/cooling. Sometimes a device is added within a wall to suck out the boundary layer, so new air can fill in and remain laminar longer. Or a device might cool the wall and stabilize the boundary layer longer. Such devices expend energy so one must be careful, say on a vehicle, that the device doesn't use more energy than it saves through the drag reduction. In other applications, like a quiet supersonic wind tunnel, the energy savings is not important, but keeping the boundary layer laminar is important so that disturbances (i.e., noise) from the turbulent boundary layers on the tunnel's walls don't affect the flow behavior on the test device.

It is not obvious why cooling should stabilize a boundary layer so we briefly discuss that here. If we apply the compressible boundary layer equations (Eq. 3.22) at the wall ($u = v = 0$), and assume no pressure gradient to isolate the effect of heat transfer, we see that:

$$0 = \frac{\partial}{\partial y}\left(\mu \frac{\partial u}{\partial y}\right)_w \tag{3.124}$$

We now expand the derivative while carefully noting the difference between μ (mu) and u (note that we drop all of the w subscripts for

simplicity, but all quantities should be evaluated at the wall).

$$\frac{\partial \mu}{\partial y}\frac{\partial u}{\partial y} + \mu \frac{\partial^2 u}{\partial y^2} = 0 \tag{3.125}$$

As briefly discussed in connection with Thwaite's method (Section 3.3) we would like the curvature to be negative for stability. More formally, stability theory suggests that a point of inflection is unstable at high Reynolds number, and since the curvature is negative as it approaches the edge velocity, it should be negative at the wall as well. Solving for the curvature:

$$\frac{\partial^2 \mu}{\partial y^2} = -\frac{1}{\mu}\frac{\partial \mu}{\partial y}\frac{\partial u}{\partial y} \tag{3.126}$$

Viscosity is positive, and the velocity gradient at the wall is positive, so to maintain negative curvature we require the viscosity gradient to be positive. Viscosity is a function of temperature so we can expand that derivative as:

$$\frac{\partial \mu}{\partial y} = \frac{\partial \mu}{\partial T}\frac{\partial T}{\partial y} \tag{3.127}$$

For a gas, $d\mu/dT$ is positive (opposite for a liquid) so for stability in the boundary layer we require the temperature gradient moving away form the wall to be positive. Thus, if we cool the wall we can create a stronger temperature gradient and delay transition.

3.5.1 Transition Prediction Methods

The e^n method is perhaps the best method for predicting transition, but is more complex than the methods discussed in this section. The H-Rx method developed by Wazzan [4] uses the e^n method (with $n = 9$) with a range of pressure gradients, surface heating, and suction. The results and then parametrized as a function of the shape factor. The result is a simple method that works well across a wide range of 2D (and axisymmetric) flows.

4. Wazzan et al., *The H-Rx method for predicting transition*, 1981.

The local Reynolds number is:

$$Re_x = \frac{V_e x}{\nu} \tag{3.128}$$

and transition is predicted if $2.1 < H < 2.8$ and

$$\log_{10}(Re_x) > -40.4557 + 64.8066H - 26.7538H^2 + 3.3819H^3 \tag{3.129}$$

This relationship is visualized in Fig. 3.12. We see that as H increases then the critical transition Reynolds number decreases (i.e., transition occurs sooner).

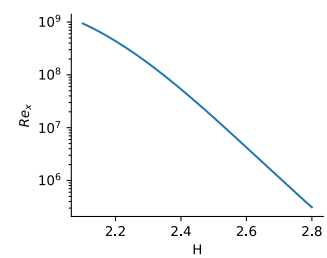

Fig. 3.12 Transition Reynolds number for the H-Rx method.

The type of transition captured by these methods is caused by Tollmien-Schlichting (TS) waves, and is only relevant for two-dimensional flows. Predicting transition in three dimensions is much more complicated and must consider crossflow instabilities and attachment line instabilities.

3.6 Drag Prediction

One of the main purposes of developing the boundary layer is to predict drag. Since we can compute c_f throughout the boundary layer, we can integrate that along the surface. However, that integration will only give us the skin friction drag (and not pressure drag). Instead, a particularly effective method is the Squire and Young formula.

$$c_d = \frac{2\theta_{TE}}{c}\left(\frac{V_{eTE}}{V_\infty}\right)^{\frac{H_{TE}+5}{2}} \tag{3.130}$$

where the subscript TE indicates the end of the boundary layer properties at the trailing edge. The formula must be applied over the upper and lower surfaces separately and added together. This formula gives total 2D viscous drag (sum of skin friction and pressure drag). If we wanted to separate out the two components we could integrate the skin friction drag as discussed above, then subtract that value from this total drag to get the pressure component.

Compaisons of this formula against against RANS CFD simulations for a variety of airfoils has suggested agreement in drag predictions within 2-3% (until stall is approached)[5]. This is remarkably good agreement for such a simple formula. Some comparisons from their paper are shown in Fig. 3.13.

5. Coder and Maughmer, *Numerical Validation of the Squire–Young Formula for Profile-Drag Prediction*, 2015.

3.7 Turbulence

To initiate a discussion on turbulence, consider the two jet flows shown in Fig. 3.14 and note the similarities and differences. One observation is that turbulent structures exist at multiple length scales, and that we notice smaller length scales at the higher Reynolds number. On the left, we see larger turbulent structures, and on the right, with a higher Reynolds number, we see much smaller turbulent structures. Another observation is that the large-scale features (e.g., spreading angle) seem to be largely independent of the Reynolds number.

These are general characteristics. Large-scale features are generally independent of Reynolds number, but the details of the turbulent

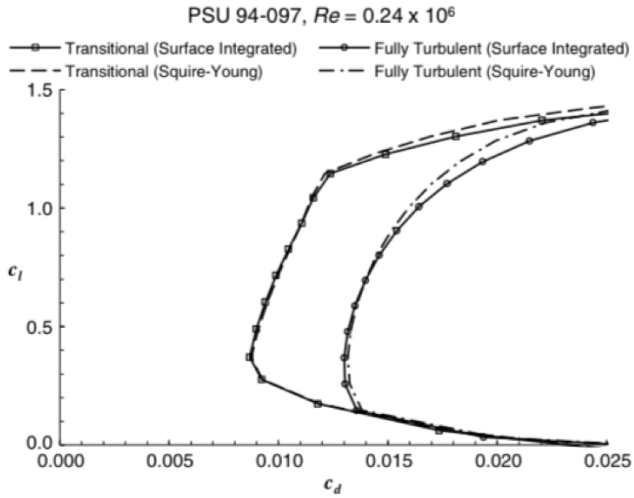

Fig. 3.13 Figure from Coder and Maughmer.[5]

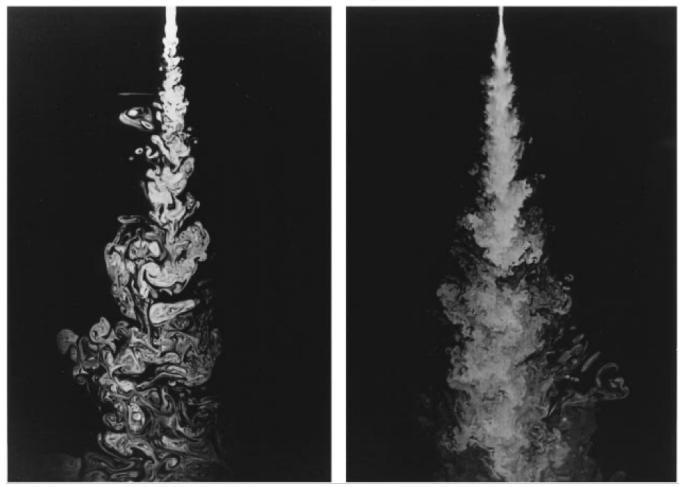

Re = 2,500 Re = 10,000

Fig. 3.14 The mixing transition in turbulent flows, Paul E. Dimotakis

structure are highly Reynolds number dependent, with smaller scales appearing as Reynolds number increases. This behavior creates the difficulty in simulating high Reynolds number flows—we have to resolve increasingly smaller and smaller scales.

3.7.1 Direct Numerical Simulation

In *direct numerical simulation* (DNS) we resolve all spatial and temporal scales of the flow (the smallest scales are known as the *Kolmogorov scale* as will be discussed later). Thus, we solve the Navier–Stokes equations without the need for any turbulence model. The cost of DNS scales with Re^3. Currently, this approach is only practical on very simple

geometries with low Reynolds numbers (approximately $O(10^3)$).*

*This video shows a DNS simulation for a small portion of a turbulent boundary layer and gives some appreciation for the scales and complexity involved: https://youtu.be/4KeaAhVoPIw.

3.7.2 Reynolds Averaged Navier Stokes and Turbulence Models

Most aerodynamic flows of interest occur at much higher Reynolds numbers where DNS is not practical. Another approach to this turbulent problem is Reynolds-averaging, which leads to solving the *Reynolds-averaged Navier–Stokes* (RANS) equations. In a RANS simulation we do not resolve the instantaneous turbulent structures, but rather solve for a time-averaged solution (think about the result from time-averaging the flow behavior shown in Fig. 3.14). We are giving up some details of the solution, and thus may lose some accuracy depending on which engineering quantities are of interest, in exchange we enable high Reynolds number solutions.

Before deriving the RANS equations (or rather an example subset of them) we need to review the concept of an expected value, or average. The expected value of some random variable X will be denoted with the following bracket notation, and is given as:

$$\langle X \rangle = E[X] = \int_{-\infty}^{\infty} x p(x) dx \tag{3.131}$$

where $p(x)$ is a probability density function for x (e.g., a normal distribution). If X can only take on discrete quantities, then the expected value would be given by the sum:

$$\langle X \rangle = \sum_{i=1}^{\infty} x_i p_i \tag{3.132}$$

where p_i is the probability associated with event x_i.

In the *Reynolds decomposition* we split every flow variable into an average component and a fluctuating component:

$$u = \langle u \rangle + u' \tag{3.133}$$

Some important properties of expectation are shown below. Expectation is a linear operator and so commutes with other linear operators like addition:

$$\langle u + v \rangle = \langle u \rangle + \langle v \rangle \tag{3.134}$$

The average value of the fluctuations is zero by definition:

$$\langle u' \rangle = 0 \tag{3.135}$$

Differentiation is also a linear operator and so it commutes:

$$\left\langle \frac{\partial u}{\partial x} \right\rangle = \frac{\partial \langle u \rangle}{\partial x} \tag{3.136}$$

The expected value of a variable is a constant and so can be pulled out of another expectation:

$$\langle\langle u\rangle v\rangle = \langle u\rangle\langle v\rangle = 0 \tag{3.137}$$

Before working out an example set of RANS equations, one quantity we will need is the expectation of the product of two random variables. We can work that out using the rules we've already established:

$$\langle uv\rangle = \langle(\langle u\rangle + u')(\langle v\rangle + v')\rangle \tag{3.138}$$

$$= \langle\langle u\rangle\langle v\rangle\rangle + \langle u'\langle v\rangle\rangle + \langle\langle u\rangle v'\rangle + \langle u'v'\rangle \tag{3.139}$$

$$= \langle u\rangle\langle v\rangle + \langle u'v'\rangle \tag{3.140}$$

Note that even though the average of u' and the average of v' are both zero, the average of their product is not necessarily zero.

We now examine the 2D incompressible Navier-Stokes equations, with Reynolds-averaging. The standard mass and momentum equations (x-direction only for brevity) are shown below.

$$\frac{\partial u}{\partial x} + \frac{\partial v}{\partial y} = 0 \tag{3.141}$$

$$\frac{\partial u}{\partial t} + u\frac{\partial u}{\partial x} + v\frac{\partial u}{\partial y} = -\frac{1}{\rho}\frac{\partial p}{\partial x} + \nu\left(\frac{\partial^2 u}{\partial x^2} + \frac{\partial^2 u}{\partial y^2}\right) \tag{3.142}$$

If we follow the same procedure shown above, introducing Reynolds-averaging, and simplifying, we obtain the following equations:

$$\frac{\partial\langle u\rangle}{\partial x} + \frac{\partial\langle v\rangle}{\partial y} = 0 \tag{3.143}$$

$$\frac{\partial\langle u\rangle}{\partial t} + \langle u\rangle\frac{\partial\langle u\rangle}{\partial x} + \langle v\rangle\frac{\partial\langle u\rangle}{\partial y} = -\frac{1}{\rho}\frac{\partial\langle p\rangle}{\partial x} + \nu\left(\frac{\partial^2\langle u\rangle}{\partial x^2} + \frac{\partial^2\langle u\rangle}{\partial y^2}\right) - \left(\frac{\partial}{\partial x}\langle u'u'\rangle + \frac{\partial}{\partial y}\langle u'v'\rangle\right) \tag{3.144}$$

Notice, that the equations appear almost identical to the original equations when we replace the instantaneous quantity (e.g., u) with a time-averaged quantity (e.g., $\langle u\rangle$). However, an extra term has been introduced as highlighted in the equation above.

Multiplying the entire equation by ρ (and considering all three dimensions) we have extra terms of the form:

$$\rho\langle u_i' u_j'\rangle \tag{3.145}$$

This quantity is called the *Reynolds stress tensor* (RST) because it has units of stress and appears in the equation in a similar way as the standard stress tensor. The problem, is that we have introduced additional unknowns that we don't have equations for, in other words, we have a closure problem. This is where *turbulence models* come in, as a way to model these additional terms.

Before discussing some turbulence models, we explore the turbulent kinetic energy (TKE) equation, which will lend some insight into the behavior of turbulence. This equation is formed by taking this new mean momentum equation, subtracting it from the original momentum equation, then multiplying by the velocity u_j. The result is:

$$\begin{aligned}\underbrace{\frac{\partial k}{\partial t} + \langle u_i \rangle \frac{\partial k}{\partial x_i}}_{Dk/Dt} + \underbrace{\frac{\partial}{\partial x_i}\left(\frac{1}{2}\langle u_i' u_j' u_j' \rangle + \frac{1}{\rho}\langle u_i' p' \rangle - 2\nu \langle u_j' s_{ij}' \rangle\right)}_{\nabla \cdot T \quad \text{transport}} \\ = \underbrace{-\langle u_i' u_j' \rangle \frac{\partial \langle u_j \rangle}{\partial x_i}}_{\text{P: production}} - \underbrace{2\nu \langle s_{ij}' s_{ij}' \rangle}_{\epsilon \,:\, \text{dissapation}}\end{aligned} \tag{3.146}$$

The quantity k is the kinetic energy of turbulence:

$$k = \frac{1}{2}\langle u_i' u_i' \rangle = \frac{1}{2}\left(u'^2 + v'^2 + w'^2\right) \tag{3.147}$$

It is proportional to the trace of the RST ($2\rho k$), and is one of the most important parameters in turbulence. Often it is reported as a nondimensional value called the *turbulence intensity*, which is the root-mean-squared of the velocity fluctuations normalized by the magnitude of the mean velocity.

$$I = \frac{\sqrt{\frac{2}{3}k}}{\|\langle u_i \rangle\|} = \frac{\sqrt{\frac{1}{3}\left(u'^2 + v'^2 + w'^2\right)}}{\sqrt{\langle u \rangle^2 + \langle v \rangle^2 + \langle w \rangle^2}} \tag{3.148}$$

The quantity s_{ij}' is the symmetric part of the stress tensor (using fluctuating components):

$$s_{ij}' = \frac{1}{2}\left(\frac{\partial u_i'}{\partial x_j} + \frac{\partial u_j'}{\partial x_i}\right) \tag{3.149}$$

Equation 3.146 has labels below various terms. The first term is the total change in kinetic energy. Energy is produced at large scales from the mean flow field (u_j). This productive term is usually positive. The transport term is a divergence moving energy from the large scales

to smaller scales. The dissipation term is always negative and shows that energy is dissipated by viscosity at the small scales where the gradients in s'_{ij} are large. The dissipation term, ε is also used to define the Kolmogorov scale, addressing how small of scales to we need to resolve in a turbulent simulation. The overall equation shows how turbulent kinetic energy flows through a fluid in an energy cascade. It is generated at large scales, transported to smaller and smaller scales, and dissipated at the smallest scales where viscosity dominates.

We now briefly introduce a few turbulence models. Recall that we need a model for the RST:

$$\rho\langle u'_i u'_j\rangle \tag{3.150}$$

Boussinesq proposed a relationship with the mean flow, in what is known as the *Boussinesq hypothesis*. The idea is to mimic the regular stress tensor (Eq. 1.102), but replace the viscosity with a new term called the *eddy viscosity* (μ_t). Note that the negative is added to cancel the negative that appears in Eq. 3.144, and make it of the same form as the stress tensor.

$$-\rho\langle u'_i u'_j\rangle = \mu_t\left(\frac{\partial\langle u_i\rangle}{\partial x_j} + \frac{\partial\langle u_j\rangle}{\partial x_i} - \frac{2}{3}\left(\frac{\partial\langle u_k\rangle}{\partial x_k}\right)\delta_{ij}\right) \tag{3.151}$$

However, this cannot be a suitable model as it has zero trace, and recall that the trace of the RST is $2\rho k$. We then add a diagonal term to produce the appropriate trace, where C is a yet unknown constant:

$$-\rho\langle u'_i u'_j\rangle = \mu_t\left(\frac{\partial\langle u_i\rangle}{\partial x_j} + \frac{\partial\langle u_j\rangle}{\partial x_i} - \frac{2}{3}\left(\frac{\partial\langle u_k\rangle}{\partial x_k}\right)\delta_{ij}\right) + C\delta_{ij} \tag{3.152}$$

Taking the trace of both sides yields: $-2\rho k = 3C$ or $C = -2/3\rho k$. Thus, we have a model for the RST (rearranged in a more standard form):

$$-\rho\langle u'_i u'_j\rangle = \mu_t\left(\frac{\partial\langle u_i\rangle}{\partial x_j} + \frac{\partial\langle u_j\rangle}{\partial x_i} - \frac{2}{3}\left(\frac{\partial\langle u_k\rangle}{\partial x_k}\right)\delta_{ij}\right) - \frac{2}{3}\rho k\delta_{ij} \tag{3.153}$$

Note the similarities to the stress tensor in Eq. 1.102 (and Eq. 1.85 with pressure included), repeated below:

$$\sigma_{ij} = \mu\left(\frac{\partial u_i}{\partial x_j} + \frac{\partial u_j}{\partial x_i} - \frac{2}{3}\left(\frac{\partial u_k}{\partial x_k}\right)\delta_{ij}\right) - p\delta_{ij} \tag{3.154}$$

This a commonly used model, although its accuracy has been shown to be poor in some scenarios. And, although we now have a model for the RST, we still have an unknown, the eddy viscosity, and so need yet another model.

Various turbulence models are used to fill this gap. We won't go into detail, but rather provide a high-level overview of some of the main ones. Perhaps the most commonly used turbulence model for CFD is the k–ϵ model. This model uses the TKE equation (Eq. 3.146), for k, the turbulent kinetic energy and an empirical PDE for ϵ (the dissipation term). The eddy viscosity is then related as:

$$\mu_t = C\rho\frac{k^2}{\epsilon} \tag{3.155}$$

where C is one of five adjustable constants used in the model.

The k–ω model is similarly based on 2 PDEs, where $\omega = \epsilon/k$. This model typically performs better in the near-wall region, in areas with large streamwise pressure gradients (although k–ϵ typically performs better when separation occurs), or for compressible flows.

The Spalart-Allmaras turbulence model is a popular one-equation model. It was designed specifically for aerospace applications with wall-bounded flows. It has been shown to work particularly well for boundary layers with adverse pressure gradients but still attached or only mildly separated. It is not a good general model, and can produce large errors for other scenarios like free shear flows, jet flows, etc.

The RST model does not use the Bousennisq hypothesis, but rather has a separate model for each term in the RST. This is the most computationally intensive of these models.

One final comment on the RANS equations is on its suitability in two-dimensions. If we refer back to the vorticty equation (Eq. 1.116) we note that the vortex stretching term is only nonzero in 3D. Vortex stretching is a critical mechanism in turbulence to transfer turbulent energy across the various scales. In other words, turbulence is fundamentally a three-dimensional phenomenon. While 2D RANS is often used, for example in airfoil simulations, and can be a useful approach, there is good reason to be even more skeptical of turbulence models in two-dimensional flows.

3.8 Turbulent Boundary Layers

We now take a closer look at the behavior within a boundary layer. Laminar boundary layers are straightforward. They are geometrically similar and the profile is known from the Blasius solution. For turbulent boundary layers, no matter how we nondimensionalize, we cannot collapse the profiles onto a single curve. This is because the layers closer to the surface act on very different length scales than layers further away. Instead, we will think of a turbulent boundary layer as being

composed of separate inner and outer layers. Figure 3.15 is a classic figure demonstrating different behavior in separate regions.

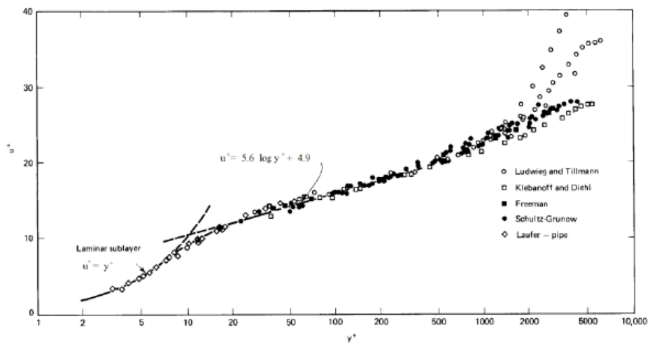

Fig. 3.15 Nondimensional velocity versus nondimensional distance from wall showing different behavior in different sublayers with a turbulent boundary layer. Figure from Clauser.[6]

6. Clauser, *The Turbulent Boundary Layer*, 1956.

Near the wall, viscosity is the most important parameter governing the fluid behavior. In this region the Reynolds stresses are negligible. At the wall the velocity fluctuations must be zero, so the Reynolds stresses are zero at the wall. Figure 3.16 depicts the viscous stresses and Reynolds stresses within a turbulent boundary layer, where we see that viscous stresses dominate in the near-wall region.

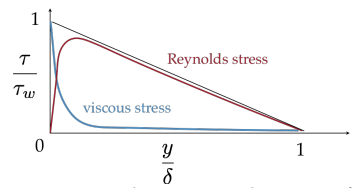

Fig. 3.16 Relative contributions of stresses within a turbulent boundary layer.

The relevant parameters near the wall are thus the viscosity (ν), density (ρ), and the shear stress at the wall (τ_w). From those quantities we can form a velocity and length scale to use in nondimensionalization. The velocity scale is called the *friction velocity*:

$$u_\tau = \sqrt{\frac{\tau_w}{\rho}} \tag{3.156}$$

and the viscous length scale is:

$$\delta_v = \frac{\nu}{u_\tau} \tag{3.157}$$

The nondimensional distance from the wall is then:

$$y^+ = \frac{y}{\delta_v} = \frac{u_\tau y}{\nu} \tag{3.158}$$

This quantity is called the *y plus* value. It is a nondimensional distance, but from the above equation can also be thought of as a Reynolds number using the relevant near-wall velocity scale. The fractional contributions of the stresses are shown again in Fig. 3.17, this time as a function of y^+.

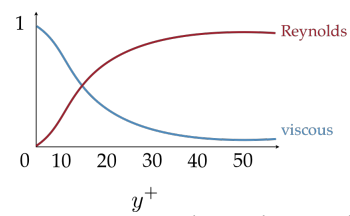

Fig. 3.17 Fractional contribution of stresses as a function of y^+ in a turbulent boundary layer.

In general, we expect the mean velocity gradient to be a function of the distance from the wall, with both the viscous length scale, and the boundary layer height as relevant length scales: However, as we've argued, for the inner portion of the boundary layer the flow behavior is independent of the outer portion of the boundary layer (i.e., independent of V_e and δ). In fact, the behavior doesn't depend on whether it is a boundary layer or any other wall shear layer (e.g., an internal flow). We then expect the mean velocity gradient to be given by

$$\frac{d\langle U\rangle}{dy} = \frac{u_\tau}{y} f\left(\frac{y}{\delta_v}\right) \tag{3.159}$$

where f is some yet unknown function with the constants u_τ/y factored out of the function so that the remaining function is nondimensional (i.e., potentially universal). We define the nondimensional velocity profile as:

$$u^+ = \frac{u}{u_\tau} \tag{3.160}$$

Then the above expression reduces to the following nondimensional relationship:

$$\begin{aligned} \frac{d\langle U\rangle}{dy} &= \frac{u_\tau}{y} f\left(\frac{y}{\delta_v}\right) \\ \frac{du^+}{dy^+} &= \frac{1}{y^+} f(y^+) \end{aligned} \tag{3.161}$$

Or in other words, u^+ can only depend on y^+ in this inner layer ($u^+ = f(y^+)$). This prediction of universal behavior with the inner layer of turbulent boundary layer is called the *law of the wall*. The inner portion of a turbulent boundary layer comprises about 10–20% of the full boundary layer height.

Within the inner layer, two sublayers are identified. The first is the *viscous sublayer* also called the *laminar inner sublayer*. This layer extends from the wall to approximately $y^+ = 5$. In this region viscosity dominates and so little mixing occurs, which is way it is referred to as a laminar inner sublayer. Near the wall, the wall shear stress dominates the behavior:

$$\tau_w = \mu \frac{\partial u}{\partial y} \tag{3.162}$$

If we rearrange, and integrate, assuming the shear stress and viscosity don't change appreciably in this small region then:

$$u = \frac{\tau_w}{\mu} y = \frac{u_\tau^2 \rho}{\mu} y \tag{3.163}$$

where we introduced the friction velocity in the last step. We now nondimensionalize by dividing the velocity by the friction velocity:

$$u^+ = \frac{u}{u_\tau} = \frac{\rho u_\tau u}{\mu} = y^+ \tag{3.164}$$

The resulting prediction is linear behavior in the viscous sublayer.

Further away we expect an intermediate region where viscosity has little effect, but where the external flow also has little effect. In this region we expect the mean rate of strain to be constant. In other words, we expect the nondimensional function that defines the mean velocity gradient, $f(y^+)$ to be constant. This is typically written as follows:

$$f(y^+) = \frac{1}{\kappa} \tag{3.165}$$

where κ is the von Karman constant. From Eq. 3.161 we then get:

$$\frac{du^+}{dy^+} = \frac{1}{y^+}\frac{1}{\kappa} \tag{3.166}$$

We integrate this expression to obtain:

$$\boxed{u^+ = \frac{1}{\kappa}\ln y^+ + C} \tag{3.167}$$

This is called the *log law*. Typical values for the two constants, obtaining from experiments on a smooth wall, are: $\kappa = 0.41$ (when using a natural log) and $C = 5$.

Figure 3.18 shows both the inner layer and the log law on a semilog scale. The inner layer applies up to about $y^+ = 5$ and the low law starts at about $y^+ = 30$. In between we have a buffer region where neither law applies. If we refer back to Fig. 3.15 we see that the log law eventually breaks down. In this outer layer there is no universal behavior, and this outer layer comprises about 80% of the boundary layer. it appears as a small region only because it is a log scale on that axis (note how it extends from about $y^+ = 1000$–5000 for that case, which is 80% of the total height.).

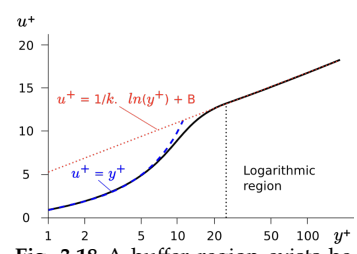

Fig. 3.18 A buffer region exists between the inner sublayer and the log law.

3.9 Large Eddy Simulation

Finally, we give a brief introduction to large eddy simulation (LES). This technique has a fidelity between DNS and RANS. The concept is motivated by the turbulent boundary layer behavior we just saw. The method explicitly solves large-scale features (e.g., large eddies), but uses a subgrid-scale model rather than trying to resolve all the small

scales like DNS does. From the above discussion we expect that we can do a reasonable job at modeling the small scales in a universal way. The larger scales have non-universal behavior, contain the most energy, and are strongly affected by geometry, so we explicitly solve for these. This technique could also be thought of as a low-pass filter (i.e., we ignore the high frequency, small scale, behavior).

4 Finite Wing

A basic wing is just a loft between two or more airfoils (Fig. 4.1). We've learned some techniques to compute forces and moments on an airfoil and would now like to understand how that relates to computing forces and moments on wings.

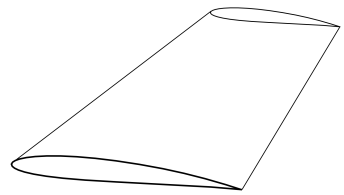

Fig. 4.1 A basic wing is just a loft between two airfoils.

4.1 Geometry

Before diving into the physics, let us get a few terms out of the way as it relates to geometry. The wingspan, or *span*, is a planar projection of the lateral extent of the wing and is denoted as b (Fig. 4.2). In other words, a vertical winglet will increase the length of the wing, but it does not increase span. This quantity is usually unambiguous, but for flexible wings we may need to specify the loading conditions at which the span is measured (e.g., span at 1g).

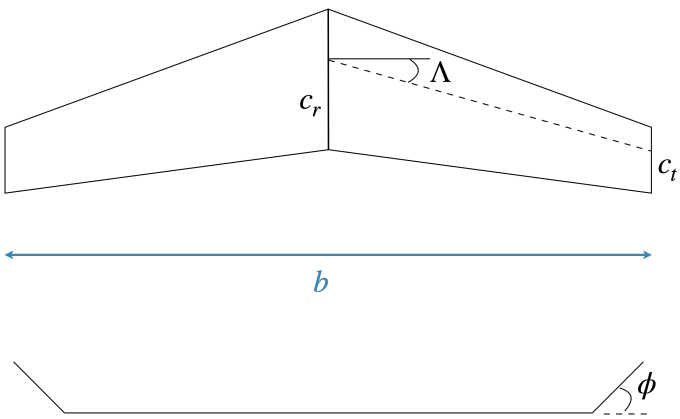

Fig. 4.2 Some nomenclature for a basic wing. Top view (top) and side view (bottom).

The wing area, or just *area*, S, is another important quantity though it can have many definitions (wetted area, projected area, gross area, etc.). Typically, we are interested in a reference area, and we note this explicitly as S_{ref}. The reference area is a flat projected area that scales with the wing, but is primarily used for normalization purposes. A typical reference area uses a trapezoidal shape whether or not the actual

wing is trapezoidal (see Fig. 4.3).

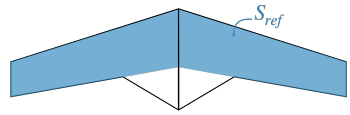

Fig. 4.3 Trapezoidal reference area.

Sweep, Λ, is a shear angle that is usually measured at the quarter-chord line, though sometimes at the leading edge. Sweep need not be constant along the wing, and instead may be a distribution. *Dihedral*, ϕ, is a rotation angle that also need not be constant along the wing and can be a distribution. Both can be seen in Fig. 4.2.

Chord, c, is rarely constant, though in simple cases it may follow a linear distribution where one only needs to know the root chord c_r and the tip chord c_t (Fig. 4.2). Another common wing design uses multiple linear segments. In the general case, the chord is a curve. *Twist* (Fig. 4.4), θ, is similarly often defined as piecewise linear, though can be a general curved shape. Twist is usually measured about the quarter chord.

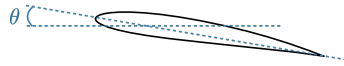

Fig. 4.4 Definition of twist.

The nondimensional quantity, *aspect ratio*, is given by:

$$AR = \frac{b^2}{S_{\text{ref}}} \tag{4.1}$$

A high aspect ratio wing and a low aspect wing are contrasted in Fig. 4.5. Another nondimensional quantity that is sometimes used is the taper ratio:

$$\lambda = \frac{c_t}{c_r} \tag{4.2}$$

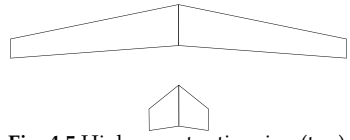

Fig. 4.5 High aspect ratio wing (top), and low aspect ratio wing (bottom).

This quantity is less direct for curved shapes, but can still apply to the trapezoidal reference area to give a qualitative understanding of the shape. A taper ratio of 1 would correspond to a constant chord wing, whereas a taper ratio of 0.1 would be higher tapered. Modern transport aircraft typically have a taper ratio of around 0.2.

The mean geometric chord is simply:

$$\bar{c} = \frac{S_{\text{ref}}}{b} \tag{4.3}$$

though this quantity isn't used very much. More relevant is the mean aerodynamic chord, which is a chord-weighted average chord. This quantity is used in stability and control calculations, to normalize pitching moment and to compute static margin, and is also typically used as the length scale in Reynolds number calculations.

$$c_{mac} = \frac{2}{S}\int_0^{b/2} c^2 dy \tag{4.4}$$

where

$$S = 2\int_0^{b/2} c\,dy \tag{4.5}$$

For a linearly tapered wing this integral evaluates to:

$$c_{mac} = \frac{2}{3}\left(c_r + c_t - \frac{c_r c_t}{c_r + c_t}\right) \tag{4.6}$$

4.2 Downwash

The flow behavior over a wing has some fundamental differences as compared to airfoils, also called infinite wings. A finite wing has a three-dimensional flow field, with a *crossflow* component of velocity perpendicular to the airfoils. In other words, a wing doesn't solely act like a series of airfoils stacked together.

A unique feature of lifting wings is that they produce a *wake vortex* as seen in Fig. 4.6. A common explanation for the vortex is that a lifting wing has higher pressure on the bottom surface as compared to the top, and so fluid will circulate around the tips as shown in Fig. 4.7. The resulting vortex is often called a tip vortex. This is a helpful conceptualization, but is a somewhat misleading explanation. It seems to suggest that a box wing (Fig. 4.8), which does not have a "tip", would not produce a vortex. It also leads to some erroneous conclusions about the benefits of winglets.

As we will see more clearly later on, these wake vortices produce *downwash*, or downward moving air, behind the wing. Downwash can be viewed more fundamentally as a consequence of Newton's third law. If a body is producing lift, colloquially we might say that means that the air is pushing the body up. Thus, by Newton's third law, the body must be pushing the air downward. Thus, any three-dimensional lifting body will leave behind a wake of downward moving air. The lift is not (and cannot) be generated uniformly along the wing. The lift must go to zero somewhere on the wing (e.g., at a wing tip where a pressure difference cannot be sustained between the upper and lower surfaces), or on a closed wing, like the box wing, the force would have to be reduced on one side to produce a net lift. In any case, variations in the lift distribution are directly related to the vorticity, and the vorticity will "roll-up" towards the center of vorticity forming a vortex, or in some cases, multiple vortices. Another way to think of vortex formation is that the downward moving air will be next to a region of still air, and that velocity gradient (which is vorticity) will induce a rotation. A more complete picture of the downwash and wake vortices can be seen in Fig. 4.9.

A major consequence of this downwash, is that energy is left behind in the wake. Or in other words, the wing produces drag. This type of drag is called *induced drag* or sometimes *vortex drag*. To completely eliminate induced drag, we would have to eliminate the downwash. In other words, if flying into still air, any disturbances made by the aircraft would need to be cancelled out, so the air behind the aircraft would also be still. But, if there is no downwash left behind, then from the above

Fig. 4.6 Picture of aircraft flying through colored smoke to visualize the wake vortex. Picture from NASA, public domain.

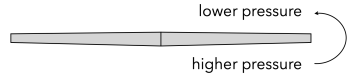

Fig. 4.7 Common explanation for tip vortex that is helpful but incomplete.

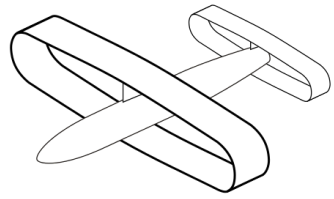

Fig. 4.8 Box or annual wing. Image from Steelpillow, Wikimedia, CC BY-SA 3.0.

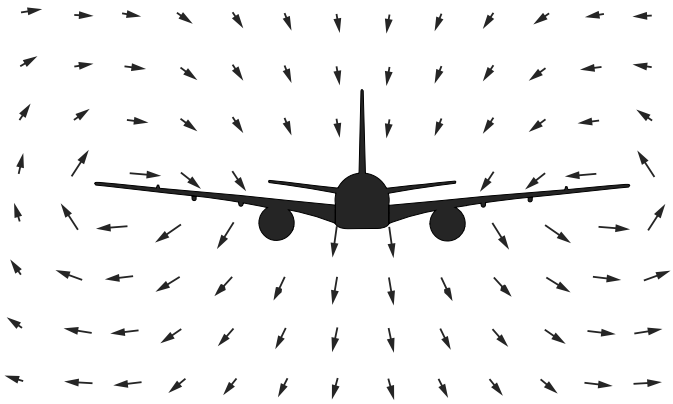

Fig. 4.9 Induced velocity from a lifting body showing the region of downwash, and circulation from the wake vortices.

arguments there would be no lift. Thus, any lifting body must always have induced drag. Although we cannot eliminate induced drag, there are things we can do to reduce it as will be discussed later.

As a side note, we can see from Fig. 4.9 that although the wake vortices induced downwash on the wing, to the sides of the wing they induced upwash, or a region of rising air. This behavior provides the motivation for formation flight. A second aircraft, or bird, positioned behind and to the side of a lead aircraft (Fig. 4.10) can fly in a region of rising air and thus reduce the energy required to maintain their lift.

The presence of downwash also changes our effective angle of attack. As depicted in Fig. 4.11, without downwash the angle of attack is the angle between the freestream velocity and the local chord line. However, the presence of downwash alters the relative incoming

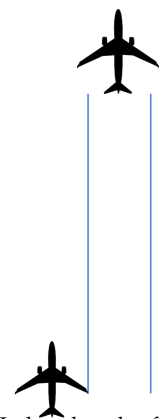

Fig. 4.10 Aircraft flying in formation can reduce their induced drag.

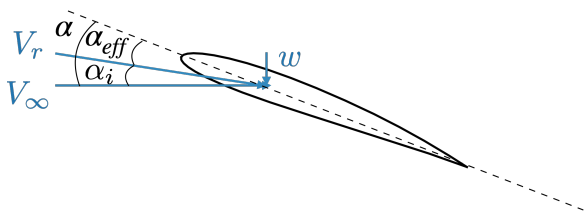

Fig. 4.11 Induced angle of attack.

velocity V_r. The effective angle of attack, α_{eff}, is reduced by the *induced angle of attack*, α_i:

$$\alpha_{eff} = \alpha - \alpha_i \tag{4.7}$$

4.3 Vortex Filaments

We continue with the assumptions of incompressible and irrotational flow, and thus are still governed by Laplace's equation (potential flow).

But in this case the singularities we use are line vortices. A cross section of a line vortex is just the point vortex we've seen before (Fig. 4.12). Or in other words, the line vortex is like the point vortex but extruded out of the plane. The circulation of the vortex is defined by the right hand rule, the fingers curl around in the direction of induced velocity and the thumb points along the line defining the direction of circulation.

An infinite vortex behaves just like the point vortex we studied in Chapter 2. In other words, the velocity has a magnitude:

$$|V| = \frac{\Gamma}{2\pi r} \tag{4.8}$$

and is a tangential direction given by the right hand rule. We can now have line vortices of any length, not just infinite. Another special case, is a semi-infinite vortex where the vortex extends to infinity in one direction only. If measuring the velocity in the plane where the vortex filament ends, its magnitude is given by:

$$|V| = \frac{\Gamma}{4\pi r}\,. \tag{4.9}$$

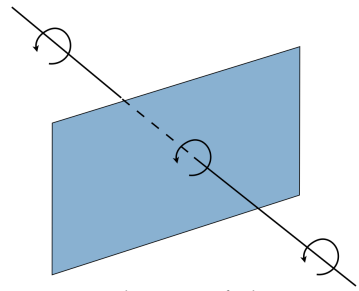

Fig. 4.12 A depiction of a line vortex. In a plane perpendicular to the line vortex the behavior is exactly that of a point vortex.

Not surprisingly, the induced velocity has half the magnitude of an infinite vortex.

For an arbitrary vortex line segment, referred to as a *vortex filament*, we need to use the *Biot-Savart Law*. This law comes from magnetostatics and describes the magnetic field induced by a constant electric current. The same equation is used in aerodynamic applications to compute the velocity induced by a filament of constant vorticity.*

*The connection to electromagnetic induction is the reason that vortex drag is referred to as induced drag.

We can derive Biot-Savart's Law as follows. First, we assume an incompressible flow:

$$\nabla \cdot \vec{V} = 0 \tag{4.10}$$

We now define

$$\vec{V} = \nabla \times \vec{A} \tag{4.11}$$

where $\vec{A}$ is an arbitrary vector since, $\nabla \cdot \nabla \times \vec{A} = 0$ for any $\vec{A}$ (a vector identity). The vorticity is given by the curl of the velocity:

$$\vec{\omega} = \nabla \times \vec{V} = \nabla \times (\nabla \times \vec{A}) = \nabla(\nabla \cdot \vec{A}) - \nabla^2 \vec{A} \tag{4.12}$$

Since, $\vec{A}$ is arbitrary, we choose it to be divergence free (i.e., $\nabla \cdot \vec{A} = 0$). The above equation then reduces to:

$$\vec{\omega} = -\nabla^2 \vec{A} \tag{4.13}$$

We recognize this equation as Poisson's equation, which has a known solution:

$$\vec{A}(\vec{q}) = \frac{1}{4\pi} \int \frac{\vec{\omega}(\vec{s})}{|\vec{q} - \vec{s}|} d^3 s \tag{4.14}$$

where q is the field location, and s is the location of the vorticity. In our case, we need the curl of this quantity (see Eq. 4.11). We can show that[†]

[†]This is straightforward to show for Cartesian coordinates.

$$\nabla \times \frac{\vec{\omega}(\vec{s})}{|\vec{q}-\vec{s}|} = \frac{\vec{\omega} \times (\vec{q}-\vec{s})}{|\vec{q}-\vec{s}|^3} \tag{4.15}$$

Thus:

$$\vec{V}(\vec{q}) = \frac{1}{4\pi} \int \frac{\vec{\omega} \times (\vec{q}-\vec{s})}{|\vec{q}-\vec{s}|^3} d^3s \tag{4.16}$$

Finally, we use a line vortex (infinitely thin) so the volume integral reduces to a line integral, where the circulation is constant along the filament $d\omega = \Gamma d\vec{l}$. We also define $\vec{r} = \vec{q} - \vec{s}$ for simplicity. In other words, $\vec{r}$ is the distance from the integration point on the filament to the evaluation point in the field where velocity is computed.

$$\boxed{\vec{V} = \frac{\Gamma}{4\pi} \int \frac{d\vec{l} \times \vec{r}}{|r|^3}} \tag{4.17}$$

Note that this is a path integral, so the vortex filament can take any arbitrary curved shape. The direction $\vec{l}$ points in the direction of positive circulation.

Often, we will use vortex filaments that are straight line segments. Let's apply the Biot-Savart law to a straight line segment as shown in Fig. 4.13. The segment $d\vec{l}$ is a distance r away from a point we want to evaluate the induced velocity at. The distance h is the perpendicular distance from the vortex to the point. For the moment we won't worry about directions, for a simple filament it is obvious from the geometry, but later we will be more rigorous about directions. The magnitude of the cross product is:

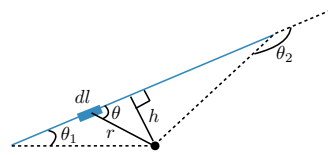

Fig. 4.13 A vortex filament and a point where the induced velocity is computed at.

$$d\vec{l} \times \vec{r} = dl\, r \sin\theta \tag{4.18}$$

From the geometry we see that

$$\sin\theta = \frac{h}{r} \tag{4.19}$$

$$\tan\theta = \frac{h}{l_h - l} \tag{4.20}$$

where l_h is the point on the vortex filament that intersects with h (a constant value), and l is a variable that moves along the filament. We use the first expression to solve for r and the second to solve for dl:

$$r = \frac{h}{\sin\theta} \tag{4.21}$$

$$dl = \frac{h}{\sin^2\theta} d\theta \tag{4.22}$$

Making these substitutions into Eq. 4.17 yields:

$$|\vec{V}| = \frac{\Gamma}{4\pi}\int_{\theta_1}^{\theta_2}\frac{\sin\theta}{h}d\theta \tag{4.23}$$

The distance h is a constant so it can be pulled out of the integral leaving us with a simple analytic expression for the magnitude of the induced velocity from the vortex segment:

$$V_\theta = \frac{\Gamma}{4\pi h}(\cos\theta_1 - \cos\theta_2) \tag{4.24}$$

Notice, that this expression returns the expected velocity magnitude for an infinite vortex (Eq. 4.8) and semi-infinite vortex (Eq. 4.9) when using $\theta_1 = 0, \theta_2 = \pi$ for the former case, and $\theta_1 = 0, \theta_2 = \pi/2$ for the latter.

To better understand how we can use vortex filaments for modeling purposes, let's consider a control volume that surrounds a vortex filament as shown in Fig. 4.14. You can imagine this control volume as a piece of paper that we wrap around the filament, without touching the filament. Let's now use Stoke's theorem (Eq. 1.26) on this control volume, with the velocity vector as the vector of interest:

$$\int_A \left(\nabla\times\vec{V}\right)\cdot d\vec{A} = \oint_C \vec{V}\cdot d\vec{\ell} \tag{4.25}$$

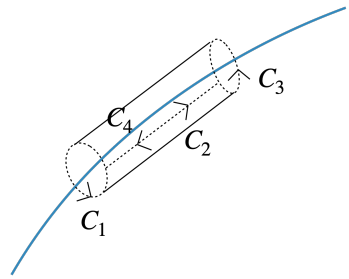

Fig. 4.14 Control volume around a vortex filament.

The quantity $\nabla\times\vec{V}$ we recognize as vorticity, and the left-hand-side as the definition of circulation (Eq. 2.1). We will use a closed-path contour starting from C_1 (around the circle), across the end of the "folded paper" (C_2), around the other circular end C_3, and back along the seam C_4 to close the path. The area enclosed by this contour does not having any vorticity crossing it. All of the vorticity is contained in the filament, and the filament does not cross the area enclosed by this contour (again imagine the area as that of a paper wrapped around the filament). Thus, the left hand side of the above integral is zero, there is no vorticity flux through the area. The contour integral around the full path must then also be zero. We break up that integral into four parts.

$$\int_{C_1}\vec{V}\cdot d\vec{\ell} + \int_{C_2}\vec{V}\cdot d\vec{\ell} + \int_{C_3}\vec{V}\cdot d\vec{\ell} + \int_{C_4}\vec{V}\cdot d\vec{\ell} = 0\,. \tag{4.26}$$

The integral along C_2 and C_4 are along the same segment, just in opposite directions, so they will cancel out. The integrals around the ends, we can see as the definition of circulation and each will contain the circulation of the filament (see Eq. 2.1 and Fig. 2.1). The two contours traverse in opposite directions, and so will have opposite signs.

$$\Gamma_1 - \Gamma_3 = 0 \tag{4.27}$$

From the above expression, we see that $\Gamma_1 = \Gamma_3$. Or in other words, *the circulation along a vortex filament must be constant*. The corollary is a filament cannot just suddenly end in the fluid, otherwise, the contour integral on one end would be zero and the above equation would not be satisfied. We can still use arbitrary vortex filaments, but we have to connect them to other filaments. The segments must form a closed path, or extend to infinity. Collectively these conditions are known as *Helmholtz's vortex theorems*.

With those requirements in mind, a simple model of a wing might look like that shown in Fig. 4.15. The bound vortex stays fixed in the wing, and from a side view, looks the same as the circulation generated from an airfoil. The new addition for a wing is the trailing vortices. The trailing vortices look like a reasonable first model for a wake vortex (Fig. 4.6). Because, the vortices cannot end in the fluid, they are closed with a starting vortex (or more typically we just extend the trailing vortices to infinity). The starting vortex is physically observable when impulsively accelerating a wing. Notice that the strength and direction of the vortices must stay constant around the loop. Based on the drawn direction of circulation, we see that the vortices all generate downwash on the inside of the rectangle formed by the vortex filament path. Thus, this model is a first step toward modeling the downwash, that is a consequence of any three-dimensional lifting body, as discussed at the beginning of this chapter. We typically omit the

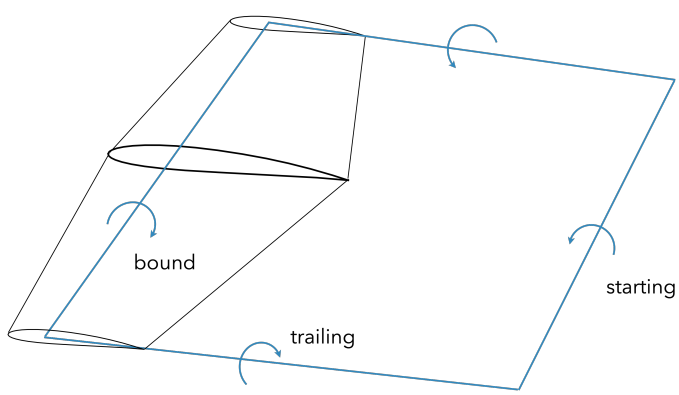

Fig. 4.15 A closed path vortex filament from a wing.

starting vortex, extending the trailing vortices to infinity, and call the resulting configuration a *horseshoe vortex* because of the horseshoe-like shape. From Eq. 4.24 we can compute the predicted downwash w at any location along the wing, based on the trailing vortices. Note that the bound vortex does not contribute any downwash at the quarter-

chord (with the bound vortex placed at the quarter-chord), since the distance from the center of the singularity is zero. The contributions from the two trailing vortices are shown in Fig. 4.16. While we do get downwash across the wing, the model is over simplified. The circulation distribution is modeled as constant along the wing with only one horseshoe vortex, and we know that the circulation must go to zero at the tips. Furthermore, this model predicts infinite downwash at the tip, an unphysical result (in fact, downwash at the tip generally isn't even large for a real wing). So a single horseshoe vortex is clearly insufficient to model a lifting wing, but it provides a starting point for improved models, two of which we will study in this chapter.

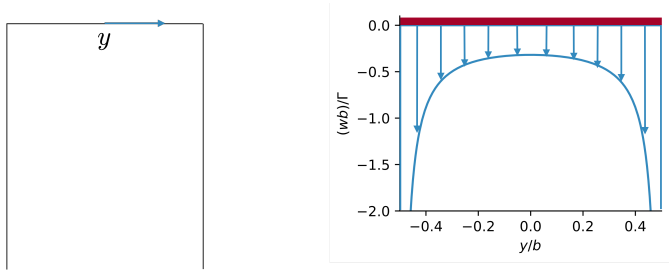

Fig. 4.16 The downwash induced at the wing from a single horseshoe vortex model. Left is a top view showing the horseshoe vortex, and the right figure is a back view showing the resultant downwash distribution.

4.4 Lifting Line Theory

If one horseshoe vortex is too crude to represent a wing, perhaps we can obtain a reasonable model by using multiple horseshoe vortices. A depiction of three horseshoe vortices, and the resulting lift distribution is shown in Fig. 4.17. The lift distribution is blocky, but is a better

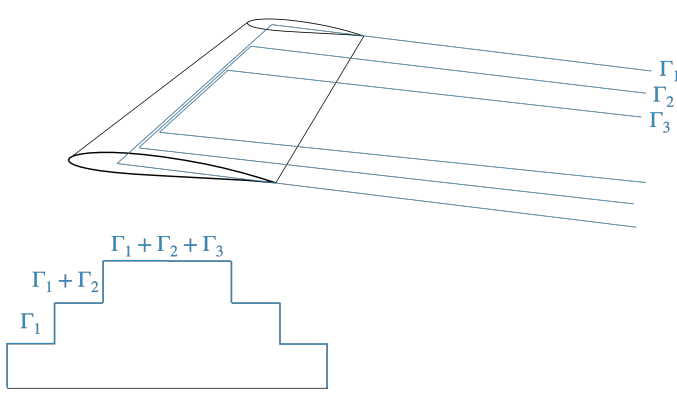

Fig. 4.17 A blocky but more realistic representation of the lift distribution as compared to a single horsesehoe vortex.

representation than the constant lift distribution produced by one

horseshoe. Notice that each additional horseshoe vortex adds an incremental circulation ($\Delta\Gamma$) to the overall circulation. In lifting line theory we extend this idea with an infinite number of horseshoe vortices, each contributing an infinitesimal change $d\Gamma$. Because we have an infinite number of vortices, it is more helpful to think of a continuously varying vorticity distribution, γ, where the vorticity is the derivative of the circulation along the *lifting line* (the line along which vorticity is distributed).

$$\gamma = \frac{d\Gamma}{dy} \tag{4.28}$$

We no longer have horseshoe vortices, but rather a vortex sheet of continuous varying vorticity. That continuously varying vorticity allows us to produce any arbitrary, smooth lift distribution.

We would like to compute the velocity induced by a vortex sheet along the lifting line. Consider Fig. 4.18, where the vorticity (γ) varies along the lifting line (as a function of a dummy variable y'), and we wish to compute the infinitesimal vertical velocity (dw) induced at some other location y. The lift distribution is increased by some $d\Gamma$ at this position, and so the corresponding strength of the trailing vortex at this particular position is: $d\Gamma = \frac{d\Gamma}{dy}dy = \gamma dy$. Each trailing vortex is a semi-infinite vortex, inducing a velocity at position y of (see Eq. 4.9):

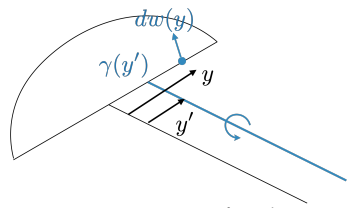

Fig. 4.18 Integration of trailing vortices along the lifting line.

$$dw(y) = -\frac{\gamma(y')dy'}{4\pi(y-y')} \tag{4.29}$$

The negative sign is needed because the circulation is decreasing with y on this side of the wing ($\gamma = d\Gamma/dy < 0$), and with a positive $(y - y')$, the resulting induced velocity is up (positive). Integrating across the lifting line gives:

$$w(y) = -\frac{1}{4\pi}\int_{-b/2}^{b/2}\frac{\gamma(y')dy'}{(y-y')} \tag{4.30}$$

From Fig. 4.11 we see that the induced angle of attack is given by (with the negative sign needed because we defined the induced velocity as positive up in the above equation):

$$\alpha_i = \tan^{-1}\left(\frac{-w}{V_\infty}\right) = \tan^{-1}\left(\frac{1}{4\pi V_\infty}\int_{-b/2}^{b/2}\frac{\gamma(y')dy'}{(y-y')}\right) \tag{4.31}$$

We can relate the lift coefficient to circulation through the Kutta-Joukowsi formula (Eq. 2.36), and the definition of the lift coefficient (eqn:lift2d):

$$L' = \rho V_\infty \Gamma = c_l \frac{1}{2}\rho V_\infty^2 c \Rightarrow c_l = \frac{2\Gamma}{V_\infty c} \tag{4.32}$$

Using the effective angle of attack from Eq. 4.7 in place of the angle of attack in Eq. 1.20, we relate the induced angle of attack to the lift coefficient across the linear portion:

$$c_l = m(\alpha - \alpha_0 - \alpha_i) \tag{4.33}$$

Putting those pieces together gives:

$$\frac{2\Gamma(y)}{V(y)c(y)} = m(y)\left(\alpha(y) - \alpha_0(y) - \tan^{-1}\left(\frac{1}{4\pi V(y)}\int_{-b/2}^{b/2}\frac{\gamma(y')dy'}{(y-y')}\right)\right) \tag{4.34}$$

This equation is known as the *fundamental equation of lifting line theory*. Given a known inflow speed, chord, and airfoil distribution, this equation, in principle, allows us to solve for the resulting lift distribution. The unknowns Γ and γ are not independent; recall that $\gamma = d\Gamma/dy$.

4.4.1 Elliptic Lift Distribution

Before looking at solving for a general situation, we start with a given solution: an elliptic lift distribution (Fig. 4.19). As we will see, an elliptic lift distribution is an efficient design from an induced drag point of view. An elliptic lift distribution is what it sounds like, the distribution of lift follows an elliptic shape:

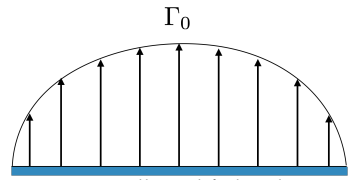

Fig. 4.19 An elliptic lift distribution.

$$\Gamma(y) = \Gamma_0\sqrt{1 - \left(\frac{y}{b/2}\right)^2} \tag{4.35}$$

where Γ_0 is the max circulation at the middle of the wing. The above is actually the circulation distribution, but the lift distribution is just a scalar multiple of this from the Kutta-Joukowski theorem:

$$L'(y) = \rho_\infty V_\infty \Gamma_0\sqrt{1 - \left(\frac{y}{b/2}\right)^2} \tag{4.36}$$

As one would expect, an elliptic lift distribution integrates nicely:

$$L = \int_{b/2}^{b/2} L'dy = \rho_\infty V_\infty \Gamma_0 b\frac{\pi}{4} \tag{4.37}$$

We equate this quantity to the lift from the definition of the lift coefficient:

$$L = C_L\frac{1}{2}\rho V_\infty^2 S \tag{4.38}$$

This allows us to relate the quantity Γ_0 to known properties of the wing:

$$\Gamma_0 = \frac{2V_\infty S C_L}{b\pi} \tag{4.39}$$

We will need the vorticity distribution to use in the fundamental lifting line equation:

$$\gamma(y') = \frac{d\Gamma}{dy}(y') = -\Gamma_0 \frac{4y}{b^2} \frac{1}{\sqrt{1-(2y/b)^2}} \tag{4.40}$$

We will now use the same type of cosine transformation we used in thin airfoil theory (Eq. 2.92), except we want the integrate from -1 to 1 (wingtip to wingtip), rather than from 0 to 1 (leading edge to trailing edge of airfoil):

$$y = \frac{b}{2}\cos\theta \text{ where } \theta = [\pi, 0] \tag{4.41}$$

Plugging the above vorticity distribution into Eq. 4.30, and using the cosine transformation gives the following equation for the induced velocity:

$$w(\theta) = -\frac{\Gamma_0}{2\pi b}\int_\pi^0 \frac{\cos\theta'}{\cos\theta - \cos\theta'} d\theta' \tag{4.42}$$

This is the same integral we saw in deriving thin airfoil theory (Eq. 2.96). Our integral corresponds directly to the $n = 1$ case (Eq. 2.98). Thus, the induced velocity distribution evaluates to:

$$w(\theta) = -\frac{\Gamma_0}{2b} \tag{4.43}$$

From this equation we see that the downwash (down because of the negative sign), is constant along the wing. In other words, *an elliptic lift distribution produces constant downwash*. This will be an important point later, but for now we note that this is a very different distribution than predicted by the overly simplified single horseshoe vortex (Fig. 4.16).

We already related our peak circulation, Γ_0, to known wing quantities (Eq. 4.39), so we plug those into this expression for downwash:

$$w = -\frac{\Gamma_0}{2b} = -\frac{V_\infty C_L}{AR\pi} \tag{4.44}$$

We then use the definition of the induced angle of attack to obtain:

$$\tan\alpha_i = \frac{-w}{V_\infty} = \frac{C_L}{\pi AR} \tag{4.45}$$

With the induced angle of attack defined in terms of known aircraft quantities (for an elliptic lift distribution), we can relate this angle to the lift and induced drag as seen in Fig. 4.20. We see that

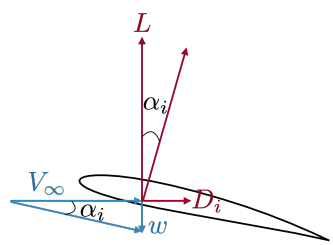

Fig. 4.20 Relationship between induced angle of attack and the lift and induced drag vectors.

$$\tan \alpha_i = \frac{D_i}{L} \tag{4.46}$$

or rearranging, and normalizing:

$$C_{Di} = C_L \tan \alpha_i \tag{4.47}$$

If we substitute the expression for an elliptic lift distribution (Eq. 4.45) we now have an equation for the induced drag produced by an elliptic lift distribution:

$$\boxed{C_{Di} = \frac{C_L^2}{\pi AR}} \tag{4.48}$$

where AR is defined using the reference area. To obtain an expression for induced drag, we multiply both sides by the dynamic pressure:

$$C_{Di}\frac{1}{2}\rho V_\infty^2 S = \frac{C_L^2}{\pi AR}\frac{1}{2}\rho V_\infty^2 S \tag{4.49}$$

Then expand the lift coefficient in terms of lift:

$$D_i = \frac{LC_L}{\pi AR} = \frac{L^2}{q_\infty S \pi AR} \tag{4.50}$$

The final result is:

$$\boxed{D_i = \frac{L^2}{q_\infty \pi b^2}} \tag{4.51}$$

While we assumed we have an elliptic lift distribution, we have not discussed how to produce such a distribution. To better understand this we use the fundamental lifting line equation (Eq. 4.34). For an elliptic lift distribution we've shown that the downwash, and thus the induced angle of attack is constant along the wing. Thus, the $\tan^{-1}$ term is a constant. The circulation term $\Gamma(y)$ is elliptic, and so if we move everything else to the right-hand side, those terms must also form an elliptic distribution. Because the induced angle of attack is constant, and if we assume that the inflow velocity, $V(y)$, is constant along the wing (as would be typical) then the remaining terms:

$$m(y)c(y)(\alpha(y) - \alpha_0(y)) \tag{4.52}$$

must form an elliptic distribution. To simplify, let's assume that we use the same airfoil throughout the wing (though not necessarily the same size airfoil). In that case, the lift curve slope (m) and the zero-lift angle of attack (α_0) would be constant along the wing. We would then need the produce $c(y)\alpha(y)$ to be elliptic. One way to achieve this is to use a wing with no twist, then $\alpha(y)$ is constant, and so the chord distribution

Fig. 4.21 The Supermarine Spitfire is a well-known example of an aircraft with an elliptic wing. Image from Adrian Pingstone, Wikimedia, public domain.

of the wing must be elliptic. This approach was perhaps most famously employed with the Spitfire (Fig. 4.21), a British WWII-era aircraft. If all we need is $c(y)\alpha(y)$ to be elliptic, that means we can produce an elliptic lift distribution with *any* arbitrary chord distribution, by appropriately twisting the wing (and thus changing $\alpha(y)$). Manufacturing an elliptic shape is more expensive, and unnecessary, so such an approach is rarely used anymore. Of course, not just any chord distribution is desirable. There are structural implications, and small chords will lead to premature stall.

4.4.2 Method of Restricted Variations

One simple way to show that the elliptic lift distribution is the minimum induced drag solution (for a fixed span and lift), is the *method of restricted variations*. In this method we consider some arbitrary lift distribution and we add differential amounts of lift at arbitrary locations (Fig. 4.22), subject to some constraints. For example, if we want to minimize induced drag, then we need the differential of induced drag to be zero. From the Kutta-Joukowski theorem the indued drag is given by:

$$D_i = \rho w \Gamma \tag{4.53}$$

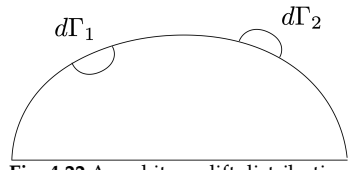

Fig. 4.22 An arbitrary lift distribution from which we add or subtract differential amounts of lift at arbitray locations.

where w is the downwash. Thus, if we add some small amount of circulation at two arbitrary locations, to maintain a minimum in induced drag we require (for an incompressible flow):

$$\delta D_i = 0 \Rightarrow w_1 \delta\Gamma_1 + w_2 \delta\Gamma_2 = 0 \tag{4.54}$$

Furthermore, we want to add these arbitrary circulations such that the lift is constant:

$$\delta L = 0 \Rightarrow \delta\Gamma_1 + \delta\Gamma_2 = 0 \tag{4.55}$$

If we combine these two equations we see that $w_1 = w_2$, but since 1 and 2 are arbitrary locations along the wing, this means that for minimum induced drag, with a fixed lift, the downwash must be constant along the wing. We already saw that an elliptic lift distribution produces constant downwash. Thus, *an elliptic lift distribution is the minimum induced drag solution for a fixed lift and span*.

This simple method can be used to produce various formulas. One example, is adding a root bending moment constraint as was shown by R. T. Jones. Such a constraint is interesting, but not usually useful as a structural constraint as it ignores thickness, and can be misleading for nonplanar wings. One minor variation is to consider minimum induced drag for a nonplanar wing. Figure 4.23 for example shows

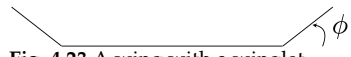

Fig. 4.23 A wing with a winglet.

a wing with a winglet. More generally, we allow to dihedral angle to vary continuously along the wing. In this case, the induced drag equation looks the same except we use the normalwash since "down" is not particularly relevant for a nonplanar wing. The normalwash is the induced velocity normal to the section of the wing. For minimum induced drag we need

$$\delta D_i = 0 \Rightarrow V_{n1}\delta\Gamma_1 + V_{n2}\delta\Gamma_2 = 0 \tag{4.56}$$

The lift equation looks similar, but we need to take only the vertical component of the circulation, which contributes to lift.

$$\delta L = 0 \Rightarrow \delta\Gamma_1 \cos\phi_1 + \delta\Gamma_2 \cos\phi_2 = 0 \tag{4.57}$$

Combing these two equations leads to the insight that the normalwash (V_n), in the farfield, should be proportional to the local dihedral angle:

$$V_n = w_0 \cos\phi \tag{4.58}$$

where w_0 is some constant.

This formula dispels another common misconception associated with winglets. A back view of a wing with a vertical winglet is depicted in Fig. 4.24. We see that the wake vortex, which induces a downwash on the wing, induces a sidewash on the winglet. We then consider a top view of the winglet, showing the airfoil in Fig. 4.25, with the wing-induced sidewash coming from right to left. Vectorially combining this velocity with the freestream results in the relative velocity V_r. From the Kutta-Jouwkoski theorem this inflow would produce a force at a right angle as depicted by the arrow emanating from the airfoil. Thus, we see that the airfoil produces a component of thrust, and is sometimes given as an explanation for why winglets are beneficial.

However, from our above derivation, we can see that this would not be an optimal winglet. The dihedral angle is 90° and so an optimally loaded winglet should be produce a net zero normalwash. Such a scenario is depicted in Fig. 4.26 where the winglet is loaded such that the normalwash of the winglet on itself, exactly cancels the normalwash induced by the wing on the winglet. Thus, no net thrust is produced. While this may seem to have eliminated any benefit, we have not considered the induced velocity of the winglet on the wing. In this scenario, the vortices generated by the winglet would produce an upwash on the main wing (near the tip), thus reducing the induced drag of the wing.

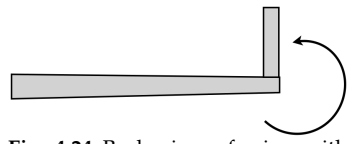

Fig. 4.24 Back view of wing with winglet.

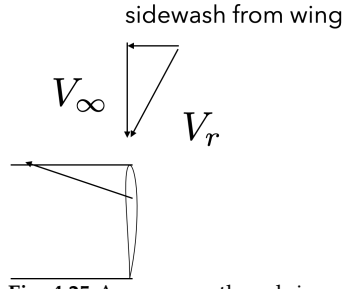

Fig. 4.25 A common, though incorrect explanation for the benefits of winglets.

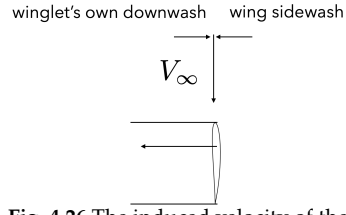

Fig. 4.26 The induced velocity of the wing on winglet cancels the induced velocity of the winglet on itself.

4.4.3 Contribution of the Bound Vortex

In lifting line theory we considered only trailing vortices in our integral. In doing so we obtained the result that the downwash, normalized by the freestream, at the wing should be $-\frac{C_L}{\pi AR}$. More generally, the induced velocity from these trailing vortices is depicted both in front of and downstream of the wing with the red curve shown in Fig. 4.27. As we go far upstream the trailing vortices have no effect, and far downstream they behave like an infinite vortex and so the induced velocity is twice as large. We now consider the bound vortex. The bound vortex may not induce a velocity on itself, but it certainly affects the wing. Far upstream and downstream the bound vortex will not induce any velocity. As we approach the bound vortex, for a straight wing, it will act like a point vortex, inducing very high velocities as we approach the lifting line as depicted with the blue line. The total induced velocity, trailing plus bound, is depicted in green. This is what the actual induced velocity distribution looks like, but this is problematic because the downwash at the wing is clearly not $-\frac{C_L}{\pi AR}$, which was the basis of our induced drag derivation. That result seems to only be applicable if we ignore the bound vortex, which does not seem justifiable.

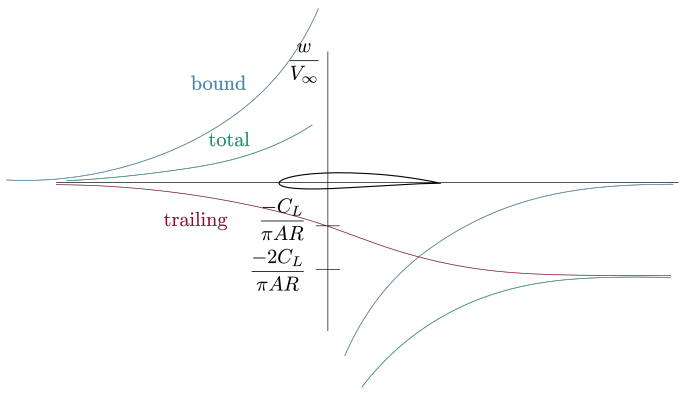

Fig. 4.27 Induced velocity from trailing and bound vortices (both separately and combined).

Fig. 4.28 Bound vorticity distributed along the wing.

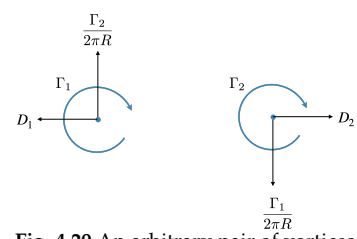

Fig. 4.29 An arbitrary pair of vortices and their mutually induced velocities.

It turns out that we can ignore the influence of the bound vortex, but only when computing drag. In the real wing, the vorticity is not all concentrated along a line, but rather the vorticity is distributed. We could depicted that with a large number of discrete vortices as seen in Fig. 4.28. Let's now consider an arbitrary pair of these vortices, one with circulation Γ_1 and the other with circulation Γ_2 (Fig. 4.29). The first vortex induced a velocity on the second vortex, in the downward

direction with magnitude

$$|w_2| = \frac{\Gamma_1}{2\pi R} \tag{4.59}$$

where R is the distance between them. Conversely, the second induces an upward velocity on the first:

$$|w_1| = \frac{\Gamma_2}{2\pi R} \tag{4.60}$$

From the Kutta-Joukowski theorem the induced drag experienced on the first vortex, from the induced velocity is:

$$D_{i1} = -\rho w_1 \Gamma_1 = -\rho \frac{\Gamma_1 \Gamma_2}{2\pi R} \tag{4.61}$$

where the negative sign came from the right hand rule. Conversely, the induced drag experienced by the second vortex is:

$$D_{i2} = \rho w_2 \Gamma_2 = \rho \frac{\Gamma_1 \Gamma_2}{2\pi R} \tag{4.62}$$

The total induced drag of the pair of vortices ($D_{i1} + D_{i2}$) is 0. Because we chose any two arbitrary vortices, this is a general result: *the total induced drag of the bound vortices always cancels*. This is true for any orientation and in three-dimensions, as long as they are bound vortices (i.e., perpindicular to the freestream velocity). This result demonstrates why the lifting line concept works and why the induced drag formulas are correct, even though we have ignored the influence of the bound vortices.

4.4.4 Lift Curve Slope Reduction

Before considering a more general case, it is also worth noting that the presence of downwash affects the lift curve slope. If we had an infinite wing, with a constant airfoil, the lift coefficient would be given by:

$$C_L = m(a - \alpha_0) \tag{4.63}$$

where m is the lift curve slope, which we saw is theoretically equal to 2π for a thin airfoil (Eq. 2.148). For a finite wing we need to include the induced angle of attack:

$$C_L = m(a - \alpha_0 - \alpha_i) \tag{4.64}$$

In the case, of an elliptic lift distribution (Eq. 4.45) this expression becomes:

$$C_L = m\left(a - \alpha_0 - \tan^{-1}\left(\frac{C_L}{\pi AR}\right)\right) \tag{4.65}$$

If we assume that the induced angle of attack is small then:

$$C_L \approx m\left(a - \alpha_0 - \frac{C_L}{\pi AR}\right) \tag{4.66}$$

We now take derivatives of both sides with respect to α:

$$\frac{dC_L}{d\alpha} = m\left(1 - \frac{dC_L}{d\alpha}\frac{1}{\pi AR}\right) \tag{4.67}$$

Solving for the lift curve slope gives:

$$C_{L,\alpha} = \frac{m}{1 + \frac{m}{\pi AR}} \tag{4.68}$$

This equation shows that if the wing had an infinite aspect ratio, then our lift curve slope would be the same as that of the airfoil, as expected. However, the presence of downwash reduces the lift curve slope of the wing. As an example, for an aspect ratio of 8, the predicted lift curve slope from the above formula would be 1.6π instead of 2π. Note that the above formula is just an approximation that assumes constant airfoils, an elliptic lift distribution, and a small induced angle of attack. Still it is a reasonable first estimate and more importantly illustrates the general behavior of a reduced lift curve slope for a finite wing.

4.4.5 General Lift Distribution

To motivate a general case, let's consider again an elliptic lift distribution:

$$\Gamma(y) = \Gamma_0\sqrt{1 - \left(\frac{y}{b/2}\right)^2} \tag{4.69}$$

but use the coordinate transformation from Eq. 4.41:

$$\Gamma(\theta) = \Gamma_0\sqrt{1 - \cos^2\theta} = \Gamma_0 \sin\theta \tag{4.70}$$

Like we did in thin airfoil theory for a cambered airfoil (Section 2.5.7), we will represent the general case with a Fourier sine series:

$$\Gamma(\theta) = 2bV_\infty \sum_{n=1}^{N} A_n \sin(n\theta) \tag{4.71}$$

The choice of constant $2bV_\infty$ is arbitrary, though we would like to choose it so that the coefficients A_n are nondimensional.

We plug the above into the fundamental lifting line equation (Eq. 4.34).

$$\alpha(\theta) - \alpha_0(\theta) = \frac{2b}{\pi c(\theta)}\sum_{n=1}^{N} A_n \sin(n\theta) + \sum_{n=1}^{N} nA_n \frac{\sin(n\theta)}{\sin\theta} \tag{4.72}$$

In the above we made use of a small angle approximation

$$\alpha_i = \tan^{-1}\left(\frac{-w}{V_\infty}\right) \approx \frac{-w}{V_\infty} \tag{4.73}$$

There are N unknowns, where N depends on how many terms we wish to include in the Fourier series, so we need N equations. This is done through a *collocation* method. This means that we choose N points along the span and apply the above equation at each of the N points, resulting in N equations and N unknowns that we can solve for simultaneously as a linear system of equations. For symmetric loadings, which is common, all the even coefficients of the series $(A_2, A_4, \ldots)$ are zero so we need not include them as unknowns. Asymmetric loadings are used as well, for example, to simulate a wing with aileron deflection.

Because of the orthogonality of the Fourier terms the integral for lift simplifies to:

$$C_L = A_1 \pi AR \tag{4.74}$$

The induced drag equation becomes:

$$C_{Di} = \frac{C_L^2}{\pi AR} \sum_{n=1}^{N} n \left(\frac{A_n}{A_1}\right)^2 \tag{4.75}$$

Even though the lift coefficient only depends on one coefficient, unlike thin airfoil theory, you can't compute A_1 independently. As we saw above with the collocation method, all of the coefficients must be computed simultaneously. Thus, accuracy improves as you include more coefficients in the Fourier series even if we only were interested in lift.

For convenience, the coefficient terms in induced drag are wrapped up into a single constant called the *inviscid span efficiency*:

$$e_{inv} = \left(\sum_{n=1}^{N} n \left(\frac{A_n}{A_1}\right)^2\right)^{-1} \tag{4.76}$$

Then, the induced drag coefficient formula simplifies to:

$$\boxed{C_{Di} = \frac{C_L^2}{\pi AR e_{inv}}} \tag{4.77}$$

or in dimensional terms:

$$\boxed{D_i = \frac{L^2}{q \pi b^2 e_{inv}}} \tag{4.78}$$

If we compare Eq. 4.77 with Eq. 4.48 we see that for an elliptic lift distribution $e_{inv} = 1$. Thus, the inviscid span efficiency could be considered a measure of how close the lift distribution is to elliptic. All planar distributions will have $e_{inv} \leq 1$, so as we saw previously, the elliptic lift distribution is the minimum induced drag solution assuming a planar lift distribution and a fixed span. A nonplanar lift distribution (e.g., adding winglets) can increase the inviscid span efficiency above 1.

Various extensions to lifting line theory have been developed over the years, often referred to as a nonlinear lifting line theory. We do not describe those in more detail here, though they can be quite useful, but rather describe an alternative approach that is perhaps more commonly used in the next section.

4.5 Vortex Lattice Method

The panel methods of Chapter 2 can be extended into three dimensions (with some additional considerations), but we will instead consider a simpler, and widely-used method, for early stage design of three dimensional lifting surfaces (e.g., wings, tails). The vortex lattice method (VLM) is essentially an extension of thin airfoil theory into three dimensions, or it could also be thought of as a simplified implementation of a 3D panel code.

In this method, a lifting surface is divided into panels, and each panel has a horseshoe vortex as shown in Fig. 4.30. The trailing vortices extends into the $+x$ direction of the body axes.

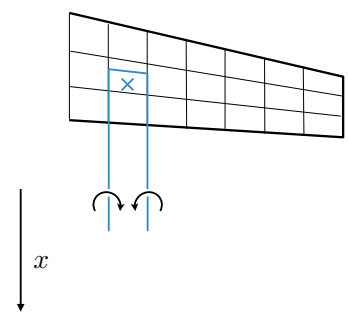

Fig. 4.30 An example paneling on a lifting surface. A horseshoe vortex is depicted on one panel, and each panel will have its own horseshoe vortex. The x denotes the control point for the given panel.

A VLM uses the thin airfoil assumption so that lifting surfaces are flat (not curved), and changes in twist are handled in the boundary condition and not the geometry. A wing may be represented with multiple flat surfaces, for example a wing and winglets. Curved surfaces require a more general 3D panel method.

A VLM can have both spanwise and chordwise panels. If only spanwise panels are used, it is called a *Weissinger* formulation. This simplification is appropriate for high aspect ratio wings where resolving the chordwise pressure distribution is less significant in obtaining an accurate lift distribution.

Because the vortex filaments automatically satisfy the governing equations, the only remaining conditions to satisfy are flow tangency and the Kutta condition. The flow tangency condition (or no-flow-through condition) will be applied at select control points. Because each horseshoe vortex has a constant (as yet unknown) strength, we can only have one control point per panel, thus maintaining an equal

number of unknowns and equations. The control point was denoted as an x in Fig. 4.30.

A vortex lattice method uses what is called a lumped vortex method, this means that distributed vorticity along each panel is all lumped into one vortex as shown in Fig. 2.23. Even with multiple chordwise panels, this approach is still used, just with the vorticity lumped into separate vortices for each chordwise panel. Back in Section 2.5.10 we already considered this exact scenario and determined from thin airfoil theory that the vorticity should be placed at the quarter chord, and the control point at the three-quarters-chord. The placing of the vortex at the quarter chord could also be motivated by the fact that it is the location of the aerodynamic center according to thin airfoil theory as seen previously in Section 2.5.9. Also note that in using the lift result from thin airfoil theory we have implicitly imposed the Kutta condition already. Thus, all that remains is satisfying flow tangency at the control points.

4.5.1 Aerodynamic Influence Coefficients (AIC)

As noted, the control point on each panel is at the section's three-quarters-chord point. There is one control point for each panel. The boundary condition is flow tangency:

$$V_n|_{cp} = 0 \tag{4.79}$$

where the cp subscript denotes a control point, and the boundary condition is applied at each control point separately. The velocity can be broken up into four terms: the freestream velocity, velocity from rigid-body rotation, self-induced velocity from the vortices, and other external velocity sources such as upstream wakes or gusts. The freestream velocity is defined as the negative of the translational motion of the vehicle (thus it is constant for the entire aircraft, unlike gusts which may vary along the aircraft and are lumped in $\vec{V}_{other}$). The flow tangency boundary condition is thus:

$$\left[(\vec{V}_\infty - \vec{\Omega} \times \vec{r}_b + \vec{V}_{ind} + \vec{V}_{other}) \cdot \hat{n}\right]_{cp} = 0 \tag{4.80}$$

where $\vec{r}_b$ is a vector from the aircraft center of gravity to a point of interest. We will move the induced term to one side, and all other terms to the other side (where the cp subscript is dropped for simplicity in notation):

$$\vec{V}_{ind} \cdot \hat{n} = -(\vec{V}_\infty - \vec{\Omega} \times \vec{r} + \vec{V}_{other}) \cdot \hat{n} \tag{4.81}$$

To keep the notation simple we will denote the velocity on the right-hand side as $\vec{V}_{ext}$ (external velocity).

$$\vec{V}_{ind} \cdot \hat{n} = -\vec{V}_{ext} \cdot \hat{n} \tag{4.82}$$

In general the rotational velocity, self-induced velocity, and other velocity sources like gusts all vary along the aircraft, and so this boundary condition will be applied separately at each control point i.

$$\vec{V}_{ind,i} \cdot \hat{n}_i = -\vec{V}_{ext,i} \cdot \hat{n}_i \tag{4.83}$$

External Velocities

Angle of attack and sideslip angle are defined in the standard way (Fig. 4.31). In this case, the the freestream velocity vector in the body axes is:

$$\vec{V}_\infty = V_\infty \begin{bmatrix} \cos\alpha\cos\beta \\ -\sin\beta \\ \sin\alpha\cos\beta \end{bmatrix} \tag{4.84}$$

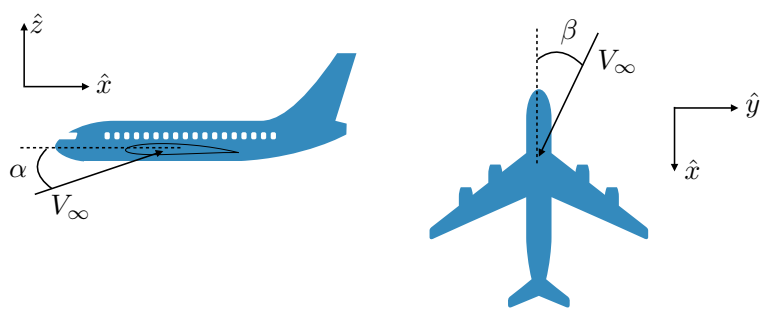

Fig. 4.31 Angle of attack and sideslip shown in body axes.

The rotational velocity is defined about the center of gravity and is simply:

$$\Omega = \begin{bmatrix} \Omega_x \\ \Omega_y \\ \Omega_z \end{bmatrix} \tag{4.85}$$

The radial vector used in determining rotational velocities is the distance from the aircraft center of gravity to the control point of interest:

$$\vec{r}_i = \vec{r}_{cp,i} - \vec{r}_{cg} \tag{4.86}$$

If we only have one chordwise panel, or even if we have a few, it generally doesn't make sense to use camber in defining the normal direction. Furthermore, camber was implicitly accounted for in the use of positioning the bound vortex and control point (recall that the

derivation assumed parabolic camber of any arbitrary magnitude). The normal vector is a function of the local twist and dihedral as shown in Fig. 4.32. Twist cannot be lumped with angle of attack for nonplanar wings. To illustrate why, imagine the twist on a winglet (sometimes called the cant angle), it moves the surface in a very different way than changing the angle of attack of the entire aircraft.

From Fig. 4.32 we can resolve $\hat{\zeta}$ and $\hat{n}$ into components as follows:

$$\hat{\zeta} = -\sin\phi\,\hat{y} + \cos\phi\,\hat{z} \tag{4.87}$$

$$\hat{n} = \sin\theta\,\hat{x} + \cos\theta\,\hat{\zeta} \tag{4.88}$$

Substituting Eq. 4.87 into Eq. 4.88 yields:

$$\hat{n} = \begin{bmatrix} \sin\theta \\ -\cos\theta\sin\phi \\ \cos\theta\cos\phi \end{bmatrix} \tag{4.89}$$

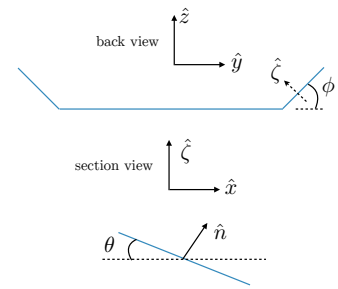

Fig. 4.32 Angles and coordinate systems used to determine normal vector to each panel. Top figure shows dihedral, while the bottom shows twist.

Using the panel discretization where y and z define the corner points of the horseshoe vortices (Fig. 4.33):

$$\sin\phi_i = \frac{z_{i+1} - z_i}{\sqrt{(y_{i+1} - y_i)^2 + (z_{i+1} - z_i)^2}} \tag{4.90}$$

$$\cos\phi_i = \frac{y_{i+1} - y_i}{\sqrt{(y_{i+1} - y_i)^2 + (z_{i+1} - z_i)^2}} \tag{4.91}$$

Induced Velocities

From the Biot-Savart law (Eq. 4.17) the induced velocity from all of the vortex filaments at control point i is:

$$\vec{V}_{ind,i} = \sum_j \frac{\Gamma_j}{4\pi} \int_j \frac{d\vec{l}_j \times \vec{r}_{ij}}{|r_{ij}|^3} \tag{4.92}$$

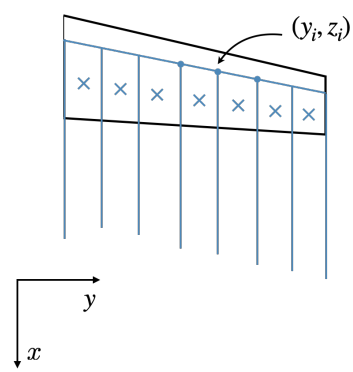

Fig. 4.33 Panel discretization defined by the corner points.

where r_{ij} is the distance from a point on the line vortex j to control point i. We can reexpress this sum by separating out the geometric terms from the circulation:

$$\vec{V}_{ind,i} = \sum_j \hat{V}_{ij}\Gamma_j \tag{4.93}$$

where $\hat{V}$ is the induced velocity at the control point, for unit circulation. Thus, the boundary condition at the ith control point (Eq. 4.83) becomes:

$$\sum_j \Gamma_j \hat{V}_{ij} \cdot \hat{n}_i = -\vec{V}_{ext,i} \cdot \hat{n}_i \tag{4.94}$$

Each control point is one equation, and putting them all together forms a linear system of equations:

$$[AIC]\Gamma = b \tag{4.95}$$

where

$$b_i = -\vec{V}_{ext,i} \cdot \hat{n}_i \tag{4.96}$$

and the aerodynamic influence coefficient matrix is given by:

$$AIC_{ij} = \hat{V}_{ij} \cdot \hat{n}_i \tag{4.97}$$

The main challenge then is to determine $\hat{V}_{ij}$

We use the velocity induced by a vortex segment (Eq. 4.24) to compute the induced velocity from a horseshoe vortex, which is comprised of three segments. This time we will need to be more careful with directions. First, we convert this expression in terms of vectors so that we can use it more generally in a computational implementation. Second, the angles θ are less convenient to work with, we would prefer to use vectors instead. We define the quantities $\vec{r}_0$, $\vec{r}_1$ and $\vec{r}_2$ as shown in Fig. 4.34. Vector $\vec{r}_0$ starts at one end of the vortex filament and ends at the other end of the filament pointing in the direction of positive circulation according to the right hand rule. Vector $\vec{r}_1$ points from the start of the filament to the point of interest, and vector $\vec{r}_2$ points from the end of the filament to the point of interest.

We use the definition of the dot product to obtain the angles.

$$\vec{r}_0 \cdot \vec{r}_1 = |\vec{r}_0||\vec{r}_1| \cos\theta_1 \Rightarrow \cos\theta_1 = \frac{\vec{r}_0 \cdot \vec{r}_1}{|\vec{r}_0||\vec{r}_1|} \tag{4.98}$$

$$\vec{r}_0 \cdot \vec{r}_2 = |\vec{r}_0||\vec{r}_2| \cos\theta_2 \Rightarrow \cos\theta_2 = \frac{\vec{r}_0 \cdot \vec{r}_2}{|\vec{r}_0||\vec{r}_2|} \tag{4.99}$$

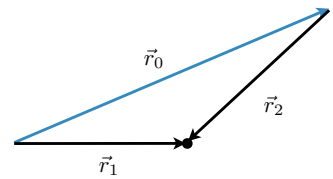

Fig. 4.34 Definitions for vectors used in horseshoe vortex derivation.

The distance h is just $r_1 \sin\theta_1$, but again we want to eliminate the explicit dependence on angles. Using the definition of the cross product:

$$|\vec{r}_0 \times \vec{r}_1| = |\vec{r}_0||\vec{r}_1| \sin\theta_1 \tag{4.100}$$

Thus,

$$h = |\vec{r}_1| \frac{|\vec{r}_0 \times \vec{r}_1|}{|\vec{r}_0||\vec{r}_1|} = \frac{|\vec{r}_0 \times \vec{r}_1|}{|\vec{r}_0|} \tag{4.101}$$

Finally, we need to determine the direction of V_θ. We have defined $\vec{r}_0$ to correspond to the direction of the circulation $\vec{\Gamma}$. Thus, the direction is a unit vector in the direction of $\vec{r}_0 \times \vec{r}_1$. In other words,

$$\vec{V}_\theta = V_\theta \frac{\vec{r}_0 \times \vec{r}_1}{|\vec{r}_0 \times \vec{r}_1|} \tag{4.102}$$

Putting all of these pieces together yields:

$$\begin{aligned}\vec{V}_\theta &= \frac{\Gamma|\vec{r}_0|}{4\pi|\vec{r}_0\times\vec{r}_1|}\frac{\vec{r}_0\times\vec{r}_1}{|\vec{r}_0\times\vec{r}_1|}\left(\frac{\vec{r}_0\cdot\vec{r}_1}{|\vec{r}_0||\vec{r}_1|}-\frac{\vec{r}_0\cdot\vec{r}_2}{|\vec{r}_0||\vec{r}_2|}\right)\\ &= \frac{\Gamma}{4\pi}\frac{\vec{r}_0\times\vec{r}_1}{|\vec{r}_0\times\vec{r}_1|^2}\left(\frac{\vec{r}_0\cdot\vec{r}_1}{|\vec{r}_1|}-\frac{\vec{r}_0\cdot\vec{r}_2}{|\vec{r}_2|}\right)\end{aligned} \tag{4.103}$$

To simplify further we can express $\vec{r}_0$ in terms of $\vec{r}_1$ and $\vec{r}_2$:

$$\vec{r}_0 = \vec{r}_1 - \vec{r}_2 \tag{4.104}$$

Making this substitution yields:

$$= \frac{\Gamma}{4\pi}\frac{\vec{r}_1\times\vec{r}_2}{|\vec{r}_1\times\vec{r}_2|^2}\left(\frac{|\vec{r}_1|^2-\vec{r}_2\cdot\vec{r}_1}{|\vec{r}_1|}-\frac{\vec{r}_1\cdot\vec{r}_2-|\vec{r}_2|^2}{|\vec{r}_2|}\right) \tag{4.105}$$

We can expand the cross product in the denominator:

$$\begin{aligned}|\vec{r}_1\times\vec{r}_2|^2 &= (\vec{r}_1\times\vec{r}_2)\cdot(\vec{r}_1\times\vec{r}_2)\\ &= (\vec{r}_1\cdot\vec{r}_1)(\vec{r}_2\cdot\vec{r}_2)-(\vec{r}_2\cdot\vec{r}_1)(\vec{r}_1\cdot\vec{r}_2)\\ &= |\vec{r}_1|^2|\vec{r}_2|^2-(\vec{r}_1\cdot\vec{r}_2)^2\end{aligned} \tag{4.106}$$

Let's also simplify the expression in parenthesis from Eq. 4.105. We will factor out a common term:

$$\begin{aligned}\left(\frac{|\vec{r}_1|^2-\vec{r}_2\cdot\vec{r}_1}{|\vec{r}_1|}-\frac{\vec{r}_1\cdot\vec{r}_2-|\vec{r}_2|^2}{|\vec{r}_2|}\right) &= \left(|\vec{r}_1|-\frac{\vec{r}_1\cdot\vec{r}_2}{|\vec{r}_1|}-\frac{\vec{r}_1\cdot\vec{r}_2}{|\vec{r}_2|}+|\vec{r}_2|\right)\\ &= \left(\frac{|\vec{r}_1||\vec{r}_2|}{|\vec{r}_2|}-\frac{\vec{r}_1\cdot\vec{r}_2}{|\vec{r}_1|}-\frac{\vec{r}_1\cdot\vec{r}_2}{|\vec{r}_2|}+\frac{|\vec{r}_1||\vec{r}_2|}{|\vec{r}_1|}\right)\\ &= (|\vec{r}_1||\vec{r}_2|-\vec{r}_1\cdot\vec{r}_2)\left(\frac{1}{|\vec{r}_2|}+\frac{1}{|\vec{r}_1|}\right)\end{aligned} \tag{4.107}$$

If we substitute Eq. 4.106 and Eq. 4.107 into Eq. 4.105 we get

$$\vec{V}_\theta = \frac{\Gamma}{4\pi}\frac{\vec{r}_1\times\vec{r}_2}{(|\vec{r}_1|^2|\vec{r}_2|^2-(\vec{r}_1\cdot\vec{r}_2)^2)}(|\vec{r}_1||\vec{r}_2|-\vec{r}_1\cdot\vec{r}_2)\left(\frac{1}{|\vec{r}_2|}+\frac{1}{|\vec{r}_1|}\right) \tag{4.108}$$

We can now factor the term in the denominator

$$|\vec{r}_1|^2|\vec{r}_2|^2-(\vec{r}_1\cdot\vec{r}_2)^2 = \left[|\vec{r}_1||\vec{r}_2|+(\vec{r}_1\cdot\vec{r}_2)\right]\left[|\vec{r}_1||\vec{r}_2|-(\vec{r}_1\cdot\vec{r}_2)\right] \tag{4.109}$$

which partially cancels with one of the terms in the numerator. The result is an expression for the induced velocity from one vortex filament in terms of only the two vectors $\vec{r}_1$ and $\vec{r}_2$.

$$\boxed{\vec{V}_\theta = \frac{\Gamma}{4\pi}\frac{\vec{r}_1\times\vec{r}_2}{(|\vec{r}_1||\vec{r}_2|+\vec{r}_1\cdot\vec{r}_2)}\left(\frac{1}{|\vec{r}_1|}+\frac{1}{|\vec{r}_2|}\right)} \tag{4.110}$$

Now we apply this formula to the horseshoe vortex shown in Fig. 4.35. For the two bound vortices we need to allow some of the vector magnitudes to extend to infinity to represent the semi-infinite vortices.

The bound vortex uses all the terms of the formula. We use subscript B to denote the vectors shown in Fig. 4.36.

$$\vec{V}_{\theta B} = \frac{\Gamma}{4\pi} \frac{\vec{r}_{1B} \times \vec{r}_{2B}}{(|\vec{r}_{1B}||\vec{r}_{2B}| + \vec{r}_{1B} \cdot \vec{r}_{2B})} \left(\frac{1}{|\vec{r_{1B}}|} + \frac{1}{|\vec{r_{2B}}|} \right) \tag{4.111}$$

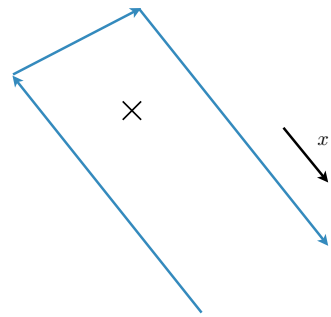

Fig. 4.35 A horseshoe vortex.

For the left vortex (Fig. 4.37) we can see that as the end of the vortex goes to infinity:

$$|\vec{r}_{1L}| \to \infty \tag{4.112}$$

$$\frac{\vec{r}_{1L}}{|\vec{r}_{1L}|} = -\hat{x} \tag{4.113}$$

If we divide the top and bottom of Eq. 4.110 by $|\vec{r}_1|$ and let $|\vec{r}_1| \to \infty$ the expression simplifies (where we use L to denote the left vortex):

$$\vec{V}_{\theta L} = \frac{\Gamma}{4\pi} \frac{-\hat{x} \times \vec{r}_{2L}}{(|\vec{r}_{2L}| - \hat{x} \cdot \vec{r}_{2L})} \left(\frac{1}{|\vec{r_{2L}}|} \right) \tag{4.114}$$

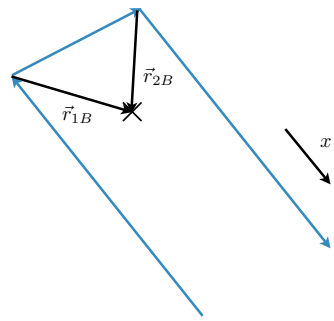

Fig. 4.36 Contribution of bound vortex induced velocity at the control point.

But note that $\vec{r}_{2L} = \vec{r}_{1B}$, so we can rewrite this contribution as:

$$\vec{V}_{\theta L} = \frac{\Gamma}{4\pi} \frac{\vec{r}_{1B} \times \hat{x}}{(|\vec{r}_{1B}| - \vec{r}_{1B} \cdot \hat{x})} \left(\frac{1}{|\vec{r_{1B}}|} \right) \tag{4.115}$$

For the right vortex (Fig. 4.38) we see that as the vortex goes off to infinity:

$$|\vec{r}_{2R}| \to \infty \tag{4.116}$$

$$\frac{\vec{r}_{2R}}{|\vec{r}_{2R}|} = -\hat{x} \tag{4.117}$$

If we divide the top and bottom of Eq. 4.110 by $|\vec{r}_2|$ and let $|\vec{r}_2| \to \infty$ the expression simplifies (where we use R to denote the right vortex):

$$\vec{V}_{\theta R} = \frac{\Gamma}{4\pi} \frac{\vec{r}_{1R} \times -\hat{x}}{(|\vec{r}_{1R}| + \vec{r}_{1R} \cdot -\hat{x})} \left(\frac{1}{|\vec{r_{1R}}|} \right) \tag{4.118}$$

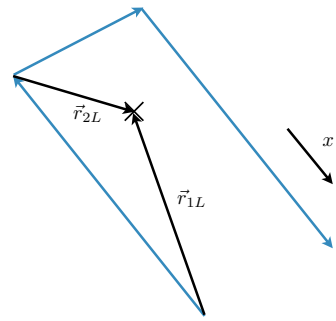

Fig. 4.37 Contributions from the left semi-infinite vortex.

But note that $\vec{r}_{1R} = \vec{r}_{2B}$, so we can rewrite this contribution as:

$$\vec{V}_{\theta R} = -\frac{\Gamma}{4\pi} \frac{\vec{r}_{2B} \times \hat{x}}{(|\vec{r}_{2B}| - \vec{r}_{2B} \cdot \hat{x})} \left(\frac{1}{|\vec{r_{2B}}|} \right) \tag{4.119}$$

Putting it all together (and dropping the B subscript): the total induced velocity at some point r measured relative to the bound vortex corners as seen in Fig. 4.36 is:

$$\vec{V} = \frac{\Gamma}{4\pi}\left[\frac{\vec{r}_1 \times \vec{r}_2}{(|\vec{r}_1||\vec{r}_2| + \vec{r}_1 \cdot \vec{r}_2)}\left(\frac{1}{|\vec{r}_1|} + \frac{1}{|\vec{r}_2|}\right) + \frac{\vec{r}_1 \times \hat{x}}{(|\vec{r}_1| - \vec{r}_1 \cdot \hat{x})}\frac{1}{|\vec{r}_1|} - \frac{\vec{r}_2 \times \hat{x}}{(|\vec{r}_2| - \vec{r}_2 \cdot \hat{x})}\frac{1}{|\vec{r}_2|}\right] \tag{4.120}$$

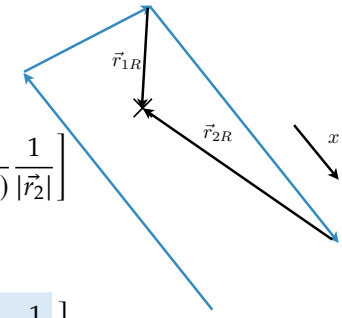

Fig. 4.38 Contributions from the right semi-infinite vortex.

Finally, we want the velocity for unit circulation and so

$$\hat{V}_{ij} = \frac{1}{4\pi}\left[\frac{\vec{r}_1 \times \vec{r}_2}{(|\vec{r}_1||\vec{r}_2| + \vec{r}_1 \cdot \vec{r}_2)}\left(\frac{1}{|\vec{r}_1|} + \frac{1}{|\vec{r}_2|}\right) + \frac{\vec{r}_1 \times \hat{x}}{(|\vec{r}_1| - r_{1x})}\frac{1}{|\vec{r}_1|} - \frac{\vec{r}_2 \times \hat{x}}{(|\vec{r}_2| - r_{2x})}\frac{1}{|\vec{r}_2|}\right] \tag{4.121}$$

where each vector points from the corner of the horseshoe vortex at position j to control point i (Fig. 4.39):

$$\vec{r}_1 = \vec{r}_{CPi} - \vec{r}_j \tag{4.122}$$

$$\vec{r}_2 = \vec{r}_{CPi} - \vec{r}_{j+1} \tag{4.123}$$

Symmetry

If the aircraft is symmetric then it is more efficient to only solve for the circulation on half of the aircraft. This reduces the size of the linear system in half. Solving a dense linear system is approximately an $O(n^3)$ operation, and the linear system solve is the main computational cost of the VLM, so if taking advantage of symmetry is possible it is generally worth doing so. This is straightforward in constructing the AIC matrix. The only change is that for each control point we need to add the influence of horseshoe vortex i as well as the influence from its mirror image $-i$. The vector $\vec{r}_{-i}$ is identical to $\vec{r}_i$ except that the sign of the y component is flipped (assuming symmetry about the x-z plane).

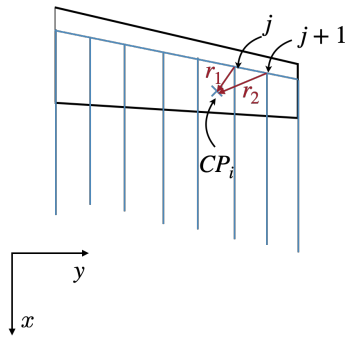

Fig. 4.39 Depiction of two vectors used in computing influence of bound vortex j at control point i.

4.5.2 Near-Field Forces and Moments

Forces and moments can be computed in the near field using the Kutta-Joukowski theorem:

$$\vec{F}_i' = \rho \vec{V}_i \times \vec{\Gamma}_i \tag{4.124}$$

First, we must compute the local velocity vector at each bound vortex. Like the boundary condition, this requires a sum of the the freestream velocity (translation), rotation, induced velocity, and other external velocities.

$$\vec{V} = \vec{V}_\infty - \vec{\Omega} \times \vec{r}_b + \vec{V}_{ind} + \vec{V}_{other} \tag{4.125}$$

This time the induced velocity is not computed at the control points, but rather at the center of the bound vortex. We can reuse Eq. 4.121, but evaluated at the center of each bound vortex. This eliminates the first term (when evaluating the influence of the panel on itself) because the bound vortex does not induce any velocity on itself. The velocity induced at the center of vortex i is:

$$\vec{V}_{ind,i} = \sum \Gamma_j \bar{V}_{ij} \tag{4.126}$$

The induced velocity per unit circulation, $\bar{V}_{ij}$, is computed using Eq. 4.121, but with the following vectors.

$$\vec{r}_1 = \vec{r}_{i,mid} - \vec{r}_j \tag{4.127}$$

$$\vec{r}_2 = \vec{r}_{i,mid} - \vec{r}_{j+1} \tag{4.128}$$

where $\vec{r}_{i,mid} = (\vec{r}_i + \vec{r}_{i+1})/2$.

Using the Kutta-Joukowski theorem, where the force is constant across a panel, results in a force for each panel of:

$$\vec{F}_i = \rho \vec{V}_i \times \vec{\Gamma}_i \Delta s_i \tag{4.129}$$

where the direction of Γ is defined by

$$\vec{\Gamma}_i \Delta s_i = \Gamma_i (\vec{r}_{i+1} - \vec{r}_i) \tag{4.130}$$

The total forces are then

$$\vec{F} = \sum_i \vec{F}_i \tag{4.131}$$

$$= \sum_i \rho \Gamma_i \left(\sum_j (\Gamma_j \hat{V}_{ij}) + \vec{V}_\infty - \vec{\Omega} \times \vec{r}_i + \vec{V}_{other,i} \right) \times (\vec{r}_{i+1} - \vec{r}_i) \tag{4.132}$$

The total moments are given by:

$$\vec{M} = \sum_i \vec{r}_{m,i} \times \vec{F}_i \tag{4.133}$$

where $\vec{r}_{m,i}$ is the vector originating from some specified reference point (often the aircraft c.g.) and ending at the location of force F_i (i.e., $\vec{r}_{m,i} = \vec{r}_{i,mid} - \vec{r}_{cg}$).

These forces and moments are in the body coordinate system. However, as aerodynamicists, we generally care about forces in the wind axes (oriented with the freestream) because that is the coordinate system where lift and drag are defined. The rotation from body axes to

wind axes is accomplished by the following rotations:

$$\begin{bmatrix} D \\ Y \\ L \end{bmatrix} = \begin{bmatrix} \cos\beta & -\sin\beta & 0 \\ \sin\beta & \cos\beta & 0 \\ 0 & 0 & 1 \end{bmatrix} \begin{bmatrix} \cos\alpha & 0 & \sin\alpha \\ 0 & 1 & 0 \\ -\sin\alpha & 0 & \cos\alpha \end{bmatrix} \begin{bmatrix} F_x \\ F_y \\ F_z \end{bmatrix} \tag{4.134}$$

We rotate moments similarly (although for dynamics leaving them in the body-coordinate system in generally preferred).

4.5.3 Simpler Alternative to Estimating Forces/Moments

The above procedure for computing the forces/moments is a bit complex for a first implementation and not necessary most of the time. For many simulations there is no sideslip, rotation, or gusts. Furthermore, if we neglect the impact of self-induction on the forces/moments we can simplify the calculations greatly. Most scenarios are symmetric, and thus the side force, rolling moment, and yawing moment calculations are unnecessary as they will end up at zero. This impact of induction on lift is almost always negligibly small, and consequently the impact on pitching moments is too. Drag is of course, a different story as it occurs because of the induced velocities, but this is most accurately computed with a far-field method anyway (discussed in following section).

In other words, we assume that the total velocity vector is:

$$\vec{V} = \begin{bmatrix} V_\infty \cos\alpha \\ 0 \\ V_\infty \sin\alpha \end{bmatrix} \tag{4.135}$$

With this assumptions the lift across the wing can be computed as:

$$\boxed{L = \rho V_\infty \sum_i \Gamma_i (y_{i+1} - y_i)} \tag{4.136}$$

where the sum occurs across each panel. This can be derived from the above equations neglecting the induction terms, or directly from the Kutta-Joukowski theorem using a wind coordinate system. To see this, note that the trailing vortices are in the x-direction and so the x-component of velocity will not contribute any force, and the z-component will only create forces in the y direction, which must all cancel out for a symmetric case. The bound vortex can, in general, have all three components. The x component is the same as the trailing vortices and contributes nothing. The z component is the same (just reversed role for x and z). The only nonzero contributor is the y component of circulation. Thus, the lift from an individual panel is:

$$\rho V_\infty \Gamma_y \Delta s \tag{4.137}$$

However, from Fig. 4.40 we see that $\Gamma_y = \Gamma \cos \Lambda$ and the length $\Delta s = dy/\cos \Lambda$ thus the lift from an individual panel can be expressed as:

$$\rho V_\infty \Gamma \Delta y \tag{4.138}$$

This expression is equally valid for nonplanar wings.

Similarly, the pitching moment is given by:

$$M = -\rho V_\infty \cos \alpha \sum_i r_{xi} \Gamma_i (y_{i+1} - y_i) \tag{4.139}$$

where r_x is the distance in the body frame from the point where the moment is computed about (usually the c.g.) to the middle of the quarter chord of each panel. Keep in mind that that this is the moment from the lift distribution and does not include any pitching moments generated by the airfoil shape. In other words, one generally needs to add the pitching moments contributed from the airfoils to obtain an accurate total pitching moment of the wing/aircraft.

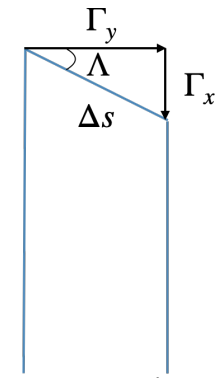

Fig. 4.40 Depiction of a vortex segment on a swept wing.

Notice that the angle of attack appears because the lift is perpendicular to V_∞ (wind frame) but the distance r_x is measured in the body frame (see Fig. 4.41). This simplified approach leaves out one additional term, the contribution to the moment from $r_z F_x$. Effectively this is the contribution of drag to the pitching moment (though not exactly, because F_x and drag occur in different axes), but this term is almost always very small as drag is much smaller than lift and r_z is much smaller than r_x.

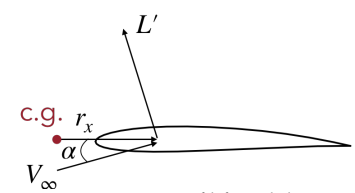

Fig. 4.41 Direction of lift and distance from c.g. to location lift is computed at.

4.5.4 Far-field Induced Drag

The induced drag can also be evaluated in the far-field using a Trefftz plane analysis with a drag-free wake. We leverage the concept discussed in Section 1.11 where forces can be determined from the velocity and pressure field on far away control surfaces. In the case of drag, for an incompressible flow, we only need to know the velocity field on a downstream plane, which is called the Trefftz plane. This procedure generally produces a more accurate estimate of induced drag.

The proper way to evaluate the drag is to evolve the wake downstream (this is called a force-free wake). Unfortunately, wake propagation is computationally intensive. A far-field analysis shows that a drag-free wake, even though the wake shape is nonphysical, produces the same induced drag as the actual force-free wake*. A drag-free wake

*Not exactly. We do need to neglect a couple of terms, though a careful analysis of a variety of wing shapes shows those terms to be negligibly small, especially for the level of fidelity we are interested in with a VLM.

(i.e., a wake that simply moves straight back in the freestream direction) is *much* simpler to compute. Using our wind coordinate system it means that the wake simply projects straight back in the $+x_w$ direction (which differs from the $+x_b$ direction we have been using, although the difference between these two is generally negligibly small for purposes of projecting the wake). The induced drag calculation then simply becomes a two-dimensional analysis computing the influence of the wake on itself.

A farfield analysis shows that the induced drag is (a general result, not specific to VLM):

$$D_i = \int \frac{\rho}{2} V_n \Gamma ds \tag{4.140}$$

where the integral is performed across the wake trace, Γ is the circulation shed at the trailing edge of the aircraft, equivalent to the potential jump across the wake, and V_n is the normlwash (induced velocity normal to the wake). For the VLM case, we have discretized spanwise panels and so the induced drag becomes a summation:

$$D_i = \frac{\rho}{2} \sum_i V_{ni} \Gamma_i \Delta s_i \tag{4.141}$$

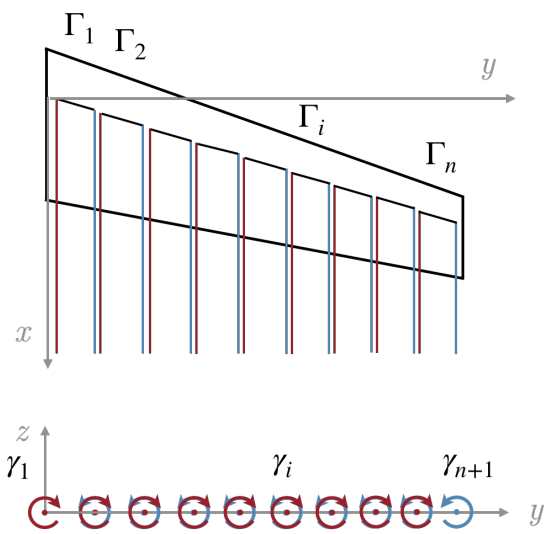

Fig. 4.42 Wake trace from horseshoe vortices in farfield. Only half of wing is shown, but the below assumes we are modeling the full wing.

Each panel sheds two vortices of opposite signs, that overlap with the neighboring vortices as shown in Fig. 4.42. These vortex strengths partially cancel. If Γ_i defines the circulation of each horseshoe vortex,

and γ_i is the net circulation of each point vortex in the far-field, then:

$$\gamma_i = \begin{cases} -\Gamma_1 & \text{for } i = 1 \\ \Gamma_{i-1} - \Gamma_i & \text{for } i = 2 \ldots n \\ \Gamma_n & \text{for } i = n+1 \end{cases} \tag{4.142}$$

Figure 4.43 diagrams the analysis we need to perform. A given point vortex j induces a velocity on the center of panel i. The center point of panel i is the projection of the control points, or if not given we will assume linear spacing:

$$\bar{y}_i = \frac{1}{2}(y_{i+1} + y_i) \tag{4.143}$$

$$\bar{z}_i = \frac{1}{2}(z_{i+1} + z_i) \tag{4.144}$$

$$\tag{4.145}$$

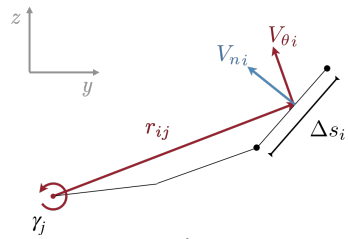

Fig. 4.43 Diagram for computing induced velocities in farfield.

Each point vortex γ_j induces a tangential velocity given by:

$$\vec{V}_{\theta,ij} = \frac{\vec{\gamma}_j \times \hat{r}_{ij}}{2\pi|r_{ij}|} = \frac{\vec{\gamma}_j \times \vec{r}_{ij}}{2\pi|r_{ij}|^2} \tag{4.146}$$

The induced velocity V_θ is always perpendicular to r_{ij}, but we want the component of velocity that is normal to panel i (the negative sign exists because downwash is positive in the induced drag calculation):

$$V_{nij} = -\vec{V}_{\theta,ij} \cdot \hat{n}_i \tag{4.147}$$

$$\tag{4.148}$$

and

$$V_{ni} = \sum_j V_{nij} \tag{4.149}$$

The induced drag is thus:

$$D_i = \frac{\rho}{2} \sum_i \sum_j \Gamma_i V_{nij} \Delta s_i \tag{4.150}$$

$$= \frac{\rho}{2} \sum_i \sum_j \Gamma_i \left(-\frac{\vec{\gamma}_j \times \vec{r}_{ij}}{2\pi|r_{ij}|^2} \right) \cdot \hat{n}_i \Delta s_i \tag{4.151}$$

$$\tag{4.152}$$

The circulation is always aligned with the x-axis because it is a drag-free wake, and thus r is always in the $y - z$ plane. Calculating this

explicitly:

$$\vec{\gamma}_j = \gamma_j \hat{x} \tag{4.153}$$

$$\vec{r}_{ij} = (\bar{y}_i - y_j)\hat{y} + (\bar{z}_i - z_j)\hat{z} \tag{4.154}$$

$$\vec{\gamma}_j \times \vec{r}_{ij} = \gamma_j(\bar{y}_i - y_j)\hat{z} - \gamma_j(\bar{z}_i - z_j)\hat{y} \tag{4.155}$$

$$\hat{n}_i = -\sin\phi_i \hat{y} + \cos\phi_i \hat{z} \tag{4.156}$$

$$\hat{n}_i \Delta s_i = -(z_{i+1} - z_i)\hat{y} + (y_{i+1} - y_i)\hat{z} \tag{4.157}$$

$$(\vec{\gamma}_j \times \vec{r}_{ij}) \cdot (\hat{n}_i \Delta s_i) = \gamma_j(\bar{z}_i - z_j)(z_{i+1} - z_i) + \gamma_j(\bar{y}_i - y_j)(y_{i+1} - y_i) \tag{4.158}$$

$$V_{nij}\Delta s_i = \frac{-\gamma_j(\bar{z}_i - z_j)(z_{i+1} - z_i) - \gamma_j(\bar{y}_i - y_j)(y_{i+1} - y_i)}{2\pi[(\bar{y}_i - y_j)^2 + (\bar{z}_i - z_j)^2]} \tag{4.159}$$

The result is that the induced drag is given by:

$$D_i = \frac{\rho}{4\pi} \sum_{i=1}^{n} \sum_{j=1}^{n+1} \Gamma_i \gamma_j k_{ij} \tag{4.160}$$

where

$$k_{ij} = \frac{(y_j - \bar{y}_i)(y_{i+1} - y_i) + (z_j - \bar{z}_i)(z_{i+1} - z_i)}{(y_j - \bar{y}_i)^2 + (z_j - \bar{z}_i)^2} \tag{4.161}$$

The sum over i occurs across each control point, whereas the sum over j occurs over each vortex at the edges of the panels.

Symmetry

If the wing and circulation distribution is symmetric, and we model only half of the wing, then the induced drag only requires a sum on half of the wing (multiplied by 2):

$$D_i = \rho_\infty \sum_{i=1}^{N} V_{ni}\Gamma_i \Delta s_i \tag{4.162}$$

If we sum only over half of the wing we have to modify the calculation of Γ_1 since the circulation in the middle of the wing exactly cancels with the other side (see Fig. 4.42).

$$\gamma_i = \begin{cases} 0 & \text{for } i = 1 \\ \Gamma_{i-1} - \Gamma_i & \text{for } i = 2 \ldots n \\ \Gamma_n & \text{for } i = n + 1 \end{cases} \tag{4.163}$$

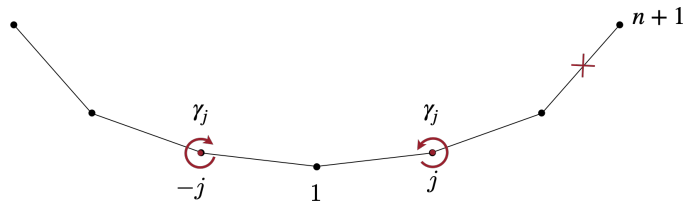

Fig. 4.44 Induced velocity in the farfield for a symmetric configuration.

Also, when calculating the induced velocity at panel i we should add not only the contribution from γ_j on the same side of the wing, but the contribution from γ_j on the opposite side of the wing as depicted in Fig. 4.44. The resulting induced drag is:

$$D_i = \frac{\rho}{2\pi} \sum_{i=1}^{n} \sum_{j=1}^{n+1} \Gamma_i \gamma_j (k_{i,j} - k_{i,-j}) \tag{4.164}$$

where

$$k_{i,\pm j} = \frac{(\pm y_j - \bar{y}_i)(y_{i+1} - y_i) + (z_j - \bar{z}_i)(z_{i+1} - z_i)}{(\pm y_j - \bar{y}_i)^2 + (z_j - \bar{z}_i)^2} \tag{4.165}$$

Compressible Flow

5

Potential flow has been a useful assumption allowing us to solve for aerodynamic flowfields around low-speed objects. The inclusion of a boundary layer model addressed a major limitation of the viscous (non-irrotational) behavior near the body. In this section we discuss fundamentals of compressible flow. We then relax the incompressibility assumption to extend potential flow to some compressible flow regimes. We will see that we can extend the methodologies we have been using to compressible flow fields if we can add a restriction on small disturbances (thin bodies, small angles of attack). Finally, we discuss shock wave and expansion theory, which are exact solutions as an alternative to the simplifications introduced for compressible potential flow.

5.1 Compressible Flow Fundamentals

We begin with a review of thermodyamics and some key concepts related to compressible flow.

5.1.1 Mach Cone

As an initial motivation to compressibility, consider a one-dimensional disturbance in a pipe. Imagine a small transmitter that makes a periodic beeping noise. In the top of Fig. 5.1 we see sound waves moving, at the speed of sound (a), in both directions. Now imagine a freestream flow in the pipe, moving left to right, at a speed less than the speed of sound. This scenario is depicted in the middle pane of Fig. 5.1. The sound waves moving to the left of the transmitter now move at the reduced speed $a - V$, relative to an inertial frame, whereas the sound waves on the right move faster at the speed $V + a$. From the figure we see that the frequency is also changed with the background moving air so that the waves are compressed to the left, and expanded to the right. If we now increase the freestream speed so that V is greater than the speed of sound, we have the scenario on the bottom of Fig. 5.1. The sound waves emitted to the right move even faster at the speed $V + a$. However, the sound waves that were emitted to the left, are

completely overwhelmed by the high speed flow, and actually move to the right at the speed $V - a$. Thus, no sound waves are transmitted upstream. In other words, if you were standing in the pipe upstream of the transmitter, you could walk all the way up to it and not hear it at all. *In supersonic flow disturbances cannot flow upstream*.

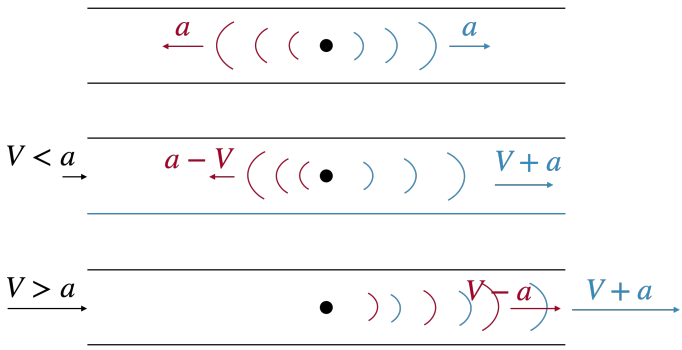

Fig. 5.1 A one-dimensional flow example with a sound wave emitter and varying freestream speeds in a pipe.

Let's now consider a similar scenario in three dimensions. In the stationary case, not drawn, spherical sound waves radiate out in all directions. Now imagine that the transmitter is moving at a subsonic speed ($M < 1$), or equivalently is stationary in a subsonic freestream. This is depicted on the left of Fig. 5.2. The scenario is similar to that

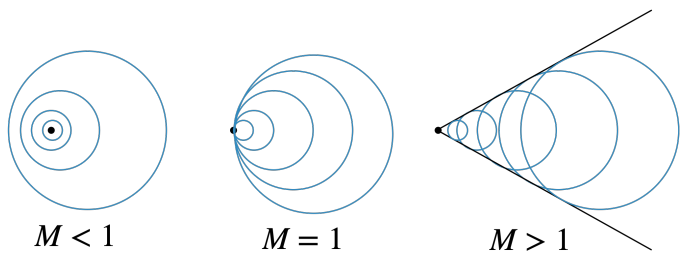

Fig. 5.2 A three-dimensional flow example with a sound wave emitter and varying freestream speeds.

of the one-dimensional case with subsonic inflow. The sound waves are compressed in the front, and expand in the back. As we increase in speed, we reach the limiting case ($M = 1$), where no sound waves are omitted forward, instead they pile up in a vertical front. The case on the right shows the scenario where the transmitter moves faster than the speed of sound ($M > 1$). In this case, all the sound waves travel to the right, like that they do in the 1D case, except that they form a *Mach cone*.

Another way to think about this shape, is that as each spherical sound wave is emitted, the transmitter flys faster than that wave, thus moving outside of it, before emitting the next wave. Instead of piling

up vertically, the sound waves pile up along the Mach cone. As the Mach number increases the Mach cone tilts flatter. Isolating one sound wave in Fig. 5.3 we can see that the angle if related by:

$$\sin \mu = \frac{a}{V} = \frac{1}{M} \tag{5.1}$$

Therefore the *Mach angle* is given by:

$$\mu = \sin^{-1}\left(\frac{1}{M}\right) \tag{5.2}$$

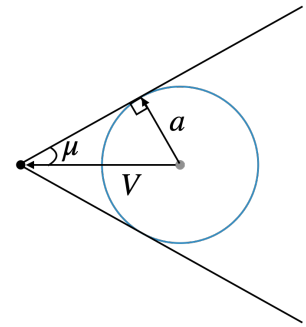

Fig. 5.3 Mach cone and one sound wave depicted.

Like the 1D case, the implication is that outside of the Mach cone you could not hear the transmitter. Notice that if you are above (or below) the transmitter, there are regions you could be where the transmitter would fly past you but you still would not have heard it yet.

For an aircraft the scenario is similar, except that the pressure waves are continuous, and they are not infinitesimally weak disturbances (which is what sound waves are). Instead, we get shock waves, which will be discussed later in this chapter. But for now we note that a Mach cone is an infinitesimally weak shock wave and represents the limiting case.

5.1.2 Ideal Gas

In fluids we are primarily interested in *intensive* properties. Intensive properties are not dependent on the size of the system, and instead are properties defined at a point. Some intensive variables, like pressure, temperature, and density, that we are already familiar with, do not have an extensive counterpart (extensive variables depend on the size of the system). Other intensive variables that do have an extensive counterpart are often referred to as *specific* quantities, and are defined per unit mass. For example, *specific volume*, v, is the volume per unit mass, or the inverse of density:

$$v = \frac{1}{\rho} \tag{5.3}$$

Specific internal energy, e, is the internal energy per unit mass, and specific entropy, s, is the entropy per unit mass. Specific enthalpy, h, is the enthalpy per unit mass and is defined as:

$$h = e + pv \tag{5.4}$$

Conceptually, you could think of enthalpy as a combination of internal energy plus work, where the work is that required to reach the given

pressure and volume. Note that even though we have used the term "work", enthalpy, like all of these other parameters, is a *state variable*, meaning that it is path independent and only depends on the current state. The variables pressure, temperature, and density that we are already familiar with are also state variables.

Thermodynamic state variables are related through an *equation of state*. Any two intensive thermodynamic quantities completely define the state. In other words, a third variable would not be independent but rather would depend on the first two. We can write any intensive property as a function of any two other intensive properties. For example:

$$e = e(s, T) \tag{5.5}$$

$$T = T(s, v) \tag{5.6}$$

$$p = p(h, T) \tag{5.7}$$

The most common equation of state is the *ideal gas law*:

$$p = p(\rho, T) = \rho R T \tag{5.8}$$

where R is the *specific gas constant*. For air, that is not chemically reacting, its value is:

$$R = 286.9 \frac{\mathrm{J}}{\mathrm{kg} \cdot \mathrm{K}} \tag{5.9}$$

An ideal gas assumes that the intermolecular forces between the gas molecules are negligible. In contrast, a *real gas* accounts for intermolecular forces. Intermolecular forces become significant if the air is at a very high pressure and a low temperature, a scenario which rarely applies in the field of aerodynamics. Sometimes vibration, dissociation, and ionization that occurs at the high temperatures of reentry vehicles are called real-gas effects, but this is a misnomer. These behaviors are not caused by intermolecular forces, but rather by chemical reactions and other high temperature effects that we shall discuss shortly.

The most general case of ideal gases occurs with chemically reacting mixtures of ideal gases. In this case chemical reactions occur, but intermolecular forces are still negligible. Air becomes a chemically reacting mixture of ideal gases above approximately 2500 K.

If there are no chemical reactions, then for an ideal gas the internal energy only depends on temperature. The proof is a bit lengthy, but traverses some concepts we need anyway.

We start with the first law of thermodynamics, which can be expressed as:

$$de = \delta q + \delta w \tag{5.10}$$

This equation states that the change in the internal energy of an isolated system is equal to the energy applied as heat (q) and as work on the surroundings (w). We use the differential de because internal energy is a state variable, whereas the changes in work and heat and noted by δ since they are, in general, path dependent. For a *reversible* process (e.g., inviscid), the work done by a fluid on a system is:

$$\delta w = -pdv \tag{5.11}$$

The second law of thermodynamics can be expressed as:

$$ds \geq \frac{\delta q}{T} \tag{5.12}$$

where s is the entropy, and T is the temperature. In an idealized process, where the heat transfer is reversible, then the expression is an equality and we place these last two equations in the first law of thermodynamics to obtain:

$$de = Tds - pdv \tag{5.13}$$

or

$$Tds = de + pdv \tag{5.14}$$

which is known as *Gibbs equation*. This is an expression of the first and second law of thermodynamics for a reversible process, or as a way to relate thermodynamic variables at a given state. We can also write this equation in terms of enthalpy by taking derivatives of its definition (Eq. 5.4) and substituting in the Gibbs equation:

$$Tds = dh - vdp \tag{5.15}$$

Or we can express in terms of the *Gibbs free energy*: $g = h = Ts$. Substituting this into Gibbs equation gives:

$$dg = vdp - sdT \tag{5.16}$$

To prove that internal energy for an ideal gas depends only on temperature, let us first assume the general case, where internal energy depends on two variables: $e = e(P, T)$. The total differential is given by:

$$de = \left(\frac{\partial e}{\partial p}\right)_T dp + \left(\frac{\partial e}{\partial T}\right)_p dT \tag{5.17}$$

We want to derive the conditions where the dependence on pressure drops out, and the internal energy thus only depends on temperature. In other words, to show under what conditions:

$$\left(\frac{\partial e}{\partial p}\right)_T = 0 \tag{5.18}$$

We can rewrite the Gibbs equation (Eq. 5.14) in terms of this derivatives:

$$\left(\frac{\partial e}{\partial p}\right)_T = T\left(\frac{\partial s}{\partial p}\right)_T - p\left(\frac{\partial v}{\partial p}\right)_T \tag{5.19}$$

If we compare one of the forms of Gibbs equation (Eq. 5.16) with a differential for $g(p,T)$:

$$dg = \left(\frac{\partial g}{\partial p}\right)_T dp + \left(\frac{\partial g}{\partial T}\right)_p dT \tag{5.20}$$

we see that:

$$v = \left(\frac{\partial g}{\partial p}\right)_T \tag{5.21}$$

and

$$s = -\left(\frac{\partial g}{\partial T}\right)_p \tag{5.22}$$

The second partial derivatives shown below must also be equal:

$$\frac{\partial^2 g}{\partial p \partial T} = \frac{\partial^2 g}{\partial T \partial p} \tag{5.23}$$

Applying that in this case gives:

$$\left(\frac{\partial v}{\partial T}\right)_p = -\left(\frac{\partial s}{\partial p}\right)_T \tag{5.24}$$

This is one of the *Maxwell relations*. We can derive other such identities in a similar way using different forms of the Gibbs equation, comparing the differentials, and equating second derivatives. For our present purposes this is the only identity we need. We substitute this into Eq. 5.19 to obtain:

$$\left(\frac{\partial e}{\partial p}\right)_T = -T\left(\frac{\partial v}{\partial T}\right)_p - p\left(\frac{\partial v}{\partial p}\right)_T \tag{5.25}$$

We now have a relationship between internal energy and the specific volume. The right side vanishes for a constant density fluid. But it also vanishes for an ideal gas ($v = \frac{RT}{p}$):

$$\left(\frac{\partial e}{\partial p}\right)_T = -T\frac{R}{p} + p\frac{R}{Tp^2} = 0 \tag{5.26}$$

Actually, it vanishes any fluid where $v = f(T/p)$. Thus, the left side of Eq. 5.17 vanishes and so $e = e(T)$ only. From the definition of enthalpy,

we can show that for an ideal gas the enthalpy also only depends on temperature.

$$h = e + pv \tag{5.27}$$
$$= e + RT \tag{5.28}$$
$$= e(T) + RT \tag{5.29}$$
$$\Rightarrow h = h(T) \tag{5.30}$$

We call this a *thermally perfect gas*.

5.1.3 Heat Capacity

A thermally perfect gas has implications on its heat capacity. The specific heat capacity is heat capacity per unit mass, where heat capacity refers to the amount of heat required to produce a unit change in temperature. For a gas, heat capacity differs significantly if the heating occurs in a fixed container (constant volume), or in the atmosphere where it can expand (constant pressure). These two quantities are called the specific heat capacity at constant volume and constant pressure respectively. Mathematically they are defined as:

$$c_v \equiv \left(\frac{\partial e}{\partial T}\right)_v \tag{5.31}$$
$$c_p \equiv \left(\frac{\partial h}{\partial T}\right)_p \tag{5.32}$$

For a thermally perfect gas, both e and h are functions only of temperature and so these become simple differentials.

$$c_v \equiv \left(\frac{de}{dT}\right)_v \tag{5.33}$$
$$c_p \equiv \left(\frac{dh}{dT}\right)_p \tag{5.34}$$

For a *calorically perfect gas*, the specific heats are also independent of temperature, and are thus considered constants.

$$e = c_v T \tag{5.35}$$
$$h = c_p T \tag{5.36}$$

For both of these latter two cases, the specific heats are related to the specific gas constant as follows. From the definitions of the specific heat capacities:

$$c_p - c_v = \frac{d}{dT}(h - e) \tag{5.37}$$

We then use the definition of enthalpy (Eq. 5.4):

$$c_p - c_v = \frac{d}{dT}(pv) \tag{5.38}$$

Now, the ideal gas law (Eq. 5.8):

$$c_p - c_v = \frac{d}{dT}(RT) = R \tag{5.39}$$

Thus,

$$c_p - c_v = R \tag{5.40}$$

Another key parameter is the ratio of specific heats:

$$\gamma = \frac{c_p}{c_v} \tag{5.41}$$

Using this equation and Eq. 5.40 we can show that:

$$c_p = \frac{\gamma}{\gamma - 1}R \tag{5.42}$$

$$c_v = \frac{1}{\gamma - 1}R \tag{5.43}$$

Thus, any two of these constants defines the gas.

To better understand the different conditions separating calorically perfect, thermally perfect, a chemically reacting mixture of ideal gases, and real gases, we consider the nature of the diatomic molecules that make up air (Fig. 5.4). In classical statistical mechanics the internal energy of a molecule is given by:

$$e = \frac{1}{2}nRT \tag{5.44}$$

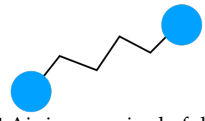

Fig. 5.4 Air is comprised of diatomic molecules.

where n is the number of degrees of freedom. Or in terms of the specific heat capacity at constant volume:

$$c_v = \frac{\partial e}{\partial T} = \frac{1}{2}nR \tag{5.45}$$

For most aerodynamic scenarios the temperature is such that the translational and rotational degrees of freedom are active. There are three translational modes, and while there are also three rotational modes, in practice only two are realized. That is because of the nature of a diatomic molecule where the moment of inertia about the internuclear axis (line joining the two atoms), is negligibly small compared to the

moments of inertia about the other two axes (not only because of the shape but also because almost all the mass of an atom is concentrated at its center). Thus, it would take an inordinately high temperature to reach this last rotational energy state. Thus, for most aerodynamic scenarios these five modes are activated, and the specific heats can be considered constant (i.e., calorically perfect):

$$c_v = \frac{5}{2}R \tag{5.46}$$

$$c_p = \frac{7}{2}R \tag{5.47}$$

$$\gamma = \frac{7}{5} = 1.4 \tag{5.48}$$

For everything in this book we will assume a calorically perfect gas.

If temperature increases beyond approximately 700 K (e.g., at higher Mach numbers), then the vibration mode is activated, which is an exchange of potential and kinetic energy along the internuclear axis. In this case, the specific heats can no longer be considered constant, but rather are a function of temperature (i.e., thermally perfect).

If temperature increases even further, beyond approximately 2500K for air, then chemical reactions begin (i.e., a chemically reacting mixture of ideal gases). Now the specific heats are a function of temperature and pressure.

To reach the "real" gas state (i.e., not an ideal gas), we would need to go the other way and decrease temperature, while simultaneously increasing pressure tremendously (say above 1,000 atm).

5.1.4 Isentropic Relations

An isentropoic flow is both adiabatic (no heat or mass transfer) and is reversible. In this case:

$$\frac{Ds}{Dt} = 0\,, \tag{5.49}$$

which means that the total derivative of the entropy is zero. In other words, the entropy is constant for a given fluid particle. If steady, then the entropy is constant along a streamline, and any many aerodynamic flows the freestream is uniform and so the entropy is then constant everywhere.

We use Gibbs equation (Eq. 5.14), rewritten as follows:

$$ds = \frac{de}{T} + \frac{p}{T}dv \tag{5.50}$$

Using the definition of the heat capacity at constant volume for a calorically perfect gas (Eq. 5.35) for the de term, and the ideal gas equation of state for the second term (Eq. 5.8) yields:

$$ds = c_v \frac{dT}{T} + R \frac{dv}{v} \tag{5.51}$$

If calorically perfect then c_v is constant with temperature and we can integrate both sides:

$$s_2 - s_1 = c_v \ln\left(\frac{T_2}{T_1}\right) + R \ln\left(\frac{v_2}{v_1}\right) \tag{5.52}$$

For an isentropic process $s_2 - s_1 = 0$ and thus we have:

$$\frac{c_v}{R} \ln\left(\frac{T_2}{T_1}\right) = -\ln\left(\frac{v_2}{v_1}\right) \tag{5.53}$$

Using the properties of a logarithm, we can rewrite both terms as:

$$\begin{aligned} \ln\left(\frac{T_2}{T_1}\right)^{\frac{c_v}{R}} &= \ln\left(\frac{v_1}{v_2}\right) \\ &= \ln\left(\frac{\rho_2}{\rho_1}\right) \end{aligned} \tag{5.54}$$

Using Eq. 5.43 and taking the exponential of both sides gives:

$$\left(\frac{T_2}{T_1}\right)^{\frac{1}{\gamma-1}} = \left(\frac{\rho_2}{\rho_1}\right) \tag{5.55}$$

Similarly, we can use Gibbs equation in terms of the enthalpy (Eq. 5.15):

$$ds = \frac{dh}{T} - v\frac{dp}{T} \tag{5.56}$$

Use the definition of the coefficient of specific heat at constant pressure, for a thermally perfect gas (Eq. 5.36), and the ideal gas law (Eq. 5.8):

$$ds = c_p \frac{dT}{T} - R\frac{dp}{p} \tag{5.57}$$

We integrate both sides and use the isentropic assumption:

$$0 = c_p \ln\left(\frac{T_2}{T_1}\right) - R \ln\left(\frac{p_2}{p_1}\right) \tag{5.58}$$

Use the logarithm properties and Eq. 5.42 gives:

$$\ln\left(\frac{T_2}{T_1}\right)^{\frac{\gamma}{\gamma-1}} = \ln\left(\frac{p_2}{p_1}\right) \tag{5.59}$$

Taking the exponential of both sides results in:

$$\left(\frac{T_2}{T_1}\right)^{\frac{\gamma}{\gamma-1}} = \left(\frac{p_2}{p_1}\right) \tag{5.60}$$

Comparing this equation with Eq. 5.55 we have the *isentropic relations* for a calorically perfect gas:

$$\frac{p_2}{p_1} = \left(\frac{\rho_2}{\rho_1}\right)^{\gamma} = \left(\frac{T_2}{T_1}\right)^{\frac{\gamma}{\gamma-1}} \tag{5.61}$$

5.1.5 Energy Equation

For incompressible flows we only needed a mass and momentum equation. Those balance laws provide 4 equations for the 4 independent variables (pressure and the three components of velocity). For compressible flows we have added another variable, ρ, and so need another equation. The internal energy and temperature are not new variables but rather are state variables defined through an equation of state (Section 5.1.2) and heat capacity equations (Section 5.1.3).

Following the same pattern as shown previously in Eq. 1.58 we can form an energy balance equation:

$$\frac{\partial}{\partial t}\int_{\forall} \rho\epsilon d\forall + \int_S \rho\epsilon(\vec{V}\cdot d\vec{A}) = \dot{W}_{in} + \dot{Q}_{in} \tag{5.62}$$

where $\epsilon = e + \frac{V^2}{2}$ is the total specific energy (specific internal energy plus specific kinetic energy), and the last two terms are the net work and heat into the system. This is a form of the first law of thermodynamics (Eq. 5.10).

Work on the fluid comes from pressure and shear stresses acting on the exterior control surface. As it is not used in this chapter will not expand on the viscous component of the work term:

$$\dot{W} = -\int_S p(\vec{V}\cdot d\vec{A}) + W_{\text{viscous}} \tag{5.63}$$

Other sources of work internal to the the control volume, for example from a shaft, may exist and would need to explicitly added.

For heat there is a volumetric heating term and a viscous term that we do not expand on here:

$$\dot{Q} = \int_{\forall} \rho\dot{q} d\forall + Q_{\text{viscous}} \tag{5.64}$$

where $\dot{q}$ is the rate of heat addition per unit mass.

If we plug this into the above energy equation it becomes:

$$\frac{\partial}{\partial t}\int_{\forall}\rho\epsilon d\forall + \int_S \rho h_T(\vec{V}\cdot d\vec{A}) = \int_{\forall}\rho\dot{q}d\forall + W_{\text{viscous}} + Q_{\text{viscous}} \tag{5.65}$$

where $h_T = h + \frac{V^2}{2}$ is the total enthalpy, and $\dot{W}_{other,in}$ refers to other work terms.

Commuting differentiation and integration, and using the divergence theorem results in:

$$\int_{\forall}\frac{\partial\rho\epsilon}{\partial t}d\forall + \int_{\forall}\nabla\cdot(\rho h_T\vec{V})d\forall = \int_{\forall}\rho\dot{q}d\forall + \text{ viscous terms} \tag{5.66}$$

We now put everything into one integral, and as before because this equation must apply to any control volume in the fluid the integrand must be zero everywhere. This gives the differential form, where we have used an inviscid assumption:

$$\frac{\partial\rho\epsilon}{\partial t} + \nabla\cdot(\rho h_T\vec{V}) = \rho\dot{q} \tag{5.67}$$

Extra work terms, like shaft work can still be explicit added to this equation.

The first term we can express in terms of total enthalpy:

$$\begin{aligned}\rho\epsilon &= \rho e + \rho\frac{V^2}{2}\\ &= \rho e + \rho\frac{V^2}{2} + \rho\frac{p}{\rho} - p\\ &= \rho e + \rho\frac{V^2}{2} + \rho p\nu - p\\ &= \rho h + \rho\frac{V^2}{2} - p\\ &= \rho h_T - p\end{aligned} \tag{5.68}$$

Substituting into the energy equation gives:

$$\frac{\partial\rho h_T}{\partial t} + \nabla\cdot(\rho h_T\vec{V}) = \frac{\partial p}{\partial t} + \rho\dot{q} \tag{5.69}$$

To make this equation more useful we expand the derivatives:

$$h_T\frac{\partial\rho}{\partial t} + \rho\frac{\partial h_T}{\partial t} + h_T\nabla\cdot(\rho\vec{V}) + \nabla h_T\cdot\rho\vec{V} = \frac{\partial p}{\partial t} + \rho\dot{q} \tag{5.70}$$

The first and third terms go to zero from the continuity equation (Eq. 1.64).

$$\rho \frac{\partial h_T}{\partial t} + \nabla h_T \cdot \rho \vec{V} = \frac{\partial p}{\partial t} + \rho \dot{q} \tag{5.71}$$

If steady and adiabatic, good assumptions for much of aerodynamics, the equations simplifies considerably to:

$$\nabla h_T \cdot \rho \vec{V} \tag{5.72}$$

In words, this equation means that total enthalpy is constant along a streamline. This result is a much simpler form of the energy equation:

$$h_{T1} = h_{T2} \tag{5.73}$$

or

$$h_1 + \frac{V_1^2}{2} = h_2 + \frac{V_2^2}{2} \tag{5.74}$$

This is a form of Bernoulli's equation, but for a compressible flow. It comes with all of the same limitations (except incompressibility): steady, along a streamline, no work or heat transfer, inviscid. The freestream for many compressible flow scenarios comes from a reservoir of constant total enthalpy, and in those cases the total enthalpy is constant everywhere. The simplicity of this equation makes it highly useful for many compressible flows.

Because we have assumed adiabatic and invscid, the flow is isentropic. Using Eq. 5.56 for constant entropy we see that:

$$dh = v dp \tag{5.75}$$

If we now invoke an incompressibility assumption we can integrate both sides to get:

$$h_2 - h_1 = \frac{1}{\rho}(p_2 - p_1) \tag{5.76}$$

Substituting this into Section 5.1.7, and multiplying through by ρ gives the classic Bernoulli equation:

$$p_1 + \frac{1}{2}\rho V_1^2 = p_2 + \frac{1}{2}\rho V_2^2 \tag{5.77}$$

or

$$p_{T1} = p_{T2} \tag{5.78}$$

where p_T is the total pressure. Note that this makes use of the incompressible definition of total pressure, a definition that is not applicable for a compressible flow. We will learn what total pressure looks like for a compressible flow later in this chapter.

5.1.6 Speed of Sound

A sound wave is an infinitesimally weak pressure wave. That means that the flow properties may change, isentropically, by some differential amount across a sound wave as pictured in Fig. 5.5 We will denote a as the speed of sound, or in other words the speed that a sound wave moves in the fluid.

We now consider a small control volume whose sides are parallel to the sound wave. Thus, the fluid enters one side of the control volume, and exits on the other side of the sound wave. Applying a mass balance across the sound wave yields:

$$\rho a A = (\rho + d\rho)(a + da)A \tag{5.79}$$

where A is some arbitrary cross-sectional size based on the control volume size. Cancelling out the area term, expanding the products on the right hand side, and neglecting the product of differential terms gives:

$$\rho a = \rho a + a d\rho + \rho da \tag{5.80}$$

$$\Rightarrow da = -\frac{a}{\rho} d\rho \tag{5.81}$$

Next, we apply a momentum balance across the sound wave. Because a sound wave is an isentropic disturbance there are no viscous terms.

$$pA + \rho a^2 A = (p + dp)A + (\rho + d\rho)(a + da)^2 A \tag{5.82}$$

$$0 = dp + 2\rho a da + a^2 d\rho \tag{5.83}$$

We substitute in the results from Eq. 5.81

$$0 = dp - 2a^2 d\rho + a^2 d\rho \tag{5.84}$$

$$\Rightarrow dp = a^2 d\rho \tag{5.85}$$

The result is:

$$\boxed{a = \sqrt{\left(\frac{\partial p}{\partial \rho}\right)_s}} \tag{5.86}$$

The subscript s denotes that this is the partial derivative at constant entropy (i.e., an isentropic process). From Eq. 5.61 we see that for a calorically perfect isentropic process we can write:

$$\frac{p}{\rho^\gamma} = \text{constant} \tag{5.87}$$

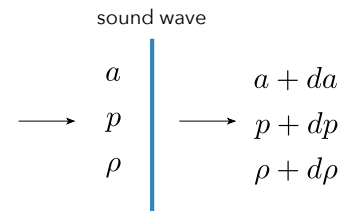

Fig. 5.5 A sound wave, or infinitely weak disturbance, across which the fluid properties change by some differential amount.

Taking derivatives and substituting into the speed of sound gives:

$$a = \sqrt{\frac{\gamma p}{\rho}} \tag{5.88}$$

For an ideal gas, which is applicable since we already made a more restrictive calorically perfect assumption, we have the following expression for the speed of sound:

$$\boxed{a = \sqrt{\gamma R T}} \tag{5.89}$$

Thus, we see that for a calorically perfect gas, the speed of sound is only a function of temperature.

This formula allows for a more convenient form of dynamic pressure in compressible flows.

$$\begin{aligned} q &= \frac{1}{2}\rho V^2 \\ &= \frac{1}{2}\rho M^2 a^2 \\ &= \frac{1}{2}\rho M^2 \frac{\gamma p}{\rho} \\ &= \frac{\gamma}{2} p M^2 \end{aligned} \tag{5.90}$$

This latter form is typically a more convenient representation of dynamic pressure for compressible flows:

$$\boxed{q = \frac{\gamma}{2} p M^2} \tag{5.91}$$

5.1.7 Total (Stagnation) Quantities

Stagnation pressure, or *total pressure*, is the equivalent pressure we would obtain if we took a point in the fluid and isentropically slowed it to stagnation. Note that total pressure is a property of the fluid at every point. It is well defined at every point in the fluid whether or not the point in question is at a stagnation point or whether or not the flow is isentropic.

Using a form of the energy equation appropriate for an isentropic process

$$h_1 + \frac{V_1}{2} = h_2 + \frac{V_2}{2} \tag{5.92}$$

For a calorically perfect gas we can substitute in Eq. 5.36:

$$c_p T_1 + \frac{V_1}{2} = c_p T_2 + \frac{V_2}{2} \tag{5.93}$$

Now let's consider condition 1 our hypothetical stagnation condition, and condition 2 the flow conditions at an arbitrary point in the fluid:

$$c_p T_T = c_p T + \frac{V}{2} \tag{5.94}$$

where T_T is called the *total temperature*. Rearranging and using the relationship between c_p and the other gas constants Eq. 5.42 as well as the equation for the speed of sound (Eq. 5.89):

$$\frac{T_T}{T} = 1 + \frac{(\gamma - 1)}{2} M^2 \tag{5.95}$$

Using the isentropic relations (Eq. 5.61) then gives us expressions for *total pressure* and *total density*:

$$\frac{p_T}{p} = \left(1 + \frac{\gamma - 1}{2} M^2\right)^{\gamma/(\gamma-1)} \tag{5.96}$$

$$\frac{\rho_T}{\rho} = \left(1 + \frac{\gamma - 1}{2} M^2\right)^{1/(\gamma-1)} \tag{5.97}$$

Note that the compressible definition for total pressure (Eq. 5.96) is very different then the incompressible counterpart ($p_T = p + \frac{1}{2}\rho V^2$)

5.1.8 Viscosity

Classical thermodynamics does not provide an expression for viscosity in terms of other thermodynamic variables. Instead we rely on kinetic theory and experiments. For a gas, a commonly-used model is called *Sutherland's Law*:

$$\mu(T) = \mu_{ref} \left(\frac{T}{T_{ref}}\right)^{3/2} \frac{T_{ref} + S}{T + S} \tag{5.98}$$

where

$$\mu_{ref} = 1.716 \times 10^{-5} \text{ kg/(m·s)} \tag{5.99}$$

$$T_{ref} = 273.15 \text{ K} \tag{5.100}$$

$$S = 110.4 \text{ K} \tag{5.101}$$

Note that the viscosity is only a function of temperature.

5.2 Full Potential Equation

We continue with the same assumption of irrotational flow:

$$\nabla \times \vec{V} = 0 \tag{5.102}$$

but now allow the fluid to be compressible. Irrotational flow can still be a useful approximation for some compressible flows. Shock waves are an irreversible process and so are not irrotational, but potential flow theory can permit infinitely weak shocks (isentropic Mach waves).

If compressible, the continuity equation becomes:

$$\nabla \cdot (\rho \vec{V}) = 0 \tag{5.103}$$

and the momentum equation, if invsicid as is necessary for irrotational flow, is:

$$\rho \vec{V} \cdot \nabla \vec{V} = -\nabla p \tag{5.104}$$

Using a vector identity we can expand the left-hand side as follows, and cross out the second term because of the irrotationality assumption.

$$\rho \left(\frac{1}{2} \nabla (\vec{V} \cdot \vec{V}) - \vec{V} \times \cancel{(\nabla \times \vec{V})} \right) = -\nabla p \tag{5.105}$$

Because we have assumed irrotational flow, there is no viscosity and no heat transfer, and the energy equation reduces to the isentropic relation (Eq. 5.61):

$$\frac{p}{\rho^\gamma} = k \tag{5.106}$$

where k is a constant. We take derivatives of the isentropic relationship and insert in the definition of the speed of sound (Eq. 5.88):

$$\nabla p = k \gamma \rho^{\gamma - 1} \nabla \rho \tag{5.107}$$

$$= \gamma \frac{p}{\rho} \nabla \rho \tag{5.108}$$

$$= a^2 \nabla \rho \tag{5.109}$$

We substitute this result into the momentum equation:

$$\rho \frac{1}{2} \nabla (\vec{V} \cdot \vec{V}) = -a^2 \nabla \rho \,, \tag{5.110}$$

and divide by ρ on both sides:

$$\frac{1}{2} \nabla (\vec{V} \cdot \vec{V}) = -a^2 \frac{\nabla \rho}{\rho} \,. \tag{5.111}$$

Next, we take the dot product with velocity on both sides of the equation.

$$\vec{V} \cdot \left(\frac{1}{2}\nabla(\vec{V} \cdot \vec{V})\right) = -a^2\vec{V} \cdot \frac{\nabla\rho}{\rho} \tag{5.112}$$

If we expand the continuity equation via the chain rule:

$$\begin{aligned} \nabla\rho \cdot \vec{V} + \rho(\nabla \cdot \vec{V}) &= 0 \\ \vec{V} \cdot \nabla\rho &= -\rho(\nabla \cdot \vec{V}) \end{aligned} \tag{5.113}$$

we see that we can substitute this term into the right side of the momentum equation:

$$\vec{V} \cdot \left(\frac{1}{2}\nabla(\vec{V} \cdot \vec{V})\right) = a^2\nabla \cdot \vec{V} \tag{5.114}$$

Rearranging gives:

$$a^2\nabla \cdot \vec{V} - \frac{1}{2}\vec{V} \cdot \nabla(\vec{V} \cdot \vec{V}) = 0 \tag{5.115}$$

Finally, we make the substitution $\vec{V} = \nabla\phi$ for the potential function.

$$\nabla^2\phi - \frac{1}{a(\phi)^2}\left(\frac{1}{2}\nabla\phi \cdot \nabla(\nabla\phi \cdot \nabla\phi)\right) = 0 \tag{5.116}$$

This equation is called the (steady) *full potential equation*. It isn't used directly very much anymore as modern numerical methods for solving the Euler equations are just as easy to work with and don't carry the limitations of isentropic or irrotational flow. However, this equation does form the basis of various small disturbance theories as we will see in this chapter. Note that for an incompressible flow the speed of sound is infinite ($a \to \infty$) and the above expression reduces to Laplace's equation as expected:

$$\nabla^2\phi = 0 \tag{5.117}$$

Actually, we haven't fully expressed the equation. We wrote that the speed of sound a is a function of ϕ but did not explicitly show this. It makes the above expression less clear, but below we show how this can be done. For a steady, adiabatic compressible flow we shows that total enthalpy is conserved along a streamline (Section 5.1.7). If we have a constant freestream, as is almost always the case for potential flow, then the upstream enthalpy is the same for every streamline and so we can say that the total enthalpy is constant everywhere. The assumptions of steady flow and constant total enthalpy are not actually necessary to derive the full potential equations. There is an unsteady version, but

the derivation is quite a bit longer and not needed for our purposes. If total enthalpy is constant we can write:

$$h + \frac{V^2}{2} = \text{const} \tag{5.118}$$

$$c_p T + \frac{1}{2}(\vec{V} \cdot \vec{V}) = \text{const} \tag{5.119}$$

$$\frac{\gamma R}{\gamma - 1} T + \frac{1}{2}(\vec{V} \cdot \vec{V}) = \text{const} \tag{5.120}$$

$$\frac{a^2}{\gamma - 1} + \frac{1}{2}(\vec{V} \cdot \vec{V}) = \text{const} \tag{5.121}$$

$$\tag{5.122}$$

where c_p is specific heat at constant pressure, and we have assumed a calorically perfect gas (Eq. 5.36), and used Eqs. 5.42 and 5.89. We now apply this equation at two points, the freesteam and an arbitrary point in the fluid.

$$\frac{a^2}{\gamma - 1} + \frac{1}{2}(\vec{V} \cdot \vec{V}) = \frac{a_\infty^2}{\gamma - 1} + \frac{1}{2} V_\infty^2 \tag{5.123}$$

or rearranging:

$$a^2 = a_\infty^2 - \frac{\gamma - 1}{2}(V_\infty^2 - \vec{V} \cdot \vec{V}) \tag{5.124}$$

Or in terms of the potential function.

$$a^2 = a_\infty^2 - \frac{\gamma - 1}{2}(V_\infty^2 - \nabla\phi \cdot \nabla\phi) \tag{5.125}$$

This equations gives the desired relationship, $a(\phi)$, and thus we see that the full potential equation only depends on one unknown: ϕ.

5.3 Small Disturbance Equations

In the remainder of this chapter we will need to make use of partial derivatives many times. In order to simplify notation we will often use the following:

$$\phi_x \equiv \frac{\partial \phi}{\partial x} \tag{5.126}$$

$$\phi_{xx} \equiv \frac{\partial^2 \phi}{\partial x^2} \tag{5.127}$$

$$\tag{5.128}$$

We now will introduce the small disturbance equations. We align our axis with the freestream, and assume that a body in the flow creates

only small disturbances relative to freestream values.

$$\phi = V_\infty x + \hat{\phi} \tag{5.129}$$

where $\hat{\phi}$ is a small disturbance in ϕ. In terms of velocities this means that:

$$\begin{aligned} u &= V_\infty + \hat{u} \\ v &= \hat{v} \\ w &= \hat{w} \end{aligned} \tag{5.130}$$

where $\hat{u}, \hat{v}, \hat{w}$ are disturbance velocities.

We start with the velocity from the full potential equation (Eq. 5.115) and introduce the perturbation velocities. It will be easier to do this one term at a time, where again we will use the subscripts to denote partial derivatives. We will also temporarily drop the hats for convenience

$$\nabla \cdot \vec{V} = u_x + v_y + w_z \tag{5.131}$$

$$\vec{V} \cdot \vec{V} = V_\infty^2 + 2V_\infty u + u^2 + v^2 + w^2 \tag{5.132}$$

$$\nabla(\vec{V} \cdot \vec{V}) = \begin{bmatrix} 2V_\infty u_x + 2uu_x + 2vv_x + 2ww_x \\ 2V_\infty u_y + 2uu_y + 2vv_y + 2ww_y \\ 2V_\infty u_z + 2uu_z + 2vv_z + 2ww_z \end{bmatrix} \tag{5.133}$$

$$\begin{aligned} \frac{1}{2}\vec{V} \cdot \nabla(\vec{V} \cdot \vec{V}) = (V_\infty + u)(V_\infty u_x + uu_x + vv_x + ww_x) + \\ v(V_\infty u_y + uu_y + vv_y + ww_y) + \\ w(V_\infty u_z + uu_z + vv_z + ww_z) \end{aligned} \tag{5.134}$$

We also need to substitute the perturbation into the definition of the speed of sound (Eq. 5.124):

$$a^2 = a_\infty^2 - \frac{\gamma - 1}{2}(V_\infty^2 - V_\infty^2 + 2V_\infty u + u^2 + v^2 + w^2) \tag{5.135}$$

$$= a_\infty^2 - \frac{\gamma - 1}{2}(2V_\infty u + u^2 + v^2 + w^2) \tag{5.136}$$

$$\tag{5.137}$$

Because u, v, w are all small, their products are even smaller and do we can drop these terms. The derivatives of u, v, w may not necessarily be small, and so we cannot drop products of derivatives times the velocities yet.

$$\begin{aligned} \frac{1}{2}\vec{V} \cdot \nabla(\vec{V} \cdot \vec{V}) \approx V_\infty^2 u_x + V_\infty u u_x + V_\infty v v_x + V_\infty w w_x \\ + V_\infty u u_x + V_\infty v u_y + V_\infty w u_z \end{aligned} \tag{5.138}$$

and

$$a^2 \approx a_\infty^2 - (\gamma - 1)V_\infty u \tag{5.139}$$

Substituting all of this into the full potential equations (Eq. 5.116) gives:

$$(a_\infty^2 - (\gamma-1)V_\infty u)(u_x + v_y + w_z) - V_\infty^2 u_x - V_\infty(2uu_x + vv_x + ww_x + vu_y + wu_z) = 0 \tag{5.140}$$

Collecting like terms yields:

$$\begin{aligned}(a_\infty^2 - (\gamma - 1)V_\infty u - V_\infty^2 - 2V_\infty u)u_x + a_\infty^2(v_y + w_z) - (\gamma - 1)V_\infty u(v_y + w_z)\\ -V_\infty(vv_x + ww_x + vu_y + wu_z) = 0\end{aligned} \tag{5.141}$$

We now simplify and divide through by a_∞^2.

$$\begin{aligned}\left(1 - M_\infty^2 - (\gamma + 1)M_\infty^2 \frac{u}{V_\infty}\right) u_x + v_y + w_z - (\gamma - 1)M_\infty^2 \frac{u}{V_\infty}(v_y + w_z)\\ -M_\infty^2 \frac{1}{V_\infty}(vv_x + ww_x + vu_y + wu_z) = 0\end{aligned} \tag{5.142}$$

Now we can see that every term has a velocity derivative term, and so those terms that are also multiplied by an additional perturbation velocity (u, v, w) will be much smaller. However, there is one term we cannot drop. We see that when the Mach number is close to 1 then the term $1 - M_\infty^2$ is small and so the remaining term in those parenthesis will be significant and can't be dropped. On the other hand, all the terms from uv_y onward are small for all Mach numbers and so we can drop them.

$$\left(1 - M_\infty^2 - (\gamma + 1)M_\infty^2 \frac{u}{V_\infty}\right) u_x + v_y + w_z = 0 \tag{5.143}$$

We can now write this in terms of the potential.

$$\boxed{\left(1 - M_\infty^2 - (\gamma + 1)M_\infty^2 \frac{\hat{\phi}_x}{V_\infty}\right) \hat{\phi}_{xx} + \hat{\phi}_{yy} + \hat{\phi}_{zz} = 0} \tag{5.144}$$

This equation is called the *transonic small disturbance equation* (TSD). As discussed, the ϕ_x term is small unless the Mach number is close to one (hence the transonic in the name), but for Mach numbers not close to one we will be able to drop the term.

In a similar process we can compute the pressure coefficient for small disturbances in a compressible flow. We cannot use the simplified C_p calculation in terms of velocities as that used Bernoulli's equation

and does not apply for compressible flow. Instead, we go back to the original definition.

$$C_p = \frac{p - p_\infty}{\frac{1}{2}\rho_\infty V_\infty^2} \tag{5.145}$$

For compressible flows it is more convenient to use a different form of the dynamic pressure in terms of the Mach number (Eq. 5.91).Substituting this into the definition of the pressure coefficient gives:

$$C_p = \left(\frac{p}{p_\infty} - 1\right)\frac{2}{\gamma M_\infty^2} \tag{5.146}$$

Now we need to go back to our energy equation (Eq. 5.119), which we apply between an arbitrary location and at freestream.

$$c_p T + \frac{1}{2}\vec{V}\cdot\vec{V} = c_p T_\infty + \frac{V_\infty^2}{2} \tag{5.147}$$

Solving for T/T_∞:

$$\frac{T}{T_\infty} = 1 + \frac{1}{2T_\infty c_p}\left(V_\infty^2 - \vec{V}\cdot\vec{V}\right) \tag{5.148}$$

Using the definition $c_p = \gamma R/(\gamma - 1)$ and substituting in the speed of sound ($a^2 = \gamma RT$) gives:

$$\frac{T}{T_\infty} = 1 + \frac{\gamma - 1}{2a_\infty^2}\left(V_\infty^2 - \vec{V}\cdot\vec{V}\right) \tag{5.149}$$

Now we make use of the isentropic relationships between pressure and tempreature (Eq. 5.61): Applying to the above equation and substituting into the pressure coefficient gives:

$$C_p = \left[\left(1 + \frac{(\gamma - 1)}{2a_\infty^2}\left(V_\infty^2 - \vec{V}\cdot\vec{V}\right)\right)^{\gamma/(\gamma-1)} - 1\right]\frac{2}{\gamma M_\infty^2} \tag{5.150}$$

So far, everything is exact, but now we can introduce the small perturbation assumption:

$$V_\infty^2 - \vec{V}\cdot\vec{V} = V_\infty^2 - (V_\infty^2 + 2V_\infty\hat{u} + \hat{u}^2 + \hat{v}^2 + \hat{w}^2) \tag{5.151}$$

$$= -(2V_\infty\hat{u} + \hat{u}^2 + \hat{v}^2 + \hat{w}^2) \tag{5.152}$$

Substituting that into the pressure coefficient gives:

$$C_p \approx \left[\left(1 - \frac{(\gamma - 1)}{2a_\infty^2}(2V_\infty\hat{u} + \hat{u}^2 + \hat{v}^2 + \hat{w}^2)\right)^{\gamma/(\gamma-1)} - 1\right]\frac{2}{\gamma M_\infty^2} \tag{5.153}$$

Now, we make use of the binomial approximation, which is:

$$(1+x)^{\alpha} \approx 1 + \alpha x + \frac{1}{2}\alpha(\alpha-1)x^2 + \dots \tag{5.154}$$

This equation can be found from a Taylor's series and applies when x is small relative to 1. In our case the 'x' term contains only perturbation velocities and so is small by definition.

$$\begin{aligned} C_p \approx \Bigg[& 1 - \frac{\gamma}{(\gamma-1)}\frac{(\gamma-1)}{2a_\infty^2}(2V_\infty\hat{u} + \hat{u}^2 + \hat{v}^2 + \hat{w}^2) \\ & + \frac{1}{2}\frac{\gamma}{(\gamma-1)}\frac{1}{(\gamma-1)}\frac{(\gamma-1)^2}{4a_\infty^4}(2V_\infty\hat{u} + \hat{u}^2 + \hat{v}^2 + \hat{w}^2)^2 - 1\Bigg]\frac{2}{\gamma M_\infty^2} \end{aligned} \tag{5.155}$$

We will retain up to second-order terms:

$$\begin{aligned} C_p &\approx \left[-\frac{\gamma}{2a_\infty^2}(2V_\infty\hat{u} + \hat{u}^2 + \hat{v}^2 + \hat{w}^2) + \frac{1}{2}\frac{\gamma}{a_\infty^4}V_\infty^2\hat{u}^2\right]\frac{2}{\gamma M_\infty^2} \\ &= -2\frac{\hat{u}}{V_\infty} - \left(\frac{\hat{u}^2 + \hat{v}^2 + \hat{w}^2}{V_\infty^2}\right) + M_\infty^2\left(\frac{\hat{u}}{V_\infty}\right)^2 \end{aligned} \tag{5.156}$$

Rearranging like terms gives our final result:

$$C_p = -\left[\frac{2\hat{u}}{V_\infty} + (1-M_\infty^2)\left(\frac{\hat{u}}{V_\infty}\right)^2 + \left(\frac{\hat{v}}{V_\infty}\right)^2 + \left(\frac{\hat{w}}{V_\infty}\right)^2\right] \tag{5.157}$$

Like the full potential equation, the TSD equation is by itself no longer of much interest (though it was of significant interest historically). Instead, we will look at the subsonic and supersonic cases separately where the Mach number is away from one and the ϕ_x term can be dropped. Some useful insights and formulas will result for these two cases.

5.4 Subsonic Small Disturbance

If the Mach number is less than approximately 0.8, and only small disturbances are introduced in the flow field, then the TSD equation (Eq. 5.144) can be reduced to:

$$\left(1 - M_\infty^2\right)\hat{\phi}_{xx} + \hat{\phi}_{yy} + \hat{\phi}_{zz} = 0 \tag{5.158}$$

The boundary conditions for inviscid flow are flow tangency, where we use the function $f(x)$ to represent the shape of the body:

$$\frac{df}{dx} = \frac{\hat{v}}{V_\infty + \hat{u}} \approx \frac{\hat{v}}{V_\infty} \tag{5.159}$$

or

$$V_\infty \frac{df}{dx} = \hat{v} = \hat{\phi}_y \tag{5.160}$$

If we drop all second order terms from the small disturbance pressure coefficient equation (Eq. 5.157) we have:

$$C_p = -\frac{2\hat{u}}{V_\infty} = -\frac{2}{V_\infty}\hat{\phi}_x \tag{5.161}$$

We repeat those three equations, without the hat to simplify the notation, and we write out the partial derivatives to make the following derivation clearer.

$$\left(1 - M_\infty^2\right)\frac{\partial^2\phi}{\partial x^2} + \frac{\partial^2\phi}{\partial y^2} + \frac{\partial^2\phi}{\partial z^2} = 0 \tag{5.162}$$

$$V_\infty \frac{df}{dx} = \frac{\partial\phi}{\partial y} \tag{5.163}$$

$$C_p = -\frac{2}{V_\infty}\frac{\partial\phi}{\partial x} \tag{5.164}$$

The first equation is almost Laplace's equation, but not quite. Perhaps with a change of variables we can transform it to Laplace's equation. We introduce the following change of variables, where A, β and C are constants (we use β as this will be an important constant, and β is conventionally used for this purpose). We scale the potential, and shape by some unknown constant. We choose x as the one variable that doesn't scale (this is general as all other scaling is relative to this). Recall that the the body is aligned in the x direction, so we scale the other coordinate directions by some other unknown constant $(1/\beta)$.

$$\phi = A\bar{\phi} \tag{5.165}$$

$$x = \bar{x} \tag{5.166}$$

$$y = \frac{1}{\beta}\bar{y} \tag{5.167}$$

$$z = \frac{1}{\beta}\bar{z} \tag{5.168}$$

$$f = C\bar{f} \tag{5.169}$$

As an example, using the chain rule, and the above change of variables, gives the following for the derivative with respect to y:

$$\frac{\partial\phi}{\partial y} = \frac{\partial\phi}{\partial\bar{y}}\frac{d\bar{y}}{dy} = \frac{\partial\phi}{\partial\bar{y}}\beta = \frac{\partial\bar{\phi}}{\partial\bar{y}}A\beta \tag{5.170}$$

Similarly, the the second derivative of y we get:

$$\frac{\partial^2 \phi}{\partial y^2} = \frac{\partial}{\partial y}\left(A\beta \frac{\partial \bar{\phi}}{\partial \bar{y}}\right) = A\beta \frac{\partial}{\partial \bar{y}}\left(\frac{\partial \bar{\phi}}{\partial y}\right) = A\beta \frac{\partial}{\partial \bar{y}}\left(\frac{\partial \bar{\phi}}{\partial \bar{y}}\frac{d\bar{y}}{dy}\right) = A\beta^2 \frac{\partial^2 \bar{\phi}}{\partial \bar{y}^2} \tag{5.171}$$

If we make the change of variable substitutions into the governing equation we get:

$$\left(1 - M_\infty^2\right)\cancel{A}\bar{\phi}_{\bar{x}\bar{x}} + \cancel{A}\beta^2 \bar{\phi}_{\bar{y}\bar{y}} + \cancel{A}\beta^2 \bar{\phi}_{\bar{z}\bar{z}} = 0 \tag{5.172}$$

If we choose to define β as:

$$\beta = \sqrt{1 - M_\infty^2} \tag{5.173}$$

then we get

$$\bar{\phi}_{\bar{x}\bar{x}} + \bar{\phi}_{\bar{y}\bar{y}} + \bar{\phi}_{\bar{z}\bar{z}} = 0 \tag{5.174}$$

which is Laplace's equation! This means that through a change of coordinates we can continue to use Laplace's equation for compressible potential flow as long as the disturbances are small and the Mach number is not too close to 1.

Next, let's check how this impacts our boundary condition. The change of coordinates gives:

$$V_\infty C \frac{d\bar{f}}{d\bar{x}} = A\beta \frac{\partial \bar{\phi}}{\partial \bar{y}} \tag{5.175}$$

Ideally, we don't want to modify the geometry when using the coordinate transformation so we would like $C = 1$ (Eq. 5.169), and we would like the ratio above $C/(A\beta)$ to also equal 1 so that we don't have to stretch the geometry when applying the boundary condition. If $C = 1$ that means we require $A = 1/\beta$. By choosing that set of constants we can use the original body shape without modification.

Finally, we need to check how our coordinate transformation impacts the computation of C_p.

$$C_p = -\frac{2}{V_\infty} A \frac{\partial \bar{\phi}}{\partial \bar{x}} \tag{5.176}$$

or since $A = 1/\beta$

$$C_p = -\frac{2}{V_\infty} \frac{\partial \bar{\phi}}{\partial \bar{x}} \frac{1}{\beta} \tag{5.177}$$

The result of the coordinate system change is:

$$\frac{\partial^2 \bar{\phi}}{\partial \bar{x}^2} + \frac{\partial^2 \bar{\phi}}{\partial \bar{y}^2} + \frac{\partial^2 \bar{\phi}}{\partial \bar{z}^2} = 0 \tag{5.178}$$

$$V_\infty \frac{d\bar{f}}{d\bar{x}} = \frac{\partial \bar{\phi}}{\partial \bar{y}} \tag{5.179}$$

$$C_p = -\frac{2}{V_\infty} \frac{\partial \bar{\phi}}{\partial \bar{x}} \frac{1}{\sqrt{1 - M_\infty^2}} \tag{5.180}$$

If we compare this set of equations to those in the original coordinate system (Eq. 5.162) we see that we successful transformed the governing equation to Laplace's equation, the boundary condition is unchanged, and the resulting C_p needs to be divided by β.

In other words, if we use the exact same process we used for solving Laplace's equation in incompressible flow (e.g., a panel method) all we need to do is multiply our resulting C_p by a correction factor:

$$C_p = \frac{C_{p_0}}{\sqrt{1 - M_\infty^2}} \tag{5.181}$$

where C_{p_0} is the pressure coefficient we would compute in the incompressible flow. This is called the *Prandtl-Glauert correction* or PG correction for short.

Furthermore, because the lift coefficient, moment coefficient, and lift curve slope are just integrals of pressure the same correction applies. For example:

$$c_l = \frac{c_{l_0}}{\sqrt{1 - M_\infty^2}} \tag{5.182}$$

Note that the effect is that as the Mach number is increased, the lift and moment coefficients are increased as well.

One unnecessary limitation in the above derivation is that we only retained the linear terms in the small disturbance pressure coefficient equation (Eq. 5.157). Retaining additional terms and following a similar process gives the *Karman-Tsien* correction, which is not much more complicated but produces more accurate results.

$$C_p = \left[\frac{\beta}{C_{p_0}} + \frac{M_\infty^2}{2(1+\beta)} \right]^{-1} \tag{5.183}$$

Again, remember the main limitation (besides those of potential flow) is the assumption of small disturbances. Most of the time aerodynamic bodies are designed to only introduce small disturbances, indeed

this is what we imply we say a vehicle has an aerodynamic shape. However, as the Mach number is increased geometries need to become increasingly thin to prevent shock waves and large disturbances. Thus, these correction methods work reasonably well for moderate Mach numbers (near 0.5), but may be quite inaccurate as we approach Mach 0.7–0.8 and above depending on the geometry.

5.5 Supersonic Thin Airfoil Theory

Starting from the TSD equation (Eq. 5.144), we can also drop the higher order term if the Mach number is approximately above 1.2. The resulting equation is

$$-\beta^2\hat{\phi}_{xx} + \hat{\phi}_{yy} + \hat{\phi}_{zz} = 0 \tag{5.184}$$

where

$$\beta = \sqrt{M_\infty^2 - 1} \tag{5.185}$$

Note that we changed the definition of β for the supersonic case. This is no longer an elliptic PDE but rather is a hyperbolic one. Like the integral boundary layer equations, that means that the information flow is directional. Disturbances cannot go upstream, as is physically consistent with the behavior of supersonic flow (information travels with the speed of sound).

In this section we will focus on airfoils (i.e., 2D):

$$-\beta^2\hat{\phi}_{xx} + \hat{\phi}_{yy} = 0 \tag{5.186}$$

This equation has the exact same form as the one-dimensional wave equation, which has known solutions:

$$\hat{\phi} = F(x - \beta y) + G(x + \beta y) \tag{5.187}$$

where F and G are arbitrary functions.

A visualization of the flow behavior is shown in Fig. 5.6. The lines are often referred to as *characteristics*. Along a characteristic the flow properties are constant. Physically, they are Mach waves or infinitely weak (isentropic) shock waves. On the upper surface only the F function applies, while G applies on the lower surface (because Mach waves only travel downstream).

Recall that the boundary condition is approximately given as:

$$V_\infty \frac{dy}{dx} = \frac{d\hat{\phi}}{dy} \tag{5.188}$$

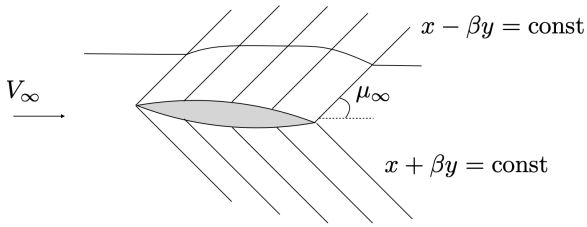

Fig. 5.6 Characteristic lines in a small disturbance supersonic flow field.

Applying this on the upper surface, and using thin-airfoil theory assumptions, as is consistent with small disturbances, yields:

$$V_\infty \left(\frac{dy}{dx}\right)_u = \left(\frac{d\hat{\phi}}{dy}\right)_{y=0^+} = -\beta F'(x) \tag{5.189}$$

If we solve this for F' we have:

$$F'(x) = -\frac{V_\infty}{\beta}\left(\frac{dy}{dx}\right)_u \tag{5.190}$$

Recall that the pressure coefficient (dropping higher order terms) is given by (Eq. 5.161):

$$C_p = -\frac{2}{V_\infty}\left(\frac{\partial\hat{\phi}}{\partial x}\right)_{y=0} \tag{5.191}$$

Evaluating on the upper surface gives:

$$C_p = -\frac{2}{V_\infty}F'(x) \tag{5.192}$$

Using the expression for F' above:

$$C_p = \frac{2}{\beta}\frac{dy}{dx} \tag{5.193}$$

The derivative dy/dx is the local slope of the airfoil, which we call θ, and β was defined previously:

$$\boxed{C_p = \frac{2\theta}{\sqrt{M_\infty^2 - 1}}} \tag{5.194}$$

This expression gives us a quick and easy way to estimate the pressure distribution on a supersonic airfoil with small disturbances. All that is needed is to know the airfoil shape (from which we get the slope θ) and the freestream Mach number. If we followed the same procedure for the lower surface we would get the same expression. Keep in mind that θ is negative for the lower surface as the slope goes the other direction.

As we did before with airfoils, we will separate the geometric description into a thickness distribution, a camber distribution, and an angle of attack. Specifically, we define the upper and lower surfaces as a superposition of camber and thickness distribution as follows:

$$y_u(x) = y_c(x) + \frac{1}{2}y_t(x) \tag{5.195}$$

$$y_l(x) = y_c(x) - \frac{1}{2}y_t(x) \tag{5.196}$$

Using the formula for the local pressure coefficient:

$$C_{p_u} = \frac{2}{\sqrt{M_\infty^2 - 1}}\left(-\alpha + \frac{dy_u}{dx}\right) \tag{5.197}$$

$$C_{p_l} = \frac{2}{\sqrt{M_\infty^2 - 1}}\left(\alpha - \frac{dy_l}{dx}\right) \tag{5.198}$$

The negative sign results from the way that θ is defined. Substituting in the camber and thickness distributions:

$$C_{p_u} = \frac{2}{\sqrt{M_\infty^2 - 1}}\left(-\alpha + \frac{dy_c}{dx} + \frac{1}{2}\frac{dy_t}{dx}\right) \tag{5.199}$$

$$C_{p_l} = \frac{2}{\sqrt{M_\infty^2 - 1}}\left(\alpha - \frac{dy_c}{dx} + \frac{1}{2}\frac{dy_t}{dx}\right) \tag{5.200}$$

The definition of the (inviscid) normal force coefficient is:

$$c_n = \frac{1}{c}\int_0^c (C_{p_l} - C_{p_u})dx \tag{5.201}$$

Substituting in the result from above gives:

$$c_n = \frac{2}{\sqrt{M_\infty^2 - 1}}\frac{1}{c}\int_0^c (2\alpha - 2\frac{dy_c}{dx})dx \tag{5.202}$$

$$= \frac{2}{\sqrt{M_\infty^2 - 1}}\frac{1}{c}\left(2\alpha\int_0^c dx - 2\int_0^c \frac{dy_c}{dx}dx\right) \tag{5.203}$$

$$= \frac{2}{\sqrt{M_\infty^2 - 1}}\frac{1}{c}\left(2\alpha c - 2\ y_c|_0^c\right) \tag{5.204}$$

$$= \frac{4\alpha}{\sqrt{M_\infty^2 - 1}} \tag{5.205}$$

The definition of the (inviscid) axial force coefficient is:

$$c_a = \frac{1}{c}\int_0^c \left(C_{p_u}\frac{dy_u}{dx} - C_{p_l}\frac{dy_l}{dx}\right)dx \tag{5.206}$$

Substituting in:

$$c_a = \frac{1}{c}\int_0^c \left(\frac{2}{\sqrt{M_\infty^2 - 1}} \left(-\alpha + \frac{dy_c}{dx} + \frac{1}{2}\frac{dy_t}{dx} \right) \left(\frac{dy_c}{dx} + \frac{1}{2}\frac{dy_t}{dx} \right) \right.$$
$$\left. - \frac{2}{\sqrt{M_\infty^2 - 1}} \left(\alpha - \frac{dy_c}{dx} + \frac{1}{2}\frac{dy_t}{dx} \right) \left(\frac{dy_c}{dx} - \frac{1}{2}\frac{dy_t}{dx} \right) \right) dx \tag{5.207}$$

Several terms appear in both expressions and so cancel out. Removing those terms leaves us with:

$$c_a = \frac{2}{\sqrt{M_\infty^2 - 1}} \frac{1}{c} \int_0^c \left(-2\alpha \frac{dy_c}{dx} + 2\left(\frac{dy_c}{dx}\right)^2 + \frac{1}{2}\left(\frac{dy_t}{dx}\right)^2 \right) dx \tag{5.208}$$

For the first term under the integral, α is a constant and can be taken out. We already saw that

$$\int_0^c \frac{dy_c}{dx} dx = 0 \tag{5.209}$$

and so that whole term is zero. We are left with:

$$c_a = \frac{4}{\sqrt{M_\infty^2 - 1}} \left(\overline{\left(\frac{dy_c}{dx}\right)^2} + \frac{1}{4}\overline{\left(\frac{dy_t}{dx}\right)^2} \right) \tag{5.210}$$

where we define

$$\overline{\zeta} = \frac{1}{c}\int_0^c \zeta(x) dx \tag{5.211}$$

as a shorthand for convenience.

Finally, lift and drag are related to the normal and axial forces as follows:

$$c_l = c_n \cos\alpha - c_a \sin\alpha \tag{5.212}$$
$$c_d = c_n \sin\alpha + c_a \cos\alpha \tag{5.213}$$

Using a small angle approximation, consistent with thin airfoil theory, yields:

$$c_l \approx c_n - c_a \alpha \tag{5.214}$$
$$c_d \approx c_n \alpha + c_a \tag{5.215}$$

Conventionally, the $c_a \alpha$ term is neglected in the lift coefficient because it is of *much* smaller magnitude than c_n (c_a is small and α is small so

their product is very small). However, in the drag calculation both $c_n\alpha$ and c_a are of similar magnitude.

$$c_l \approx c_n \tag{5.216}$$

$$c_d \approx c_n\alpha + c_a \tag{5.217}$$

Thus:

$$\begin{aligned} c_l &= \frac{4\alpha}{\sqrt{M_\infty^2 - 1}} \\ c_d &= \frac{4}{\sqrt{M_\infty^2 - 1}}\left(\alpha^2 + \overline{\left(\frac{dy_c}{dx}\right)^2} + \frac{1}{4}\overline{\left(\frac{dy_t}{dx}\right)^2}\right) \end{aligned} \tag{5.218}$$

The (inviscid) pitching moment coefficient is:

$$c_{mle} = \frac{1}{c^2}\int_0^c \left(\left(C_{p_u} - C_{p_l}\right)x + C_{p_u}\frac{dy_u}{dx}y_u - C_{p_l}\frac{dy_l}{dx}y_l\right)dx \tag{5.219}$$

Making substitutions:

$$\begin{aligned} c_{mle} = \frac{1}{c^2}\frac{2}{\sqrt{M_\infty^2 - 1}}\int_0^c \Bigg[&\left(-2\alpha + 2\frac{dy_c}{dx}\right)x + \left(-\alpha + \frac{dy_c}{dx} + \frac{1}{2}\frac{dy_t}{dx}\right)\left(\frac{dy_c}{dx} + \frac{1}{2}\frac{dy_t}{dx}\right)(y_c + y_t) - \\ &\left(\alpha - \frac{dy_c}{dx} + \frac{1}{2}\frac{dy_t}{dx}\right)\left(\frac{dy_c}{dx} - \frac{1}{2}\frac{dy_t}{dx}\right)(y_c - y_t)\Bigg]dx \end{aligned} \tag{5.220}$$

Removing terms that cancel:

$$\begin{aligned} c_{mle} = \frac{1}{c^2}\frac{2}{\sqrt{M_\infty^2 - 1}}\int_0^c \Bigg[&-2\alpha x + 2\frac{dy_c}{dx}x + y_c\left(-2\alpha\frac{dy_c}{dx} + 2\frac{dy_c}{dx}^2 + \frac{1}{2}\frac{dy_t}{dx}^2\right) + \\ &y_t\left(-\alpha\frac{dy_t}{dx} + 2\frac{dy_c}{dx}\frac{dy_t}{dx}\right)\Bigg]dx \end{aligned} \tag{5.221}$$

Neglecting all second order terms:

$$c_{mle} \approx \frac{1}{c^2}\frac{2}{\sqrt{M_\infty^2 - 1}}\int_0^c \left[-2\alpha x + 2\frac{dy_c}{dx}x\right]dx \tag{5.222}$$

$$= \frac{1}{c^2}\frac{2}{\sqrt{M_\infty^2 - 1}}\left[-2\alpha\frac{c^2}{2} + \int_0^c 2\frac{dy_c}{dx}x\,dx\right] \tag{5.223}$$

The second term we can integrate by parts:

$$c_{mle} = \frac{1}{c^2}\frac{2}{\sqrt{M_\infty^2 - 1}}\left[-\alpha c^2 + 2(xy_c)_0^c - \int_0^c y_c\,dx\right] \tag{5.224}$$

The second term is zero, leading to

$$c_{mle} = -\frac{2}{\sqrt{M_\infty^2 - 1}}\left[\alpha + \frac{1}{c^2}\int_0^c y_c dx\right] \tag{5.225}$$

Substituting in the definition of the chord-averaged variable.

$$c_{mle} = -\frac{2}{\sqrt{M_\infty^2 - 1}}\left[\alpha + \frac{\overline{y_c}}{c}\right] \tag{5.226}$$

The aerodynamic center can be computing by noting the the moment at any other location can be found as:

$$M'(x) = M'_{le} + L'x \tag{5.227}$$

$$c_m(x) = c_{mle} + c_l\frac{x}{c} \tag{5.228}$$

The definition of the aerodynamic center is the location where $dc_m/d\alpha = 0$ or in other words, the pitching moment is independent of angle of attack.

$$\frac{dc_{mac}}{d\alpha} = \frac{dc_{mle}}{d\alpha} + \frac{dc_l}{d\alpha}\frac{x_{ac}}{c} = 0 \tag{5.229}$$

$$\Rightarrow \frac{x_{ac}}{c} = \frac{-dc_{mle}/d\alpha}{dc_l/d\alpha} \tag{5.230}$$

Using the results from the above equations gives:

$$\frac{x_{ac}}{c} = \frac{2/\beta}{4/\beta} = \frac{1}{2} \tag{5.231}$$

Thus, in supersonic thin airfoil theory the aerodynamic center is at the half chord, not the quarter chord as in subsonic thin airfoil theory.

Example 5.1 Diamond airfoil

As an example consider the diamond airfoil shown in Fig. 5.7. There is no camber, but the thickness over the first half of the airfoil is given by:

$$y_t = 2x\tan\theta \tag{5.232}$$

and for the latter half is:

$$y_t = 2(c - x)\tan\theta \tag{5.233}$$

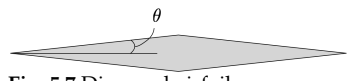

Fig. 5.7 Diamond airfoil.

If we evaluate the thickness term that appears in the integral:

$$\frac{1}{4}\overline{\left(\frac{dy_t}{dx}\right)^2} = \frac{1}{4c}\int_0^c \left(\frac{dy_t}{dx}\right)^2 dx \tag{5.234}$$

$$= \frac{1}{4c}\left[\int_0^{c/2}\left(\frac{dy_t}{dx}\right)^2 dx + \int_{c/2}^c \left(\frac{dy_t}{dx}\right)^2 dx\right] \tag{5.235}$$

$$= \frac{1}{4c}\left[4\tan^2\theta\frac{c}{2} + 4\tan^2\theta\frac{c}{2}\right] = \tan^2\theta = \left(\frac{t}{c}\right)^2 \tag{5.236}$$

The resulting drag coefficient estimate for the diamond airfoil is thus:

$$c_d = \frac{4}{\sqrt{M_\infty^2 - 1}} \left(\alpha^2 + \left(\frac{t}{c} \right)^2 \right) \tag{5.237}$$

Shock-expansion theory, discussed in the next section, is more accurate as it does not rely on the small disturbance assumptions and is well suited for numerical simulations. Although these simple methods are less exact, they give rise to analytic expressions that allow for back-of-the-envelope estimation and provide insight into the main factors that affect supersonic airfoils.

5.6 Shock Waves

Normal shock waves are perpendicular to the flow direction, whereas oblique shock waves occur at an angle relative to the flow. It is convenient to conceptually differentiate between normal shock waves and oblique shock waves, although theoretically we could treat every shock wave as a normal shock wave with an appropriate change of reference. The physics does not change between the two types, it is just a convenient construct to align with flow directions.

5.6.1 Normal Shock Waves

We determined the speed of sound by placing a control volume around a sound wave, which is an infinitely weak, isentropic, pressure wave (Section 5.1.6). To analyze shock waves, we use a similar process. However, a shock wave is not isentropic, and fluid properties change by a finite, discontinuous amount. Shock waves are not actually discontinuities, but are extremely thin regions (typically on the order of microns) across which fluid properties change rapidly. From the macro fluid level they appear discontinuous and are generally treated as such.

Consider the shock wave and control volume shown in Fig. 5.8. A mass, momentum, and energy balance yields:

$$\rho_1 u_1 = \rho_2 u_2 \tag{5.238}$$

$$p_1 + \rho_1 u_1^2 = p_2 + \rho_2 u_2^2 \tag{5.239}$$

$$h_1 + \frac{u_1^2}{2} = h_2 + \frac{u_2^2}{2} \tag{5.240}$$

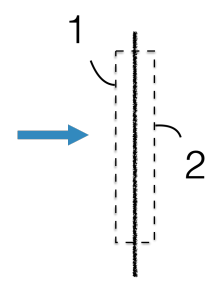

Fig. 5.8 Control volume around a shock wave.

In the latter two equations we have assumed that the flow is inviscid at the boundaries of the control volume. The shock wave itself is highly

viscous, but that viscous behavior is confined to the interior of the control volume. We make the control volume just large enough so that the boundaries are outside the large velocity gradients that occur within the shock wave.

If we assume a calorically perfect gas we can add the ideal gas equation of state and the simple relationship for specific heats:

$$p = \rho R T \tag{5.241}$$

$$h = c_p T \tag{5.242}$$

We now have five equations and five unknowns that we can solve algebraically. In the more general case, where specific heats vary with temperature and potentially pressure, these equations can still be solved but a numerical solution may be necessary.

Solving for the five unknowns results in the following shock jump equations:

$$\frac{u_2}{u_1} = \frac{\rho_1}{\rho_2} = \frac{2 + (\gamma - 1)M_1^2}{(\gamma + 1)M_1^2} \tag{5.243}$$

$$\frac{p_2}{p_1} = 1 + \frac{2\gamma}{\gamma + 1}(M_1^2 - 1) \tag{5.244}$$

$$\frac{T_2}{T_1} = \frac{h_2}{h_1} = \frac{p_2}{p_1}\frac{\rho_1}{\rho_2} \tag{5.245}$$

These ratios are plotted as a function of Mach number in Fig. 5.9.

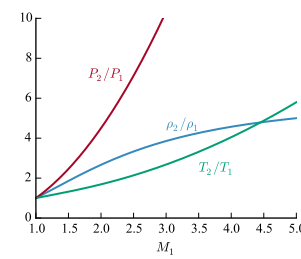

Fig. 5.9 Shock jump relationships.

From the derivation we can also show that the upstream Mach number is always supersonic and the downstream Mach number is always subsonic (with the speeds measured relative to the shock wave). The downstream Mach number is as follows:

$$M_2 = \sqrt{\frac{2 + (\gamma - 1)M_1^2}{2\gamma M_1^2 - (\gamma - 1)}} \tag{5.246}$$

and is plotted in Fig. 5.10: The downstream Mach number asymptotes to:

$$\lim_{M_1 \to \infty} M_2 = \sqrt{\frac{\gamma - 1}{2\gamma}} \approx .378 \tag{5.247}$$

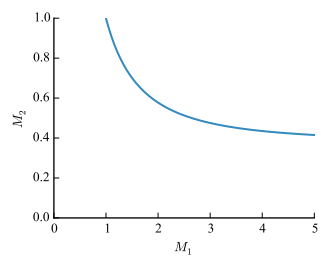

Fig. 5.10 Mach number downstream of a normal shockwave.

This is not to say that the downstream speed asymptotes, indeed the temperature keeps rising with increasing Mach number as shown in Fig. 5.9, and so the speed of sound and thus the actually speed must keep rising as well.

A shock wave, while viscous, is still adiabatic and so the total temperature is preserved:

$$T_{T1} = T_{T2} \tag{5.248}$$

Total pressure will not be constant, however, because of viscosity. We use the total pressure definition (Eq. 5.96) separately for the upstream and downstream properties.

$$\frac{p_{T1}}{p_1} = \left(1 + \frac{\gamma - 1}{2} M_1^2\right)^{\gamma/(\gamma-1)} \tag{5.249}$$

$$\frac{p_{T2}}{p_2} = \left(1 + \frac{\gamma - 1}{2} M_2^2\right)^{\gamma/(\gamma-1)} \tag{5.250}$$

We now divide the two equations by each other:

$$\frac{p_{T2}}{p_{T1}} = \frac{p_2}{p_1} \frac{\left(1 + \frac{\gamma-1}{2} M_2^2\right)^{\gamma/(\gamma-1)}}{\left(1 + \frac{\gamma-1}{2} M_1^2\right)^{\gamma/(\gamma-1)}} \tag{5.251}$$

We now substitute in Eq. 5.244 and Eq. 5.246:

$$\frac{p_{T2}}{p_{T1}} = \left(1 + \frac{2\gamma}{\gamma+1}(M_1^2 - 1)\right) \frac{\left(1 + \frac{\gamma-1}{2}\left(\frac{2+(\gamma-1)M_1^2}{2\gamma M_1^2-(\gamma-1)}\right)\right)^{\gamma/(\gamma-1)}}{\left(1 + \frac{\gamma-1}{2} M_1^2\right)^{\gamma/(\gamma-1)}} \tag{5.252}$$

After some simplification we arrive at the, still rather lengthy, equation for the total pressure drop across a normal shock wave:

$$\frac{p_{T2}}{p_{T1}} = \left(\frac{\gamma+1}{2\gamma M_1^2 - (\gamma-1)}\right)^{\frac{1}{\gamma-1}} \left(\frac{(\gamma+1)M_1^2}{2 + (\gamma-1)M_1^2}\right)^{\frac{\gamma}{\gamma-1}} \tag{5.253}$$

This total pressure drop is plotted as a function of upstream Mach number in Fig. 5.11. Notice that the total pressure drop is relatively small for Mach numbers not much greater than one, but then starts to drop precipitously. This is why many proposed supersonic transports fly at Mach numbers that are only modestly above Mach 1. As the Mach number increases further the total pressure drop becomes very significant and thus the amount of energy burned increases rapidly with higher speeds. The relationship between Mach number and total pressure loss is not the same for an airplane, as the shock waves along an aircraft are not all normal shock waves. More general shock waves are discussed in the following section. However, the qualitative behavior is still relevant.

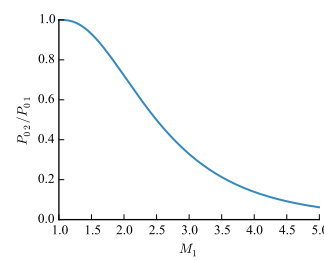

Fig. 5.11 Total pressure drop across a normal shockwave.

5.6.2 Oblique Shock Waves

An oblique shock wave forms at an angle between that of a normal shock wave (perpindicular) and that of a Mach wave (depicted with the angle μ in Fig. 5.2 and Eq. 5.2). Oblique waves are weaker than a normal shock wave, weaker in the sense that they produce less entropy or less total pressure loss, and thus less drag for a flight vehicle. A Mach wave is the limit of an infinitely weak oblique shock wave. Like a normal shock wave, an oblique shock wave is nonisentropic and behind the wave the pressure, density, and temperature all increase discretely. Unlike a normal shock wave, the Mach number behind an oblique shock wave may still be supersonic.

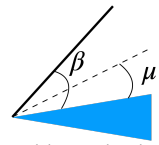

Fig. 5.12 An oblique shock wave angle (β) compared to a Mach wave angle (μ).

An oblique shock wave formed at an inside corner is depicted in Fig. 5.13. We call θ the turning angle, it is the angle change for the fluid flow. We call β the shock angle. It is the angle of the shock wave and produces the discrete change in direction for the flow, as well as the accompanying pressure, temperature, density increase.

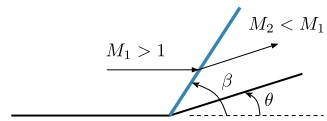

Fig. 5.13 An oblique shock wave.

Oblique shock waves are not really a special case, it is just a normal shock wave relative to the flow perpendicular to the wave (the tangential component of the flow is unaffected). However, it is convenient to rework the equations in a frame of reference relative to the incoming flow.

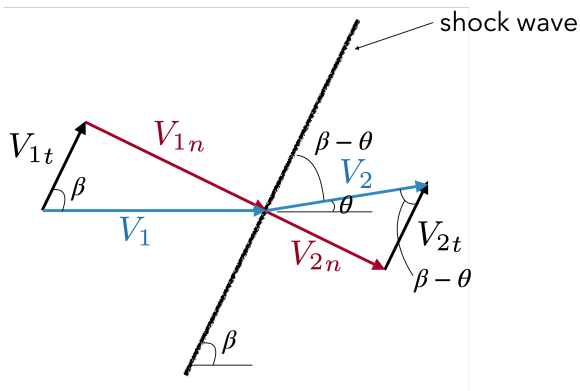

Fig. 5.14 Velocity components before and after an oblique shock wave.

Figure 5.14 depicts the velocity components upstream and downstream of an oblique shock. We have broken up the velocity vectors into components both normal to (subscript n) and tangential to (subscript t) the shock wave. The tangential component is unaffected, and the normal component follows the normal shock jump equations derived previously. From the previous discussion we now that the downstream normal component is always subsonic, however the downstream total

velocity vector may be, and often is, supersonic.

The incoming normal Mach number, as shown in Fig. 5.14, is:

$$M_{1n} = M_1 \sin\beta \tag{5.254}$$

and the exit Mach number is:

$$M_{2n} = M_2 \sin(\beta - \theta) \tag{5.255}$$

We can use the incoming normal Mach number in Eqs. 5.243 to 5.245 to compute the downstream pressure, density, and temperature (using M_{1n} in place of M_1 in the previous equations). However, this normal number depends on the shock angle β and that is not known beforehand. We only know the turning angle θ based on the problem geometry.

To relate these angles with known properties we refer back to Fig. 5.14 and note that:

$$\tan\beta = \frac{V_{1n}}{V_{1t}} \tag{5.256}$$

and

$$\tan(\beta - \theta) = \frac{V_{2n}}{V_{2t}} \tag{5.257}$$

We subtract these two equations, recalling that $V_{1t} = V_{2t}$ so:

$$\tan\beta - \tan(\beta - \theta) = \frac{V_{1n} - V_{2n}}{V_{1t}} \tag{5.258}$$

We expand the left hand side with a trig identity, and on the right hand side we divide top and bottom by V_{1n}.

$$\tan\beta - \frac{(\tan\beta - \tan\theta)}{1 + \tan\beta\tan\theta} = \frac{1 - \frac{V_{2n}}{V_{1n}}}{\frac{V_{1t}}{V_{1n}}} \tag{5.259}$$

On the left hand side we put the two terms on a common denominator, add, then simplify. On the right we use Eq. 5.243 to express the jump in velocity across the shock wave (nothing that we need to use the normal component of the upstream Mach number), and from Fig. 5.14 we see that the term in the denominator is just $1/\tan\beta$.

$$\frac{\tan^2\beta\tan\theta + \tan\theta}{1 + \tan\beta\tan\theta} = \tan\beta\left(1 - \frac{(2 + (\gamma - 1)M_{1n}^2)}{(\gamma + 1)M_{1n}^2}\right) \tag{5.260}$$

On the left we factor out $\tan\theta$ from the two terms in the numerator and use a trig identity on the remaining portion. On the right we expand with a common denominator and add the two terms.

$$\frac{\tan\theta(\sec^2\beta)}{1 + \tan\beta\tan\theta} = \tan\beta\left(\frac{2M_{1n}^2 - 2}{(\gamma + 1)M_{1n}^2}\right) \tag{5.261}$$

Using Eq. 5.254 we express M_{1n} in terms of the upstream Mach number. We move the sec^2 term to the denominator and expand $tan\beta$ to make the cancellations more obvious.

$$\frac{\tan\theta)}{\cos^2\beta(1+\tan\beta\tan\theta)} = \frac{\sin\beta}{\cos\beta}\left(\frac{2{M_1}^2\sin^2\beta-2}{(\gamma+1){M_1}^2\sin^2\beta}\right) \tag{5.262}$$

One the right side the $\sin\beta$ terms cancel. A $\cos\beta$ cancels across both sides. The remaining $\cos\beta$ term is distributed across the parenthetical term.

$$\frac{\tan\theta}{\cos\beta+\sin\beta\tan\theta)} = \left(\frac{2{M_1}^2\sin^2\beta-2}{(\gamma+1){M_1}^2\sin\beta}\right) \tag{5.263}$$

We now try to isolate θ by dividing both numerator and denominator of the left side term by $\tan\theta$.

$$\frac{1}{\left(\frac{\cos\beta}{\tan\theta}+\sin\beta\right)} = \left(\frac{2{M_1}^2\sin^2\beta-2}{(\gamma+1){M_1}^2\sin\beta}\right) \tag{5.264}$$

To isolate θ we invert both sides then subtract $\sin\beta$ from both sides.

$$\frac{\cos\beta}{\tan\theta} = \left(\frac{(\gamma+1){M_1}^2\sin\beta}{2{M_1}^2\sin^2\beta-2}\right)-\sin\beta \tag{5.265}$$

We now put the right hand side on a common denominator and add:

$$\frac{\cos\beta}{\tan\theta} = \left(\frac{(\gamma+1){M_1}^2\sin\beta-2{M_1}^2\sin^3\beta+2\sin\beta}{2{M_1}^2\sin^2\beta-2}\right) \tag{5.266}$$

On the right side we can factor a $\sin\beta$ term out of the numerator. Then we invert both sides and multiply by $\cos\beta$.

$$\tan\theta = \frac{\cos\beta}{\sin\beta}\left(\frac{2{M_1}^2\sin^2\beta-2}{(\gamma+1){M_1}^2-2{M_1}^2\sin^2\beta+2}\right) \tag{5.267}$$

We can simplify a bit more.

$$\tan\theta = \frac{1}{\tan\beta}\left(\frac{2({M_1}^2\sin^2\beta-1)}{(\gamma{M_1}^2+{M_1}^2(1-2\sin^2\beta)+2}\right) \tag{5.268}$$

Then using a trig identity on the denominator, leading to our final expression.

$$\tan\theta = \frac{2}{\tan\beta}\left(\frac{{M_1}^2\sin^2\beta-1}{{M_1}^2[\gamma+\cos(2\beta)]+2}\right) \tag{5.269}$$

We now have an explicit expression for θ in terms of β and M_1, although more typically what we want is β given M_1 and θ as inputs. In the latter case, this is still an implicit equation. Still the explicit form is convenient for creating graphs.

This oblique shock relationship is plotted in Fig. 5.15 for a few different incoming Mach numbers. Notice that for a given turning

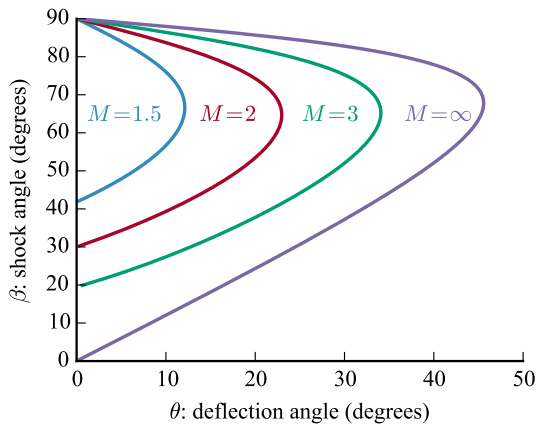

Fig. 5.15 Oblique shock relationship for different turning angles.

angle (θ) there are two solutions. These are called the *weak solution* and the *strong solution*. The weak solution typically occurs naturally. The strong solution may occur if downstream conditions require it—for example if we change the back pressure in an engine or wind tunnel. The limits of the weak and strong solution are Mach waves and normal shocks respectively, and occur at deflection angles of zero.

We also see that there is a maximum deflection angle, θ_{max} for a given Mach number. For the weak solution the downstream Mach number is supersonic, except for a small region of solutions near θ_{max}. For geometries that require a turning angle larger than this, an oblique shock will not occur, and instead a detached *bow shock* will form.

A bow shock is depicted in Fig. 5.16. As suggested by the numbered points, a bow shock passes through all points in the oblique shock relationships shown in Fig. 5.15. Point 1 corresponds to a normal shock. Point 2 is a strong oblique shock (with subsonic flow behind it). Point 3 is the dividing line between subsonic and supersonic downstream flow. Notice that this point occurs near to, but not at, θ_{max} Point 4 is a weak oblique shock. The shock angle is changing continuously through the bow shock, but asymptotes to that of a Mach wave (point 5). A blunt body will necessarily create a detached bow shock since a large turning angle is required.

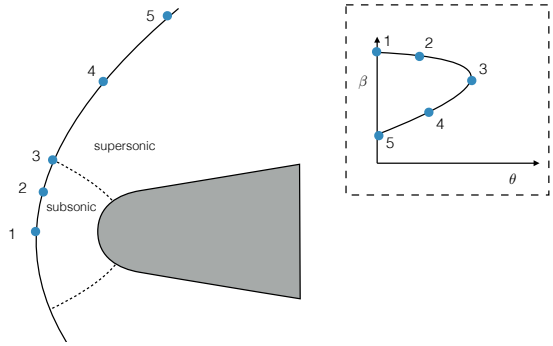

Fig. 5.16 A detatced bow shock wave.

5.7 Expansion Fans

An *expansion fan* also known as an expansion wave, or a Prandtl-Meyer expansion wave is essentially the opposite of an oblique shock. Through an expansion fan the Mach number increases, and pressure, density, and temperature all decrease. Whereas oblique shock waves occur on an inside corner, or more generally where the fluid turns in on itself, expansion fans occur on outside corners or where the fluid turns away from itself. Unlikely, a shock wave, an expansion fan occurs across a continuous region (the streamlines curve smoothly), and is isentropic. It is a continuous region consisting of an infinite number of Mach waves, each creating an infinitesimal isentropic change. The Mach waves starting at the incoming mach number:

$$\sin \mu_1 = \frac{1}{M_1} \tag{5.270}$$

and end at the exit Mach number:

$$\sin \mu_2 = \frac{1}{M_2} \tag{5.271}$$

This is depicted in Fig. 5.17.

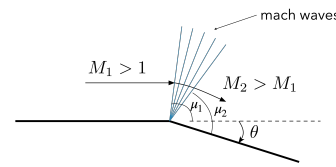

Fig. 5.17 An expansion fan.

7. Anderson, *Modern Compressible Flow: With Historical Perspective*, 2003.

The following derivation for analyzing an expansion fan is similar to that of Anderson.[7] Consider the flow through a Mach wave as exaggerated in Fig. 5.18. The turning angle is some infinitesimal amount $d\theta$ through which the velocity increases by some infinitesimal amount dV. We know that the change in velocity can only occur in a direction normal to the Mach wave (as it is the limit of an infinitely weak oblique shock wave). Thus, we can draw the velocity relationships as shown in Fig. 5.19. We can now relate the velocity vectors to the angles using the law of sines. The angles we can work out from the known information as shown in Fig. 5.20.

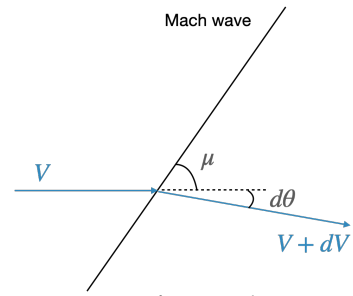

Fig. 5.18 Infinitesimal turning through a Mach wave.

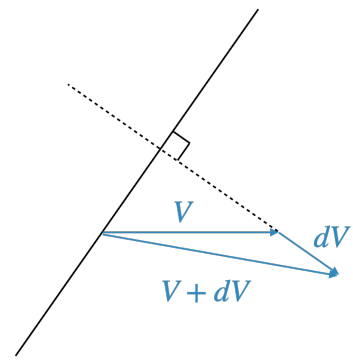

Fig. 5.19 The change in velocity occurs at a right angle to the Mach wave.

$$\frac{\sin\left(\frac{\pi}{2} + \mu\right)}{V + dV} = \frac{\sin\left(\frac{\pi}{2} - \mu - d\theta\right)}{V} \tag{5.272}$$

The trig expressions can be simplified as:

$$\frac{\cos\mu}{V+dV} = \frac{\cos(\mu+d\theta)}{V} \tag{5.273}$$

The right hand trig function we expand using the sum formula:

$$\frac{\cos\mu}{V+dV} = \frac{\cos\mu\cos d\theta - \sin\mu\sin d\theta}{V} \tag{5.274}$$

Since $d\theta$ is an infinitesimal amount, in the limit $\cos d\theta \to 1$ and $\sin d\theta \to d\theta$. The resulting equation is then:

$$\frac{\cos\mu}{V+dV} = \frac{\cos\mu - \sin\mu d\theta}{V} \tag{5.275}$$

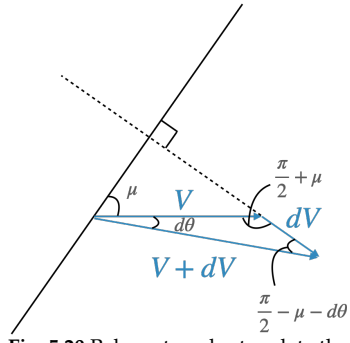

Fig. 5.20 Relevant angles to relate the velocity change and angle change.

We cross multiply:

$$\frac{\cos\mu}{\cos\mu - \sin(\mu)d\theta} = \frac{V+dV}{V} \tag{5.276}$$

Simplifying:

$$\frac{1}{1-\tan(\mu)d\theta} = 1 + \frac{dV}{V} \tag{5.277}$$

The left hand side we can expand using the series expansion:

$$\frac{1}{1-x} = 1 + x + x^2 + \ldots \text{ for } |x| < 1 \tag{5.278}$$

In our case, the x term is infinitesimally small so we can drop all higher order terms, which will be exact in the limit.

$$1 + \tan(\mu)d\theta = 1 + \frac{dV}{V} \tag{5.279}$$

We can cancel the ones, and since we know that $\sin\mu = 1/M$ (Eq. 5.2), we know that $\tan\mu = 1/\sqrt{M^2-1}$

$$\frac{1}{\sqrt{M^2-1}}d\theta = \frac{dV}{V} \tag{5.280}$$

Thus, we can relate the angle change to the velocity change as:

$$d\theta = \sqrt{M^2-1}\frac{dV}{V} \tag{5.281}$$

Now we wish to find the total angle change across a series of continuous Mach waves. In other words, we need to integrate both sides.

$$\int_{\theta_1}^{\theta_2} d\theta = \int_{M_1}^{M_2} \sqrt{M^2-1}\frac{dV}{V} \tag{5.282}$$

The right integrand is in terms of V but we would like it to be in terms of the Mach number. We can expand derivatives of velocity in terms of Mach number ($V = Ma$):

$$dV = Mda + adM \tag{5.283}$$

Thus:

$$\frac{dV}{V} = M\frac{da}{V} + \frac{1}{M}dM \tag{5.284}$$

The speed of sound is given by (Eq. 5.89):

$$a = \sqrt{\gamma RT} \tag{5.285}$$

Rather than using the static fluid properties we could also express in terms of total conditions:

$$a_T = \sqrt{\gamma RT_T} \tag{5.286}$$

Dividing these two equations gives:

$$\frac{a_T}{a} = \sqrt{\frac{T_T}{T}} = \sqrt{1 + \frac{(\gamma - 1)}{2}M^2} \tag{5.287}$$

where the latter expression comes from the definition of total temperature (Eq. 5.95). We write this expression in terms of a:

$$a = a_T\left(1 + \frac{(\gamma - 1)}{2}M^2\right)^{-1/2} \tag{5.288}$$

Taking derivatives gives:

$$da = -a_T\frac{1}{2}\left(1 + \frac{(\gamma - 1)}{2}M^2\right)^{-3/2}\frac{(\gamma - 1)}{2}2MdM \tag{5.289}$$

$$= -a\frac{1}{2}\left(1 + \frac{(\gamma - 1)}{2}M^2\right)^{-1}(\gamma - 1)MdM \tag{5.290}$$

$$= -V\frac{\frac{(\gamma-1)}{2}}{1 + \frac{(\gamma-1)}{2}M^2}dM \tag{5.291}$$

Substituting this expression back into Eq. 5.284:

$$\frac{dV}{V} = \frac{\frac{-(\gamma-1)}{2}M}{1 + \frac{(\gamma-1)}{2}M^2}dM + \frac{1}{M}dM \tag{5.292}$$

$$= \frac{\frac{-(\gamma-1)}{2}M^2 + 1 + \frac{(\gamma-1)}{2}M^2}{M\left(1 + \frac{(\gamma-1)}{2}M^2\right)}dM \tag{5.293}$$

$$= \frac{1}{M\left(1 + \frac{(\gamma-1)}{2}M^2\right)}dM \tag{5.294}$$

We now have an expression in terms of Mach number that we can substitute into Eq. 5.282:

$$\Delta\theta = \int_{M_1}^{M_2} \frac{\sqrt{M^2 - 1}}{M\left(1 + \frac{(\gamma-1)}{2}M^2\right)} dM \tag{5.295}$$

This expression can be analytically integrated, and as the result is somewhat long, we use the shorthand ν to represent the function.

$$\nu(M) = \sqrt{\frac{\gamma+1}{\gamma-1}} \tan^{-1} \sqrt{\frac{\gamma-1}{\gamma+1}(M^2-1)} - \tan^{-1}\sqrt{M^2-1} \tag{5.296}$$

Thus, the change in angle across the expansion fan is then computed as:

$$\Delta\theta = \nu(M_2) - \nu(M_1) \tag{5.297}$$

6 Propellers and Turbines

Both propellers and turbines use rotating blades but for different purposes. A propeller is designed to produce thrust and thus propel a vehicle, and in the process a torque is produced that opposes the blade motion and thus requires input power to maintain the rotation (top half of Fig. 6.1). A turbine is designed to produce a torque in the direction of blade motion and thus extract power from the moving fluid, and in the process a drag force is produced (bottom half of Fig. 6.1).

In Fig. 6.1 a streamtube passing through the rotor disk is also shown. A streamtube is a collection of streamlines. The propeller imparts momentum in the direction of the freestream and thus the streamtube area decreases (continuity equation). Conversely, the turbine extracts momentum leaving behind a wake of slower speeds and thus the streamtube area expands.

For conceptual design an effective method to analyze turbines and propellers is blade element momentum (BEM) theory. BEM theory is a combination of momentum balances and blade element (airfoil) analyses. The next two sections derive the theory from the perspective of a propeller and then from a perspective of a turbine. Both can be easily unified in a single derivation,[8] but when first learning the methods it is easier to comprehend when using the conventions of the application of interest. Reading only one of these sections is necessary. The two sections are written to stand alone, and because there is a lot of commonality between the two applications there is a lot of repeat material.

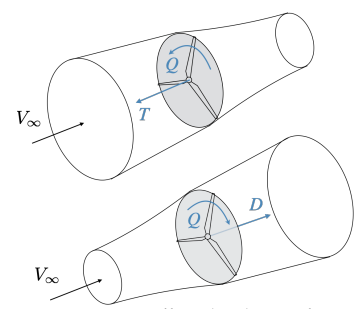

Fig. 6.1 Propeller (top) produces thrust and requires power (to overcome the resistive torque) to operate, whereas a turbine (bottom) produces torque and is accompanied by a resulting drag.

8. Ning, *Using Blade Element Momentum Methods with Gradient-Based Design Optimization*, 2021.

6.1 Blade Element Momentum Theory: Propellers

We will perform the derivation first from the perspective of a propeller and then from the perspective of a wind turbine. Note that we use the term propellers to generically refer to any turbomachine that adds momentum to the fluid.

6.1.1 Linear Momentum Balance

We will use a streamtube as our control volume, but rather than use one large streamtube across the entire rotor, we use an infinitesimally thin annulus streamtube at a given radial location of the rotor (Fig. 6.2). For convenience we define three stations as shown in the figure: upstream, at the rotor disk, and in the wake.

Figure 6.3 shows the control volume from a side view. First, we perform a mass balance. In the following derivation we neglect any variations in density. Compressibility, if necessary, is included in the blade element formulation.

$$\rho V_\infty A_\infty = \rho V_d A_d = \rho V_w A_w \tag{6.1}$$

Notice that as the velocity increases, the cross sectional area decreases.

Next, we apply an x-momentum balance across the entire control volume, where we take the positive direction for x as downwind:

$$\rho V_\infty(-V_\infty A_\infty) + \rho V_w(V_w A_w) = T \tag{6.2}$$

We make no assumption about the direction of the thrust, but rather let the equations determine the direction of thrust. The standard definition for thrust is the force opposite to V_∞. However, in the momentum balance we need to use the force the propeller exerts on the fluid, which is in the opposite direction, and is thus positive above. Combining these two expressions yields:

$$T = \rho A_d V_d (V_w - V_\infty) \tag{6.3}$$

It is not obvious that the pressure terms from the sides of the control volume cancel, but they do. We can come up with the same result more rigorously, with a cylindrical control volume that does not follow the streamlines, but the details are omitted here.

Let us now use a second control volume just across the disk. We will call the x location just upstream of the disk station 2, and just downstream will be called station 3. Performing a momentum balance yields (again neglecting any density changes across the disk):

$$\rho V_2(-V_2 A_2) + \rho V_3(V_3 A_3) = T + p_2 A_2 - p_3 A_3 \tag{6.4}$$

Because $A_2 = A_3 = A_d$ and the velocity must vary continuously through the disk ($V_2 = V_3$) the above expression simplifies to:

$$T = A_d(p_3 - p_2) \tag{6.5}$$

Combining the two expressions for thrust (Eqs. 6.3 and 6.5) yields:

$$\rho V_d(V_w - V_\infty) = (p_3 - p_2) \tag{6.6}$$

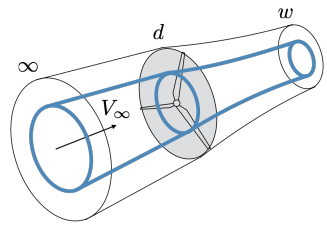

Fig. 6.2 The blue annulus streamtube is used as our control volume in the derivation of this section. The stations are denoted by ∞: far upstream, d: the rotor disk, and w in the far wake.

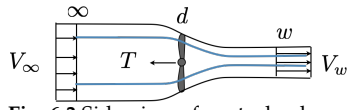

Fig. 6.3 Side view of control volume with resultant force T shown in typical thrust direction ($-x$ direction for our coordinate system).

To relate the pressure change from station 2 to 3, we use Bernoulli's equation (Eq. 5.77). We cannot apply Bernoulli's equation from station 2 to station 3 directly because work is done on the fluid between those stations. However, we can apply the equation upstream of the turbine and downstream of the turbine separately.

First, from station ∞ to station 2:

$$p_\infty + \frac{1}{2}\rho V_\infty^2 = p_2 + \frac{1}{2}\rho V_2^2 \tag{6.7}$$

then from station 3 to station w:

$$p_3 + \frac{1}{2}\rho V_3^2 = p_w + \frac{1}{2}\rho V_w^2 \tag{6.8}$$

If we subtract the two equations and simplify using $V_2 = V_3$, and assume our control volume is large enough so that $p_\infty = p_w$ we have

$$p_3 - p_2 = \frac{1}{2}\rho(V_w^2 - V_\infty^2) \tag{6.9}$$

This expression for the pressure drop is inserted into Eq. 6.6

$$\begin{aligned} \rho V_d(V_w - V_\infty) &= (p_3 - p_2) \\ \rho V_d(V_w - V_\infty) &= \frac{1}{2}\rho(V_w^2 - V_\infty^2) \\ V_d(V_w - V_\infty) &= \frac{1}{2}(V_w - V_\infty)(V_w + V_\infty) \\ V_d &= \frac{1}{2}(V_w + V_\infty) \end{aligned} \tag{6.10}$$

This yields the result that the velocity at the disk is half way between the upstream and downstream velocity. A similar relationship was derived for a lifting wing when we showed that the downwash at the wing is half of the downwash in the farfield.

With this relationship, we can generically relate the velocities at the 3 stations using the unknown induced velocity u (Fig. 6.4).

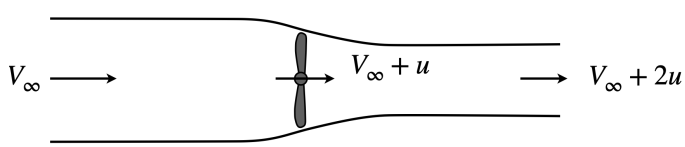

Fig. 6.4 Depiction of the induced velocity in at the rotor disk and in the farfield.

By convention one typically nondimensionalizes u as follows:

$$\begin{aligned} V_d &= V_\infty + u \\ &= V_\infty\left(1 + \frac{u}{V_\infty}\right) \\ &= V_\infty(1 + a) \end{aligned} \tag{6.11}$$

The quantity a is called the *axial induction factor*. Similarly, we can express the far-field velocity as:

$$V_w = V_\infty(1 + 2a) \tag{6.12}$$

With these definitions, we can express thrust in terms of the axial induction factor (using Eqs. 6.5, 6.6, 6.11, and 6.12):

$$\begin{aligned} T &= \rho A_d V_d (V_w - V_\infty) \\ &= \rho A_d V_\infty (1 + a)(V_\infty(1 + 2a) - V_\infty) \\ &= \rho A_d V_\infty^2 (1 + a)(2a) \end{aligned} \tag{6.13}$$

6.1.2 Extensions and Modifications to the Basic Methodology

The basic momentum theory ignores the hub and tip vortices that affect the induced velocity. Various correct methods exist; we use the simple analytical expression developed by Prandtl.[9]

9. Glauert, *Airplane Propellers*, 1935.

$$\begin{aligned} f_{tip} &= \frac{B}{2}\left(\frac{R - r}{r|\sin\phi|}\right) \\ F_{tip} &= \frac{2}{\pi}\arccos(\exp(-f_{tip})) \\ f_{hub} &= \frac{B}{2}\left(\frac{r - R_{hub}}{R_{hub}|\sin\phi|}\right) \\ F_{hub} &= \frac{2}{\pi}\arccos(\exp(-f_{hub})) \\ F &= F_{tip}F_{hub} \end{aligned} \tag{6.14}$$

The absolute value is necessary because our definition permits both positive and negative inflow angles. This hub/tip-loss factor (which is always between 0 and 1) is applied directly to the thrust.

$$T = 2a(1 + a)\rho A_d V_\infty^2 F \tag{6.15}$$

The tip loss function is visualized in Fig. 6.16

Another common modification is adjusting for high induction factors, but this is only applicable to turbines and is not discussed here.

We will use a disk area that is infinitesimally thin $A_d = 2\pi r$ so that we get a thrust per unit length. The final form for the thrust per unit length at a given radial section is then:

$$T' = 4a(1 + a)\rho V_\infty^2 \pi r F \tag{6.16}$$

If a is positive then the rotor is acting as a propeller, if negative it is acting as a turbine (and thus produces drag instead of thrust).

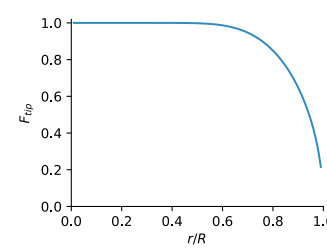

Fig. 6.5 Tip loss function, which goes to zero at the tip, to simulate a finite rotor.

6.1.3 Efficiency

For propellers, a quantity we often care about is the efficiency. So far we have been discussing the flow field from a frame fixed with the propeller (i.e., the left side of Fig. 6.6). In other words, in our frame of reference the propeller is not moving, freestream air is coming in at speed V_∞ and a wake is left behind at speed V_w. An understanding of efficiency is perhaps easier to see from a ground-fixed frame. To achieve that we simply vectorially subtract V_∞ from all the velocities (right side of Fig. 6.6). Now the propeller (i.e., with the aircraft) is moving with speed V_∞ into still air and leaving behind a wake with speed $V_w - V_\infty$.

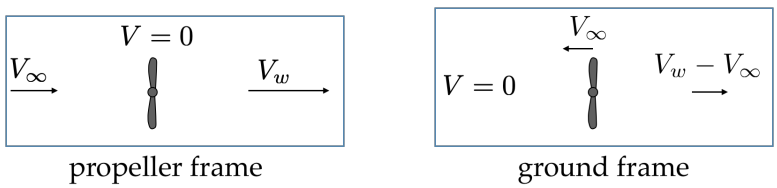

Fig. 6.6 Propeller shown in the frame of the propeller and in a ground-fixed frame.

The propulsive efficiency is given by the useful power out (TV_∞) divided by all the power put into the system (power out plus power left behind in the wake):

$$\eta = \frac{TV_\infty}{TV_\infty + \frac{1}{2}\dot{m}(V_w - V_\infty)^2} \tag{6.17}$$

If we plug in our expression for thrust (Eq. 6.16) and note that the mass flow rate is: $\dot{m} = \rho A_d V_d$ then this efficiency calculation can be simplified to:

$$\eta = \frac{2}{1 + \frac{V_w}{V_\infty}} \tag{6.18}$$

and our thrust in Eq. 6.13 can be written as:

$$T = \dot{m}(V_w - V_\infty) \tag{6.19}$$

What these equations tell us is that for maximum efficiency we would like $V_w = V_\infty$. In other words, we would like to leave no energy behind in the wake. However, that also means that the propeller produces zero thrust. Conversely, if we make V_w larger than we can increase our thrust, but at the expense of decreased efficiency. Another parameter we can change to increase thrust is to increase the mass flow rate $\dot{m}$, which generally means increasing the size of the propeller (A_d). Increasing propeller diameter allows us to increase propulsive thrust without sacrificing efficiency. Of course, increasing propeller diameter comes with its own tradeoffs specific to the application, but in general

leads to increased weight and noise. Additionally, increasing diameter may increase the tip Mach number, leading to shock waves, completely eliminating any efficiency gains.

6.1.4 Angular Momentum

Similar to the linear momentum case, where an induced velocity is produced in opposition to the force on the rotor, the rotation of the blades is accompanied by an induced swirl velocity in the opposite direction to that of the torque on the rotor. Unlike, the linear momentum case where the induced velocity change occurs across a large control volume, the rotational velocity change occurs only across the rotor disk. Conservation of momentum yields the same result as the linear case, where the induced velocity at the disk is halfway between its upstream and downstream values. In this case, upstream and downstream is just upstream and downstream of the rotor disk, instead of in the farfield. The induced rotational velocity is 0 upwind of the rotor, v in the plane of the rotor, and $2v$ downstream of the rotor (opposing the direction of the torque on the rotor). Just like before, we define a normalized version of this induced velocity, which we call the tangential induction factor: $a' = v/V_y$, where V_y is the tangential inflow velocity and in the absence of wind or other motion is just Ωr.

The angular momentum balance can be obtained by taking the position vector $\vec{r}$ crossed into the momentum equation. In this case we take r as the radial distance from the center of the turbine. We repeat the linear momentum equation from Eq. 1.75, except that we represent the pressure and shear terms generically as a sum of forces.

$$\frac{\partial}{\partial t}\int_{\forall}\rho\vec{V}d\forall + \int_A \rho\vec{V}\left(\vec{V}\cdot d\vec{A}\right) = \sum\vec{F} \tag{6.20}$$

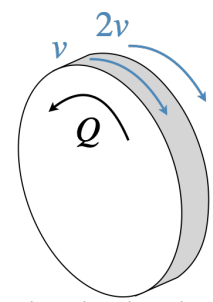

Fig. 6.7 The induced swirl velocity is in the direction opposite to that of the torque on the rotor.

Perform the cross product yields:

$$\frac{\partial}{\partial t}\int_{\forall}\rho(\vec{r}\times\vec{V})d\forall + \int_A(\vec{r}\times\vec{V})\rho\left(\vec{V}\cdot d\vec{A}\right) = \sum\vec{r}\times\vec{F} \tag{6.21}$$

Although a rotating turbine is fundamentally unsteady, we are typically interested in time-averaged quantities (e.g., torque, thrust). Once time averaged, the time-dependent term goes to zero. Then, to express this equation more concisely we use the mass flow rate $\dot{m} = \rho\vec{V}\cdot d\vec{A}$, and recognize the right hand side as torque (Q):

$$\int_A\left(\vec{r}\times\vec{V}\right)\dot{m} = \sum\vec{Q} \tag{6.22}$$

We use a disk-shaped control volume that surrounds the rotor disk, and assume no axial component of velocity exists on the sides of the control volume. We are then interested in only the inflow and outflow velocity vectors into the control volume. Figure 6.8 uses an ground-centered inertial control volume, rather than a blade-centric control volume to show the velocity triangles. This is a somewhat unconventional frame of reference and orientation for a turbine/propeller, but is commonly used in turbomachinery analysis, and is convenient for this particular analysis. The figure illustrates the inflow and outflow on either side of the control volume, and notes the direction of blade rotation For a propeller the direction of torque opposes the rotation direction and so the induced velocity is in the direction of rotation as shown in the figure (opposite of the torque).

We define a positive torque as is conventional for propellers, which is that a positive torque opposes the direction of motion (i.e., torque is about our $-x$ axis and is thus negative in our chosen axes.) This means that the propeller must input power to overcome this resistive torque. Although that is a negative torque for our coordinate system, the momentum equations need the torque the rotor exerts on the fluid (not the torque the fluid exerts on rotor), and so we flip the sign again:

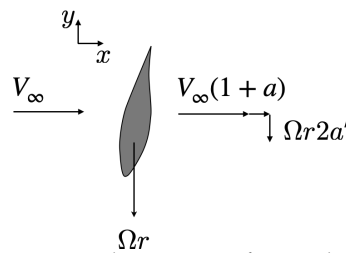

Fig. 6.8 Velocity vectors for angular momentum balance.

$$\begin{aligned} r\Omega r 2a'\dot{m} &= Q \\ \Omega r^2 2a'\dot{m} &= Q \end{aligned} \tag{6.23}$$

Using the results from the previous section:

$$\dot{m} = \rho V_d A_d = \rho V_\infty (1+a) A_d \tag{6.24}$$

adding the hub/tip loss factor, and using our infinitesimal annual ring area results in:

$$Q' = 4a'(1+a)\rho V_\infty \Omega r^2 \pi r F \tag{6.25}$$

For a turbine the sign of a' would reverse and consequently the sign for the torque and power would automatically switch as well.

6.1.5 Blade Element Theory

We have considered the momentum part of the theory, and now consider the blade element portion. Blade element is just another name for 2D airfoil theory. Consider the airfoil from a section of the blade shown in Fig. 6.9. The inflow plus induced velocities from the previous sections are shown resulting in the total inflow velocity vector W. The angle θ, from the plane of rotation to the airfoil chord line, is called the twist angle. The angle ϕ, from the plane of rotation to the inflow velocity

vector, is called in the inflow angle. The angle between the velocity vector and the chord line is the angle of attack:

$$\alpha = \theta - \phi \tag{6.26}$$

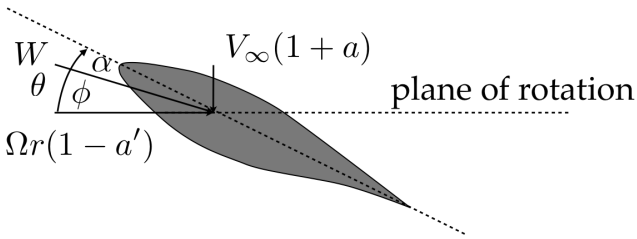

Fig. 6.9 Definition for positive twist and coordinate system for the blade element theory.

With a known angle of attack we can compute the sectional lift and drag coefficient from 2D airfoil data. The lift and drag coefficients may in general also be functions of the Reynolds number and Mach number.

$$\begin{aligned} c_l &= f_L(\alpha, Re, M) \\ c_d &= f_D(\alpha, Re, M) \end{aligned} \tag{6.27}$$

These lift and drag coefficients are generally computed from a spline so that the results vary smoothly. Because we do not know the induction factors yet we usually approximate the Reynolds number (and Mach number) using:

$$\begin{aligned} W_0 &= \sqrt{V_\infty^2 + (\Omega r)^2} \\ Re &= \frac{\rho W_0 c}{\mu} \end{aligned} \tag{6.28}$$

The impact of this approximation is usually negligible as Reynolds number changes occur across orders of magnitude. Instead of using Mach number as one of the inputs in the spline, we could just correct the lift coefficient with a Prandtl-Glauert rule:

$$c_l = \frac{c_{l0}}{\sqrt{1 - M^2}} \tag{6.29}$$

Using the Kutta-Joukowski theorem, the directions for the lift and drag coefficients, c_l and c_d are as shown in Fig. 6.10.

We need to resolve these forces into the normal and tangential directions as shown in the figure. These directions are consistent with the way we have defined thrust and torque in the momentum equations.

$$\begin{aligned} c_n &= c_l \cos\phi - c_d \sin\phi \\ c_t &= c_l \sin\phi + c_d \cos\phi \end{aligned} \tag{6.30}$$

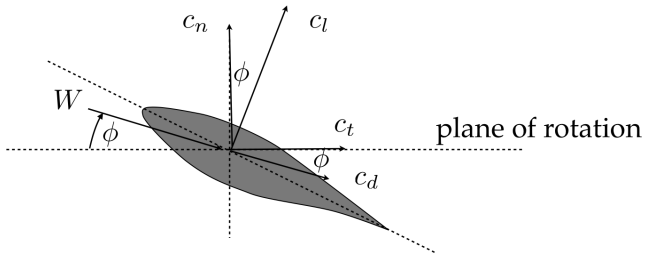

Fig. 6.10 Directions for the lift and drag forces from the Kutta Joukowski theorem.

To compute the total thrust and torque for this blade section we then multiply by the local dynamic pressure (not freestream, including induction) and the chord. This gives us the forces/moments per unit length for one blade, and so to get the forces for the entire rotor we need to multiply by the number of blades B:

$$\begin{aligned} T' &= BN' \\ T' &= Bc_n \frac{1}{2}\rho W^2 c \end{aligned} \tag{6.31}$$

$$\begin{aligned} Q' &= BrT' \\ Q' &= Brc_t \frac{1}{2}\rho W^2 c \end{aligned} \tag{6.32}$$

where

$$W = \sqrt{[V_\infty(1+a)]^2 + [\Omega r(1-a')]^2} \tag{6.33}$$

The above formulation is equally applicable to turbines, except that the positive direction of camber is usually flipped for turbine operation (imagine flipping the airfoil upside down). Regardless of the camber direction, any blade can operate as both a turbine or propeller with appropriate twist, but if we want an efficient turbine we would flip the camber. This is equivalent to modifying the airfoil functions as:

$$\begin{aligned} f_L &= -c_l(-\alpha, Re, M) \\ f_D &= c_d(-\alpha, Re, M) \end{aligned} \tag{6.34}$$

6.1.6 Blade Element Momentum

We can now combine the results from momentum theory and blade element theory. We first equate the linear momentum equations (thrust), and next the angular momentum equations (torque). Finally, we discuss the residual equation which determines whether or not we have consistency between the momentum and blade element theories.

We equate the thrust from momentum theory and blade element theory. Before doing so we define the nondimensional parameter:

$$\sigma' = \frac{Bc}{2\pi r} \tag{6.35}$$

which is called the local solidity. It is a measure of how much area the blades occupy relative to the disk area for a given radial station (hence local solidity and not total solidity). We now equate the two thrust equations:

$$\begin{aligned} 4a(1+a)\rho V_\infty^2 \pi r F &= B c_n \frac{1}{2}\rho W^2 c \\ 4a(1+a)F &= \sigma' c_n \left(\frac{W}{V_\infty}\right)^2 \end{aligned} \tag{6.36}$$

To simplify further we need to relate the inflow velocity to the induction factors. By referring to Fig. 6.11 we can come up with the following expressions:

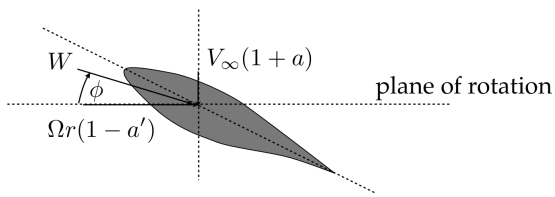

Fig. 6.11 Inflow angle and inflow velocities.

$$\sin\phi = \frac{V_\infty(1+a)}{W} \tag{6.37}$$

or

$$\cos\phi = \frac{\Omega r(1-a')}{W} \tag{6.38}$$

These can be rearranged as:

$$\frac{W}{V_\infty} = \frac{1+a}{\sin\phi} \tag{6.39}$$

or

$$\frac{W}{\Omega r} = \frac{1-a'}{\cos\phi} \tag{6.40}$$

We will use the first substitution for this thrust equation:

$$\begin{aligned} 4a(1+a)F &= \sigma' c_n \left(\frac{W}{V_\infty}\right)^2 \\ 4a(1+a)F &= \sigma' c_n \frac{(1+a)^2}{\sin^2\phi} \\ 4aF &= \sigma' c_n \frac{(1+a)}{\sin^2\phi} \end{aligned} \tag{6.41}$$

This equation can now be solved for a. After some algebraic manipulation the result is:

$$a = \frac{1}{\frac{4F\sin^2\phi}{\sigma' c_n} - 1} \tag{6.42}$$

We repeat a similar process for the torques. Equating the torques from momentum and blade element theories results in:

$$\begin{aligned} 4a'(1+a)\rho V_\infty \Omega r^2 \pi r F &= B r c_t \frac{1}{2}\rho W^2 c \\ 4a'(1+a)F &= \sigma' c_t \frac{W}{V_\infty}\frac{W}{\Omega r} \end{aligned} \tag{6.43}$$

We now substitute the relationships for W. This time we use one of each of the two equations:

$$\begin{aligned} 4a'(1+a)F &= \sigma' c_t \frac{(1+a)}{\sin\phi}\frac{(1-a')}{\cos\phi} \\ 4a'F &= \sigma' c_t \frac{1}{\sin\phi}\frac{(1-a')}{\cos\phi} \end{aligned} \tag{6.44}$$

We can now solve this for a':

$$a' = \frac{1}{\frac{4F\sin\phi\cos\phi}{\sigma' c_t} + 1} \tag{6.45}$$

The above equations allow us to compute the induction factors. However, we have to be careful as these calculations depend on ϕ and the angle of attack, which in turn depend on the induction factors (Fig. 6.9). Thus, we have a circular dependency and need to use an iterative method, or a root solver. Traditionally, this is done by considering a and a' as the unknowns and using the two equations above to form two residuals. However, we can greatly simplify the solution of these equations by considering ϕ and W as the unknowns [8,10]. The inflow velocity has no direct dependence in the BEM equations (other than in Reynolds number, which operates on a log scale and so the impact is negligible). This means that we can reduce the residuals to one equation, which is advantageous because one dimensional root finding problems can be solved with guaranteed convergence. The solution of the residual ensures compatibility between the blade element and momentum theories. From Fig. 6.11 we can write:

8. Ning, *Using Blade Element Momentum Methods with Gradient-Based Design Optimization*, 2021.

10. Ning, *A Simple Solution Method for the Blade Element Momentum Equations with Guaranteed Convergence*, 2014.

$$\tan\phi = \frac{V_\infty(1+a)}{\Omega r(1-a')} \tag{6.46}$$

This equation could be rearranged in many ways to form a residual equation, but as demonstrated in the above cited papers a numerically advantageous form is:

$$\mathcal{R}(\phi) = \frac{\sin\phi}{1+a} - \frac{V_\infty}{\Omega r}\frac{\cos\phi}{(1-a')} = 0 \tag{6.47}$$

In summary we define a residual function as follows:

$$\text{function } \mathcal{R}(\phi) \tag{6.48}$$

$$\alpha = \theta - \phi \tag{6.49}$$

$$c_l = f(\alpha, Re, M) \tag{6.50}$$

$$c_d = f(\alpha, Re, M) \tag{6.51}$$

$$c_n = c_l \cos\phi - c_d \sin\phi \tag{6.52}$$

$$c_t = c_l \sin\phi + c_d \cos\phi \tag{6.53}$$

$$a = \frac{\sigma' c_n}{4F\sin^2\phi - \sigma' c_n} \tag{6.54}$$

$$a' = \frac{\sigma' c_t}{4F\sin\phi\cos\phi + \sigma' c_t} \tag{6.55}$$

$$\text{return } \frac{\sin\phi}{1+a} - \frac{V_\infty}{\Omega r}\frac{\cos\phi}{(1-a')} \tag{6.56}$$

Generally, the solution will be in the bracket: $\phi = (0, \pi/2]$ (note the open bracket at zero). Thus, a method like Brent's method can be used to yield fast and robust convergence. If airfoil data has not been extended to such high angles, a smaller range may suffice.

This procedure yields a solution at one radial station of the blade (Fig. 6.22). Once we solve a section on the blade for the correct inflow angle ϕ^* we can recalculate the resulting loads and induction factors for that section:

$$c_n, c_t, a, a' = f(\phi^*) \tag{6.57}$$

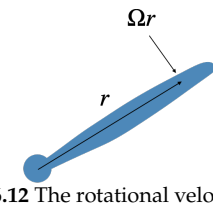

Fig. 6.12 The rotational velocity at a given radial station on the blade.

We then compute the inflow velocity:

$$W^2 = (V_\infty(1+a))^2 + (\Omega r(1-a'))^2 \tag{6.58}$$

and the thrust and torque per unit length:

$$T' = Bc_n \frac{1}{2}\rho W^2 c \tag{6.59}$$

$$Q' = Brc_t \frac{1}{2}\rho W^2 c \tag{6.60}$$

We then need to repeat these procedure at multiple radial stations given by our chosen blade discretization. We then integrate across the blade to get total thrust and torque:

$$T = \int_{r_h}^{r_t} T' dr \tag{6.61}$$

$$Q = \int_{r_h}^{r_t} Q' dr \tag{6.62}$$

where r_h and r_t correspond to the hub and tip radius respectively. Right at the hub/tip the loads go to zero and so we need not compute at those points (indeed we cannot compute right at those points). Finally, from the torque we can compute the required power.

$$P = Q\Omega \tag{6.63}$$

While not necessary, it is often convenient to normalize using typical propeller conventions. The thrust, torque, and power coefficients are given by:

$$C_T = \frac{T}{\rho n^2 D^4} \tag{6.64}$$

$$C_Q = \frac{Q}{\rho n^2 D^5} \tag{6.65}$$

$$C_P = \frac{P}{\rho n^3 D^5} \tag{6.66}$$

where n is the number of revolutions per second:

$$n = \frac{\Omega}{2\pi} \tag{6.67}$$

and D is the diameter. The efficiency is given by:

$$\eta = \frac{P_{out}}{P_{in}} = \frac{TV_\infty}{Q\Omega} = \frac{C_T \rho n^2 D^4 V_\infty}{C_P \rho n^3 D^5} = J\frac{C_T}{C_P} \tag{6.68}$$

All of these outputs are functions of the advance ratio (another nondimensional parameter, recall discussion in Ex. 1.2):

$$J = \frac{V_\infty}{nD} \tag{6.69}$$

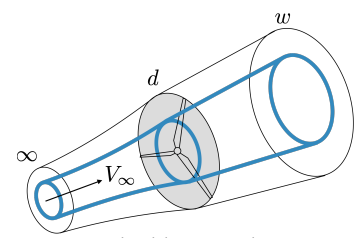

Fig. 6.13 The blue annulus streamtube is used as our control volume in the derivation of this section. The stations are denoted by ∞: far upstream, d: the rotor disk, and w in the far wake.

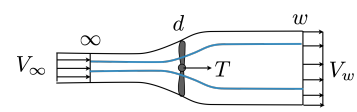

Fig. 6.14 Side view of control volume with resultant force T. Note that this is a drag force but is called thrust in the wind turbine community.

*Perhaps because it can be considered as a thrust force acting on the wind turbine tower, and that is generally the primary reason why this force is of interest in wind turbine applciations.

6.2 Blade Element Momentum Theory: Turbines

We now repeat the above derivations, but from the perspective of a turbine. This section will be briefer as we can reuse most of the same concepts, although there are a few unique considerations.

6.2.1 Linear Momentum Balance

We again use infinitesimally thin annulus streamtubes at each radial station along the rotor (Fig. 6.13), and adopt the same three stations: upstream, at the rotor disk, and in the wake.

Figure 6.14 shows the control volume from a side view. Note that the net force on the blade is actually a drag force, but in the wind

energy community it is referred to as a thrust* and so we will adopt that convention here. First, we perform a mass balance.

$$\rho V_\infty A_\infty = \rho V_d A_d = \rho V_w A_w \tag{6.70}$$

Notice that as the fluid slows down, the cross-sectional area increases.

Next, we apply an x-momentum balance across the entire control volume, where we take the positive direction for x as downwind:

$$\rho V_\infty(-V_\infty A_\infty) + \rho V_w(V_w A_w) = -T \tag{6.71}$$

The standard definition for thrust for a wind turbine is positive in the direction of V_∞. However, in the momentum balance we need to use the force the turbine exerts on the fluid, which is in the opposite direction, and is thus negative above. Combining these two expressions yields:

$$T = \rho A_d V_d (V_\infty - V_w) \tag{6.72}$$

It is not obvious that the pressure terms from the sides of the control volume cancel, but they do. We can come up with the same result more rigorously, with a cylindrical control volume that does not follow the streamlines, but the details are omitted here.

Let us now use a second control volume just across the disk. We will call the x location just upstream of the disk station 2, and just downstream will be called station 3. Performing a momentum balance yields :

$$\rho V_2(-V_2 A_2) + \rho V_3(V_3 A_3) = -T + p_2 A_2 - p_3 A_3 \tag{6.73}$$

Because $A_2 = A_3 = A_d$ and the velocity must vary continuously through the disk ($V_2 = V_3$) the above expression simplifies to:

$$T = A_d(p_2 - p_3) \tag{6.74}$$

Combining the two expressions for thrust (Eqs. 6.72 and 6.74) yields:

$$\rho V_d(V_\infty - V_w) = (p_2 - p_3) \tag{6.75}$$

To relate the pressure change from station 2 to 3, we use Bernoulli's equation (Eq. 5.77). We cannot apply Bernoulli's equation from station 2 to station 3 directly because work is done on the fluid between those stations. However, we can apply the equation upstream of the turbine and downstream of the turbine separately.

First, from station ∞ to station 2:

$$p_\infty + \frac{1}{2}\rho V_\infty^2 = p_2 + \frac{1}{2}\rho V_2^2 \tag{6.76}$$

then from station 3 to station w:

$$p_3 + \frac{1}{2}\rho V_3^2 = p_w + \frac{1}{2}\rho V_w^2 \tag{6.77}$$

If we subtract the two equations and simplify using $V_2 = V_3$, and assume our control volume is large enough so that $p_\infty = p_w$ we have

$$p_2 - p_3 = \frac{1}{2}\rho(V_\infty^2 - V_w^2) \tag{6.78}$$

This expression for the pressure drop is inserted into Eq. 6.75

$$\begin{aligned} \rho V_d(V_\infty - V_w) &= (p_2 - p_3) \\ \rho V_d(V_\infty - V_w) &= \frac{1}{2}\rho(V_\infty^2 - V_w^2) \\ V_d(V_\infty - V_w) &= \frac{1}{2}(V_\infty - V_w)(V_\infty + V_w) \\ V_d &= \frac{1}{2}(V_\infty + V_w) \end{aligned} \tag{6.79}$$

This yields the result that the velocity at the disk is half way between the upstream and downstream velocity. A similar relationship was derived for a lifting wing when we showed that the downwash at the wing is half of the downwash in the farfield.

With this relationship, we can generically relate the velocities at the 3 stations using the unknown induced velocity u (Fig. 6.15).

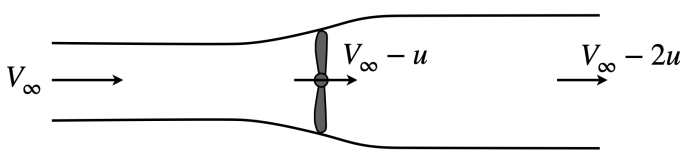

Fig. 6.15 Depiction of the induced velocity in at the rotor disk and in the farfield.

By convention one typically nondimensionalizes u as follows:

$$\begin{aligned} V_d &= V_\infty - u \\ &= V_\infty\left(1 - \frac{u}{V_\infty}\right) \\ &= V_\infty(1 - a) \end{aligned} \tag{6.80}$$

The quantity a is called the *axial induction factor*. Similarly, we can express the far-field velocity as:

$$V_w = V_\infty(1 - 2a) \tag{6.81}$$

With these definitions, we can express thrust in terms of the axial induction factor (using Eqs. 6.74, 6.75, 6.80, and 6.81):

$$\begin{aligned} T &= \rho A_d V_d (V_\infty - V_w) \\ &= \rho A_d V_\infty (1-a)(V_\infty - V_\infty(1-2a)) \\ &= \rho A_d V_\infty^2 (1-a)(2a) \end{aligned} \tag{6.82}$$

We then nondimensionalize this expression to form the thrust coefficient using turbine conventions. We use V_∞ as the reference velocity in the dynamic pressure, and the local annulus area as the reference area.

$$\begin{aligned} C_T &= \frac{T}{\frac{1}{2}\rho V_\infty^2 A_d} \\ &= 4a(1-a) \end{aligned} \tag{6.83}$$

One way to express the power is:

$$P = T V_d \tag{6.84}$$

Using Eqs. 6.80 and 6.82 we have:

$$P = \rho A_d V_\infty^3 (1-a)^2 2a \tag{6.85}$$

We normalize to compute the power coefficient:

$$\begin{aligned} C_P &= \frac{P}{\frac{1}{2}\rho V_\infty^3 A_d} \\ &= 4a(1-a)^2 \end{aligned} \tag{6.86}$$

To find the optimal induction for maximizing power we take derivatives of this expression with respect to a:

$$\begin{aligned} \frac{dC_P}{da} = 4a(2)(1-a)(-1) + 4(1-a)^2 &= 0 \\ -2a + (1-a) &= 0 \\ a^* &= 1/3 \end{aligned} \tag{6.87}$$

Thus, to maximize power, with no constraints, the optimal induction factor at each section is 1/3.[†] The corresponding maximum power coefficient is:

$$C_P(a = 1/3) = \frac{16}{27} \approx 0.59 \tag{6.88}$$

This is the maximum theoretical power coefficient for a turbine, and is known as the *Betz limit*.

[†] In practice there are many constraints, like thrust constraints, structural constraints, etc., and so the optimal induction is typically less than this value.

6.2.2 Extensions and Modifications to the Basic Methodology

The basic momentum theory ignores the hub and tip vortices that affect the induced velocity. Various correct methods exist; we use the simple analytical expression developed by Prandtl.[9]

9. Glauert, *Airplane Propellers*, 1935.

$$
\begin{aligned}
f_{tip} &= \frac{B}{2}\left(\frac{R-r}{r|\sin\phi|}\right) \\
F_{tip} &= \frac{2}{\pi}\arccos(\exp(-f_{tip})) \\
f_{hub} &= \frac{B}{2}\left(\frac{r-R_{hub}}{R_{hub}|\sin\phi|}\right) \\
F_{hub} &= \frac{2}{\pi}\arccos(\exp(-f_{hub})) \\
F &= F_{tip}F_{hub}
\end{aligned}
\tag{6.89}
$$

The absolute value is necessary because our definition permits both positive and negative inflow angles. This hub/tip-loss factor (which is always between 0 and 1) is applied directly to the thrust.

$$
C_T = 4a(1-a)F \tag{6.90}
$$

The tip loss function is visualized in Fig. 6.16

One unique consideration for turbines is dealing with high induction factors. The velocity in the wake from the momentum balance is shown in Eq. 6.81. If a increases above 0.5, then the equation predicts wake velocities that reverse direction. This reversal is non-physical, as the real flow entrains momentum in the wake through turbulence. Empirical data is needed to determine the behavior as a approaches 0.5 and beyond. Notional behavior of the thrust coefficient with large induction factors is seen in Fig. 6.17.

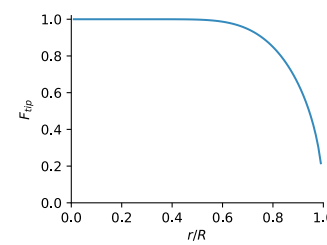

Fig. 6.16 Tip loss function, which goes to zero at the tip, to simulate a finite rotor.

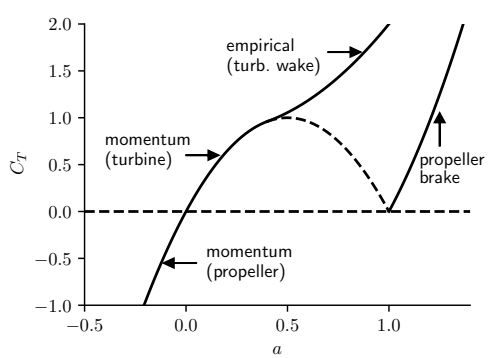

Fig. 6.17 Thrust coefficient as a function of axial induction factor

Various extension methods exist for the turbulent wake region. A common simple method is the quadratic fit from Glauert.[11] However, the Glauert correction does not maintain continuity when the tip/hub loss corrections are included. Buhl provided a small modification of Glauert's method to provide that continuity.[12] However, that modification leads to nonzero thrust loads when the tip correction is zero, which can be problematic for some optimization parameterizations. So we use a small modification of that approach.[‡]

11. Glauert and Committee, *A General Theory of the Autogyro*, 1926.

12. Buhl Jr., *A New Empirical Relationship between Thrust Coefficient and Induction Factor for the Turbulent Windmill State*, 2005.

[‡]Pointed out in a personal communication from Kenneth Lønbæk.

$$C_T = \left(\frac{14}{9}a^2 - \frac{4}{9}a + \frac{8}{9}\right)F \quad \text{for } 0.4 \leq a \leq 1 \tag{6.91}$$

Additional considerations are needed for induction factors larger than 1, the propeller brake region. The current expression Eq. 6.83 predicts a change in sign in the thrust force for induction factors greater than 1. However, repeating the momentum balance shows that the force still acts as a drag device (i.e., thrust in the wind turbine convention).

$$C_T = -4a(1+a)F \quad \text{for } a \geq 1 \tag{6.92}$$

For this case the rotor behaves like a propeller (requiring power input) but with a large negative pitch so that the thrust is reversed allowing the rotor to act like an aerodynamic brake.

6.2.3 Angular Momentum

Similar to the linear momentum case, where an induced velocity is produced in opposition to the force on the rotor, the rotation of the blades is accompanied by an induced swirl velocity in the opposite direction to that of the torque on the rotor. Unlike, the linear momentum case where the induced velocity change occurs across a large control volume, the rotational velocity change occurs only across the rotor disk. Conservation of momentum yields the same result as the linear case, where the induced velocity at the disk is halfway between its upstream and downstream values. In this case, upstream and downstream is just upstream and downstream of the rotor disk, instead of in the farfield. The induced rotational velocity is 0 upwind of the rotor, v in the plane of the rotor, and $2v$ downstream of the rotor (opposing the direction of the torque on the rotor). Just like before, we define a normalized version of this induced velocity, which we call the tangential induction factor: $a' = v/V_y$, where V_y is the tangential inflow velocity and in the absence of wind or other motion is just Ωr.

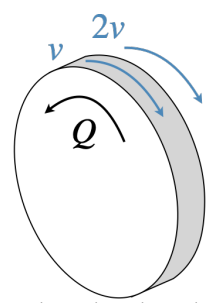

Fig. 6.18 The induced swirl velocity is in the direction opposite to that of the torque on the rotor.

The angular momentum balance can be obtained by taking the position vector $\vec{r}$ crossed into the momentum equation. In this case we

take r as the radial distance from the center of the turbine. We repeat the linear momentum equation from Eq. 1.75, except that we represent the pressure and shear terms generically as a sum of forces.

$$\frac{\partial}{\partial t}\int_{\forall}\rho\vec{V}d\forall + \int_{A}\rho\vec{V}\left(\vec{V}\cdot d\vec{A}\right) = \sum\vec{F} \tag{6.93}$$

Perform the cross product yields:

$$\frac{\partial}{\partial t}\int_{\forall}\rho(\vec{r}\times\vec{V})d\forall + \int_{A}(\vec{r}\times\vec{V})\rho\left(\vec{V}\cdot d\vec{A}\right) = \sum\vec{r}\times\vec{F} \tag{6.94}$$

Although a rotating turbine is fundamentally unsteady, we are typically interested in time-averaged quantities (e.g., torque, thrust). Once time averaged, the time-dependent term goes to zero. Then, to express this equation more concisely we use the mass flow rate $\dot{m} = \rho\vec{V}\cdot d\vec{A}$, and recognize the right hand side as torque (Q):

$$\int_{A}\left(\vec{r}\times\vec{V}\right)\dot{m} = \sum\vec{Q} \tag{6.95}$$

We use a disk-shaped control volume that surrounds the rotor disk, and assume no axial component of velocity exists on the sides of the control volume. We are then interested in only the inflow and outflow velocity vectors into the control volume. Figure 6.19 uses an ground-centered inertial control volume, rather than a blade-centric control volume to show the velocity triangles. This is a somewhat unconventional frame of reference and orientation for a turbine/propeller, but is commonly used in turbomachinery analysis, and is convenient for this particular analysis. The figure illustrates the inflow and outflow on either side of the control volume, and notes the direction of blade rotation. For a turbine the direction of torque is in the same direction as the rotation direction and so the induced velocity opposes the rotational direction as shown in the figure.

We define a positive torque as is conventional for turbines, which is that a positive torque is in the direction of motion (i.e., torque is about our $+x$ axis). The momentum equations need the torque the rotor exerts on the fluid (not the torque the fluid exerts on rotor), and so we flip the sign:

$$\begin{aligned} -r\Omega r2a'\dot{m} &= -Q \\ \Omega r^2 2a'\dot{m} &= Q \end{aligned} \tag{6.96}$$

Using the results from the previous section:

$$\dot{m} = \rho V_d A_d = \rho V_\infty(1-a)A_d \tag{6.97}$$

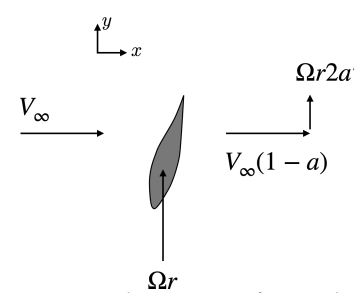

Fig. 6.19 Velocity vectors for angular momentum balance.

and adding the hub/tip loss factor results in:

$$Q' = \Omega r^2 2a' \rho V_\infty (1-a) A_d F \tag{6.98}$$

We normalize the torque in a similar way to thrust (but with an extra term for the radius):

$$\begin{aligned} C_Q &= \frac{Q'}{\frac{1}{2}\rho V_\infty^2 A_d r} \\ &= 4a'(1-a)\lambda_r F \end{aligned} \tag{6.99}$$

where

$$\lambda_r = \frac{\Omega r}{V_\infty} \tag{6.100}$$

is called the *local tip-speed ratio*.

6.2.4 Blade Element Theory

We have considered the momentum part of the theory, and now consider the blade element portion. Blade element is just another name for 2D airfoil theory. Consider the airfoil from a section of the blade shown in Fig. 6.20. The inflow plus induced velocities from the previous sections are shown resulting in the total inflow velocity vector W. The angle θ, from the plane of rotation to the airfoil chord line, is called the twist angle. The angle ϕ, from the plane of rotation to the inflow velocity vector, is called in the inflow angle. The angle between the velocity vector and the chord line is the angle of attack:

$$\alpha = \phi - \theta \tag{6.101}$$

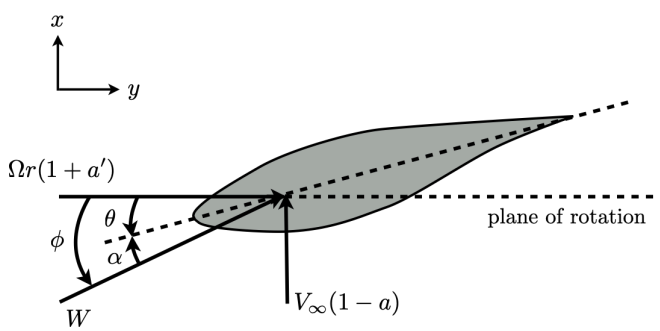

Fig. 6.20 Definition for positive twist and coordinate system for the blade element theory.

With a known angle of attack we can compute the sectional lift and drag coefficient from 2D airfoil data. The lift and drag coefficients may in general also be functions of the Reynolds number (for wind

turbines Mach numbers are generally low enough to be considered incompressible).

$$\begin{aligned} c_l &= f_L(\alpha, Re) \\ c_d &= f_D(\alpha, Re) \end{aligned} \tag{6.102}$$

These lift and drag coefficients are generally computed from a spline so that the results vary smoothly. Because we do not know the induction factors yet we usually approximate the Reynolds number using:

$$\begin{aligned} W_0 &= \sqrt{V_\infty^2 + (\Omega r)^2} \\ Re &= \frac{\rho W_0 c}{\mu} \end{aligned} \tag{6.103}$$

The impact of this approximation is usually negligible as Reynolds number changes occur across orders of magnitude.

Using the Kutta-Joukowski theorem, the directions for the lift and drag coefficients, c_l and c_d are as shown in Fig. 6.21.

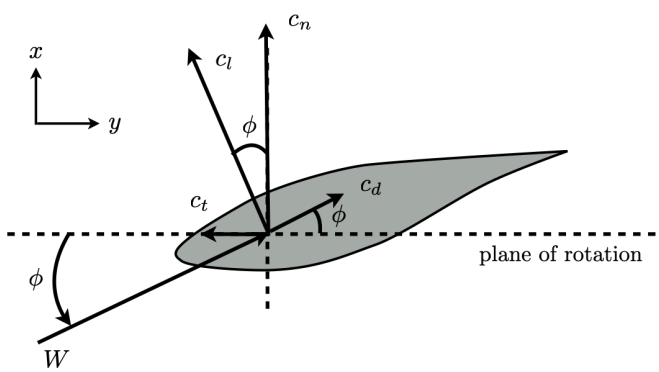

Fig. 6.21 Directions for the lift and drag forces from the Kutta Joukowski theorem.

We need to resolve these forces into the normal and tangential directions as shown in the figure. These directions are consistent with the way we have defined thrust and torque in the momentum equations.

$$\begin{aligned} c_n &= c_l \cos\phi + c_d \sin\phi \\ c_t &= c_l \sin\phi - c_d \cos\phi \end{aligned} \tag{6.104}$$

To compute the total thrust and torque for this blade section we then multiply by the local dynamic pressure (not freestream, including induction) and the chord. This gives us the forces/moments per unit length for one blade, and so to get the forces for the entire rotor we need to multiply by the number of blades B:

$$\begin{aligned} T' &= BN' \\ T' &= Bc_n \frac{1}{2}\rho W^2 c \end{aligned} \tag{6.105}$$

$$
\begin{aligned}
Q' &= BrT' \\
Q' &= Brc_t \frac{1}{2}\rho W^2 c
\end{aligned}
\tag{6.106}
$$

where

$$
W = \sqrt{[V_\infty(1-a)]^2 + [\Omega r(1+a')]^2} \tag{6.107}
$$

If we use the same normalizations from the previous section we obtain:

$$
C_T = c_n \sigma' \left(\frac{W}{V_\infty}\right)^2 \tag{6.108}
$$

where

$$
\sigma' = \frac{Bc}{2\pi r} \tag{6.109}
$$

is called the *local solidity* and is a ratio of the area of the blades relative to the disk area, at a given radius.[§] Using Fig. 6.20 we can relate the velocities as:

[§]Total solidity, or sometimes just solidity, is the ratio of the total blade area relative to total disk area.

$$
\sin\phi = \frac{V_\infty(1-a)}{W} \tag{6.110}
$$

Thus, the local thrust coefficient from blade element theory is:

$$
C_T = c_n \sigma' \left(\frac{(1-a)}{\sin\phi}\right)^2 \tag{6.111}
$$

We repeat the same process for the torque coefficient. The velocities can be related using Eq. 6.110 or with

$$
\cos\phi = \frac{\Omega r(1+a')}{W} \tag{6.112}
$$

For the torque coefficient is will be convenient to use one of each substitution in place of W.

$$
\begin{aligned}
C_Q &= c_t \sigma' \left(\frac{W}{V_\infty}\right)^2 \\
&= c_t \sigma' \lambda_r \left(\frac{(1-a)(1+a')}{\sin\phi\cos\phi}\right)
\end{aligned}
\tag{6.113}
$$

6.2.5 Blade Element Momentum

We can now combine the results from momentum theory and blade element theory. We first equate the linear momentum equations (thrust), and next the angular momentum equations (torque). Finally, we discuss the residual equation which determines whether or not we have consistency between the momentum and blade element theories.

We equate the thrust from momentum theory and blade element theory. In the wind turbine case, the thrust coefficient from momentum theory had three expressions. For $a < 0.4$ we have:

$$\begin{aligned} 4a(1-a)F &= c_n\sigma' \left(\frac{(1-a)}{\sin\phi}\right)^2 \\ 4aF &= c_n\sigma' \frac{(1-a)}{\sin^2\phi} \end{aligned} \tag{6.114}$$

It will be convenient to group some of these terms into a new nondimensional factor

$$\kappa = \frac{c_n\sigma'}{4F\sin^2\phi} \tag{6.115}$$

With that definition the solution for a is:

$$\boxed{a = \frac{\kappa}{1+\kappa}} \tag{6.116}$$

The criteria for this equation was expressed in terms of a, but this is not convenient as that is the quantity we are solving for. Instead, we will express the criteria in terms of κ. We require that

$$\begin{aligned} \frac{\kappa}{1+\kappa} &\le 0.4 \\ \kappa &\le 0.4(1+\kappa), \quad \text{(assuming } 1+\kappa > 0 \\ &\qquad \text{or in other words } \kappa > -1) \\ 0.6\kappa &\le 0.4 \\ \kappa &\le \frac{2}{3} \end{aligned} \tag{6.117}$$

Thus, this first cases applies if $-1 \le \kappa < 2/3$.

For the next case, $0.4 < a < 1$, we use the empirical momentum formula:

$$\left(\frac{14}{9}a^2 - \frac{4}{9}a + \frac{8}{9}\right)F = c_n\sigma'\left(\frac{1-a}{\sin\phi}\right)^2 \tag{6.118}$$

This yields a quadratic formula that can be solved for a. After simplification it yields (noting that only the negative sign in the quadratic formula is physically possible):

$$\boxed{a = \frac{\gamma_1 - \sqrt{\gamma_2}}{\gamma_3}} \tag{6.119}$$

where

$$\begin{aligned}\gamma_1 &= 2\kappa - \frac{1}{9}\\ \gamma_2 &= 2\kappa - \frac{1}{3}\\ \gamma_3 &= 2\kappa - \frac{7}{9}\end{aligned} \tag{6.120}$$

Using a similar process to express the criteria in terms of κ insteae of a, we can show that the equation applies when $\kappa > 2/3$ (and thus the denominator will never be zero).

The case for $a > 1$, the propeller break region, leads to a similar equation to the first case, but with a negative sign. The result is:

$$a = \frac{\kappa}{\kappa - 1} \tag{6.121}$$

If $a > 1$ then from Fig. 6.20 we see that the angle ϕ would need to change signs. Thus, this case only applies when $\phi < 0$. This case is exactly the same as the first momentum case, if we replace κ with $-\kappa$.

We can consolidate these three cases as shown in Algorithm 1. Note that $\kappa = -1$ is only physically consistent if $V_\infty = 0$.[8] For nonzero inflow, we know that κ cannot equal -1 so if any intermediate iterations produces κ = -1 we can simply return a nonzero residual and continue iterating.

8. Ning, *Using Blade Element Momentum Methods with Gradient-Based Design Optimization*, 2021.

Algorithm 1 Solve for the axial induced velocity.

```
if φ < 0 then
    κ = −κ
end if

if κ ≤ 2/3 then
    a = κ/(1 + κ)                    if κ = −1 return any nonzero residual.
else
    a = (γ1 − √γ2)/γ3
end if
```

We repeat a similar process for the torques, except in this case there iis only one equation. Equating the torque coefficients from momentum and blade element theories results in:

$$\begin{aligned}4a'(1-a)\lambda_r F &= c_t \sigma' \lambda_r \left(\frac{(1-a)(1+a')}{\sin\phi\cos\phi}\right)\\ 4a'F &= c_t\sigma'\left(\frac{(1+a')}{\sin\phi\cos\phi}\right)\end{aligned} \tag{6.122}$$

For convenience we define the nondimensional quantity:

$$\kappa' = \frac{c_t \sigma'}{4F \sin\phi \cos\phi} \tag{6.123}$$

We can now solve this for a':

$$a' = \frac{\kappa'}{1 - \kappa'} \tag{6.124}$$

The above equations allow us to compute the induction factors. However, we have to be careful as these calculations depend on ϕ and the angle of attack, which in turn depend on the induction factors (Fig. 6.20). Thus, we have a circular dependency and need to use an iterative method, or a root solver. Traditionally, this is done by considering a and a' as the unknowns and using the two equations above to form two residuals. However, we can greatly simplify the solution of these equations by considering ϕ and W as the unknowns.[8,10] The inflow velocity has no direct dependence in the BEM equations (other than in Reynolds number, which operates on a log scale and so the impact is negligible). This means that we can reduce the residuals to one equation, which is advantageous because one dimensional root finding problems can be solved with guaranteed convergence. The solution of the residual ensures compatibility between the blade element and momentum theories. From Fig. 6.20 we can write:

8. Ning, *Using Blade Element Momentum Methods with Gradient-Based Design Optimization*, 2021.

10. Ning, *A Simple Solution Method for the Blade Element Momentum Equations with Guaranteed Convergence*, 2014.

$$\tan\phi = \frac{V_\infty(1-a)}{\Omega r(1+a')} \tag{6.125}$$

$$= \frac{(1-a)}{\lambda_r(1+a')} \tag{6.126}$$

This equation could be rearranged in many ways to form a residual equation, but as demonstrated in the above cited papers a numerically advantageous form is:

$$\mathcal{R}(\phi) = \frac{\sin\phi}{1-a} - \frac{\cos\phi}{\lambda_r(1+a')} = 0 \tag{6.127}$$

In summary we define a residual function as follows:

$$\text{function } \mathcal{R}(\phi) \tag{6.128}$$
$$\alpha = \phi - \theta \tag{6.129}$$
$$c_l = f(\alpha, Re) \tag{6.130}$$
$$c_d = f(\alpha, Re) \tag{6.131}$$
$$c_n = c_l \cos\phi + c_d \sin\phi \tag{6.132}$$
$$c_t = c_l \sin\phi - c_d \cos\phi \tag{6.133}$$
$$\kappa = \frac{\sigma' c_n}{4F \sin^2\phi} \tag{6.134}$$
$$\text{Compute } a \text{ from Algorithm 1} \tag{6.135}$$
$$\kappa' = \frac{\sigma' c_t}{4F \sin\phi \cos\phi} \tag{6.136}$$
$$a' = \kappa'/(1-\kappa') \tag{6.137}$$
$$\text{return } \frac{\sin\phi}{1-a} - \frac{\cos\phi}{\lambda_r(1+a')} \tag{6.138}$$

Generally, the solution will be in the bracket: $\phi = (0, \pi/2]$ (note the open bracket at zero). Thus, a method like Brent's method can be used to yield fast and robust convergence. If airfoil data has not been extended to such high angles, a smaller range may suffice.

This procedure yields a solution at one radial station of the blade (Fig. 6.22). Once we solve a section on the blade for the correct inflow angle ϕ^* we can recalculate the resulting loads and induction factors for that section:

$$c_n, c_t, a, a' = f(\phi^*) \tag{6.139}$$

We then compute the inflow velocity:

$$W^2 = (V_\infty(1-a))^2 + (\Omega r(1+a'))^2 \tag{6.140}$$

and the thrust and torque per unit length:

$$T' = Bc_n \frac{1}{2}\rho W^2 c \tag{6.141}$$
$$Q' = Brc_t \frac{1}{2}\rho W^2 c \tag{6.142}$$

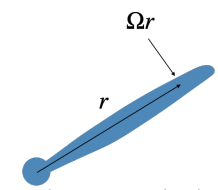

Fig. 6.22 The rotational velocity at a given radial station on the blade.

We then need to repeat these procedure at multiple radial stations given by our chosen blade discretization. We then integrate across the

blade to get total thrust and torque:

$$T = \int_{r_h}^{r_t} T' dr \tag{6.143}$$

$$Q = \int_{r_h}^{r_t} Q' dr \tag{6.144}$$

where r_h and r_t correspond to the hub and tip radius respectively. Right at the hub/tip the loads go to zero and so we need not compute at those points (indeed we cannot compute right at those points). Finally, from the torque we can compute the required power.

$$P = Q\Omega \tag{6.145}$$

While not necessary, it is often convenient to normalize using typical turbine conventions. The thrust, torque, and power coefficients are given by:

$$C_T = \frac{T}{\frac{1}{2}\rho V_\infty^2 \pi R^2} \tag{6.146}$$

$$C_Q = \frac{Q}{\frac{1}{2}\rho V_\infty^2 \pi R^3} \tag{6.147}$$

$$C_P = \frac{P}{\frac{1}{2}\rho V_\infty^3 \pi R^2} \tag{6.148}$$

where R is the rotor radius. All of these outputs are functions of the tip-speed ratio

$$\lambda = \frac{\Omega R}{V_\infty} \tag{6.149}$$

6.3 Airfoil Data Corrections

The accuracy of the blade element methodology hinges on providing accurate airfoil data, namely the tables of lift and drag coefficients as functions of angle of attack (and potentially of Reynolds number and Mach number as well). Unfortunately, static airfoil tables, whether from experimental data or computational simulation, are rarely useful as is.

First, the airfoil forces, particularly the maximum lift, is significantly affected by rotation. Most airfoil data is based on non-rotating conditions. The Coriolis and centrifugal forces, generated from rotation, tend to delay stall and allow for higher lift coefficients. Rotation corrections are needed to account for this behavior.

Second, corrections for Reynolds number and/or Mach number may be needed. Ideally, airfoil coefficients are provided at multiple

Reynolds/Mach numbers. If so, we can interpolate directly on the data as Reynolds number and Mach number vary in the simulation. If such data is not available, corrections can account for modest variations. Mach number variation is rarely needed for wind turbines, or propellers designed for low-speed aircraft.

Third, the angle of attack range from most airfoil data sources is too limited. As compared to wings, the angle of attack along blades varies much more significantly. This is because rotation changes the local inflow speed, from small speeds near the hub to large speeds at the tip, and thus the local inflow angle varies considerably. Thus, we usually need to provide airfoil data across a larger range of angles of attack. For wind turbines, the incoming wind can change direction significantly, and startup and stopping introduces large changes in rotation speed that can be important loading conditions. All of these considerations lead to an even wider range of angles that need to be considered. Thus, for wind turbines in particular, we typically extrapolate the data across the full circle from $\alpha = -180°$ to $180°$. For propellers, the extrapolation can be much more modest and in some cases may not be needed at all depending on the conditions being analyzed (e.g., the range of advance ratios simulated).

If not extrapolated to large angles, we should reduce the solution range shown below Eq. 6.56 to not extend all the way to $\pi/2$. That is a wide enough value to bracket the solution without requiring any information, but a tighter bracket can work as well if we use information specific to our propeller. Knowing the twist angles, and provided angles of attack (assuming a solution exist within the range of provided data), we could provide a smaller upper bound on ϕ (Eq. 6.26).

6.3.1 Rotation Corrections

As discussed in Section 1.10, fluid moving in a rotating reference frame experiences additional apparent forces, namely a Coriolis force and a centrifugal force.* These forces are negligibly small for the flow around a rotor, except in the boundary layer or in areas of separation where the fluid is moving slowly.

*Himmelskamp was the first to identify that the lift curves on sections of a rotating propeller blade differed significantly from the 2D wind tunnel data.[13] Although theoretical explanations did not come for some time after.

13. Himmelskamp, *Profile investigations on a rotating airscrew*, 1947.

The hub and tip vortices induce radial motion along the blade. The hub vortex induces flow towards the tip, and the tip vortex induces flow towards the hub, with the effects most pronounced near the ends. From Eq. 1.131 we can see the Coriolis force associated with these radial velocity components induces a force towards the trailing edge near the hub, and towards the leading edge near the tip (Fig. 6.23). These apparent forces act as a favorable and adverse pressure gradient

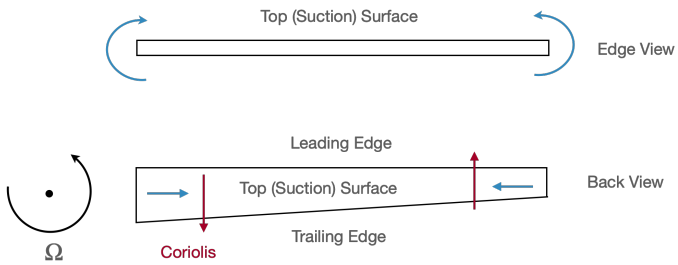

Fig. 6.23 Coriolis force generated from radial flow along blade.

respectively. Thus, near the hub, stall is delayed to higher lift coefficients because of the favorable pressure gradient. Conversely, near the tip, stall happens sooner than otherwise would occur on a non-rotating section.

In addition to the Coriolis force, there is a centrifugal force directed from hub to tip. This force accentuates the radial flow from the hub vortex, and somewhat counteracts the radial flow from tip vortex. Thus, we expect an even higher increase in maximum lift coefficients near the hub, and a more subdued impact on maximum lift decreases near the tip. Additionally, the radial flow from the centrifugal force extends the region of separation out further from the hub, an effect called *centrifugal pumping*. Thus, the effects of stall delay occur further out on the blade, although they are still most pronounced near the hub.

Many rotation corrections models exit. Sometimes these are called 3D corrections, as they correct 2D non-rotating data to account for the three-dimensional effects of radial flow. Although a basic motivation for the behavior was described above, the flow mechanisms are complex and still not fully understood. None of the models is considered highly generalizable, though many share similar features.

A common form is:

$$c_{l3D} = c_{l2D} + f_l\left(\frac{c}{R}, \frac{r}{R}, \lambda, \ldots\right)(c_{l_{pot}} - c_{l2D}) \tag{6.150}$$

where c_{l2D} is the provided non-rotating data, c_{l3D} is the rotationally-corrected data, $c_{l_{pot}}$ is the idealized potential flow solution (Eq. 2.147), and f_l is a function that differs between the methods. Note that although the theoretical lift curve slope is 2π (Eq. 2.148), and we can use that, it is usually preferable to use the lift curve slope from the actual data as determined by regression.

A similar expression is used for drag:

$$c_{d3D} = c_{d2D} + f_d\left(\frac{c}{R}, \frac{r}{R}, \lambda, \ldots\right)(c_{d0} - c_{d2D}) \tag{6.151}$$

where c_{d0} is the drag coefficient at zero degrees angle of attack. However, there is less agreement on rotation-based drag models. In fact, there is

not even agreement on whether the drag should increase or decrease (though most now predict an increase).

Many such models exist, only a few of which are highlighted below. One of the original models, is from Snell,[14,15] which identified the local solidity (c/r when stripping away constants) as a critical parameter in predicting the enhancement in lift coefficient near the hub. This model is simply:

$$f_l = 3.1\left(\frac{c}{r}\right)^2 \tag{6.152}$$

For lower tip-speed ratios this model can be improved with:[16]

$$f_l = 3.1\left(\frac{c}{r}\right)^2 \frac{\Omega r}{W} \tag{6.153}$$

where W is the local inflow velocity Eq. 6.33 or Eq. 6.107. If we ignore the smaller contribution from induction that the last term can be approximated as:

$$\frac{\Omega r}{W} \approx \frac{\lambda_r^2}{1+\lambda_r^2} \tag{6.154}$$

where λ_r is the local tip-speed ratio (Eq. 6.100). Note that the local tip-speed ratio is related to the tip-speed ratio Eq. 6.149 as:

$$\lambda_r = \frac{\lambda}{r/R} \tag{6.155}$$

This model does not have a corresponding drag formula.

Another popular model is from Du and Selig:[17]

$$f_l = \frac{1}{2\pi}\left[12.63(c/r)\left(\frac{a-(c/r)^{\frac{d}{\Lambda(r/R)}}}{b+(c/r)^{\frac{d}{2\Lambda(r/R)}}}\right)-1\right] \tag{6.156}$$

where a, b, and d are tunable parameters set to 1 by default, and Λ is a modified tip speed ratio:

$$\Lambda = \frac{\Omega R}{\sqrt{V_x^2+(\Omega R)^2}} = \frac{\lambda}{\sqrt{1+\lambda^2}} \tag{6.157}$$

Although a similar drag formula was proposed, it predicts a decrease in drag and is thus not often used.

Because these models are driven by the Coriolis force from the hub vortex, and the centrifugal pumping pushing the separation location further inboard, it should not be applied near the tip. For $r/R > 0.8$, no correction is applied (though the correction naturally drops off anyway with increasing radial location).

14. Snel, *Scaling laws for the boundary layer flow on rotating wind turbine blades*, 1991.

15. Snel et al., *Sectional prediction of lift coefficients on rotating wind turbine blades in stall*, 1994.

16. Lindenburg, *Investigation into Rotor Blade Aerodynamics: Analysis of the stationary measurements on the UAE phase-VI rotor in the NASA-Ames wind tunnel*, 2003.

17. Du and Selig, *A 3-D Stall-Delay Model for Horizontal Axis Wind Turbine Performance Prediction*, 1998.

Additionally, both of these methods will continue to provide enhanced lift coefficients at large angles of attack. In practice the correction should only be applied in full up to some maximum angle. After about 30 degrees the corrections is tapered off towards zero (e.g., until 50 degrees [16] or until 90 degrees[18]).

For drag, one approach is to use the simple result from Eggers [19] that relates the tangential force correction and the normal force correction as follows:

$$\Delta c_t = 0.12 \Delta c_n \tag{6.158}$$

where these terms refer to corrections in tangential and normal force respectively. We can relate these back to changes in lift and drag from the definitions of these coordinate systems Fig. 6.21

$$\Delta c_d = \Delta c_n \sin\phi - \Delta c_t \cos\phi \tag{6.159}$$

$$\Delta c_l = \Delta c_n \cos\phi + \Delta c_t \sin\phi \tag{6.160}$$

If we substitute Eq. 6.158 into the above two equations we have:

$$\Delta c_d = \Delta c_n \left(\sin\phi - 0.12\cos\phi\right) \tag{6.161}$$

$$\Delta c_l = \Delta c_n \left(\cos\phi + 0.12\sin\phi\right) \tag{6.162}$$

We now solve Eq. 6.162 for c_n and substitute it into Eq. 6.161 we have the relationship:

$$\Delta c_d = \Delta c_l \left(\frac{\sin\phi - 0.12\cos\phi}{\cos\phi + 0.12\sin\phi}\right) \tag{6.163}$$

With this technique we could then use any model for the lift correction, (i.e., Eq. 6.150 written in the form $c_{l3D} = c_{l2D} + \Delta c_l$) then compute a corresponding drag correction from Eq. 6.163 that we apply as follows:

$$c_{d3D} = c_{d2D} + \Delta c_d \tag{6.164}$$

Note that Eggers defines his own correction for the normal force although that isn't expounded on here.

While the above formulas were expressed in terms of the tip-speed ratio, the advance ratio (Eq. 6.69), used for propellers, is related to the tip speed ratio (Eq. 6.149) by:

$$\lambda = \pi / J \tag{6.165}$$

Rotation corrections can be done on the fly (i.e., computed at each iteration of the analysis), or they can be pre-computed and built into the airfoil polars that are fixed throughout the analysis. While on-the-fly is

16. Lindenburg, *Investigation into Rotor Blade Aerodynamics: Analysis of the stationary measurements on the UAE phase-VI rotor in the NASA-Ames wind tunnel*, 2003.

18. Laino et al., *Validation of the AeroDyn Subroutines Using NREL Unsteady Aerodynamics Experiment Data*, 2002.

19. Eggers Jr et al., *An Assessment of Approximate Modeling of Aerodynamic Loads on the uae Rotor*, 2003.

perhaps ideal, pre-computation is more common because the combined variation in airfoil data, post-stall behavior, rotation corrections, and extrapolation (discussed later in this section) can sometimes lead to unphysical results (e.g., abrupt changes, discontinuities, reversals, etc.). By pre-computing, all airfoil polars can be inspected and adjusted as needed.

The difficulty with pre-computing is that the corrections depend on the radial station (r), and so even in the case when a single airfoil is used for the entire blade, separate airfoil files should be created at each station. For wind turbines this is not so onerous as the airfoil typically varies across the blade anyway. However, sometimes the amount of effort is not justified for some blades where the rotational corrections are relatively modest, and the operating conditions explored are minimal and typical, so just one rotationally-corrected airfoil might be used for the whole blade. This can sometimes be justifiable as high angles of attack only occur near the root for normal operation, precisely where such corrections would be most needed.

6.3.2 Reynolds and Mach Number Corrections

Another correction that may be needed is for Reynolds number. If Reynolds number variation is significant, it is generally more accurate for the airfoil force coefficients to be provided at multiple Reynolds numbers (whether from computations or experiments). Then, the lift and drag at a given Reynolds number is computed through interpolation.

However, if such data is not available, an on-the-fly Reynolds number correction could be used instead. From Eq. 3.49 we have an analytic solution to the skin friction coefficient for laminar flow over a flat plate.

$$C_f = \frac{1.328}{\sqrt{Re_L}} \tag{6.166}$$

For a flat plate the skin friction coefficient is also the drag coefficient. For other shapes, the drag would still be (approximately) proportional to the skin friction coefficient. We represent this proportionality with some constant k:

$$c_d = \frac{k}{\sqrt{Re_L}} \tag{6.167}$$

If we know the drag at some Reynolds number, which we denote as condition 0, and wish to estimate the drag at some other Reynolds number (no subscript) we have the following ratio:

$$\frac{c_d}{c_{d0}} = \frac{\sqrt{Re_0}}{\sqrt{Re}} \tag{6.168}$$

A turbulent boundary layer is more likely and so we can repeat the same analysis with an empirical flat plate skin friction coefficient (Eq. 3.53). In this case:

$$\frac{c_d}{c_{d0}} = \left(\frac{Re_0}{Re}\right)^{0.2} \tag{6.169}$$

Both cases can be represented as:

$$c_d = c_{d0}\left(\frac{Re_0}{Re}\right)^p \tag{6.170}$$

where $p = 0.5$ for a purely laminar boundary layer, $p = 0.2$ for a turbulent boundary layer, or some other empirical value may be used based on additional data.

This equation provides a simple way to estimate the drag for modest changes in Reynolds number (at least within the same flow regime of laminar or turbulent), given the drag coefficient at some known Reynolds number (c_{d0}, Re_0). For modest changes in Reynolds number, lift typically shows little variation and so may be neglected within this approximation. While this method is not as accurate as providing data at multiple Reynolds number, it is straightforward to apply and may be sufficient in many cases.

For changes in Mach number similar approaches can be utilized. Ideally, data is provided at different Mach numbers. But, if not, the Prandtl-Glauert correction could be used (Eq. 5.182).

$$c_l = \frac{c_{l0}}{\sqrt{1 - M_\infty^2}} \tag{6.171}$$

where c_{l0} corresponds to the incompressible lift coefficient. This correction affects only the lift and neglects any changes in drag. Again, such corrections can be useful if other data is not available, and the variations in Mach number are relatively modest. Unfortunately, the Karman-Tsien correction cannot be used as the correction is for pressure coefficients and does not result in a simple proportionality constant that could be factored out of an integral for forces (as does the Prandtl-Glauert method).

6.3.3 Extrapolation

As discussed previously sometimes it is desirable to extend the angle of attack range of the airfoil data all the way from $-180°$ to $180°$. This may be for physical reasons (wind turbine startup/stop scenarios which have high angles), numerical solution approaches (which may

use a large bracket for robustness and simplicity), or optimization robustness (in which intermediate solutions may have large twist angles). Experimental data rarely exists at such high angles, so extrapolation approaches are used. Fortunately at high angles, airfoils behave like a flat plate and so the behavior can be captured in a relatively universal way.

The Viterna method is the most commonly used extrapolation approach.[20] The extrapolation begins at an angle of attack α_s, which corresponds to the angle of attack at stall, the angle of attack at maximum lift (after rotation corrections), or some other location in the stalled region depending on the extent of reliable data. The extrapolation of lift and drag for angles larger than α_s (or less than $-\alpha_{ns}$ where α_{ns} corresponds to stall at negative angles of attack) is:

20. Viterna and Janetzke, *Theoretical and Experimental Power from Large Horizontal-Axis Wind Turbines*, 1982.

$$c_l = \frac{c_{d\,max}}{2}\sin(2\alpha) + A\frac{\cos^2\alpha}{\sin\alpha} \tag{6.172}$$

$$c_d = c_{d\,max}\sin^2(\alpha) + B\cos\alpha \tag{6.173}$$

where A and B are constants defined as:

$$A = (c_{l_s} - c_{d\,max}\sin\alpha_s\cos\alpha_s)\frac{\sin\alpha_s}{\cos^2\alpha_s} \tag{6.174}$$

$$B = c_{d_s} - \frac{c_{d\,max}\sin^2\alpha_s}{\cos\alpha_s} \tag{6.175}$$

The maximum drag coefficient, $c_{d\,max}$, is estimated from flat plate experiments as:

$$c_{d\,max} = \begin{cases} 1.11 + 0.018AR & \text{for } AR < 50 \\ 2.01 & \text{for } AR \geq 50 \end{cases} \tag{6.176}$$

The aspect ratio AR is defined as the blade radius divided by the chord at 75% radius:

$$AR = \frac{R}{c_{0.75R}} \tag{6.177}$$

This method is generally considered reasonably accurate. However, like the rotation corrections, it can sometimes produce nonphysical results with abrupt changes or discontinuities so some care is needed in implementation and usually it is used as a preprocessing step so that the outputs can be inspected. Usually it is applied after rotation corrections, another reason favoring precomputed rotational corrections.

6.3.4 Dynamic Stall

While everything we have discussed so far is based on static aerodynamics, wind turbine and propeller aerodynamics are also subject to

dynamic behavior. This dynamic behavior may arise because of wind fluctuations (e.g., turbulence), motion of the blades (e.g., aeroelasticity) or both. If the dynamic behavior is slow†, then the steady approache can be used reasonably well with instantaneous dynamic inputs. This approach where static models are used with instantaneous time-varying inputs is known as *quasi-static*. However, as the dynamic behavior increases in speed, then the physical behavior can differ quite significantly from quasi-static predictions. The topic of unsteady aerodynamics is discussed more broadly in a separately chapter. In this section, just a brief overview of the impact on rotors is noted.

†What is meant by "slow" is defined more precisely in the next paragraph.

The degree of unsteadiness is quantified by a nondimensional number called the Strohaul number:

$$St = \frac{fL}{V} \tag{6.178}$$

where f is the frequency of the unsteady behavior, L is some characteristic length, and V is the fluid velocity. For aerodynamics the reduced frequency is more commonly used:

$$k = \frac{\omega c}{2V} \tag{6.179}$$

where ω is the circular frequency ($w = 2\pi f$) and a length scale of $c/2$ is used because of results from unsteady thin airfoil theory. If the reduced frequency is small (say, $k < 0.05$) then the behavior can be considered quasi-static. Otherwise, a dynamic model is needed.

The lift, drag, and moment coefficients of airfoils in dynamic stall exhibit hysteresis, meaning that as angle of attack is rapidly increased then decreased the lift and drag curves do not follow the same path back down as they did going up. Figure 6.24 depicts an example, where an airfoil is under going a pitching motion with an amplitude of 4 degrees. Note that the dynamic lift coefficient not only differs from the static lift coefficient, but that the lift coefficient when the angle of attack is increased differs from that when the angle of attack is decreased.

Perhaps the most well known dynamic stall model is the Beddoes-Leishman model, which arose out of the rotorcraft community.[21,22] However, rotorcraft and wind turbine blades have different dynamic stall behavior, as the thin airfoils in rotorcraft are more susceptible to leading edge stall, and travel at speeds where compressibility is critical. Wind turbines on the other hand have much thicker airfoil shapes, and have other unique considerations like lead-lag vibration. Some dynamic stall models that are specific to or commonly used in wind turbine applications include the Øye model[23] or the Risø model.[24]

21. Beddoes, *A synthesis of unsteady aerodynamic effects including stall hysteresis*, 1976.

22. Leishman and Beddoes, *A Semi-Empirical Model for Dynamic Stall*, 1989.

23. Øye, *Dynamic stall simulated as time lag of separation*, 1991.

24. Hansen et al., *A Beddoes–Leishman Type Dynamic Stall Model in State-space and Indicial Formulations*, 2004.

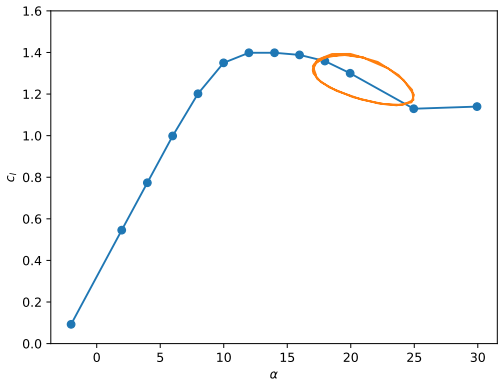

Fig. 6.24 Static airfoil lift coefficient in dotted line. Cyclic behavior created from a pitching airfoil with a reduced frequency of 0.1, and a pitching amplitude of 4 degrees centered at 21 degrees angle of attack.

6.4 Wakes

While the details of wake development behind a propeller or turbine are complex, we can generally obtain reasonable approximations for two scenarios: in the near-field and far-field. In the near field, assuming that the wake does not deform (i.e., moves straight back for a wing, or continues in a rigid helicoidal shape for a rotor), is generally a reasonable approximation. We could, for example, use the induced velocities computed aft of the blade:

$$V_{\text{axial}} = 2V_\infty a \tag{6.180}$$

and

$$V_{\text{swirl}} = 2\Omega r a' \tag{6.181}$$

These velocities are depicted in Fig. 6.25. Note that we don't use the velocities right at the disk. Instead, we are interested in behavior aft of the rotor, which includes a factor of 2 as computed previously. The downstream result of the previous sections is considered near-field in the overall wake development, as the transition occurs quickly. This type of near-field model can work well if we are reasonably close to the rotor disk, typically within about one rotor diameter.

This type of model is sometimes used for tractor configurations with the propeller forward of the wing. The wake of the propeller impinges on the wing and modifies the input velocities (e.g., computed using a VLM Section 4.5). Because the velocities in the propeller wake increase in speed, in a *blown wing* concept multiple propellers can be used to significantly increase the effective freestream velocity as seen by the wing, allowing takeoff with much shorter runways. Sometimes additional corrections are used to modify the effect of the axial and

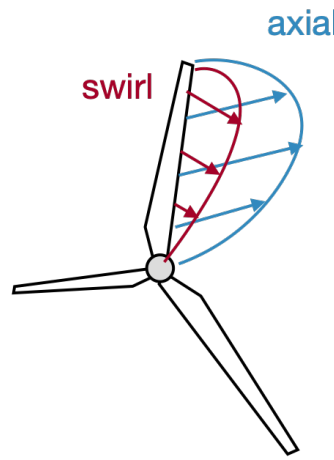

Fig. 6.25 The induced velocities in the near field of the rotor computed based on the induction at the rotor.

swirl velocities on the wing velocities, to better match experimental data.

The other type of approximation that is sometimes used is a far-field wakes. While the former type is more common for propellers, this latter time is common for wind turbines. Far-field wake models are motivated by the observed self-similarity of bluff-body wakes. This means that after some distance, if properly normalized, the velocity deficit profile collapses to a single curve. Thus, we expect that a model can be developed to predict the behavior of a far-field wake in a reasonably universal way. Self-similarity usually begins after a few rotor diameters.

For a turbine, the velocity is decreased in the wake, which reduces the power available to downstream turbines. Furthermore, the wake increases turbulence increasing the fatigue loads on downstream turbines. Thus, in a wind farm, wind turbines are far apart (usually at least 6 diameters spacing) to reduce negative wake interactions. At these separation distances a far-field assumption can be a reasonable approximation.

One of the simplest turbine wake models is the Jensen model.[25] We start a control volume at a point downstream of the rotor, where the wake has developed as discussed in the previous sections (V_w), and continues in a self-similar manner forward of that point (Fig. 6.26). From this point it expands linearly into the far-field (V_f).

25. Jensen, *A Note on Wind Generator Interaction*, 1983.

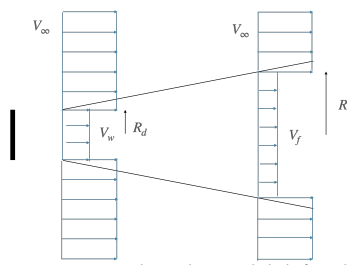

Fig. 6.26 Simple wake model defined by a linearly expanding wake from the rotor disk.

We now apply a mass balance to a cylindrical control volume starting downstream of the disk, where we assume the starting diameter is identical to that of the rotor disk, and end at an arbitrary location in the farfield.

$$\rho V_d \pi R_d^2 + \rho V_\infty (\pi R^2 - \pi R_d^2) = \rho V_w \pi R^2 \tag{6.182}$$

Cancelling like terms and simplifying results in:

$$V_d R_d^2 + V_\infty (R^2 - R_d^2) = V_w R^2 \tag{6.183}$$

We now solve for the wake velocity:

$$V_w = V_d \left(\frac{R_d}{R}\right)^2 + V_\infty \left(1 - \left(\frac{R_d}{R}\right)^2\right) \tag{6.184}$$

Using the definition for the initial wake velocity in terms of an induction

factor (Eq. 6.81) results in:

$$
\begin{aligned}
V_w &= V_\infty(1-2a)\left(\frac{R_d}{R}\right)^2 + V_\infty\left(1-\left(\frac{R_d}{R}\right)^2\right) \\
V_w &= V_\infty\left(1+(1-2a-1)\left(\frac{R_d}{R}\right)^2\right) \\
V_w &= V_\infty\left(1-2a\left(\frac{R_d}{R}\right)^2\right)
\end{aligned}
\tag{6.185}
$$

We have already assumed that the radius expands linearly with downstream distance x, starting from the disk, which we express as:

$$R = R_d + kx \tag{6.186}$$

The parameter k is called the *wake growth rate*, and is the slope of the linear wake profile. The rotor diameter (D) is more commonly used than radius, so we also make that change:

$$
\begin{aligned}
V_w &= V_\infty\left(1-2a\left(\frac{D/2}{D/2+kx}\right)^2\right) \\
&= V_\infty\left(1-2a\left(\frac{D}{D+2kx}\right)^2\right) \\
&= V_\infty\left(1-2a\left(1+\frac{2kx}{D}\right)^{-2}\right)
\end{aligned}
\tag{6.187}
$$

Turbine wake models are typically expressed in terms of the velocity deficit:

$$\delta = \frac{\Delta V}{V_\infty} = \frac{V_\infty - V_w}{V_\infty} = 1 - \frac{V_w}{V_\infty} \tag{6.188}$$

In this case the velocity deficit is:

$$\delta = \frac{2a}{\left(1+\frac{2kx}{D}\right)^2} \tag{6.189}$$

The original Jensen model assumed that the rotor was optimally loaded for maximum power (Eq. 6.87, $a = 1/3$), but a later version generalized to express the induction in terms of the induction factor.[26] Using the momentum theory expression for thrust coefficient (Eq. 6.83), we can solve for the induction factor:

26. Katić et al., *A simple model for cluster efficiency*, 1986.

$$a = \frac{1}{2}\left(1-\sqrt{1-C_T}\right) \tag{6.190}$$

In solving the quadratic equation for a, we know that the negative sign is the correct branch based on physically realizable induction factors for this momentum region (Fig. 6.17). We substitute this expression into the velocity deficit:

$$\frac{\Delta V}{V_\infty} = \frac{1 - \sqrt{1 - C_T}}{\left(1 + \frac{2kx}{D}\right)^2} \tag{6.191}$$

We now have the final model:

$$\delta(x, r) = \begin{cases} \left(1 - \sqrt{1 - C_T}\right) / \left(1 + \frac{2kx}{D}\right)^2 & \text{for } |r| \leq D/2 + kx \\ 0 & \text{otherwise} \end{cases} \tag{6.192}$$

The initial Jensen model assumed an expansion rate of $k = 0.1$ although this is an adjustable constant. Today, more typical values are $k = 0.075$ for onshore turbines, and $k = 0.04$ for offshore.

This was a useful initial model that has served the community well, but is not often used today as it is over-simplistic and has been replaced by better models. The resulting velocity profile contains an unphysical jump, and there is no dependence on other critical parameters like freestream turbulence.

Many turbine wake models exist, we highlight just one more recent model that is well used, which we will call the BP model as it was developed by Bastankhah and Porté-Agel model.[27] The BP model uses a self-similar Gaussian distribution to describe the wake deficit, allowing for a continuous and smooth velocity profile that matches experimental data much better. Additionally, rather than satisfy only a mass balance, both a mass and a momentum balance are used. The wake growth rate is also computed as a function of turbulence intensity. Several parameters in the model are tuned based on LES simulations. The derivation is not discussed here, but we rather provide a summary. The full model allows for changes in yaw angle, wake deflection, variations both laterally and vertically (rather than an axisymmetric model), but we ignore these considerations for simplicity in the expression shown here. The result is:

27. Bastankhah and Porté-Agel, *Experimental and theoretical study of wind turbine wakes in yawed conditions*, 2016.

$$\delta(x, r) = \left(1 - \sqrt{1 - \frac{C_T D^2}{8\sigma^2}}\right) \exp\left(-0.5 \left[\frac{r}{\sigma}\right]^2\right) \tag{6.193}$$

where σ is the wake width (as a standard deviation) defined as:

$$\sigma = k^*(x - x_0) + \frac{D}{2\sqrt{2}} \tag{6.194}$$

Note that k^* is defined slightly differently than the wake growth rate mentioned earlier ($k^* = d\sigma/dx$ as opposed to $k = dD/dx$). A different definition is necessary since a Gaussian distribution has no "edge". The physical effect is the same, both denote a growth rate in the width of the wake, but the actual numbers used will not be the same. The location x_0, the point at which self-similarly is assumed to begin, is computed as:

$$x_0 = \frac{D(1 + \sqrt{1 - C_T})}{\sqrt{2}(\alpha^* I + \beta^*(1 - \sqrt{1 - C_T}))} \tag{6.195}$$

where $\alpha^* = 2.32$, $\beta^* = 0.154$, and I is the turbulence intensity (Eq. 3.148). This model was later extended so the wake growth rate could be computed as a function of turbulence intensity:[28]

$$k^* = 0.3837\, I + 0.003678 \tag{6.196}$$

28. Niayifar and Porté-Agel, *Analytical Modeling of Wind Farms: A New Approach for Power Prediction*, 2016.

Figure 6.27 shows an example comparing the Jensen model and the BP model for some specific parameter choices noted in the figure caption. The main highlight is to contrast the constant wake deficit versus the smooth Gaussian deficit.

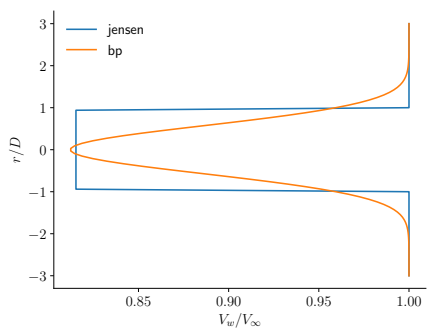

Fig. 6.27 Both wake models are at $x = 6D$ with $C_T = 0.889$. The Jensen model used $k = 0.075$, and the BP used $I = 0.14$.

The above discussion provides only an introduction to turbine wake models. Various additional considerations are needed in a wind farm model. Downstream turbines are often only partially overlapped by an upstream wake, and typically an area overlap ratio is used to modify the velocity deficits. When multiple wakes intersect the velocity deficits must be combined in some way. Some common approaches include a root-mean-square deficit or a linear sum of deficits. As the wind changes direction, typically expressed as a probability distribution called a wind rose, the wakes needed to be recomputed. Some models assume independent calculations, while others require a downstream marching approach to compute the effect of velocity deficits in a

sequential manner. Wind shear, wake deflection, stratification, amongst other considerations, can be important in obtaining good velocity and power predictions in a wind farm.

7 CFD

This chapter does not overview the CFD process or dive into any theory. We simply visit a few fluid calculations that are relevant to CFD applications.

7.1 Sizing the Prism Layer Mesh

In inviscid CFD an unstructured (or structured) mesh can be used all the way to the body. However, in viscous CFD it is important to use a structured mesh near the body. A structured mesh typically uses quadrilaterals, hexahedrons, or prims cells. We will generically refer to these structured boundary layer cells as prism cells in the below discussion. Prism cells serve multiple purposes. They can more easily be made high aspect ratio, which is important to efficiently capture a boundary layer as flow quantities change much more rapidly normal to the surface as compared to streamwise. Prism cells aligned with the flow in the boundary layer also reduce numerical diffusion allowing for more accurate solutions. This layer is called the *prism layer*. This section discusses some techniques to size the mesh in the prism layer.

First, we need to choose an overall height for the prism layer. As an estimate, we could use the boundary layer displacement thickness from Schlichting's empirical formulas for turbulent boundary layers (Eq. 3.50):

$$H = \frac{0.046x}{Re_L^{0.2}} \tag{7.1}$$

where H is the total height of the prism layer and $Re_L = V_e L/\nu$ with L the boundary layer length. Since we generally don't know V_e before computing the flow field, we will use the freestream velocity: $Re_L = V_\infty L/\nu$.

Next, we need to determine the height of the first cell. While various wall models exist, in the following we assume that we want to fully resolve the prism layer. In that case our first cell height should give a y^+ value of 1 in order to resolve the viscous sublayer. Recall that y^+ is a

Reynolds number applicable near a wall:

$$y^+ = \frac{u_\tau y}{\nu} \tag{7.2}$$

where $u_\tau = \sqrt{\tau_w/\rho}$ is the friction velocity.

If we need y^+ equal to 1 (or some other value like 30 if using a wall model) then we can solve for the y value that is the height of our first cell (which we call h):

$$\begin{aligned} h &= \frac{\nu y^+}{u_\tau} \\ &= \nu y^+ \sqrt{\frac{\rho}{\tau_w}} \\ &= \nu y^+ \sqrt{\frac{\rho}{c_f \frac{1}{2}\rho V_e^2}} \\ &= \frac{\nu y^+}{V_e}\sqrt{\frac{2}{c_f}} \end{aligned} \tag{7.3}$$

The Reynolds number (again using V_∞ instead of the unknown V_e is):

$$Re_L = \frac{V_\infty L}{\nu} \tag{7.4}$$

We solve this for ν and plug into the above equation:

$$h = \frac{y^+ L}{Re_L}\sqrt{\frac{2}{c_f}} \tag{7.5}$$

This provides an estimate for the height of the first cell in the prism layer in order to achieve a desired $y+$ value. We still need an estimate for c_f but can use the Schlichting formulas for that too.

$$c_f = \frac{0.0592}{Re_L^{0.2}} \tag{7.6}$$

Now that we know the size of the prism layer, and the size of the first cell, we need to determine how many cells span the prism layer. Equivalently, we could determine the growth rate. The growth rate is more fundamental, so it makes more sense to choose a growth rate (e.g., 1.2) and then pick the number of cells accordingly.

CFD packages have different methods to space the cells in the prism layer, but one common approach is geometric progression. The formula for geometric progression is:

$$H = h\left(\frac{r^n - 1}{r - 1}\right) \tag{7.7}$$

where H is the overall height, h the height of the first cell, r the growth rate, and n the total number of cells. In our case, we want to solve for n:

$$n = \log_r \left(\frac{H}{h}(r-1) + 1 \right) \tag{7.8}$$

Thus, we have a procedure to size the mesh in the prism layer.

7.2 Matching Mach and Reynolds Number Simultaneously

Matching Mach number and Reynolds number simultaneously for many aerospace applications is difficult if not impossible experimentally. For CFD applications we can of course match both simultaneously, but this is a source of frequent error if we aren't careful.

In CFD a compressible freestream boundary condition is typically specified with Mach number, pressure, and temperature. Obviously, we set the freestream Mach number to the desired match. But what pressure and temperature do we use in order to match Reynolds number?

Let's start with the definitions of Mach number and Reynolds number (based on chord in this case):

$$M_\infty = \frac{V_\infty}{a}, \quad Re = \frac{\rho V_\infty c}{\mu}$$

How does temperature and pressure affect these equations? The speed of sound and the dynamic viscosity are both functions of temperature, and the density is a function of pressure and temperature through a thermodynamic equation of state (generally the ideal gas law). In other words:

$$M_\infty = \frac{V_\infty}{a(T)}, \quad Re = \frac{\rho(p,T) V_\infty c}{\mu(T)}$$

The freestream velocity appears in both equations, so we solve for it in one equation and plug it into the other.

$$Re = \frac{\rho(p,T) M_\infty a(T) c}{\mu(T)}$$

We note that we have a degree of freedom. We can either choose a pressure and then solve for the corresponding temperature that satisfies the equation, or we can specify temperature and then choose the corresponding pressure that satisfies the equation. Intuitively that should make sense. We should be able to match Mach and Reynolds Number at any condition by appropriately choosing the other variables.

The density has a simple relationship between pressure and temperature through the ideal gas law:

$$p = \rho RT$$

where the specific gas constant $R = 286.9$ J/(kg-K) for air. Substituting that into our main equation results in:

$$Re = \frac{pM_\infty a(T)c}{RT\mu(T)}$$

The speed of sound also has a simple relationship with temperature:

$$a = \sqrt{\gamma RT}$$

where $\gamma = 1.4$ for an ideal diatomic gases (and air is essentially entirely composed of diatomic gases). Substituting in:

$$Re = \frac{pM_\infty \sqrt{\gamma RT}c}{RT\mu(T)} = \frac{pM_\infty \sqrt{\gamma}c}{\sqrt{RT}\mu(T)}$$

The only thing we haven't substituted in is the dynamic viscosity dependence on temperature. We won't directly substitute in an expression, just because it is a bit long. For an ideal gas, the dynamic viscosity can be found from Sutherland's law:

$$\mu = \mu_{ref}\left(\frac{T}{T_{ref}}\right)^{3/2}\frac{T_{ref}+S}{T+S}$$

where $T_{ref} = 273.15$, $S = 110.4$, $\mu_{ref} = 1.716 \times 10^{-5}$ kg/(m-s).

We can see that the easiest way to solve this equation is to choose T, and then compute p (note that the units for T are Kelvin in all of these equations):

$$p = \frac{Re\ \mu(T)\sqrt{RT}}{M_\infty c\sqrt{\gamma}}$$

By choosing a T, we know everything on the right hand side and can directly solve for p.

The opposite approach is also possible (choose p then solve for T), but is more work. We move everything related to T to the left-hand side.

$$\sqrt{T}\mu(T) = \frac{pM_\infty c\sqrt{\gamma}}{Re\sqrt{R}}$$

We actually can solve for T explicitly through a quadratic function, but it's messy and is easier just to solve the above numerically as a root finding problem:

$$f(T) = \sqrt{T}\mu(T) - \frac{pM_\infty c\sqrt{\gamma}}{Re\sqrt{R}} = 0$$

We use a root finding algorithm to find the T that satisfies $f(T) = 0$ (where again T is in Kelvin).

Either approach is fine, but remember that when you set the temperature and pressure in your boundary condition, you should also use those values to set the initial conditions (or at least something close). If your initial conditions are very far from the steady state solution, you may have numerical issues and a difficult time converging. If you change pressure, it may be easiest to just change the reference pressure and then your gauge pressure can remain at zero elsewhere.

Bibliography

1 Buresti, G., "A note on Stokes' hypothesis," *Acta Mechanica*, Vol. 226, No. 10, June 2015, pp. 3555–3559, ISSN: 1619-6937. DOI: 10.1007/s00707-015-1380-9 — cited on p. 24

2 Cebeci, T. and Bradshaw, P., *Physical and Computational Aspects of Convective Heat Transfer*, 1st ed. Springer, 1988. ISBN: 978-1-4612-3918-5 DOI: 10.1007/978-1-4612-3918-5 — cited on p. 93

3 Moran, J., *An Introduction to Theoretical and Computational Aerodynamics*. Dover Publications, 1984. — cited on p. 94

4 Wazzan, A. R., Gazley, C., and Smith, A., "The H-Rx method for predicting transition," RAND Corporation, Santa Monica, CA, 1981. — cited on p. 99

5 Coder, J. G. and Maughmer, M. D., "Numerical Validation of the Squire–Young Formula for Profile-Drag Prediction," *Journal of Aircraft*, Vol. 52, No. 3, May 2015, pp. 948–955. DOI: 10.2514/1.C033021 — cited on pp. 100, 101

6 Clauser, F. H., "The Turbulent Boundary Layer," *Advances in Applied Mechanics*, Vol. 4, Dryden, H. and von Kármán, T., Eds., 1956, pp. 1–51, ISSN: 0065-2156. DOI: https://doi.org/10.1016/S0065-2156(08)70370-3 — cited on p. 107

7 Anderson, J. D., *Modern Compressible Flow: With Historical Perspective*. 2003. ISBN: 1259027422 — cited on p. 184

8 Ning, A., "Using Blade Element Momentum Methods with Gradient-Based Design Optimization," *Structural and Multidisciplinary Optimization*, May 2021. DOI: 10.1007/s00158-021-02883-6 — cited on pp. 188, 198, 211, 212

9 Glauert, H., *Airplane propellers*, *Aerodynamic Theory*, Springer, 1935, pp. 169–360. — cited on pp. 191, 204

10 Ning, A., "A Simple Solution Method for the Blade Element Momentum Equations with Guaranteed Convergence," *Wind Energy*, Vol. 17, No. 9, September 2014, pp. 1327–1345. DOI: 10.1002/we.1636 — cited on pp. 198, 212

11 Glauert, H. and Committee, A. R., *A General Theory of the Autogyro*. HM Stationery Office, November 1926. cited on p. 205

12 Buhl Jr., M. L., "A New Empirical Relationship between Thrust Coefficient and Induction Factor for the Turbulent Windmill State," NREL/TP-500-36834, National Renewable Energy Laboratory, August 2005. cited on p. 205

13 Himmelskamp, H., *Profile investigations on a rotating airscrew*. Ministry of Aircraft Production, 1947. cited on p. 215

14 Snel, H., "Scaling laws for the boundary layer flow on rotating wind turbine blades," *4th IEA symposium on aerodynamics for wind turbines, Rome*, 1991. cited on p. 217

15 Snel, H., Houwink, R., and Bosschers, J., "Sectional prediction of lift coefficients on rotating wind turbine blades in stall," ECN-C-93-052, Netherlands Energy Research Foundation (ECN), December 1994. cited on p. 217

16 Lindenburg, C., "Investigation into Rotor Blade Aerodynamics: Analysis of the stationary measurements on the UAE phase-VI rotor in the NASA-Ames wind tunnel," ECN-C–03-025, July 2003. cited on pp. 217, 218

17 Du, Z. and Selig, M., "A 3-D Stall-Delay Model for Horizontal Axis Wind Turbine Performance Prediction," *1998 ASME Wind Energy Symposium*, ser. AIAA-1998-21, January 1998. cited on p. 217

18 Laino, D. J., Hansen, A. C., and Minnema, J. E., "Validation of the AeroDyn Subroutines Using NREL Unsteady Aerodynamics Experiment Data," *Wind Energy*, Vol. 5, 2002, pp. 227–244. DOI: 10.1002/we.69 cited on p. 218

19 Eggers Jr, A. J., Chaney, K., and Digumarthi, R., "An Assessment of Approximate Modeling of Aerodynamic Loads on the uae Rotor," *41st Aerospace Sciences Meeting and Exhibit*, ser. AIAA-2003-0868, January 2003. DOI: 10.2514/6.2003-868 cited on p. 218

20 Viterna, L. A. and Janetzke, D. C., "Theoretical and Experimental Power from Large Horizontal-Axis Wind Turbines," DOE/NASA/20320-4, National Aeronautics and Space Administration, Lewis Research Center, September 1982. cited on p. 221

21 Beddoes, T., "A synthesis of unsteady aerodynamic effects including stall hysteresis," *Vertica*, Vol. 1, No. 2, 1976, pp. 113–123. cited on p. 222

22 Leishman, J. G. and Beddoes, T. S., "A Semi-Empirical Model for Dynamic Stall," *Journal of the American Helicopter Society*, Vol. 34, No. 3, July 1989, pp. 3–17, ISSN: 2161-6027. DOI: 10.4050/jahs.34.3 cited on p. 222

23 Øye, S., "Dynamic stall simulated as time lag of separation," *Proceedings of the 4th IEA Symposium on the Aerodynamics of Wind Turbines*, Vol. 27, Rome, Italy, 1991, p. 28. cited on p. 222

24 Hansen, M. H., Gaunaa, M., and Madsen, H. A., "A Beddoes–Leishman Type Dynamic Stall Model in State-space and Indicial Formulations," Risø-R-1354, Risø National Laboratory, Roskilde, Denmark, 2004. cited on p. 222

25 Jensen, N. O., "A Note on Wind Generator Interaction," RISØ-M-2411, Risø National Laboratory, November 1983. cited on p. 224

26 Katić, I., Højstrup, J., and Jensen, N. O., "A simple model for cluster efficiency," *Eurorpean Wind Energy Association Conference and Exhibition*, Rome, Italy, October 1986. cited on p. 225

27 Bastankhah, M. and Porté-Agel, F., "Experimental and theoretical study of wind turbine wakes in yawed conditions," *Journal of Fluid Mechanics*, Vol. 806, October 2016, pp. 506–541, ISSN: 1469-7645. DOI: 10.1017/jfm.2016.595 cited on p. 226

28 Niayifar, A. and Porté-Agel, F., "Analytical Modeling of Wind Farms: A New Approach for Power Prediction," *Energies*, Vol. 9, No. 9, September 2016, p. 741, ISSN: 1996-1073. DOI: 10.3390/en9090741 cited on p. 227